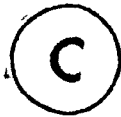


THE EFFECT OF RANDOMLY  
VARYING ADDED MASS ON THE  
DYNAMICS OF A FLEXIBLE  
CYLINDER IN TWO-PHASE  
AXIALLY FLOWING FLUID

by



CHRISTOPHE KLEIN

Under the supervision of Prof. M.P. Paidoussis

A thesis submitted to  
the Faculty of Graduate Studies and Research  
in partial fulfillment of the requirements  
for the degree of Master of Engineering

Department of Mechanical Engineering  
McGill University  
Montreal, Que., Canada

October, 1981

January 1982

re - Christophe KLEIN- M.Eng. thesis

DYNAMICS OF FLEXIBLE CYLINDER IN TWO-PHASE FLOW

## ABSTRACT

This thesis investigates the effect of randomly varying added mass on the dynamics of a flexible cylinder in an external axial two-phase flow, bounded by a rigid immobile channel.

The behaviour of a cylinder in two-phase flow has been found to be very different and less predictable than in single-phase flow. Experiments have shown that damping is significantly higher in simulated two-phase flows, depending on the flow regime, and that the hydrodynamic or added mass decreases with increasing void fraction, but at a higher rate than that of the mixture density.

The hypothesis is made that these effects might arise from random fluctuations of the hydrodynamic mass.

After an attempt to find a theoretical formulation of this probabilistic problem, based on a model of the fluid-structure interaction at the molecular level, a numerical approach is adopted. This simulation consists in applying random perturbations on the added mass coefficient of a one-degree-of-freedom system, and investigating their effect on the response frequency and damping.

A first digital analysis of the free vibrations of this system is conducted in the time domain. A second digital analysis of the free vibrations is also undertaken, but this time in the frequency domain. Finally, an analog simulation of both free and forced vibrations of the system is carried out by means of an analog computer and a FFT electronic frequency analyser.

All three studies exhibit a behaviour in agreement with the effects sought, but occurring with a magnitude much lower than expected.

## SOMMAIRE

### L'EFFET DE FLUCTUATIONS ALEATOIRES DE LA MASSE AJOUTÉE SUR LE COMPOTEMENT DYNAMIQUE D'UN CYLINDRE FLEXIBLE DANS UN ÉCOULEMENT FLUIDE DIPHASIQUE ET AXIAL

Cette thèse traite de l'effet de fluctuations aléatoires de la masse ajoutée sur le comportement dynamique d'un cylindre flexible soumis à un écoulement externe, axial et diphasique, limité par un conduit rigide et immobile.

Il a été établi que le comportement d'un cylindre dans un écoulement diphasique est très différent et moins prévisible que dans un écoulement monophasique. Des expériences ont montré que l'amortissement est nettement plus élevé dans des écoulements diphasiques simulés, suivant le régime d'écoulement, et que la masse hydrodynamique, ou masse ajoutée, décroît lorsque le pourcentage de vapeur s'accroît, mais ceci plus rapidement que ne le fait la densité du mélange.

On émet l'hypothèse que ces effets proviendraient de fluctuations aléatoires affectant la masse hydrodynamique.

Après une tentative de formulation théorique de ce problème probabiliste basée sur un modèle à l'échelle moléculaire de l'interaction entre fluide et solide, on a choisi une approche numérique. Cette simulation consiste à appliquer des perturbations aléatoires sur le coefficient de masse ajoutée d'un système à un degré de liberté, et à étudier leur action sur la fréquence et l'amortissement de la réponse.

On entreprend une première analyse digitale des vibrations libres de ce système, dans le domaine temporel. Puis on entreprend une seconde analyse digitale, également des vibrations libres, mais cette fois il s'agit d'une étude fréquentielle. Finalement on mène à bien une analyse analogue, à la fois des vibrations libres et forcées du système, au moyen d'un calculateur analogique et d'un analyseur de fréquences FFT électronique.

Ces études aboutissent toutes trois à la mise en évidence des effets recherchés, mais avec une amplitude beaucoup plus faible que souhaitée.

### ACKNOWLEDGEMENT

The author wishes to express his indebtedness to:

Professor M.P. Paidoussis, Chairman of the Department of Mechanical Engineering, McGill University, for his guidance, encouragement, valuable suggestions and criticisms, and general supervision as Research Director for this project; also for the large amount of time spent in reviewing this manuscript;

Professor D.R. Axelrad, Professor Emeritus, Mechanical Engineering, McGill University, for his valuable advice and large amount of time spent to find a theoretical probabilistic model;

Messrs L.N. Carlucci and M.J. Pettigrew of Atomic Energy of Canada, CRNL, for useful suggestions on direction of this research and for providing experimental data with which the theoretical results herein obtained could be compared;

Dr. P. Thibault, Mr. J. Gagnon and Mr. M. Ostoja-Starzewski for many critical discussions and useful ideas;

Miss J. Newman for an excellent typing job; and

Atomic Energy of Canada Ltd. for the financial assistance provided to this research and to the author.

## TABLE OF CONTENTS

	<u>Page No.</u>
ABSTRACT	i
SOMMAIRE	ii
ACKNOWLEDGEMENT	iv
TABLE OF CONTENTS	v
1. <u>CHAPTER I - INTRODUCTION</u>	1
2. <u>CHAPTER II - PROBLEM FORMULATION</u>	8
2.1 Fluid Damping and Hydrodynamic Mass in Two-Phase Flow	8
2.1.1 Two-Phase Flow Modelling	8
2.1.2 Results Obtained by Carlucci	10
2.2 Equation of Small Lateral Motions	12
2.3 Probabilistic Formulation Attempt	16
2.4 One-degree-of-Freedom Model Finally Adopted	20
3. <u>CHAPTER III - DIGITAL ANALYSIS OF THE FREE VIBRATIONS IN THE TIME DOMAIN</u>	24
3.1 Method of Analysis	24
3.2 Results and Discussion	27
3.2.1 Numerical Importance of the Hydrodynamic Mass and Damping Effects Observed by Carlucci	30
3.2.2 Response of the System to Pseudo-Random Added Mass Perturbations	35
3.2.3 Response of the System to Deterministic Added Mass Perturbations	39
3.2.4 Response of the System to Deterministic Added Mass Perturbations; Parametric Resonances	41

	<u>Page No.</u>
4. <u>CHAPTER IV</u> - DIGITAL ANALYSIS OF THE FREE VIBRATIONS IN THE FREQUENCY DOMAIN	45
4.1 Introduction	45
4.2 Results Obtained in the Frequency Range (0 - 160 Hz)	49
4.2.1 Response of the System to Deterministic Added Mass Perturbations; Parametric Resonance	52
4.2.2 Response of the System to Pseudo-Random Added Mass Perturbations	55
4.3 Results Obtained in the Frequency Range (0 - 40 Hz)	61
5. <u>CHAPTER V</u> - ANALOG ANALYSIS OF THE FREE AND FORCED VIBRATIONS IN THE FREQUENCY DOMAIN	71
5.1 Description of Equipment and Method	71
5.1.1 Digital Signal Analyser and Analog Computer	71
5.1.2 Machine Equation on Analog Computer	73
5.2 Free Vibration Results	78
5.3 Forced Vibration Results	80
6. <u>CHAPTER VI</u> - CONCLUSION	85
7. REFERENCES	88
8. FIGURES 1 - 46	
9. APPENDIX A	
Discretization of the Equation of Small Lateral Motions in an Attempt to Obtain a Fokker-Planck Equation	A1
10. APPENDIX B	
Some Elements on the Probabilistic Formulation of the Fluid-Structure Interaction	B1

	<u>Page No.</u>
10. APPENDIX B (cont'd)	
B.1 Membrane in Planar Turbulent Flow	B1
B.2 Investigation of the Random Loading Force $A(t)$	B4
B.3 Integration of the Generalized Langevin Equation over a Specific Time Interval $\Delta T$	B6
11. APPENDIX C	
Complements to the Digital Time Domain Analysis of Chapter III	C1
C.1 Runge - Kutta Method	C1
C.2 Generation of Pseudo-Random Gaussian Perturbations	C2
C.3 Determination of the Mean $\mu$ and Variance $\sigma^2$ of the Random Fluctuator $\alpha(t)$	C7
C.4 Study of Convergence of the Runge - Kutta Solutions	C11
C.5 Listing of the Program	C13
C.6 Various Series of Computer Runs Investigated	C19
12. APPENDIX D	
Complements to the Digital Frequency Domain Analysis of Chapter IV	D1
D.1 Fast Fourier Transform	D1
D.2 Various Schemes of $\alpha(t)$ Generated in the Digital Study	D7
D.3 Listing of the Program	D13
13. APPENDIX E	
Complements to the Analog Frequency Domain Analysis of Chapter V	E1
E.1 Measurement Characteristics of the HP 5420A Digital Signal Analyser	E1
E.2 The EAI 1000 Analog Computer	E7

1.

CHAPTER I  
INTRODUCTION

The study of flow-induced vibrations of structural components has been greatly intensified in recent years [1].

Some spectacular failures come indeed to mind to point out how important these vibrations may become in some cases. One exciting example is the famous oscillation in November 1940 of the Tacoma Narrows Bridge in Washington State; four months after its opening, the fine suspension Bridge swayed violently in a steady wind of about 42 miles per hour and was ultimately destroyed. But the worst accident to be quoted here occurred on March 27, 1980 in the North Sea, when the Alexander L. Keilland semi-submersible oil platform capsized in heavy seas, after one of its five supporting legs had buckled and then fractured; a total of 123 oil workers and engineers perished in the disaster, most of them trapped in near-freezing waters 80 metres deep.

Undoubtedly the greatest amount of research has been performed in the aeroelasticity field, since the criterion of minimizing the dead-weight compared to vehicle performance characteristics is of utmost importance in the aerospace industry. Some useful information on plate and shell problems can be found in Refs. [2-4].

Other problems have also been investigated as for instance the behaviour of urban winds between high skyscrapers or, especially in Canada, the galloping of ice-coated transmission lines in a steady wind. In the early 1960's it has also been attempted to transport oil cheaply by sea in a nylon-rubber oil barge or "dracone"; although this was a commercially acceptable proposition, Hawthorne [5] and Paidoussis [6] showed that rigid

body oscillations occur at low towing speeds, whilst flexural instabilities of buckling and flutter type occur at higher towing speeds.

Our interest in this thesis is in the dynamics of flexible slender cylinders immersed in external two-phase axially flowing fluid.

The topic of flow-induced vibrations of cylinders has received growing attention from researchers because of repeated and sometimes very costly equipment failures in the power generating industry, having even led to some complete plant stoppages. As a matter of fact, such devices as boilers, heat exchangers, steam generators and nuclear reactors have primarily been designed for heat transfer or other specific purposes, whereas flow-induced vibrations used to be considered, not so long ago, as a secondary design parameter.

Unlike the case of cross-flow-induced vibrations where large amplitude oscillations develop even at moderate flow velocities, the subject of parallel-flow-induced vibrations is rather new. The first experimental study was reported by Burgreen et al. [7] in the late 1950's. Later Paidoussis [8] formulated an equation of motion and performed the first stability analysis of a solitary cylinder in unconfined steady incompressible axial flow. He showed that small flow velocities damp free motions of the cylinder and diminish its natural frequencies, whereas increasing flow velocities eventually destabilize the system, first by buckling (divergence) and finally by flutter. It is these instabilities which have been given the name of fluidelastic instabilities - fluidelastic being a generic word for both aeroelastic and hydroelastic. A number of refinements were included in subsequent work [9,10] and, among others, the study was extended to the case of several cylinders arranged in a cluster [10]. At this stage, the

expression of the hydrodynamic or "added" mass was refined in order to take into account the effect of confinement of the flow either by a narrow channel or by surrounding but still immobile cylinders. The next important step was to include the fact that adjacent cylinders do not remain passive, but on the contrary undergo complex hydrodynamically coupled motions; this was first achieved by Chen [11] and has since then been extended and also verified by a whole set of experiments [12]. One of the main effects of flow channel confinement and of hydrodynamic coupling to neighbouring cylinders is to severely lower the stability threshold. It was also observed that, once the system becomes unstable, it is subjected to a succession of buckling and flutter instabilities with increasing flow, of progressively more complex modal shape.

Nevertheless, the critical flow speeds leading to fluidelastic instabilities remain still higher than the flow velocity ranges usually encountered in industrial applications, that is why only the small-amplitude or "sub-critical" vibrations are of current interest. Normally such small vibrations, typically  $10^{-3}$  to  $10^{-1}$  cm, would be neglected, were it not for the often extremely close spacing of the cylinders in the array, with inter-cylinder gap-to-radius ratios of the order of  $10^{-1}$ . [A bundle of nuclear-reactor fuel elements is reproduced in Fig. 1]. Hence, although very small, these vibrations may cause intercylinder impact, which may result in fretting-wear damage. Several mechanisms of sub-critical vibrations have been proposed and they have been reviewed in Refs. [13,14]; it is now widely accepted that these vibrations are a random response to the random fluid pressure forces developed in the flow field.

On the whole, several review papers are available in the literature on vibrations of cylinders induced by axial (and cross) flow [15-19, 21,22].

A new classification of these vibrations has been proposed very recently by Paidoussis [21], distinguishing between three main types of behaviour: (i) response to pressure fluctuations in the flow at all flow velocities; (ii) parametric resonances at specific flow speeds or excitation frequencies; (iii) fluidelastic instabilities for very high flow velocities [see Fig. 2].

Unfortunately most studies deal with single-phase flows, and relatively little has been done on two-phase flows [22]. Moreover, no substantial research has yet been conducted on one of the key issues of the problem, namely the quite complex fluid-structure interaction in two-phase flows [22,23,26]. Generally speaking, the presence of the second phase induces a randomly varying fluid density and introduces two major aspects to the problem: (i) a much altered pressure field exhibiting a drastic shift, depending on the flow regime, of the frequency distribution of the pressure force, and also bringing a higher susceptibility to subcritical vibration; (ii) parametric excitation due to the periodicity existing in the distribution of the virtual mass and which has been studied extensively by Hara [24-26]. Actual systems often involve high temperature and high pressure steam-water mixtures, with the steam quality varying along the rods due to surface boiling; Pettigrew and Gorman [27] report the only experiment with such a heated system. As a matter of fact, simulations involving boiling systems are costly and difficult to instrument, hence simulation experiments using non-condensable gases have commonly been conducted — the most

popular mixture being the air-water mixture [28-33]. In these experiments, various parameters have been found to be of interest, such as void fraction, fluid density, average flow velocity, etc. Paidoussis and Pettigrew [31] have conducted some experiments on confined cylinders in both liquid and two-phase flows, to test the validity of the aforementioned theory, e.g. [12] or [21], predicting the onset of fluidelastic instabilities and the succession, with increasing flow, of buckling and flutter instabilities of progressively more complex modal shape. In the case of liquid flow, agreement between theory and experiment was found to be qualitatively good and quantitatively fair — taking the experimental difficulties into account. But as far as the two-phase flow is concerned, theory completely failed to predict the lack of noticeable instabilities which has been observed in the experiments.

More recently Carlucci [32,33] has investigated experimentally the behaviour of fluid damping and hydrodynamic mass of a cylinder in simulated two-phase flow (also an air-water mixture). He has found that damping in two-phase flow is significantly higher than in single-phase flow, whereas the hydrodynamic mass decreases with increasing void fraction, but at a higher rate than that of the mixture density.

A first attempt has been made by Ostoja-Starzewski [34,35] to find out whether these discoveries can be attributed to the compressibility of the two-phase fluid stream. Of course, two-phase flow is anything but incompressible, hence the motivation for that investigation. Another starting point of that study was the fact that the speed of sound in two-phase mixtures can be much lower than in either of its two constituents (easily one tenth, and even  $1/50^{\text{th}}$  at low pressures: cf. Fig. 3), which allows the

Mach number  $M$  to reach values close to 1\* for operational values of the flow velocity. Using a homogeneous-flow model of the two-phase flow, Ostoja-Starzewski found, by means of three different mathematical models, that the effect of compressibility is in qualitative agreement with Carlucci's results, but nevertheless quantitatively seriously underestimates the observed behaviour.

Even more recently Schumann [36] conducted a theoretical research on a somewhat related problem: the fact that the effective density of a two-phase mixture of solid particles and inviscid compressible fluid differs from the average density, due to relative accelerations between the phases. His study on virtual density and speed of sound in a fluid-solid mixture is based on Hamilton's principle and a general homogenization method.

This research represents in fact a second attempt to discover the underlying mechanism of the two effects observed by Carlucci. The basic hypothesis made here is that these effects could be attributed to random fluctuations of the hydrodynamic mass of the cylinder, this randomness arising from the highly non-homogeneous nature of two-phase flow. A fundamental approach was first envisaged, which would have led to a completely probabilistic description of the fluid-structure interaction. The principle of such an approach would be to first consider the coupled motion of the structure and the two-phase flowing fluid from a microdynamic point of view, i.e. at the molecular level, and then to develop a statistical method by which a transition to the global hydrodynamic formulation could be achieved. (Some elements of this approach will be found in Appendix B.) But such a task being beyond the scope of a M.Eng. thesis, it was decided to limit the

---

\*This arises since  $M = U/c$ , where  $U$  is the flow velocity and  $c$  the sonic speed [34].

work to a purely numerical simulation, with the aim of studying mainly the effect of a randomly varying virtual mass on the response of a one-degree-of-freedom oscillator. A digital study of the free vibrations of this system is first conducted in the time domain and is given in Chapter III. A second digital analysis of the same free vibrations is also undertaken, but this time in the frequency domain, and is presented in Chapter IV. Finally, an analog simulation of both free and forced vibrations of this system is carried out, in the frequency domain, by means of an analog computer; this last analysis is the topic of Chapter V.

## CHAPTER II

### PROBLEM FORMULATION

#### 2.1 Fluid Damping and Hydrodynamic Mass in Two-Phase Flow

##### 2.1.1 Two-Phase Flow Modelling

As the random pressure fluctuations in the turbulent boundary layer are considered to be the main forcing mechanism exciting the structural component vibrations, it may be worthwhile to see under which conditions the pressure disturbances are transmitted in two-phase flow. Phase distribution (flow regime) has for instance been shown to strongly influence the frequency distribution of the pressure force [22].

Modelling of two-phase flow and of the continuous heat and mass transfer occurring between the phases is an extremely important subject for the design of many major items of equipment found in chemical and power plants. But due to the continuous variation of all the thermal and hydraulic properties of the flowing fluid, the mechanisms of phase changes in channel flow remain a poorly understood phenomenon; this is so despite the efforts of many investigators for more than a century, which have resulted in more than 10,000 papers published on boiling and two-phase flow. A general review on convective boiling and condensation, i.e. in the presence of a forced flow, has been given by Collier [37], mostly for single-component systems, i.e. a pure liquid and its vapour, and more particularly the water/steam system. The methods used to analyse a two-phase flow are based on those already validated for single-phase flows, and the general procedure consists in writing down the basic equations governing the conservation of mass, energy and momentum, and then in seeking to solve them

by means of various simplifying assumptions. Three main types of assumptions have been made, as follows.

(i) The "homogeneous" flow model, in which the two-phase flow is assumed to be a single-phase flow having pseudo-properties obtained by suitably averaging the properties of the individual phases. This is the simplest model and has for instance been adopted by Ostoja-Starzewski [34].

(ii) The "separated" flow model, in which the two phases are artificially separated, and two sets of basic equations are written, one for each phase.

(iii) The "flow pattern" models, which represent the most sophisticated approach and in which the two phases are considered to be arranged in one of several prescribed geometries. These geometries are based on the various configurations or flow patterns observed when a gas and a liquid flow together in a channel. Commonly, six main flow regimes are distinguished in vertical flow: (1) bubbly flow, (2) slug flow, (3) churn flow, (4) wispy-annular flow, (5) annular flow, and (6) drop or mist flow. Churn and wispy-annular flows are included by some authors, respectively, into the categories of slug and annular flows [cf. Fig. 4]. Transitional flows are also noted [Fig. 5] and often exact characterization is quite difficult.

Fig. 6 shows the flow pattern map of Hewitt and Roberts [38] as given by Collier [37], on which the range of test conditions investigated by Carlucci [33] have been superimposed. This map has been obtained [38] from observations on low-pressure air-water and high-pressure steam-water flow in small diameter vertical tubes, and should be regarded no more than a rough guide.

It should also be mentioned here that in horizontal flow, the flow patterns are complicated by asymmetry of the phases resulting from the

influence of gravity. The different flow patterns are illustrated in Fig. 7 and a map of them by Baker [39] is also given.

### 2.1.2 Results Obtained by Carlucci

With the vertical flow pattern map [Fig. 6] in mind, let us now review Carlucci's results [33] in more detail. His visual observation of the slug, churn and low velocity bubbly flow patterns coincided reasonably well with those indicated on the map, but at higher mixture velocities the true flow pattern became increasingly more difficult to be visually identified. In particular the distinction between high velocity bubbly flow and annular or wispy annular flow was not possible, all three flow patterns appearing frothy or foamy on the flow tube surface.

Fig. 8 gives typical results showing the variation of the compliance magnitude with void fraction, and indicates the respective changes in damping and resonance frequency. Fig. 9 gives more information on the variation of the total fluid damping ratio  $\zeta_t$  with void fraction, and for different values of the mass flux. From both Figs. 8 and 9, it may be seen that maximum values of  $\zeta_t$  are obtained for void fractions ranging from 30 to 60 percent, whereas  $\zeta_t$  becomes minimal at void fractions of zero value and between 80 and 100 percent. Comparison between Figs. 9(a) and 9(b) shows that  $\zeta_t$  is higher in the smaller diameter flow tube, indicating a confinement effect. But, on the contrary, the mass flux does not appear to greatly affect the magnitude of  $\zeta_t$ ; however, because of the wide range of mass flux studied, the functional dependance of  $\zeta_t$  on void fraction is affected by the various flow patterns encountered [Fig. 6]. Total fluid damping ratio  $\zeta_t$  can be decomposed in three different components: a viscous

damping ratio  $\zeta_v$ , a flow-dependent damping ratio  $\zeta_f$ , and a two-phase damping ratio  $\zeta_{tp}$ . Thus we have

$$\zeta_t = \zeta_v + \zeta_f + \zeta_{tp} \quad (2-1)$$

Their variation with void fraction is given in Fig. 10. To sum up, fluid damping has been found to be significantly higher in two-phase flow than in single-phase flow, and a maximum or maxima have been exhibited at void fractions of 30% to 60%.

The variation of hydrodynamic mass with void fraction is shown in Fig. 11. Clearly, the hydrodynamic mass appears to decrease linearly with void fraction but at a greater rate than the mixture density line. It can also be noticed that it approaches a value of essentially zero at void fractions of 70% to 80%. This illustrates the fact that in annular flow the cylinder is dynamically decoupled from the flow tube wall since, in this flow pattern, most of the liquid flows as a thin film on the flow tube and cylinder surfaces. It might be useful to recall here the origin of the concept of hydrodynamic mass: when a structure vibrates in a fluid, the fluid gives rise to a two-part fluid-reaction force, one part of which may be interpreted as a flow-induced damping, whereas the other part is an acceleration-dependent, inertial force which may be thought to be associated with an "added" mass, as far as the dynamic response of the structure is concerned. Generally the hydrodynamic, or added, mass of a cylindrical rod is assumed to be equal to the mass of fluid displaced by the rod [40]. This is only true when the rod is submerged in an infinite fluid; however, for a confined cylinder, or one belonging to a fuel bundle, the added mass is affected by the duct wall and, for the cluster, by adjacent rods. Chen

and Wambsganss [9] and Paidoussis [10] have used an expression of the form

$$m_h = \chi m_f \quad (2-2)$$

where  $m_h$  and  $m_f$  are respectively the hydrodynamic mass and the mass of fluid displaced by unit length of the cylinder, and  $\chi$  is an expression equal to 1 for unconfined flow and greater than 1 otherwise, increasing when the flow channel decreases. Carlucci [33] uses the same expression and in his case  $\chi$  depends on the ratio of the flow tube inside diameter  $D_i$  to the cylinder diameter  $D$ :

$$\chi = \frac{(D_i/D)^2 + 1}{(D_i/D)^2 - 1} \quad (2-3)^*$$

This expression which has been derived for homogeneous inviscid flow may not be well suited to describe the complex reality hidden behind the notion of hydrodynamic mass in two-phase flow.

## 2.2 Equation of Small Lateral Motions

Our very first approach to the problem intended to start from the formulations obtained by Paidoussis and other investigators for the motion of a cylinder immersed in single-phase axially flowing fluid. We then hoped to be able to extend it to two-phase flow while incorporating a randomly varying added mass.

The system under consideration consists of a solitary flexible slender cylinder in external axial two-phase flow contained by a rigid channel, as depicted in Fig. 12. The cylinder, considered to be an Euler-

Bernoulli beam, is of finite length  $L$ , mass  $m$  per unit length, uniform cylinder cross section of diameter  $D$  and area  $A$ , flexural rigidity  $EI$  and internal damping of the Kelvin-Voigt type. Moreover, the cylinder is supposed to be pinned-pinned with the downstream end free to slide axially.

As far as the two-phase fluid flow is concerned, it is modelled by a macroscopically homogeneous flow, of mean flow velocity  $U$  and of fluid density  $\rho$ .  $D_h$  is the hydraulic diameter and is equal to  $4A_{ch}/S_{tot}$ ,  $A_{ch}$  being the channel flow area and  $S_{tot}$  being the total surface area in channel, per unit length. It is also assumed that the flow over the beam is not affected by the supports, as if the finite length cylinder were a portion of an infinitely long beam, the remainder of which is perfectly rigid.

The derivation of the equation of small lateral motions for a cylinder in external axial flow is not presented here and may be found in [10]. To obtain it, a force balance was taken for a small element of the cylinder, considering the various forces applied to this element.

Since we chose the homogeneous flow model, there is no difference between vertical and horizontal flow, except that for the latter configuration gravity effects may be neglected.

The equation of motion of a horizontal cylinder in a single plane  $[(x,y)$ -plane of Fig. 12] immersed in axial flow then reads

$$\begin{aligned} \mu I \frac{\partial^5 y}{\partial x^4 \partial t} + EI \frac{\partial^4 y}{\partial x^4} + \left[ \frac{\partial}{\partial t} + U \frac{\partial}{\partial x} \right] [m_h \left( \frac{\partial y}{\partial t} + U \frac{\partial y}{\partial x} \right)] \\ - \frac{1}{2} \rho D U^2 \left\{ C_f \left( 1 + \frac{D}{D_h} \right) (L - x) + D C_b \right\} \frac{\partial^2 y}{\partial x^2} + \frac{1}{2} \rho D U^2 C_f \left( \frac{D}{D_h} \right) \frac{\partial y}{\partial x} \\ + \frac{1}{2} \rho D U C_f \left( \frac{\partial y}{\partial t} + U \frac{\partial y}{\partial x} \right) + m \frac{\partial^2 y}{\partial t^2} = 0, \end{aligned} \quad (2-4)$$

where  $y = y(x, t)$ ,  $C_f$  is the frictional coefficient and  $C_b$  is the form drag coefficient at the end  $x=L$ . The boundary conditions may be taken as

$$y(0, t) = \frac{\partial y(0, t)}{\partial x} = y(L, t) = \frac{\partial y(L, t)}{\partial x} = 0. \quad (2-5)$$

For a two-phase flow, this equation will have some stochastic coefficients. We assume that  $EI$ ,  $\mu I$ ,  $L$ ,  $D$ ,  $D_h$ ,  $C_f$ ,  $C_b$  and  $m$  will remain constant, and express  $m_h$  as

$$m_h = \chi \rho A. \quad (2-2')$$

We then identify the stochastically-varying quantities as  $\rho$ ,  $U$ , and combinations of these terms (such as  $\rho U$ ,  $\rho U^2$ , ...), as well as their derivatives.

Expressing  $\rho$  and  $U$  as

$$\rho = \rho(x, t), \quad U = U(x, t),$$

we obtain

$$\begin{aligned} & \mu I \frac{\partial^5 y}{\partial x^4 \partial t} + EI \frac{\partial^4 y}{\partial x^4} + \chi A \left[ \rho \frac{\partial^2 y}{\partial t^2} + 2\rho U \frac{\partial^2 y}{\partial x \partial t} + \rho U^2 \frac{\partial^2 y}{\partial x^2} \right] \\ & - \frac{1}{2} \rho D U^2 \left\{ C_f \left( 1 + \frac{D}{D_h} \right) (L - x) + D C_b \right\} \frac{\partial^2 y}{\partial x^2} \\ & + \left\{ \chi A \left[ \frac{\partial(\rho U)}{\partial t} + U \frac{\partial(\rho U)}{\partial x} \right] + \frac{1}{2} \rho D U^2 C_f \left( 1 + \frac{D}{D_h} \right) \right\} \frac{\partial y}{\partial x} \\ & + \left\{ \chi A \left[ \frac{\partial \rho}{\partial t} + U \frac{\partial \rho}{\partial x} \right] + \frac{1}{2} \rho D U C_f \right\} \frac{\partial y}{\partial t} + m \frac{\partial^2 y}{\partial t^2} = 0. \end{aligned} \quad (2-6)$$

This equation is then rendered nondimensional, since nondimensional quantities are familiar to all researchers in the field and allow comparison between

various systems.

This is carried out by setting

$$\begin{aligned} \xi &= \frac{x}{L}, & \eta &= \frac{y}{L}, & \tau &= \left[ \frac{EI}{m + \bar{\rho}A} \right]^{\frac{1}{2}} \frac{t}{L^2}, \\ h_0 &= \frac{D}{D_h}, & u &= \left( \frac{\bar{\rho}A}{EI} \right)^{\frac{1}{2}} \bar{U}L, & \alpha_0 &= \left[ \frac{I}{E(\bar{\rho}A + m)} \right]^{\frac{1}{2}} \frac{\mu}{L^2}, \\ \beta_0 &= \frac{\bar{\rho}A}{\bar{\rho}A + m}, & c_f &= \frac{4}{\pi} c_f, & c_b &= \frac{4}{\pi} c_b, & \epsilon &= \frac{L}{D}. \end{aligned} \quad (2-7)$$

We also introduce the mean values of  $\rho$ ,  $U$ ,  $\rho U$  and  $\rho U^2$ :

$$\rho = \bar{\rho} s_1, \quad U = \bar{U} s_2, \quad \rho U = \bar{\rho U} s_3, \quad \rho U^2 = \bar{\rho U^2} s_4. \quad (2-8)$$

Having done all this, and assuming, moreover, that  $\eta(\xi, \tau) \approx 0(\epsilon)$ , and  $s_i(\xi, \tau) \approx 0(\epsilon)$  for all  $i$ , we finally end up with an equation of the form:

$$\begin{aligned} A_1 \frac{\partial^5 \eta(\xi, \tau)}{\partial \xi^4 \partial \tau} + A_2 \frac{\partial^4 \eta(\xi, \tau)}{\partial \xi^4} + A_3 s_4(\xi, \tau) \frac{\partial^2 \eta(\xi, \tau)}{\partial \xi^2} \\ + A_4 s_3(\xi, \tau) \frac{\partial^2 \eta(\xi, \tau)}{\partial \xi \partial \tau} + \left[ A_5 \frac{\partial s_3(\xi, \tau)}{\partial \tau} + A_6 s_4(\xi, \tau) \right] \frac{\partial \eta(\xi, \tau)}{\partial \xi} \\ + \left[ A_7 \frac{\partial s_1(\xi, \tau)}{\partial \tau} + A_8 \right] \frac{\partial \eta(\xi, \tau)}{\partial \tau} + \left[ A_9 + A_{10} s_1(\xi, \tau) \right] \frac{\partial^2 \eta(\xi, \tau)}{\partial \tau^2} = 0, \end{aligned} \quad (2-9)$$

where  $A_1$  to  $A_{10}$  are constants. The expressions of these constants will be found in Appendix A. The boundary conditions may be taken as

$$\eta(0, \tau) = \frac{\partial \eta(0, \tau)}{\partial \xi} = 0, \quad \eta(1, \tau) = \frac{\partial \eta(1, \tau)}{\partial \xi} = 0. \quad (2-10)$$

Several solution schemes were then considered to find some statistical solution to this equation. The most elaborate of these will be found in Appendix A. It consisted first in expressing all the stochastically varying quantities in terms of only one of them, chosen to be the principal random variable. Then the goal was to transform the equation of motion into an equation of the type:

$$\frac{d^2w(t)}{dt^2} + \lambda \frac{dw(t)}{dt} + \psi_w(t) = f(t), \quad (2-11)$$

where  $\lambda$  is a constant and  $w$  is a function of time to be found, on which a Fokker-Planck formulation should be tried out, following Morton and Corrsin [41]. Obtaining such a type of equation was attempted by means of the Galerkin discretization method. Unfortunately we had to realize that we could not obtain, by this method, a solution in the form of a probability distribution of the fluid density or of its velocity. Moreover, the whole procedure seemed contradictory since it was hoped to obtain a probabilistic solution of an equation which is basically deterministic. It was therefore decided to try a new approach and look into a purely probabilistic formulation of the fluid-structure interaction.

### 2.3 Probabilistic Formulation Attempt

The usual phenomenological laws of matter, like equations of state or transport equations, are deterministic laws. They are also average laws since they deal in macroscopic variables like pressure, temperature and electrical current, which represent the aggregate effect of millions of molecular interactions. But in many cases, even a simplified

deterministic model becomes intractable, either because the equations governing the system are too complex, or because they cannot even be derived. This occurs for a rolling die or for thermal agitation of molecules in a gas. Hence comes the need for a theory of stochastic processes, based on the mathematical tools developed by the probability theory. These tools have first been widely used by engineers in the field of telecommunications, since very often the signals to be dealt with are actually of random nature. In the same way, a control systems engineer can no longer neglect the statistical properties of the perturbations applied to the system he is optimizing. But in the past decades, the theory of stochastic processes has played an increasingly important role in nearly all the fields of science: physics, biology, medicine, economics, etc. In the physical sciences, this theory arose out of the study initiated by Einstein [42] in 1905 on the erratic movement (Brownian motion) of small particles suspended in a liquid. Major contributions to the problem of Brownian motion have been given by Uhlenbeck and Ornstein [43], Chandrasekhar [44], and Wang and Uhlenbeck [45]. A more recent mathematical critical review on the subject may also be found in Ref. [47]. More generally speaking, a great amount of literature has already been published on stochastic processes, and two fundamental books by Doob [48] and Feller [49] should be cited here. Other pieces of work might also be mentioned here, such as these of Papoulis [50], Stern et al. [51], Yaglom [52] more precisely on stationary random functions, Beran [53] and Samuels [54] on statistical continuum theories, Bharucha - Reid [55] mainly on Markov processes, and more recently Montroll and Lebowitz [56] on fluctuation phenomena (selected papers), and Axelrad [57] on micromechanics of solids.

To come back to the problem of a flexible slender cylinder immersed in axially flowing two-phase fluid, let us attempt to approach the coupled motion of the structure and the fluid from a local point of view, i.e. molecular level. By a corresponding statistical method, a transition to the global hydrodynamic formulation can be achieved.

With this aim in mind, a model is adopted, according to which the individual fluid particles moving along the boundary of the structure (see Appendix B and Figs. 13) have a behaviour represented by a "generalized Langevin equation" expressed by

$$m \frac{d^2 \vec{r}}{dt^2} + \beta \frac{d\vec{r}}{dt} + \omega_0^2 \vec{r} = \vec{A}(t), \quad (2-12)$$

where  $\vec{r}$  denotes the random position vector of the molecule:  $\vec{r} = \vec{r}(x,y)$

and in which:

$m$  is the fluid particle mass;

$\beta$  is the Stokes' drag denoting the interaction between the fluid particle and the surface of the solid body (this friction exists in the x-direction only);

$-\omega_0^2 \vec{r}$  is a harmonic-type attraction between the considered particle and its neighbours;

$\vec{A}(t)$  is the random loading force (equivalent to the random pressure on the structural member).

This equation may be split into a set of two equations accounting for the longitudinal and transverse components in the velocity field  $\vec{u} = \vec{u}(\vec{r}, t)$  (see Appendix B). This model incorporates the friction effects in the longitudinal direction only, whilst the transverse force is coupled to the local inertia of the structure in the unstable mode of motion. Hence the dynamics

of the system is assumed, for simplicity, to be two-dimensional.

The solution of the generalized Langevin equation in terms of the excitation force  $\vec{A}(t)$  accounts for the perturbation of the otherwise undisturbed lattice - structure of the fluid flow. Furthermore, this solution leads to a velocity distribution  $P(\vec{u})$  at a given instant of time for a prescribed mode of surface motion of the solid in the flow field.

At this stage of investigation, one can consider two different studies, namely:

- a) If the velocity distribution  $P(\vec{u})$  or the linear momentum distribution  $P(\rho\vec{u})$  only, is sought, one can define the respective probability distribution and obtain its evolution with time in form of a set of Fokker-Planck equations. Their solutions have to satisfy the given boundary and initial conditions, which also serve to determine the constants in the evolution equations.
- b) If, however, the density fluctuations in the fluid are of main interest, it would be better to use the Chapman-Kolmogorov evolution relation for the probability of the density distribution functions, for example

$$\frac{d P(\rho)_{t_1}}{dt} = Q^D P(\rho)_t, \quad (2-13)$$

where  $Q^D$  is the probability transition matrix (two-dimensional).

More information on the whole procedure up to the derivation of the set of the two coupled Fokker-Planck equations (cf. point a) above) can be found in Appendix B. But completing the whole probabilistic study described above has proved to be beyond the scope of a M.Eng. thesis, even though from this first attempt, it is strongly felt that, in order to achieve a proper formulation with respect to the random pressure and/or

density fields, one has to use the molecular-hydrodynamic approach\* as proposed, for example, by Hansen and McDonald [58], Boon and Yip [59] and others.

#### 2.4 One-Degree-of-Freedom Model Finally Adopted

It was finally decided to dwell on a numerical simulation of a one-degree-of-freedom system, in which a randomly-varying added mass is incorporated. The purpose of this study is to investigate the effects of these random fluctuations of the hydrodynamic mass on the response of the system. More particularly, our attention is focused on the comparison between the cases with and without these fluctuations, in order to see whether our results are in agreement with the ones obtained by Carlucci [33] and presented above in Section 2.1.2. If this is the case, then a good chance exists that the key of the mechanism, affecting the damping and the hydrodynamic mass in two-phase flow, lies actually in the hypothesis made, namely that the observed behaviour is due to random variations affecting the added mass. It is also supposed that our system is rather "static" in the sense that it is assumed that, with this model, we are placed at a given void fraction which remains constant all over the experiments (the void fraction is not taken into account explicitly in the model, but it is supposed to be somewhere in the "interesting" range, i.e. between 30 and 60 percent). Hence the only parameter investigated here will be the random fluctuations of the hydrodynamic mass. It is finally supposed that,

---

\* However, not all the investigators in the field agree on whether analysis of the fluid-structure interaction should be studied by the probabilistic approach. For instance Schlechtendahl argues against this direction, as quoted on page 193 of Ref. [23].

at this stage, it is sufficient to investigate a one-degree-of-freedom system, and that, if the desired effects do not prove to be significant, there is relatively little chance to see them occur for a higher degree-of-freedom system.

The system studied is

$$[M + m_h(t)]\ddot{x} + C\dot{x} + Kx = \begin{cases} 0 \\ f_o(t) \end{cases}, \quad (2-14)$$

in which  $x$  is the response of the structural system and  $M$ ,  $C$ ,  $K$  are respectively its mass, coefficient of viscous damping and spring constant.  $m_h(t)$  is its hydrodynamic mass and is composed of two terms, viz.

$$m_h(t) = \overline{m}_h + \mu(t), \quad (2-15)$$

where  $\overline{m}_h$  is the mean value and is assumed to be constant and  $\mu(t)$  are the fluctuations of  $m_h(t)$  about  $\overline{m}_h$ .

Hence, the total mass appearing in equation (2-14), sometimes called "virtual mass" by some authors (e.g. [9] or [16]), reads

$$M + m_h(t) = M + \overline{m}_h + \mu(t),$$

in which  $M + \overline{m}_h$  is constant.

Dividing all the terms of equation (2-14) by  $M + \overline{m}_h$ , we obtain

$$[1 + \alpha(t)]\ddot{x} + 2\zeta\omega_n\dot{x} + \omega_n^2x = \begin{cases} 0 \\ f(t) \end{cases}, \quad (2-16)$$

where

$$\omega_n = \sqrt{\frac{K}{M + \overline{m}_h}} \quad (2-16', a)$$

is the circular (undamped) natural frequency, including  $\overline{m}_h$ ;

$$\zeta = \frac{C}{2(M + \overline{m}_h)\omega_n} = \frac{C}{2\sqrt{K(M + \overline{m}_h)}} \quad (2-16', b)$$

is the viscous damping factor;

$$f(t) = \frac{f_o(t)}{M + \overline{m}_h} \quad (2-16', c)$$

is the forcing function (if considered); and

$$\alpha(t) = \frac{\mu(t)}{M + \overline{m}_h} \quad (2-16', d)$$

is the dimensionless fluctuating part of the hydrodynamic mass which is the parameter of interest in this study.

When  $\alpha(t) = 0$ , the treatment of this equation is classical and the analytical solution is easily obtained. Let us seize here the opportunity to mention two good textbooks on vibration analysis by Meirovitch [60] and Thomson [61].

For the unforced case, for an underdamped system, the solution is

$$x_d = B_d e^{-\zeta\omega_n t} \cos(\omega_d t + \Phi), \quad (2-17)$$

in which  $B$  and  $\Phi$  are constants depending on the initial conditions, and

$$\omega_d = \omega_n \sqrt{1 - \zeta^2}. \quad (2-18)$$

For the forced case, the general solution is a superposition of a transient response (general solution of the equation without forcing

function) and of a steady-state response (particular solution of the complete equation). If the forcing function is

$$f(t) = F \cos \omega_f t,$$

where  $\omega_f$  is hence the circular forcing frequency, then the general solution reads

$$x = Be^{-\zeta\omega_n t} \cos(\omega_d t + \phi) + \frac{F}{M + m_h} \frac{(\omega_n^2 - \omega_f^2) \cos \omega_f t + 2\zeta\omega_f \omega_n \sin \omega_f t}{(\omega_n^2 - \omega_f^2)^2 + (2\zeta\omega_f \omega_n)^2}. \quad (2-19)$$

After a certain time, the transient response (first term) damps out and there remains only the steady state response (second term).

For  $\alpha(t) \neq 0$ , the equation can hardly be solved analytically if at all; that is why we resort to numerical methods to achieve this purpose. A Runge-Kutta iteration method is used in the case of the digital computation (Chapters III and IV), whereas the equation is solved directly on the analog computer in the case of the analog computation (Chapter V). Various schemes are considered for generating both deterministic and random  $\alpha(t)$ , the main interest relating, of course, to the latter case. This random  $\alpha(t)$  should more properly be denoted as "pseudo-random" since in the digital simulation, the series of random variates are obtained by means of a Monte-Carlo random number generating technique, while in the analog simulation,  $\alpha(t)$  is produced by a noise generator incorporated to the frequency analyser available for the study. Having generated  $\alpha(t)$ , the response of the system is then investigated as will be described in detail in the chapters that follow.

CHAPTER III  
DIGITAL ANALYSIS OF THE FREE  
VIBRATIONS IN THE TIME DOMAIN

3.1 Method of Analysis

The first numerical analysis undertaken was performed in the time domain, since it was the easiest to implement. As a matter of fact, it simply consists in plotting the solution of equation (2-16), obtained by means of the Runge-Kutta scheme (presented in detail in Appendix C.1), versus time, which is one of the variables of the scheme, the variates of which are separated by a constant step-size  $h$ .

This digital analysis is conducted on the Amdahl V7 digital computer of McGill University. In the beginning of the study, the digital solution obtained is plotted directly by the printer at the same time as the numerical output is released. These plots are obtained by using a subroutine from the International Mathematical and Statistical Libraries\* (IMSL), namely the subroutine USPLTD. These printer plots are discrete, and the characters used for each data point are numerals, each specific to each function plotted (up to ten functions can thus be superimposed upon the same plot). For multiple plots, the character M is used in the event of coincidence by two or more functions. A typical plot is shown in Fig. 14. More complete information on the USPLTD and all other IMSL subroutines that will be used later on may be found in Ref. [62]. The use of IMSL subroutines allows the whole program to be written in Fortran WATFIV language, and moreover in double precision since all those subroutines at McGill University

---

\*An extensive collection of mathematical and statistical subroutines written in Fortran.

are available in that precision. Later in the study, the functions will be plotted in a smooth and nicer form by using a Calcomp 663 digital incremental plotter (for more information, see Ref. [63]). In this case, the program will undergo minor changes in order to be run in Fortran IV language (compiler H) and the points to be plotted will have to be given in single precision. The programs considered here could therefore also be run on the IBM 360/370 Series computers.

Nevertheless, the results discussed in this chapter are those obtained from the discrete USPLTD plots. Four different solutions are calculated and printed out. The numbers 1, 2, 3, 4 appearing on the plots (cf. Fig. 14) — to be referred to as Curves 1, 2, 3, 4 — are identified below.

Curve 1 is the control curve corresponding to the analytical solution of equation (2-16) with  $\alpha(t) = 0$  and without forcing function, i.e. this solution is simply given by equation (2-17) for free motions of a damped oscillator.

Curve 2 corresponds exactly to the same equation, but this time the numerical solution (obtained by the Runge-Kutta method) is considered.

Curve 3 denotes the numerical solution to equation (2-16) still without forcing function but with a deterministic  $\alpha(t) \neq 0$ ; this deterministic  $\alpha(t)$  is chosen to be equal to

$$\alpha(t) = \sum_{i=1}^5 a_i \sin(\omega_i t + \phi_i). \quad (3-1)$$

The values of the parameters  $a_i$ ,  $\omega_i$  and  $\phi_i$ , as well as these of  $\omega_n$  and  $\zeta$ , will be specified in the second part of this chapter, when the results are discussed. Let us just indicate here that in all cases we finally took

$$a_i = 0 \quad \text{for all } i,$$

and

$$a_1 = a_2 = a_3 = a_4 = a_5 = \frac{\alpha}{5}, \quad (3-2)$$

the parameter

$$\bar{\alpha} = \sum_{i=1}^5 a_i \quad (3-3)$$

being thus introduced.

Curve 4 represents the random case, i.e. a random  $\alpha(t)$  is used, and is the case of main interest here. The equation considered is the same as for Curve 3, except that  $\alpha(t)$  is now obtained by a Monte-Carlo pseudo-random algorithm, assuming a normal, i.e. Gaussian, probability density distribution. The method used to generate the random variates of  $\alpha(t)$  is explained in Appendix C.2. Moreover, the mean  $\mu$  and variance  $\sigma^2$  of the pseudo-random  $\alpha(t)$  are assumed to be the same as those of the deterministic  $\alpha(t)$  described by equation (3-1) [on this, see Appendix C.3]. To give an idea on the signal generated, Figs. 15(a),(b) and 16(a),(b) show respectively time records and histograms of the random perturbation  $\alpha(t)$  obtained.

Initial sets of results were obtained by using 300 calculation points per 3 cycles of oscillation, which corresponds to the time length chosen to be printed on one page of USPLTD plot. A study of convergence, which may be found in Appendix C.4, indicated that 500 points is more accurate and this value has thus been adopted for subsequent runs. This study of convergence is mainly based on analysing the discrepancies between the

two reference curves (i.e., those obtained for  $\alpha(t) = 0$ ), namely Curve 1 (analytical solution) and Curve 2 (numerical solution). Comparison between these two solutions gives a measure of the lack of precision originating from the use of the numerical integration scheme. One interesting item to note is that there seems to be a very slight systematic shift towards lower frequencies. By using 500 calculation points per 3 cycles, the frequency of Curve 1 was found to be exactly the value chosen, i.e.  $f_n = 15$  Hz, whereas the frequency of Curve 2 was 14.97 Hz\*. If the hypothesis is made that this systematic shift is nearly constant, then all the frequencies that will be obtained from the USPLTD plots should be all increased by 0.03 Hz.

Finally, a listing of the whole program may be found in Appendix C.5.

### 3.2 Results and Discussion

The ranges of the parameters of practical interest [cf. equations (2-16) and (3-1), (3-2), (3-3)] are taken to be as follows — as recommended by CRNL<sup>†</sup>, who sponsored part of this work:

- (i) natural frequency:  $f_n = 15$  to 60 Hz; (3-4,a)
- (ii) perturbation frequencies:  $f_i = \omega_i/2\pi = 5$  to 25 Hz; (3-4,b)
- (iii) damping factor:  $\zeta = 0.005$  to 0.1; (3-4,c)
- (iv) perturbation amplitudes:  $\pm 0.01 \leq \bar{\alpha} \leq 0.2$ . (3-4,d)

These conditions will henceforth, for convenience, be referred to as "realistic".

\* These two frequencies (of Curves 1 and 2) were found by three measurements, over 15, 30 and 45 cycles of oscillation, which gave the same results.

<sup>†</sup> Chalk River Nuclear Laboratories — more specifically by Messrs L.N. Carlucci and M.J. Pettigrew of CRNL.

In most cases, for convenience, the ratio of  $f_i$  and  $f_n$  was taken to be an integer. Also, in all cases, the initial conditions are taken to be

$$x(0) = 1, \quad \dot{x}(0) = 0. \quad (3-5)$$

However, as rather "uninteresting" results are obtained for parameters in the ranges as defined by (i) - (iv) above, other ranges are also investigated, which give more "interesting" results, albeit of possibly limited practical value. One of the main changes introduced is to look into higher values of  $\bar{\alpha}$ , up to  $\bar{\alpha} = 1$ , in order to allow clearer identification of the weak effect observed for a small  $\bar{\alpha}$ .

Eight series of calculations have been conducted, each consisting in three or four computer runs. To recognize them, they have been denoted by the letters A to H and are presented in Appendix C.6. In fact, two main categories are to be distinguished.

- The first one (Series A, B and C) considers the ranges of parameters described in (i) - (iv) above (except for higher  $\bar{\alpha}$  in some cases) and is discussed in Section 3.2.3 below.
- The second one (Series D to H) considers also the ranges of parameters (i), (iii) and (iv) above (also higher  $\bar{\alpha}$  in some cases), but replaces the perturbation frequencies range (ii) mostly by:

$$(ii)': f_i = \omega_i/2\pi = 30, 150, 240, 300, 450 \text{ Hz.} \quad (3-6)$$

This case is more concerned with the occurrence of a parametric resonance; and it is discussed in Section 3.2.4 below.

But first is discussed, in Section 3.2.1, the numerical importance of the two effects observed by Carlucci. Then are given, in Section 3.2.2, the results concerning Curve 4, since they are of main interest. As a matter of fact, Curve 4 does not differ between the two categories distinguished above (and discussed in Sections 3.2.3 and 3.2.4). This is so because, due to the method adopted to generate the random variates (given in Appendix C.2), Curve 4 does not depend on the perturbation frequencies  $f_i$ , but only on the value of the mean  $\mu$  and the variance  $\sigma^2$  of the distribution considered. It is shown in Appendix C.3 that

$$\mu = 0, \quad (3-7,a)$$

$$\sigma = \frac{\bar{\alpha}}{\sqrt{10}}; \quad (3-7,b)$$

hence Curve 4 depends on  $\bar{\alpha}$  only.

The results discussed below are obtained from the series which have been run with 500 points of calculation per 3 cycles and with  $\zeta = 0.005$  (Series B, C, G) or  $\zeta = 0$  (Series H). These series are also those which have been run over the largest number of cycles.

### 3.2.1 Numerical Importance of the Hydrodynamic Mass and Damping Effects Observed by Carlucci

Before giving our own results, it is of interest to indicate the order of magnitude of the two effects shown by Carlucci's experiments, and which it is intended to verify on the one-degree-of-freedom model.

Let us first show how a frequency increase can be interpreted in terms of a hydrodynamic mass decrease. For this, the system is considered to stay at a given void fraction of  $v$  percent, for which the mean value of the added mass is denoted by  $\bar{m}_{h,v}$ . It is about this mean value that the fluctuations  $\mu(t)$  are considered, according to equation (2-15). The circular natural frequency  $\omega_{\text{hom},v}$ , for the homogeneous model (with the hydrodynamic mass proportional to the mixture density), is obtained from equation (2-16',a) as

$$\omega_{\text{hom},v} = \sqrt{\frac{K}{M + \bar{m}_{h,v}}} \quad (3-8,a)$$

In case the added mass perturbations are included, we obtain a new circular natural frequency  $\omega_{\text{resp},v}$  given by

$$\omega_{\text{resp},v} = \sqrt{\frac{K}{M + \bar{m}_{h,v} + \delta \mu_{\text{rms}}}} \quad (3-8,b)$$

in which  $\delta = +1$  or  $-1$ , according to whether a hydrodynamic mass increase or decrease is considered.

If we observe a frequency increase, i.e.,

$$\omega_{\text{resp},v} > \omega_{\text{hom},v}$$

this implies that

$$\frac{\omega_{\text{resp},v}^s}{\omega_{\text{hom},v}^s} = \sqrt{\frac{M + \overline{m}_{h,v}}{M + \overline{m}_{h,v} + \delta\mu_{\text{rms}}}} > 1$$

hence

$$M + \overline{m}_{h,v} > M + \overline{m}_{h,v} + \delta\mu_{\text{rms}}$$

from which we finally get

$$\delta\mu_{\text{rms}} < 0$$

$\mu_{\text{rms}}$  being always a positive quantity, this implies that  $\delta = -1$  has to be taken.

We effectively see that, according to the one-degree-of-freedom model, a frequency increase is equivalent to a hydrodynamic mass decrease, if all other parameters are kept constant.

Let us now quantify the clear hydrodynamic mass decrease appearing on Fig. 11, with the aim in mind to express it in terms of a frequency increase. As already stressed, the hydrodynamic mass decreases with increasing void fraction; but at a higher rate than that of the mixture density. The hydrodynamic mass line proportional to the mixture density appears on Fig. 11 in form of a straight line (rather a dashed line) extending from  $\overline{m}_{h,0}/\overline{m}_{h,0} = 1$  for a zero void fraction to  $\overline{m}_{h,100}/\overline{m}_{h,0} = 0$  for a void fraction of 100%. The experimental values of the added mass lie below this line, and an experimental straight line can also be drawn according to these points (it is not shown on Fig. 11). The experimental values (divided by  $\overline{m}_{h,0}$ ) thus decrease from 1 for a zero void fraction and approach a value of zero at a void fraction of about 66 to 70%. We intend to place ourselves at a given void

fraction that we assume to remain constant. Since the interesting void fraction range extends between 30 and 60%, we adopt the value of 50%. At this void fraction are obtained the values  $\bar{m}_{h,50}/\bar{m}_{h,0} = 0.50$  (from the dashed line proportional to the mixture density) and  $(\bar{m}_{h,50} + \mu)/\bar{m}_{h,0} \approx 0.28$  (from the experimental line).

It is now necessary to translate this hydrodynamic mass decrease in terms of a frequency increase. Let us first start from Fig. 8. At a zero void fraction,  $f_{\text{hom},0}$  is equal to 32 Hz\*, whereas for a void fraction of 100%, we read  $f_{\text{hom},100} = 40$  Hz\*. From this, using also equation (3-8,a), we obtain the following relations:

$$f_{\text{hom},0} = \frac{1}{2\pi} \sqrt{\frac{K}{M + \bar{m}_{h,0}}} = 32 \quad (3-9,a)$$

$$f_{\text{hom},100} = \frac{1}{2\pi} \sqrt{\frac{K}{M + \bar{m}_{h,100}}} = 40. \quad (3-9,b)$$

We also know (from considerations above on Fig. 11) that  $\bar{m}_{h,100} \approx 0$ , hence

$$40/32 = \sqrt{\frac{M + \bar{m}_{h,0}}{M}}$$

Squaring this equation, we obtain

$$(5/4)^2 = \frac{M + \bar{m}_{h,0}}{M},$$

from which we finally get

$$\bar{m}_{h,0} = [(5/4)^2 - 1]M = 0.5625 M.$$

\*These experimental values of the oscillation frequency are between twice and thrice the numerical values used in the following sections and chapters.

Coming back to our point at 50% void fraction, we have  $\bar{m}_{h,50}/\bar{m}_{h,0} = 0.50$ .  
From this, we easily obtain [using equation (3-8,a)]

$$\begin{aligned} f_{\text{hom},50} &= \frac{1}{2\pi} \sqrt{\frac{K}{M + \bar{m}_{h,50}}} \\ &= \frac{1}{2\pi} \sqrt{\frac{K}{M \times 0.5 \times 0.5625M}} \end{aligned}$$

From (3-9,b), using  $\bar{m}_{h,100} = 0$ , we get

$$\sqrt{\frac{K}{M}} = 80\pi$$

hence

$$\sqrt{K} = 80\pi\sqrt{M}$$

From this,

$$\begin{aligned} f_{\text{hom},50} &= \frac{80\pi}{2\pi} \sqrt{\frac{M}{M(1 + 0.5 \times 0.5625)}} \\ &= 40 \sqrt{\frac{1}{1 + 0.5 \times 0.5625}} \end{aligned}$$

We finally obtain

$$f_{\text{hom},50} = 35.3 \text{ Hz.} \quad (3-10,a)$$

This is the value calculated for the homogeneous mixture. For the actual two-phase flow, we can extrapolate the two compliance curve plots of Fig. 8 closest to the void fraction of 50% (those for void fractions of 40 and 54%), and thus we approximate the value of  $f_{\text{resp},50}$  to 37.4 Hz.

We could equally use the result obtained from Fig. 11, namely

$$\overline{m}_{h,50} + \mu = 0.28 \overline{m}_{h,0},$$

and plug it into equation (3-8,b), which gives us

$$\begin{aligned} f_{\text{resp},50} &= \frac{1}{2\pi} \sqrt{\frac{K}{M + \overline{m}_{h,50} + \mu}} \\ &= 40 \sqrt{\frac{1}{1 + 0.28 \times 0.5625}} \\ &= 37.2 \text{ Hz.} \end{aligned}$$

We thus have the following estimation:

$$f_{\text{resp},50} = 37.3 \text{ Hz.} \quad (3-10,b)$$

From (3-10,a) and (3-10,b), we obtain the relative amplitude of the hydrodynamic mass decrease effect, at a 50% void fraction, expressed in terms of a frequency increase. It is

$$\frac{f_{\text{resp},50} - f_{\text{hom},50}}{f_{\text{hom},50}} = \frac{37.3 - 35.3}{35.3} = 5.7\%.$$

Thus the frequency increase effect we wish to observe should be of the order of about 6%.

As far as the second effect found by Carlucci is concerned, namely the important increase in damping, an examination of Figs. 8 and 9 shows us that, at a void fraction of 50%, damping is at least 100% higher than its value at a zero void fraction.

It is these two effects that we now wish to verify on our one-degree-of-freedom system.

### 3.2.2. Response of the System to Pseudo-Random Added Mass Perturbations

This response is obtained for four different values of  $\bar{\alpha}$ , namely: 0.25, 0.50, 0.75 and 1. Curve 4 is best examined

- on run G1\* for  $\bar{\alpha} = 0.25$ , and this over 60 cycles of oscillation;
- on runs C2\* and C3\*, respectively for  $\bar{\alpha} = 0.50$  and  $\bar{\alpha} = 0.75$ , over 30 cycles only (as a matter of fact Curve 4 cannot be observed with accuracy over more than 30 cycles on runs G2 and G3, because of the parametric

---

\* See Appendix C.6.

resonance affecting Curve 3, which renders Curve 4 indistinguishable on the USPLTD plots used<sup>†</sup>);

- on run G4 for  $\bar{\alpha} = 1$ , again over 60 cycles of oscillation (in G4, Curve 4 exhibits higher values than Curve 3, hence this plot can be used here).

As far as the general behaviour of Curve 4 is concerned, Curve 4 behaves almost like the "control" Curve 1 for the three first values  $\bar{\alpha} = 0.25$ , 0.50 and 0.75, that is to say it shows vibration with about the same, if not slightly higher amplitude, as may be seen on the  $x_{rms}$  values below (see also Figs. 17, 18 and 19). It nevertheless exhibits a certain shift towards higher frequencies. However, when  $\bar{\alpha} = 1$ , the behaviour of Curve 4 deviates from the typical oscillation of a sinusoid, i.e. it begins to display some random excursions starting from the 20<sup>th</sup> cycle, and finally becomes unbounded (unstable), reaching a value of about 11 after 60 cycles (see Figs. 20 or 21); it is recalled here that the initial conditions are given by equation (3-5).

To illustrate more completely what has just been said above, we shall give the values of both  $x_{rms}$  and the effective frequency of oscillation. Actually, two sets of  $x_{rms}$  values are given:  $x_{rms}(1)$  has been calculated over 30 cycles of oscillation with  $\zeta = 0$  (Series H) and should be

---

<sup>†</sup>This is due to a property of the USPLTD plots which has not yet been mentioned here. The range of the y-axis is indeed constant on the output page (51 print positions) and adjusts automatically in order to extend fully from the minimum value  $y_{min}$  to the maximum value  $y_{max}$  of the function  $y$  to be plotted. In our program, we have specified (on the "control" Curve 1) a maximum of +1 and a minimum of -1, so that the plots of the decaying cases have all their y-axis of the same scale. However, when Curves 3 or 4 become unbounded, the range of the y-axis is determined by the extremum value(s)  $y_{extr}$  such as  $|y_{extr}| > 1$ .

compared to  $x_{\text{rms}}$  (Curve 1) = 0.707 obtained with exactly the same condition, whereas  $x_{\text{rms}}$  (2) has been calculated over 60 cycles with  $\zeta = 0.005$  (Series G) and should be compared with  $x_{\text{rms}}$  (Curve 1) = 0.360. As far as the effective frequency of Curve 4 is concerned, the number of cycles chosen for the measurement is divided by the corresponding total time of oscillation. A mean value of the frequency is thus obtained, and it can be added that, qualitatively, this frequency seems to be constant; hence, it is believed that the mean values below are given to a good approximation. For  $\bar{\alpha} = 0.25$ , the number of cycles considered is 60 (run G1), for  $\bar{\alpha} = 0.50$  and 0.75, it is 30 (runs C2 and C3), whereas for  $\bar{\alpha} = 1$  it is only 20 (runs C4 or G4) since, as already mentioned, the sinusoidal behaviour is disturbed just after that, hence a measurement over more cycles would be meaningless.

The results obtained are given in the table below.

$\bar{\alpha}$	$\sigma$	$x_{\text{rms}}(1)^{\S}$	$x_{\text{rms}}(2)^{\S}$	$f_{\text{eff}}(\text{Hz})$
0.25	0.079	0.715	0.364	15.02*
0.50	0.158	0.752	0.377	15.18*
0.75	0.237	0.743	0.362	15.47*
1.00	0.316	0.980 <sup>†</sup>	2.22	16.16*

<sup>§</sup> It is recalled that the  $x_{\text{rms}}(1)$  values are obtained over 30 cycles with  $\zeta = 0$  (compare to  $x_{\text{rms}}$  (Curve 1) = 0.707), whereas the  $x_{\text{rms}}(2)$  values are calculated over 60 cycles with  $\zeta = 0.005$  (compare to  $x_{\text{rms}}$  (Curve 1) = 0.360).

<sup>†</sup> This will become much larger if  $x_{\text{rms}}$  were taken over more than 30 cycles (see for instance  $x_{\text{rms}}(2)$ ).

\* If the hypothesis is made that the very slight shift to lower frequencies due to the use of the Runge-Kutta scheme (cf. the remarks on the study of convergence, made at the end of Section 3.1 or in Appendix C.4), is constant, then all the frequencies obtained should be increased by 0.03 Hz and the actual frequencies would respectively read: 15.05, 15.21, 15.50 and 16.19 Hz.

The results of  $x_{rms}(1)$  indicate that, unless  $\bar{\alpha}$  is large (1.00), the  $x_{rms}$  lie in the vicinity of  $\sqrt{2}/2$  which is the classical value for a sinusoid, as obtained by Curve 1. The results of  $x_{rms}(2)$  show more significantly the fact that Curve 4 becomes essentially unbounded for  $\bar{\alpha}=1$ . From all considerations on amplitude and  $x_{rms}$  values of the response, it is deduced that a critical standard deviation  $\sigma_{crit}$  exists for instability and lies somewhere between  $0.237 < \sigma_{crit} < 0.316$ .

But the most interesting item to be discussed here is the effective (or average) frequency, in view of its importance vis-à-vis the observed added mass coefficients in two-phase flow; these were found to be lower than those calculated on the basis of homogeneous models of the two-phase medium. We observe indeed a clear shift to higher effective frequencies as the amplitude of perturbations increases. This translates, of course, to lower added mass coefficients (as compared to homogeneous model, where effectively  $m_h(t) = \bar{m}_h$  is taken, i.e.  $\alpha(t)=0$ ); this agrees qualitatively with the observations made by Carlucci (see Section 2.1.2). However by examining our values<sup>5</sup> given in the table above, we obtain a frequency shift of  $(15.05 - 15)/15 \approx 0.3\%$  for the upper suggested "realistic" value of  $\bar{\alpha}$  (i.e.,  $\bar{\alpha}=0.25$ ). This is undoubtedly a very weak effect, when compared to the experimentally observed 6% frequency shift (see previous Section 3.2.1). For the higher "unrealistic" values, we obtain of course a more significant frequency shift, albeit of only 1.4% for  $\bar{\alpha}=0.50$  and 3.3% for  $\bar{\alpha}=0.75$ . It is only for the highly unrealistic value of

---

<sup>5</sup>We use the corrected values, obtained by addition of 0.03 Hz — see last footnote on p.37.

$\bar{\alpha} = 1$  that we obtain a shift of 7.9%.

As far as damping is concerned, unfortunately no important damping effect could be found in this attempt.

### 3.2.3 Response of the System to Deterministic Added Mass Perturbations

In this section, Curve 3 is examined as the response of the system to a deterministic perturbation  $\alpha(t)$  defined by equation (3-1) and characterized by the "realistic" range of perturbation frequencies

$$f_i = 5, 10, 15, 20, 25 \text{ Hz.} \quad (3-11)$$

This means that the computer runs to be investigated here belong to Series A, B, C (see Appendix C.6).

For a small  $\bar{\alpha}$  ( $\bar{\alpha} = 0.25$ ), it is seen in Fig. 17 that for  $f_n$  ( $f_n = 15 \text{ Hz}$ ) lying within the range of the  $f_i$  (run B1 or C1), Curve 3 is essentially coincident with Curve 1; i.e. the deterministic case for "small" perturbation amplitudes is little different from the deterministic case with zero mass perturbation. Moreover,  $x_{\text{rms}}$  for Curve 3 is very little different than that of Curve 1 (it is smaller by 2%).

In Fig. 22 is shown a case with the same  $\bar{\alpha}$  ( $\bar{\alpha} = 0.25$ ) but with  $f_n$  ( $f_n = 60 \text{ Hz}$ ) higher than any of the  $f_i$  (run B3). The results of Curve 3 are somewhat different from those obtained above. Even if the amplitude is about the same, with a  $x_{\text{rms}}$  of Curve 3 also little different than that of Curve 1 (larger by 1%), on the contrary, for the first few cycles of oscillation, the effective frequency diminishes to about 58 Hz, rather than remaining at 60 Hz, but later this effect appears to diminish, even though the fre-

quency continues to fluctuate slightly about 60 Hz. When  $f_n = 30$  Hz (run B2), this effect (lower frequency) is not yet noticeable and the response is similar to that obtained for  $f_n = 15$  Hz. It could be mentioned here that, as far as Curve 4 is concerned in the three runs of Series B, its behaviour is not affected<sup>†</sup> by the relative position of  $f_n$  compared to the  $f_i$ , and that is why this question was not examined in Section 3.2.2. The reason for this lies naturally in the method (presented in Appendix C.2) used for generating the pseudo-random variates of  $\alpha(t)$ , which does not take the perturbation frequencies  $f_i$  into account. Since the same number of discretization points is used per 3 cycles (500), exactly the same random variates are used at the respective stages of integration; this accounts for the identical results.

Let us now come back to the other cases (Series C) computed for  $f_n = 15$  Hz, and stick to this value for the rest of this chapter. The cases with added mass perturbations of larger amplitudes are considered, namely  $\bar{\alpha} = 0.50, 0.75$  and  $1$  (respectively runs C2, C3 and C4). Figs. 19 and 20 show the response for  $\bar{\alpha} = 0.75$  and  $\bar{\alpha} = 1$ , respectively. Curve 3 displays an unusual beating phenomenon (especially in Fig. 20), its amplitude being sometimes higher and sometimes lower than that of "control" Curve 1. Curve 3 also displays an increased frequency of oscillation, which nevertheless remains smaller than the frequency shift observed for Curve 4 (see Section 3.2.2).

To conclude this section, let us give the  $x_{rms}$  values of Curve 3 (which should be compared with  $x_{rms}$  (Curve 1) = 0.474) and its effective frequency, both calculated over 30 cycles of oscillation, with  $\zeta = 0.005$ .

---

<sup>†</sup>Except that its frequency will be 15, 30 or 60 Hz according to  $f_n$ .

$\bar{\alpha}$	$x_{rms}$	$f_{eff}(Hz)^{\dagger}$
0.25	0.465	15.01
0.50	0.502	15.08
0.75	0.541	15.23
1.00	0.494	$\approx 15.60$

We can see very clearly that, as far as the effective frequency is concerned, the deterministic effect is in the same direction as the random effect (it indicates a decrease of the added mass), but its magnitude is smaller.

#### 3.2.4 Response of the System to Deterministic Added Mass Perturbations; Parametric Resonances

The perturbation frequencies mostly considered in this last section of Chapter III are given by equation (3-6),

$$f_i = 30, 150, 240, 300, 450 \text{ Hz.}$$

They are beyond the recommended "realistic" range for two-phase flow as measured by Carlucci, et al. and given by equation (3-4,b). Nevertheless, we shall examine this case for it gives rise to the fundamentally interesting phenomenon of parametric resonance. Series D to H are considered for that purpose (see Appendix C.6).

Whenever harmonic perturbations are present in the axial flow about cylindrical structures, there exists the distinct possibility that they may cause parametric resonances, otherwise known as parametric insta-

---

<sup>†</sup>The same remark given in footnote \* concerning the frequencies of the previous table (in Section 3.2.2) also applies to the frequencies given in this table.

bilities [64]. It has been shown that such resonances may occur if the circular frequency of the periodic flow component,  $\omega_p$ , lies in the vicinity of a fractional multiple of one of the natural frequencies of the cylinder,  $\omega_n^i$ , i.e. if  $\omega_p \approx 2\omega_n^i / K$ , where  $K=1,2,3,\dots$ . The most important of these resonances, the so-called principal primary parametric resonance, occurs when  $K=1$ , so that  $\omega_p \approx 2\omega_n^i$  - a well-established result from the analogous problem of a column subjected to a harmonically perturbed axial load [65].

In cases where  $f_1 = 2f_n$ , irrespective to the other frequencies  $f_i$ , parametric resonance oscillations were observed (Curve 3) for all  $\bar{\alpha}$  tested, however with an unusual behaviour occurring for  $\bar{\alpha}=1$ . A typical case is shown in Fig. 18, for  $\bar{\alpha}=0.50$  (run G2). It is interesting to note that Curve 3, in the first few cycles, is diminished in amplitude vis-à-vis Curve 1 and then, after  $N_{\min}$  cycles, reaches a minimum characterized by the ratio  $R_{\min} = [\text{amplitude Curve 3}] / [\text{amplitude Curve 1}]$ . Then Curve 3 increases again, equals Curve 1 in amplitude after  $N_1$  cycles, and finally continues to increase steadily (the system is highly unstable, in the sense that it displays amplified oscillations). The values of  $N_{\min}$ ,  $R_{\min}$  and  $N_1$  are given in the table in the next page.

It is also noted that the frequency  $f_{\text{initial}}$  in the first few cycles becomes larger, but later this effect evaporates after a sufficient number of cycles (after the amplitude has "taken off"). The values of  $f_{\text{initial}}$  are calculated over  $N_{\min}$  cycles of oscillation and are also given in the next page.

It is most interesting to notice that if  $\bar{\alpha}=1$  (run G4), i.e. the higher parametric amplitude envisaged here, Curve 3 is no longer unbounded! Instead, it displays some kind of amplitude and frequency quasi-periodic

variations, similar to beating (see Fig. 21). This does not follow the conventional pattern for parametric resonance oscillations.

The table giving the parameters described above is now presented, with an addition of two sets of  $x_{rms}$  values, exactly the same as for Curve 4 in Section 3.2.2.  $x_{rms}(1)$  has been calculated over 30 cycles of oscillation with  $\zeta = 0$  (Series H) and should be compared to  $x_{rms}$  (Curve 1) = 0.707, whereas  $x_{rms}(2)$  has been calculated over 60 cycles with  $\zeta = 0.005$  (Series G) and should be compared with  $x_{rms}$  (Curve 1) = 0.360.

$\bar{\alpha}$	$N_{min}$	$R_{min}$	$N_1$	$x_{rms}(1)$	$x_{rms}(2)$	$f_{initial}$ (Hz)
0.25	27	0.29	45	0.336	0.244	15.09
0.50	6	0.48	12	3.93	39.79	15.32
0.75	3	0.55	6	22.2	516.6	15.66
1.00	1½	0.58	3½	1.52	0.679	16.25

The frequency shift observed is higher than any other observed before, i.e. of Curve 3 (in Section 3.2.3) and even of Curve 4 (in Section 3.2.2). But it should not be forgotten that this is only an initial frequency measured over a small number of cycles ( $N_{min}$ ) and that after, let us say,  $N_1$  cycles, the frequency remains sensibly constant at about 15 Hz.

The results for the sets of  $x_{rms}$  values are indicative of the peculiar behaviour relating to parametric resonance instabilities described earlier in this section. Thus, for  $\bar{\alpha} = 0.25$ , one obtains  $x_{rms}(1) < \sqrt{2}/2$ , which is the classical value for a sinusoid as obtained by Curve 1; this displays the initial reduction in amplitude referred to earlier; if more cycles had been taken, then  $x_{rms}(1) > \sqrt{2}/2$  would have been obtained. For  $\bar{\alpha} = 0.50$  and 0.75, we note that  $x_{rms}(1)$  is very large, reflecting parametric

resonances, but for  $\bar{\alpha} = 1$ , a much smaller  $x_{rms}(1)$  is obtained, reflecting the beating phenomenon described earlier, rather than a monotonic increase of amplitude (after an initial decrease) characteristic of  $\bar{\alpha} = 0.50$  and  $0.75$  (and also of  $\bar{\alpha} = 0.25$  if a large enough number of cycles were investigated).

The cases tested in Series F, where  $f_n = f_1$ , at least for the  $\zeta$  and  $\bar{\alpha}$  involved, displayed no parametric resonance. Hence, within the ranges tested, it is obvious that principal primary resonant oscillations do occur, but secondary resonances do not (see Refs. [64] and [65]).

CHAPTER IV  
DIGITAL ANALYSIS OF THE FREE  
VIBRATIONS IN THE FREQUENCY DOMAIN

4.1 Introduction

The results obtained in Chapter III (for Curve 4) agree qualitatively with Carlucci's observations, at least as far as the shift towards higher frequencies is concerned. This shift means indeed that the observed added mass is lower than that calculated on the basis of the homogeneous model of two-phase flow, for which  $m_h(t) = \bar{m}_h$  is taken. However, quantitatively speaking, the effect that we observed remains weak, compared to what Carlucci reported. On the other hand, damping has not been found to be higher, and on the contrary it even seemed to be a little lower, as the  $x_{rms}$  values given in Section 3.2.2 indicate it (for  $\bar{\alpha} = 0.25$ , these values are higher by 1% than those found for  $\bar{\alpha} = 0$ ). This obviously does not accord with the observation of a significantly higher damping reported by Carlucci. Thus, the study in the time domain conducted in Chapter III has proven not to be quite conclusive.

One reason for this relative failure is thought to lie in the way the pseudo-random added mass perturbations, i.e.  $\alpha(t)$ , are generated (cf. Appendix C.2). As a matter of fact, no restriction on frequency content was included in the Monte-Carlo method used to generate the random variates of  $\alpha(t)$ , as has already been mentioned in Section 3.2.3 when Series B were examined. In Fig. 23, the power spectrum of this pseudo-random  $\alpha(t)$  is shown, and it may be seen that it effectively contains all frequencies and could be considered as an approximate white noise. This is by far not the

case of the deterministic  $\alpha(t)$ , used for Curve 3 of Chapter III, which includes specifically five frequencies  $f_i$ , thus favouring certain predominant frequencies to perturb the added mass. Studies being conducted by AECL\*, subsequent to Carlucci's work, suggest that the random perturbations  $\alpha(t)$  should actually be of narrow frequency band. Hence two new aspects must be added to the present analysis. On the one hand, new schemes for generating random perturbations of the hydrodynamic mass have to be developed, capable of producing a narrow-banded  $\alpha(t)$ , or rather  $\alpha(f)$  where  $f$  stands for the frequency. On the other hand, to enable such a study in the frequency domain, the frequencies themselves must appear explicitly in the analysis. The whole study must therefore be transferred from the time domain into the frequency domain. Since we have already implemented the Monte-Carlo method (for generating the random perturbations) and the Runge-Kutta scheme (for solving the differential equation), it was decided to undertake this frequency analysis on the same digital computer used before (Amdahl V7 of McGill University).

To carry out the study in the frequency domain, we want to calculate the power spectra of both the added mass perturbations  $\alpha(t)$  and the system response  $x(t)$ . This leads us to introduce the Fourier transform, since the power spectrum  $G_{xx}(f)$  of a time function  $x(t)$  is defined as the Fourier transform of its autocorrelation  $R_{xx}(\tau)$ , i.e.

$$G_{xx}(f) = \int_{-\infty}^{\infty} e^{-i2\pi f \tau} R_{xx}(\tau) d\tau. \quad (4-1)$$

The autocorrelation function itself is a time average (for an ergodic process) defined by

---

\* Atomic Energy of Canada Limited.

$$R_{XX}(\tau) = \lim_{T \rightarrow \infty} \frac{1}{2T} \int_{-T}^T x(t) x(t+\tau) dt. \quad (4-2)$$

Much has been written on the Fourier transform, but we shall only quote the book by Bracewell [66]. However, calculating numerically a Fourier transform, as the one given by equation(4-1) for instance, is not an easy task, and, anyway, the Fourier transform cannot be integrated in its continuous form, but has to be discretized and truncated. Fortunately, a very efficient algorithm for calculating this discrete Fourier transform (DFT) was "rediscovered" in 1965 by Cooley and Tukey [67], after the results of the mathematicians C.C. Danielson and Cornelius Lanczos which were "lost" in 1942. This powerful algorithm is called fast Fourier transform (FFT) and reduces significantly computing time and cost, making thus possible rapid transformations between time and frequency domains. Calculations that once took minutes and cost dollars can now be done in seconds for a few cents. The Cooley-Tukey algorithm takes advantage of the redundancy in the nested multiplications to reduce the number of transform operations to  $N_{DFT} \log_2(N_{DFT})$  rather than the traditional  $N_{DFT}^2$  operations of the discrete Fourier transform in order to realize this speed-up;  $N_{DFT}$  denotes the number of samples of the time function used for the DFT. More information may be found in Brigham [68], in Bergland [69] and also in Appendix D.1, on the DFT and on the FFT algorithm, as well as on three problems or "pitfalls" encountered in using them, namely aliasing, leakage and the picket-fence effect. A program for computing the FFT algorithm is given on page 164 of Ref. [68] and another one on page 184 of Ref. [70], but in this study we shall use a subroutine taken from the IMSL Library [62]. This subprogram computes directly the power spectrum and is therefore called FTGPS (Fast

Fourier transform estimates of power spectra and cross spectra of time series). During its run, the FTFPS subroutine calls the FFTRC subroutine (also taken from the IMSL Library) which computes the fast Fourier transform of a real valued sequence. But before calling FFTRC, the FTFPS routine uses a symmetric data window which is approximately the Parzen spectral window. Let  $N_t$  be the number of input samples of the time domain (i.e. the number of data to be transformed). We also introduce  $L$ , which is an input parameter used to segment the time series.  $L$  must be a power of two, and  $N_t$  must be evenly divisible by  $L$ . The number  $N_{ps}$  of sampled frequencies obtained by calling FTFPS is equal to  $N_{ps} = (L/2) + 1$ . Those spectral estimates are taken at frequencies

$$f_i^{PS} = \frac{i-1}{L\Delta t}, \quad (4-3)$$

where  $i=1,2,\dots,(L/2)+1$  and  $\Delta t$  is the period of sampling of the time series. As a final remark on the FTFPS sub-program, let us mention that the output (power spectrum) is returned into units which are the square of the input data.

To come back to the random perturbations of the added mass, two main ranges of FTFPS parameters have been chosen, and they help to distinguish the two following sections. In Section 4.2, the frequency range (0-160 Hz)\* with  $N_{ps} = 1025$  (i.e.  $L = 2048$ ) and  $\zeta = 0.005$  is mainly considered, whereas in Section 4.3 this range is reduced to (0-40 Hz) with  $N_{ps} = 513$  (i.e.  $L = 1024$ ) and  $\zeta = 0.02$ . As for the various schemes of  $\alpha(t)$  generated in this chapter, they are classified in Appendix D.2. For the sake of

---

\* It might be wondered why such a large range is adopted for studying a much smaller range: (5-25 Hz). This is merely to make sure that we will not miss any effect below 160 Hz.

completeness, the cases studied in Chapter III are also mentioned, and on the whole eleven schemes are distinguished. Each particular scheme has been denoted by a small letter from a to k given in brackets (e.g. [a], [b],...). To indicate whether the scheme is considered in Section 4.2 or 4.3, this small letter within brackets is preceded respectively by the capital letter A or B (e.g. A[a] stands for scheme [a] considered in Section 4.2, and B[i] denotes scheme [i] of Section 4.3).

In the previous chapter, the deterministic  $\alpha(t)$  (scheme [b] leading to former Curve 3) was taken as a sum of five sine functions. In this chapter, it will be a function of N sine functions, with nevertheless mostly N=5 in Section 4.2, but with mostly N=33 in Section 4.3. Hence  $\bar{\alpha}$  is defined more generally than in equation (3-3) by

$$\bar{\alpha} = \sum_{j=1}^N a_j = N a_j. \quad (4-4)$$

The results are both printed on the computer output and plotted by means of the Calcomp 663 digital incremental plotter. On the legend of these plots may be read the parameters ALPHA and SIGMA which stand respectively for  $\bar{\alpha}$  and  $\sigma$ . Finally, a typical listing of the program used may be found in Appendix D.3.

#### 4.2 Results Obtained in the Frequency Range (0 - 160 Hz)

Most of the results given here are indeed obtained, unless otherwise specified, in the frequency range (0 - 160 Hz) with the number of power spectral estimates  $N_{ps}$  equal to 1025. Using these values means that 6.4 spectral samples are obtained per Hertz or, said in an equivalent way, that

the resolution obtained is  $\Delta f = 0.156$  Hz (frequency interval between two consecutive spectral estimates).

In this section, damping is generally taken as  $\zeta = 0.005$ , as it was suggested and chosen in Chapter III. The natural frequency of the system is typically taken as 12, 13, 14 or 15 Hz. Moreover, the number  $N_t$  of samples of the time function is chosen to be 4096 (at least when the frequency range and  $N_{ps}$  are those indicated above).  $N_t$  is thus effectively evenly divisible by  $L$  as it should, since  $L = 2048$  (see at the end of the previous section). On the other hand, the step-size  $h = \Delta t$ , which is the period of sampling of the time function, is determined by using equation (4-3).

We have

$$f_1^{ps} = 0$$

$$f_{N_{ps}}^{ps} = \frac{N_{ps} - 1}{L\Delta t}$$

and also

$$f_{N_{ps}}^{ps} - f_1^{ps} = FR,$$

where FR stands for the frequency range. Hence

$$\frac{N_{ps} - 1}{L\Delta t} = FR,$$

from which we get

$$h = \Delta t = \frac{N_{ps} - 1}{L \cdot FR} \quad (4-5)$$

Numerically speaking, we obtain

$$\Delta t = \frac{1024}{2048 \times 160} = \frac{1}{320} = 3.125 \text{ ms.} \quad (4-6)$$

The total sampling time  $T_t$  is then

$$T_t = N_t \cdot \Delta t = 4096/320 = 12.8 \text{ s.}$$

Hence the total number of cycles  $N_c(f)$  investigated for a signal of frequency  $f$  is

$$N_c(f) = \frac{T_t}{T} = T_t \cdot f, \quad (4-7)$$

where  $T = 1/f$ .

We thus notice, since the natural frequency  $f_n$  lies between 12 and 15 Hz, that the time signal will be analysed over approximately its 170 first cycles<sup>†</sup>. This is about two and half times the highest number of cycles considered in the time domain study conducted in Chapter III.

This also means that a signal of frequency 5 Hz will be considered over 64 cycles, whereas over 320 cycles for a frequency of 25 Hz. Hence we obtain 64 time samples over one period of a signal of frequency 5 Hz, about 24 samples for a signal of frequency  $f_n$ , and 12.8 samples when the frequency is 25 Hz (5 and 25 Hz are respectively the lower and upper limits of the frequency band desired for the pseudo-random  $\alpha(t)$ ).

We will now discuss the results obtained, first for the deterministic perturbations  $\alpha(t)$  (Schemes [b] and [a]) in Section 4.2.1, and then for the pseudo-random  $\alpha(t)$  (Schemes [c], [d], [e] and [f]) in Section 4.2.2.

---

<sup>†</sup>Over 150 cycles if  $f_n = 12$  Hz, and 190 cycles if  $f_n = 15$  Hz.

#### 4.2.1 Response of the System to Deterministic Added Mass Perturbations; Parametric Resonance

Only considered with  $N=5$ , Case A[b]\* has been run for two values of  $\bar{\alpha}$ :  $\bar{\alpha}=0.25$  and  $\bar{\alpha}=0.75$ . For  $\bar{\alpha}=0.25$ , the natural frequencies  $f_n=12$  Hz and  $f_n=15$  Hz were considered (in Chapter III, only  $f_n=15$  Hz was envisaged). For  $\bar{\alpha}=0.75$ , the study was extended to five values of  $f_n$ : 11, 12, 13, 14 and 15 Hz. Let us now give the numerical results of the runs in which  $f_n=12$  Hz and  $f_n=15$  Hz.

Scheme of $\alpha(t)$	Input			Results			
	$\bar{\alpha}$	$\sigma$	$f_n$ (Hz)	$[\alpha(\omega)]_{\max}$	$f_{\text{resp}}$	$\Delta f_{\frac{1}{2}\text{pp}}$	$A_{\text{resp}}$
[a]	0	-	12	0	12.03	0.125	20.69
[b]	0.25	-	12	0.96	12.03	0.12	24.19
[b]	0.75	-	12	8.65	12.5	0.254	$7.9 \times 10^{19}$
[a]	0	-	15	0	15.0	0.12	13.63
[b]	0.25	-	15	0.96	15.0	0.125	14.41
[b]	0.75	-	15	8.65	15.31	0.12	13.7

=Main table=

In this table as well as in the next ones,  $[\alpha(\omega)]_{\max}$  is the amplitude of the highest peak in the power spectrum of  $\alpha(t)$ ,  $f_{\text{resp}}$  is the frequency at which the peak in the power spectrum of system response occurred,  $\Delta f_{\frac{1}{2}\text{pp}}$  is the frequency interval at the half-power point, and  $A_{\text{resp}}$  is the amplitude of the response peak.

It is seen, especially when  $\bar{\alpha}=0.75$ , that parametric resonance occurs when  $f_n=12$  Hz, but does not occur when  $f_n=15$  Hz. The other runs done for  $\bar{\alpha}=0.75$  show that for the other values of  $f_n$ , this parametric

\* See Appendix D.2.

resonance does not occur, as can be seen in the additional table below.

$f_n$	$f_{\text{resp}}$	$\Delta f_{\frac{1}{2}pp}$	$A_{\text{resp}}$
11	11.25	0.13	26.98
13	13.125	0.12	13.67
14	14.22	0.154	8.915

=Additional table=

In common: Scheme [b];  $\bar{\alpha} = 0.75$ ;  $[\alpha(\omega)]_{\text{max}} = 8.65$ .

In fact, the result for  $f_n = 12$  Hz and  $\bar{\alpha} = 0.75$  is very clear since it indicates that the frequency at which the resonance occurs is actually 12.5 Hz. This proves that we are dealing with the primary resonance associated to the frequency  $f_5 = 25$  Hz (since  $25/12.5 = 2$ ). Actually, the power spectrum of the system response for  $f_n = 12$  Hz and  $\bar{\alpha} = 0.75$  displays even more interesting features as far as parametric resonance is concerned (see Fig. 24). Four smaller peaks can be seen, but in reality they are not so small, since the scale of the y-axis is determined by the peak at 12.5 Hz with an amplitude of nearly  $10^{20}$ . The next peak in importance after the one at 12.5 Hz is found for a frequency of 7.5 Hz. Visibly this is the primary parametric resonance due to  $f_3 = 15$  Hz ( $15/7.5 = 2$ ). The third interesting peak is found for a frequency of 2.5 Hz and is the primary resonance associated to  $f_1 = 5$  Hz ( $5/2.5 = 2$ ). Hence three primary parametric resonances have been displayed. The two smaller remaining peaks occur at frequencies of 17.5 Hz and 22.5 Hz, but it is not exactly known to which combination of perturbation frequencies  $f_i$  they are the response. It is however felt that they represent secondary parametric resonances responding respectively to frequencies of 17.5 Hz ( $17.5/17.5 = 1$ ) and 22.5 Hz ( $22.5/22.5 = 1$ ). These two

frequencies of 17.5 Hz and 22.5 Hz can possibly be present in  $\alpha(t)$  by some addition of certain frequencies  $f_i$  according to the trigonometrical formula

$$\sin p + \sin q = 2 \sin \frac{p+q}{2} \cos \frac{p-q}{2}$$

(we have  $\frac{10+25}{2} = \frac{15+20}{2} = 17.5$  and  $\frac{20+25}{2} = 22.5$ ).

It is recalled that in Chapter III (Section 3.2.4), only one principal parametric resonance (for  $f_n = 15$  Hz:  $30/15 = 2$ ) and no secondary resonance were found. But  $f_n = 12$  Hz was not envisaged at that time.

Coming back to the main table above, it is seen that, contrary to intuition, the absolute value of the response when  $f_n = 12$  Hz is higher than when  $f_n = 15$  Hz. However, this is not a conventional forced-vibration system; hence, this should not be interpreted as an ordinary resonance effect.

The results concerning  $\Delta f_{\frac{1}{2}pp}$  are not significant, but as for the frequency, it is seen that for  $f_n = 15$  Hz and  $\bar{\alpha} = 0.75$ , we have  $f_{resp} = 15.31$  Hz, whereas in Chapter III (end of Section 3.2.3) it was found to be 15.23 Hz, all the input parameters being the same. Taking the resolution of the spectral solution into consideration ( $\Delta f = 0.156$  Hz), this is a good result.

Another observation is that even in this deterministic case, there are variations in  $A_{resp}$  as  $\bar{\alpha}$  changes, as seen when  $f_n = 15$  Hz; however, the effect is not systematic.

Finally to illustrate these results, the power spectra for  $\bar{\alpha} = 0.25$  are shown in Figs. 25(a), (b) and (c). In Fig. 25(a) may be seen the five deterministic peaks, exactly equal; next to the ordinate showing the relative amplitude is indicated the absolute value — in this example 0.96. The sharp

peak of the system response is shown in Figs. 25(b) and (c) for  $f_n = 15$  Hz and 12 Hz, respectively. When  $f_n = 12$  Hz, a very small peak appears just to the right of the main peak and denotes the impending rise of the parametric resonance.

#### 4.2.2 Response of the System to Pseudo-Random Added Mass Perturbations

The purpose of this set of calculations, as already explained in the introduction to this chapter, is to study the effect of random added mass perturbations  $\alpha(t)$  of narrow frequency band. It is for this reason that various models have been developed for  $\alpha(t)$ , starting from the less elaborate scheme [c] which was investigated in Chapter III and is completely pseudo-random. With scheme [d] the effect of having pseudo-random amplitudes is of interest, whereas schemes [e] and [f] consider pseudo-random frequencies, in the hope that one might thus be able to "broaden" the  $N$  sharp response peaks obtained for the deterministic scheme [b] (cf. Fig. 25(a)). Finally it is hoped that if we can "broaden" these deterministic peaks enough, they will "join" and form one quasi-continuous frequency band (eventually the number  $N$  of peaks will have to be increased within the range considered — between 5 Hz and 25 Hz — in order to "help" them to "join" up more easily).

Quantitative comparisons of the results are also made, in order to examine the following specific questions:

- (i) how do the actual frequencies of oscillation compare to the natural frequencies of the system;
- (ii) whether the width of the response peak broadens with more random perturbations in the added mass;
- (iii) whether the vibration amplitude changes systematically with increasing randomness in the added mass.

It is reasonable to expect that if the hydrodynamic mass should decrease and the effective damping should increase with increasing randomness in the added mass, one would expect to see (a) an increase of the effective oscillation frequency, (b) a broadening of the vibration amplitude peak in the power spectrum of the system response, and (c) a reduced amplitude of the vibration peak.

We shall now examine the results obtained with these different models.

Scheme [c]: This is the random scheme which has been adopted in the previous chapter (Section 3.2.2), and on which all the random discussion was conducted. The values of  $\bar{\alpha}$  and  $\sigma$  are related by

$$\sigma = \bar{\alpha}/\sqrt{2N}, \quad (4-8,b)$$

and we also have

$$\mu = 0, \quad (4-8,a)$$

as may be seen in Appendix D.2.

As for Case A[b] in the previous Section 4.2.1, Case A[c]<sup>\*</sup> has only been run for  $N=5$ , and for  $\bar{\alpha}=0.25$  and  $0.75$  (hence  $\sigma=0.25/\sqrt{10}$  and  $0.75/\sqrt{10}$ , respectively).

Fig. 23 shows the power spectrum of  $\alpha(t)$  for  $\bar{\alpha}=0.25$  (and  $\sigma=0.25/\sqrt{10}$ ). As may be seen, the form of  $\alpha(t)$  is really wide-band random, the energy being distributed on all frequencies (and this probably goes far beyond 160 Hz). However, the response of the system is of narrow band, displaying a sharp peak at  $f=f_n$  exactly as on Fig. 25(b). For  $f_n=12$  Hz,

---

\* See Appendix D.2.

the parametric resonance which appeared in Case A[b] does not occur at all. In this sense, the random  $\alpha(t)$  actually has a damping effect.

Let us now view the results obtained.

Scheme of $\alpha(t)$	Input			Results		
	$\bar{\alpha}$	$\sigma$	$f_n$ (Hz)	$[\alpha(\omega)]_{\max}$	$f_{\text{resp}}$	$A_{\text{resp}}$
[a]	0	-	12	0	12.03	20.69
[c]	0.25	$0.25/\sqrt{10}$	12	0.0326	12.03	20.66
[c]	0.75	$0.75/\sqrt{10}$	12	0.2938	12.34	17.79
[a]	0	-	15	0	15.0	13.63
[c]	0.25	$0.25/\sqrt{10}$	15	0.0326	15.0	12.60
[c]	0.75	$0.75/\sqrt{10}$	15	0.2938	15.47	9.22

We see that the frequency of the response increases with  $\bar{\alpha}$ , which goes in the direction sought and agrees with what was found in Chapter III. In Section 3.2.2, we found indeed that, for  $\bar{\alpha} = 0.75$  (and  $f_n = 15$  Hz),  $f_{\text{resp}} = 15.47$  Hz, and here we get the same value, which proves that there is good agreement between the two methods. However, we obtain also an interesting result that we could not get previously, i.e., we see that  $A_{\text{resp}}$  decreases when  $\bar{\alpha}$  increases, both for  $f_n = 12$  Hz and  $f_n = 15$  Hz. Hence, a certain damping effect appears here.

As in the previous Case A[b], the amplitude when  $f_n = 12$  Hz is higher than when  $f_n = 15$  Hz.

Scheme [d]: In this case, pseudo-random amplitudes are considered. Fig. 26 shows the power spectrum of  $\alpha(t)$  for  $N = 5$  and  $\bar{\alpha} = 0.25$ . The five peaks still appear very distinctly, and the power spectra of the response, which were obtained for the same parameters ( $f_n = 12$  and 15 Hz;  $\bar{\alpha} = 0.25$  and 0.75) dis-

play, as might have been foreseen, the same behaviour as for the deterministic case A[b]. No "broadening" of the deterministic peaks can be obtained with scheme [d]. This is clearly not a useful model.

Scheme [e]: A great deal of work has been done with this model, for which the deterministic frequencies  $f_i$  are perturbed by a random fluctuator. Now, the two parameters  $\bar{\alpha}$  and  $\sigma$  can be chosen to vary independently; hence, in Figs. 27(a) - (c) is shown the power spectrum of  $\alpha(t)$  for a given  $\bar{\alpha}$  ( $\bar{\alpha} = 0.25$ ) but for increasing  $\sigma$  ( $\sigma = 0.25, 0.50$  and  $1$ ). As may be seen, we are still considering the value  $N=5$ . It is seen that when  $\sigma$  is small (Fig. 27(a)) the dominant frequencies stand out clearly, in a background of "noise". However, with increasing  $\sigma$ , the "noise" becomes more pronounced, so that in Fig. 27(c) it is difficult to pick out the predominant frequencies - although, on closer examination, it may be established that they are still there. Actually, the amplitudes of Figs. 27(a) - (c) indicate that it is not the "noise" which increases in such a proportion, but that rather the amplitudes of the deterministic peaks progressively decrease, until they are "swallowed" by the "noise". Unfortunately, the establishment of this fact indicates that the desired effect of a broadening of the peaks is much less important than the observed effect of the peaks vanishing in the general "noise".

As far as the response is concerned, it cannot be said to change very much when the system is subjected to any of the  $\alpha(t)$  considered above and seen in Figs. 27(a) - (c). It consists of one sharp peak at  $f = f_n$ , similar to the one shown in Fig. 25(b). Nevertheless, it should be mentioned that for  $\bar{\alpha} = 0.75$  and  $f_n = 12$  Hz the parametric resonance, which was observed in Case A[b] at a frequency of 12.5 Hz, still appears but at a much reduced

level (since with scheme [e], an amplitude of the order of only  $10^7$  to  $10^2$  — decreasing when  $\sigma$  increases — is obtained, whereas for scheme [b], it reached  $10^{20}$ ).

Let us now give the quantitative results obtained for  $\bar{\alpha} = 0.25$ ,  $f_n = 14$  Hz and  $N = 5$  (these are the runs for which  $\alpha(t)$  is shown in Figs. 27(a)-(c)).

Scheme of $\alpha(t)$	Input			Results			
	$\bar{\alpha}$	$\sigma$	$f_n$ (Hz)	$[\alpha(\omega)]_{\max}$	$f_{\text{resp}}$	$\Delta f_{\frac{1}{2}\text{pp}}$	$A_{\text{resp}}$
[a]	0	0	14	0	14.06	0.216	12.45
[e]	0.25	0.25	14	0.298	14.06	0.13	14.11
[e]	0.25	0.50	14	0.0782	14.06	0.125	13.43
[e]	0.25	1.00	14	0.0285	14.06	0.128	12.65

It is noted that with increasing  $\sigma$ ,  $[\alpha(\omega)]_{\max}$  decreases (what has already been explained by the vanishing of the five deterministic peaks), and so does  $A_{\text{resp}}$ . However, there is no significant broadening of the response, nor a significant frequency shift.

Although promising, the desired goal of achieving narrow banded  $\alpha(t)$  has really not been achieved. Therefore, two further attempts were undertaken. The first consists in increasing the number of predominant frequencies from  $N = 5$  to  $N = 17$ . Fig. 28 shows the power spectrum of  $\alpha(t)$  for this new value of  $N$ , and for  $\bar{\alpha} = 0.25$  and  $\sigma = 0.50$ . As it may be noticed, increasing  $N$  has not changed things very much. (The value of  $[\alpha(\omega)]_{\max}$  is 0.0133 in Fig. 28, which is smaller than 0.0782 in Fig. 27(b), also obtained for  $\bar{\alpha} = 0.25$  and  $\sigma = 0.50$ , but with  $N = 5$ . This is due to the fact that the amplitude  $\frac{\bar{\alpha}}{N}$ , common to all sine functions of scheme [e], is now

$\frac{\bar{\alpha}}{17}$  instead of  $\frac{\bar{\alpha}}{5}$ , previously [cf. equation (4-4)]. The other parameters obtained are:  $f_{\text{resp}} = 14.06$  Hz,  $\Delta f_{\frac{1}{2}\text{pp}} = 0.177$  Hz, and  $A_{\text{resp}} = 13.47$ .)

The second attempt made amounts to decreasing the discrimination of the calculation - which means reducing the resolution  $\Delta f$  in the power spectrum calculations. It should be stressed that this is the only part of Section 4.2 in which the range (0 - 160 Hz) and  $N_{\text{ps}} = 1025$  are not adopted. In fact we consider here the range (0 - 80 Hz) and  $N_{\text{ps}} = 129$ , which gives us 1.6 spectral samples per Hertz, or a resolution of  $\Delta f = 0.625$  Hz. Decreasing the discrimination of the calculation makes actually things "look" a great deal more successful [Figs. 29(a) and (b)]; the response displays also a broader peak [Fig. 29(c)]. But we know that in fact this is artificial and that things are not really better. We now indicate the quantitative results obtained with these range and value of  $N_{\text{ps}}$ , and for  $N = 17$  and  $f_n = 13$  Hz.

Scheme of $\alpha(t)$	Input			Results			
	$\bar{\alpha}$	$\sigma$	$f_n$ (Hz)	$[\alpha(\omega)]_{\text{max}}$	$f_{\text{resp}}$	$\Delta f_{\frac{1}{2}\text{pp}}$	$A_{\text{resp}}$
[e]	0.25	0.25	13	0.0111	13.12	0.50	14.45
[e]	0.75	0.25	13	0.10	13.12	0.46	13.76
[e]	0.25	0.50	13	0.0072	13.12	0.51	14.50
[e]	0.75	0.50	13	0.0646	13.12	0.47	13.36

Range = (0, 80 Hz) and  $N_{\text{ps}} = 129$ .

It is seen that, as  $\bar{\alpha}$  increases,  $A_{\text{resp}}$  decreases very slightly and  $\Delta f_{\frac{1}{2}\text{pp}}$  remains almost the same. However, these results are not very reliable, because of the small number of points in the spectrum.

Scheme [f]: The results of this case are very similar to those obtained with scheme [e]; as a matter of fact, both schemes consider pseudo-random perturbations on the frequencies. It was noted, nevertheless, that for a given  $\bar{\alpha}$  the "broad-banded" form of  $\alpha(t)$  emerges at higher values of  $\sigma$  than was the case with scheme [e]. Also, for  $\bar{\alpha} = 0.75$  and  $f_n = 12$  Hz, the remaining effect of parametric resonance displays higher amplitudes (from  $10^{12}$  to  $10^3$ , decreasing with increasing  $\sigma$ ) than it did with scheme [e]. Hence schemes [e] and [f] display the same qualitative results, but the effective damping is lower for the latter scheme.

#### 4.3 Results Obtained in the Frequency Range (0 - 40 Hz)

The first part of the frequency domain analysis (Section 4.2) has proved to be a relative success, since good agreement with the time domain results (Chapter III) could be reached for the common schemes [b] and [c], especially as far as the effective frequency of oscillation is concerned. Moreover, it was possible to observe a more conclusive damping effect due to the random added mass perturbations, in the case where parametric resonance\* occurs (what was already found in Chapter III), as well as in the case of the completely pseudo-random scheme [c] (what could not have been displayed previously).

Nevertheless, the desired goal of generating a narrow-banded pseudo-random  $\alpha(t)$  could not be achieved with any of the three new schemes introduced, namely scheme [d] (with randomly perturbed amplitudes  $a_i$ ) and

---

\*When  $f_n = 12$  Hz and with large amplitudes of  $\alpha(t)$ . This was observed for schemes [e] and [f], where  $f_n = 12$  Hz displays a much reduced parametric resonance compared to scheme [b].

[e] and [f] (with randomly perturbed frequencies  $f_j$ ). In fact, instead of observing a broadening of the sharp peaks corresponding to the  $N$  frequencies  $f_j$ , with increasing  $\sigma$  [cf. Figs. 27(a) - (c)], it was noticed that the peaks — still very sharp — decrease in amplitude until they become no longer distinguishable from the surrounding "noise". Increasing the number  $N$  of perturbation frequencies  $f_j$  did not alter this pattern of behaviour.

In this section, another digital attempt will be undertaken to come closer to the aim of producing such an  $\alpha(t)$  of narrow frequency band. Therefore two improvements are introduced; the first one consists in choosing certain better system and analysis parameters, and the second one in testing more sophisticated models of the added mass perturbations  $\alpha(t)$ .

The parameter improvements are the following:

- (i) we increase the value of  $\zeta$  from 0.005 to 0.02, in order to obtain a broader peak for the system response, which will make it easier to measure  $\Delta f_{\frac{1}{2}pp}$ ;
- (ii) we choose the value  $f_n = 14$  Hz for the natural frequency of the system, to avoid any effect of the parametric resonance observed at  $f_n = 12$  Hz (this parametric resonance occurring actually at 12.5 Hz); we also discard  $f_n = 13$  Hz for the same reason, even though no really important effect of this parametric resonance has been observed at that frequency; furthermore, we do not choose  $f_n = 15$  Hz, since 15 Hz is precisely one of the deterministic frequencies involved in  $\alpha(t)$ ;
- (iii) we reduce the frequency range studied from (0 - 160 Hz) down to (0 - 40 Hz), and this is sufficient since we want the frequency band of  $\alpha(t)$  to spread between 5 and 25 Hz, and also since we have not discovered any unsuspected effect above 40 Hz affecting the system response (in Section 4.2);

(iv) we also reduce the number  $N_{ps}$  of points used to calculate the power spectra of  $\alpha(f)^*$  and  $x(f)^*$  from 1025 down to 513<sup>†</sup> (hence  $L = 1024$ ); this is possible since we reduce the frequency range by four times.

Thanks to all this, our results on the three parameters of interest (response frequency, frequency interval at the half-power point, and amplitude of the response peak) will be of much better comparative value.

Having chosen these frequency ranges (iii) and number of calculation points (iv), we obtain 12.8 calculated points per Hertz or, in other words, the width of one calculated frequency interval or resolution  $\Delta f$  is equal to 0.078 Hz approximately. This means that the accuracy of the power spectra obtained is twice better as it was in Section 4.2.

Having done (i), (iii) and (iv), we notice on the output data that, since the response peak is broader, we obtain about 20 significant points to plot this peak, whereas only 3 such points were available for the very sharp peaks of Section 4.2. This is quite an appreciable improvement.

However, one question might give some trouble and stems from the choice of  $N_{ps}$ ,  $L$  and  $N_t$  (here  $N_t = 2048$ ). In fact, equation (4-5) gives a period of sampling of the time record  $\Delta t$  equal to

$$\Delta t = \frac{512}{1024 \times 40} = \frac{1}{80} = 12.5 \text{ ms.}$$

The value is four times bigger than before. Hence there will be four times

---

\* Where  $f$  stands for the frequency.

<sup>†</sup> With 513 points, the computing time is half of what it would be with 1025 points; moreover the program can be run in CLASS 2, whilst a 1025 points program requires CLASS 3.

less sampling points per cycle of oscillation, i.e. 16 samples per cycle if  $f = 5$  Hz, about 6 samples if  $f = f_n$ , and only 3.2 samples if  $f = 25$  Hz. As we can see it, there exists a conflict between accuracy in the time domain of the input and accuracy in the frequency domain of the output. The total sampling time is

$$T_t = N_t \cdot \Delta t = 2048/80 = 25.6 \text{ s.}$$

This is twice the time length covered before, hence the number of cycles considered will also double, which represents about 340 cycles of the response (128 cycles of a signal of 5 Hz and 640 cycles if  $f = 25$  Hz).

As for the models of  $\alpha(t)$  to be tested, they include three former ones, namely schemes [a] (reference with  $\alpha(t) = 0$ ), [b] (deterministic reference = sum of  $N$  sine functions) and [e] (pseudo-random perturbations of the frequencies  $f_j$ ). The new schemes introduced here are denoted from [g] to [k], and consist mainly of more refined deterministic variations of the frequencies  $f_j$  (schemes [g], [h] and [j]) on which pseudo-random perturbations may also be added (schemes [i] and [k]). For further information on these schemes, see Appendix D.2.

Let us finally note that in every run with non-null  $\alpha(t)$ , the value  $\bar{\alpha} = 0.25$  is used. Also, in every run in which pseudo-random  $RO_j^\dagger$  sequences are generated and used, the mean  $\mu_j = 0$  and standard deviation  $\sigma_j = 0.25$  are used.

We now review the different schemes and examine the power spectrum of  $\alpha(f)$ , as well as the results concerning the response  $x(f)$ .

Scheme [a]: This is the reference case with  $\alpha(t) = 0$ . Two runs are conducted, the first one being the only run of this Section 4.3 which is not

---

<sup>†</sup> $RO_j$  is defined in Appendix D.2.

considering  $N_{ps} = 513$ . The results obtained are given below.

Input				Results		
Scheme of $\alpha(t)$	$N_{ps}$	Frequency Range (Hz)	# points / Hz	$f_{resp}$ (Hz)	$\Delta f_{\frac{1}{2}pp}$ (Hz)	$A_{resp} \times 10^{-4}$
[a]	1025	0 - 40	25.6	13.87	0.520	1.81
[a]	513	0 - 40	12.8	13.9	0.524	14.36

$$\alpha(t) = 0$$

This Case B[a] is interesting mostly because it allows comparison of the results for the two different values of  $N_{ps}$ . The damping being more important now ( $\zeta = 0.02$ ), the response  $x(t)$  will decay rapidly and we notice actually that the response amplitude of the first run ( $1.81 \times 10^{-4}$ ; for  $N_{ps} = 1025$ ) is eight times smaller than for the second run ( $14.36 \times 10^{-4}$ ; for  $N_{ps} = 513$ ). This example shows us one limitation of the FTFS method, since we are limited by the time span studied, and maybe in Section 4.2 we did not go far enough in time to obtain some expected results. We also understand that this method would not be well suited for the study of the forced vibrations of the system, since in that case a much bigger number of cycles should be investigated.

Another limitation lies in the discreteness of the method itself, and this is illustrated by the results concerning the effective response frequency. For the first run the response peak, or more exactly the maximum frequency estimate obtained, is located at the discrete frequency abscissa  $f_{r1} = 13.8671875$  Hz, whilst for the second run, this frequency point is not present and the peak is obtained for  $f_{r2} = 13.90625$  Hz (see Fig. 30). But this problem is inherent to any digital method, and the results have to be

given with an indication of the resolution of the method. One thing is sure from both runs, it is that the response frequency is smaller than the natural frequency of the system (14 Hz), but it is not known exactly where it occurs. (There might however exist a very slight difference between  $f_{r1}$  and  $f_{r2}$ , due to the Runge-Kutta method used over different time lengths.) The unexpected lower frequency found may be due partially to the higher damping used ( $\zeta = 0.02$  instead of 0.005).

From now on, all subsequent runs will have in common:  $N_{ps} = 513$ , range = (0,40 Hz),  $f_n = 14$  Hz,  $\zeta = 0.02$  and  $\bar{\alpha} = 0.25$ . Moreover, for all pseudo-random runs, the value  $\sigma = 0.25$  is adopted (only the "realistic" value is considered).

Scheme [b]: This is the deterministic reference case and consists simply of a sum of  $N$  sine functions. In Case B[b], four values of  $N$  are considered:  $N = 5, 9, 17, 33$ . The perturbation frequencies  $f_i$  stretch between 5 and 25 Hz and their respective values may be found in Appendix D.2.

Let us give the results right now.

Input		Results			
Scheme of $\alpha(t)$	$N$	$[\alpha(\omega)]_{\max}$	$f_{\text{resp}}$	$\Delta f_{\frac{1}{2}pp}$	$A_{\text{resp}} \times 10^{-4}$
[b]	5	0.4809	13.9	0.531	13.63
[b]	9	0.1484	13.9	0.529	14.39
[b]	17	0.0416	13.9	0.520	14.43
[b]	33	0.01104	13.9	0.524	14.44

[Fig. 31]

$\bar{\alpha} = 0.25$  and  $\sigma = 0$

The most visible, and also expected affect is the strong decrease of  $[\alpha(\omega)]_{\max}$  as  $N$  increases. This comes simply from the choice of  $a_i$  as

$a_i = \frac{\bar{\alpha}}{N}$  for all  $i$  (equation (4-4)), hence since we want  $\bar{\alpha}$  to be constant,  $a_i$  decreases as  $N$  increases.

We also notice a slight increase of  $A_{resp}$ , which is only certain when passing from  $N=5$  to  $N=9$ . To be complete, we should compare these amplitude values with the one obtained from the second run of Case B[a], and then we see that this conclusion does not hold since  $A_{resp}$  of Case B[a] is even smaller than  $A_{resp}$  of the second run of this case ( $14.36 < 14.39$ ). The imprecision on  $A_{resp}$  does not allow us to conclude anything else but that  $A_{resp}$  is constant. The same conclusion can be made about  $f_{resp}$  and  $\Delta f_{\frac{1}{2}pp}$ .

From this point on, we could continue to give in a similar way the results for the other schemes considered, since in fact schemes [e] and [g] have also be run for the same four values of  $N$ . But it is believed that a comparative discussion is more interesting, and for this purpose, we shall only consider the runs for which  $N=33$  has been adopted. As a matter of fact, it is with this highest value of  $N$  that the chance is the biggest to obtain a narrow-banded  $\alpha(t)$ .

But before giving the results for  $N=33$ , let us have a qualitative review of the power spectrum of  $\alpha(t)$  obtained with the different schemes (also for  $N=33$ ). In Fig. 31(a) are seen the 33 deterministic peaks characteristic of the reference case [b] (already discussed above), whereas Fig. 31(b) displays the associate system response. This will be the only response peak shown in this section, since for all the other schemes investigated, the shape of the response peak was found to be similar.

In Fig. 32 is given the power spectrum of  $\alpha(t)$ , corresponding to scheme [e]. It exhibits a wide-band spectrum, very different from the sharp

peaks obtained for  $N=5$  in Section 4.2.2 [cf. Fig. 27(a)]. It is more similar to what is obtained for the completely pseudo-random scheme [c] (cf. Fig. 23). Unfortunately, the same kind of behaviour is observed in Figs. 33, 34, 35 (scheme [g]) and in Fig. 36 (scheme [h]).

However, a better result is achieved in Fig. 37, actually the first good result up to now, as far as the aim of generating a narrow-banded  $\alpha(t)$  is concerned. This relative success is found for scheme [h] with  $\mu_i = 0.2$  for all  $i$  and  $\lambda = 2$  (cf. Appendix D.2), which means that the exact scheme considered is

$$\alpha(t) = \frac{\bar{\alpha}}{33} \sum_{i=1}^{33} \sin[\omega_i(1 + 0.2 \sin(20\pi t))t],$$

for which the values of  $\omega_i$  may also be found in Appendix D.2.

This result is considered to be a success because the "bell"-shape of a narrow frequency band appears, but this success is only relative since the broadening of the outstanding peaks (corresponding to the frequencies  $f_i$ ) is not sufficient to give us a real frequency band.

We have mentioned before that this is the first case displaying a good result, but unfortunately it is also the last. Another problem seen indeed in Fig. 37 is that the potential narrow frequency band does not spread exactly between 5 and 25 Hz, but rather between 12 and 28 Hz, which is a little too far from the suggested "realistic" conditions desired [cf. equation (3-4,b)]. To obtain the same kind of spectrum, but shifted to the "left" on the frequency abscissa, we proceed to a systematic shift of the perturbation frequencies  $f_i$  and therefore reduce all of them by 3 Hz. In other words, we replace the frequencies (5, 5.625, ..., 25 Hz) by (2, 2.625, ..., 22 Hz). However, this does not produce the expected result as we may

notice it in Fig. 38 (scheme [j]) and in Fig. 39 (scheme [k]). The desired shape of Fig. 37 has actually disappeared, and there only remains a wide band spectrum, as found in Figs. 32 to 36. We are thus forced to recognize that there is little hope in obtaining a narrow-banded  $\alpha(t)$  by means of such a digital method.

However, it may still be interesting to give the quantitative results obtained for all these runs, conducted with  $N=33$  (except for scheme [a], of course, since  $\alpha(t)=0$ ).

Input					Results				
Scheme	Nature*	$\mu_j$	$\lambda$	$\sigma$	$[\alpha(\omega)]_{\max} \times 10^{-4}$	$f_{\text{resp}}$	$\Delta f_{\frac{1}{2}\text{pp}}$	$A_{\text{resp}} \times 10^{-4}$	Figure
[a]	d	-	-	-	-	13.9	0.524	14.36	-
[b]	d	-	-	-	110.4	13.9	0.524	14.44	Figs. 31
[e]	pr	-	-	0.25	38.62	13.9	0.520	14.54	Fig. 32
[g]	d	0.2	5	-	41.89	13.9	0.533	12.75	Fig. 33
[g]	d	0.2	2	-	79.97	13.9	0.519	13.60	Fig. 34
[g]	d	0.1	5	-	45.28	13.9	0.513	13.37	Fig. 35
[h]	d	0.2	5	-	41.71	13.9	0.533	14.34	Fig. 36
[h]	d	0.2	2	-	77.55	13.9	0.525	12.94	Fig. 37
[j]	d	0.2	1	-	64.18	13.9	0.519	14.57	Fig. 38
[k]	pr	0.2	1	0.25	33.25	13.9	0.512	14.51	Fig. 39

The general observation is that, as well as being unable to obtain good results from the qualitative point of view, these results are also not very enlightening<sup>§</sup>. It is true that most of these schemes are deterministic and that the deterministic scheme [b] has been found in Chapter III, for

\* Nature: d denotes a deterministic scheme, and pr a pseudo-random one.

§ The results of  $f_{\text{resp}}$ , which seems to be constant, are a good example of this.

C instance, to display less important effects (e.g. effective frequency) than the pseudo-random scheme [c]. Another reason is that here we took  $\bar{\alpha} = 0.25$ , which is the lowest value of  $\bar{\alpha}$  studied, and the effects have always proved to remain weak for such a low  $\bar{\alpha}$ .

7 It could be mentioned here that the two lowest values of  $[\alpha(\omega)]_{\max}$  are found precisely for the two pseudo-random cases (schemes [e] and [k]). Comparison between schemes [j] and [k] is also interesting, since the latter is the pseudo-random perturbed version of the former. According to  $A_{\text{resp}}$ , damping seems to be higher ( $14.51 \times 10^{-4} < 14.57 \times 10^{-4}$ ) but not according to  $\Delta f_{\frac{1}{2}\text{pp}}$  ( $0.512 < 0.519$ ) since for higher damping,  $\Delta f_{\frac{1}{2}\text{pp}}$  would increase.

Another reason for the lack of significant results of this section may be the small number per cycle of discrete data taken from the time domain signal, at least for the highest frequencies considered.

## CHAPTER V

ANALOG ANALYSIS OF THE FREE AND  
FORCED VIBRATIONS IN THE FREQUENCY DOMAIN5.1 Description of Equipment and Method5.1.1 Digital Signal Analyser and Analog Computer

The motivation for this last analysis lies in the failure of the digital methods to generate pseudo-random added mass perturbations of narrow frequency band. Of course, we could still improve these methods by introducing digital filters. But this is considered to be too complicated, especially when considering a certain rigidity inherent in the FTFPS power spectrum sub-program as for the choice of the parameters of interest. High computer times (up to \$160 CPU charge occurred for certain digital runs) are also a factor to be taken into account against the digital methods.

This is why we decided to switch from the Amdhal V7 computer to our Hewlett-Packard vibration analysis equipment. The main piece of this equipment consists of a HP 5420A Digital Signal Analyser. This electronic device performs a variety of time domain and frequency domain measurements. To link the time domain to the frequency domain, it also makes use of the FFT algorithm, described in Appendix D.1 and used in Chapter IV. One valuable advantage of the analyser is the possibility of processing not only one ensemble of  $N_t$  time domain samples — as it was done previously with the FTFPS sub-program — but on the contrary a whole series of them. A very important number of these ensembles (up to 32,767) can be processed one after the other, as soon as  $N_t$  time data have been sampled. The process used to obtain the final result is a signal averaging which, in this case, is an overlapped processing. Although time windowing of measured data records is a necessity when using digital processors — and

this is in order to avoid aliasing (cf. Appendix D.1) — one of the deleterious effects of windowing is the loss of the information contained in the original data. Much of the coherent information buried in noise can thus be recovered by using time records that overlap one another, resulting in variance reduction that depends upon the window shape. Hence over 1000 oscillation cycles can be analysed—which is very interesting for the forced case. Several windowing functions are available according to the nature of the input signal. We choose to enter a randomly varying signal, hence the Hanning window is selected and the result obtained is actually a power spectral density (p.s.d.) which is given in volts<sup>2</sup>/Hz. Additional information on the measurement characteristics of this frequency analyser may be found in Appendix E.1, and even more in Chapter 5 of the analyser manual [71].

Paradoxically, this digital signal analyser accepts only analog signals as input. As a matter of fact, since we have already solved the differential equation (2-16) on the digital computer, it would be desirable to analyse these digital solution data on the HP 5420A analyser. But this is not possible because, even though the analyser processes digital numbers, it is not designed to accept digital input. The solution of storing the digital response obtained previously, and transforming it into an analog signal was first considered, but could not be implemented because of both hardware and software incompatibilities between the IBM and HP systems.

For this reason, it is decided to solve equation (2-16) on an analog computer, namely the EAI 1000 Analog Computer. More information on this computer may be found in Appendix E.2, as well as in its reference and maintenance manual [72]. More general information on analog computers may also be found in Refs. [73] and [74]. A practical advantage of using an analog computer lies in the fact that, once the equation has been scaled and plugged on the EAI 1000, it becomes much easier to change the

parameters of interest than in a deck of computer cards.

In this approach, we no longer use a Monte-Carlo method to generate the pseudo-random  $\alpha(\omega)$ , but simply pick up the signal obtained from the Noise Source incorporated in the ADC element of the analyser (Analog/Digital Converter HP 54410A). Then this noise, whose spectrum is flat (wide-band) in the frequency range considered for analysis, is filtered to the desired frequency band by means of the Krohn-Hite filter model 3323. In Figs. 40(a)-(c) is shown the power spectral density of  $\alpha(\omega)$  for three different values of averages obtained by overlapped processing (this number of averages is noted #A on the display of the analyser). For only one average taken [Fig. 40(a)], the narrow band is not yet very good, still exhibiting sharp peaks as was found in the digital analysis of Chapter IV. However, when the number of averages is increased, the narrow band is much more marked, as may be seen in Fig. 40(b) [#A = 100] and especially in Fig. 40(c) [#A = 1000]. This is in agreement with what was stressed earlier, namely that overlapped processing recovers coherent signals buried in noise. As far as the forcing function is concerned, it is obtained, when considered, from the HP 3300A Function Generator. In Fig. 41 may be found the schematic description of the experiment.

### 5.1.2 Machine Equation on Analog Computer

In actual magnitude and time scales, equation (2-16) may be written

$$[1 + \alpha(t)]\ddot{x} + 2\zeta\omega_n\dot{x} + \omega_n^2x = \begin{cases} 0 \\ \omega_n^2 f^0 \sin \omega_f t \end{cases} \quad (5-1)$$

in which  $f^0$  is constant.

This equation must undergo some changes in order to fit the analog computer requirements (maximum voltage =  $\pm 5$  volts), as described below.

a) Magnitude scaling

The maxima are calculated in the unforced case with no damping. This means that the solution given by equation (2-17) now reads

$$x(t) = B \cos(\omega_n t + \phi).$$

Its first and second derivatives with respect to time are

$$\dot{x}(t) = -\omega_n B \sin(\omega_n t + \phi),$$

$$\ddot{x}(t) = -\omega_n^2 B \cos(\omega_n t + \phi).$$

By introducing the initial conditions\*,  $x(0) = x_{IC}$  and  $\dot{x}(0) = 0$ , we find that  $B = x_{IC}$  and  $\phi = 0$ .

Hence,

$$x(t) = x_{IC} \cos(\omega_n t)$$

$$\dot{x}(t) = -x_{IC} \omega_n \sin(\omega_n t)$$

$$\ddot{x}(t) = -x_{IC} \omega_n^2 \cos(\omega_n t)$$

from where we get

$$|x(t)|_{\max} = x_{IC} \quad (5-2,a)$$

$$|\dot{x}(t)|_{\max} = x_{IC} \omega_n \quad (5-2,b)$$

---

\* Slightly different from initial conditions (3-5).

$$|\ddot{x}(t)|_{\max} = x_{IC} \omega_n^2. \quad (5-2,c)$$

For the forced case, it is just necessary to lower the initial value of  $x_{IC}$  in order to avoid overflow when increasing  $f^\circ$ .

Let us now introduce the machine variables:

Actual variable	Expected maximum	Computer variable
$x$	$x_{IC}$	$\left[ \frac{x}{x_{IC}} \right]$
$\dot{x}$	$\omega_n x_{IC}$	$\left[ \frac{\dot{x}}{\omega_n x_{IC}} \right]$
$\ddot{x}$	$\omega_n^2 x_{IC}$	$\left[ \frac{\ddot{x}}{\omega_n^2 x_{IC}} \right]$

Having done this and dividing by  $\omega_n^2 x_{IC}$ , equation (5-1)

becomes

$$(1 + \alpha(t)) \left[ \frac{\ddot{x}}{\omega_n^2 x_{IC}} \right] + 2\zeta \left[ \frac{\dot{x}}{\omega_n x_{IC}} \right] + \left[ \frac{x}{x_{IC}} \right] = \begin{cases} 0 \\ F^\circ \sin \omega_f t \end{cases}, \quad (5-3)$$

where

$$F^\circ = \frac{f^\circ}{x_{IC}}$$

#### b) Time scaling

The typical value that we choose for the natural frequency of our system is  $f_n = 14$  Hz for reasons previously explained (cf. Section 4.3).

With the magnitude-scaled equation above, we have to set two potentiometers at the value  $\omega_n$ , one to pass from  $\left[ \frac{\ddot{x}}{\omega_n^2 x_{IC}} \right]$  to  $\left[ \frac{\dot{x}}{\omega_n x_{IC}} \right]$ , another

to pass from  $[\frac{\dot{x}}{\omega_n x_{IC}}]$  to  $[\frac{x}{x_{IC}}]$ ; or we could at least use the value  $\frac{\omega_n}{10}$  since the integrators are equipped with one input of gain 10.

Calculating  $\omega_n$  we find

$$f_n = 14 \text{ Hz} \rightarrow \omega_n = 2\pi f_n = 87.965 \text{ rad/s,}$$

hence

$$\frac{\omega_n}{10} = 8.796 \approx 8.80 \text{ rad/s.}$$

But it is impossible to set any potentiometer to the latter value 8.80, even more to the value 88, since potentiometers can only vary between 0 and +1. Hence we have to reduce the gain around the program loops (which remained constant in the magnitude scaling). By changing the gain of all integrators by the same amount, we do what is called time scaling.

For reasons of convenience, we adopt a time scaling coefficient of 10. Hence the machine time will be

$$\tau = 10t, \tag{5-4}$$

which means that everything occurs ten times slower, and so all the frequencies are ten times smaller, as shown below on a given problem frequency  $f_a$  and machine frequency  $F_a$ .

$$\text{Problem frequency: } f_a = \omega_a / 2\pi$$

$$\text{Computer frequency: } F_a = \Omega_a / 2\pi$$

We have

$$f_a = 1/t_a \quad \text{and} \quad F_a = 1/T_a,$$

in which  $t_a$  and  $T_a$  are obviously the periods associated respectively to  $f_a$  and  $F_a$ .

According to equation (5-4), we obtain

$$T_a = 10t_a,$$

from which we get

$$F_a = \frac{1}{T_a} = \frac{1}{10t_a} = \frac{f_a}{10}; \quad (5-5)$$

so we actually proved that the computer frequencies are 10 times smaller than the problem frequencies.

Hence our new natural frequency is

$$F_n = 1.4 \text{ Hz}, \quad (5-6)$$

and the values of the two potentiometers placed before the two integrators are 0.880. The advantage of studying ten times slower motions is the fact that they can be followed much easier on the oscilloscope and, moreover, their time records can be plotted directly by an analog plotter (a frequency of 14 Hz would be too fast to be followed by such a plotter). This possibility allows time record comparison between the reference solutions obtained for  $\alpha(t) = 0$ . Thus the comparison between Curve 1 of Chapter III and the analog solution (for  $\alpha(t) = 0$ ), carried out for the same natural frequency and value of  $\zeta$ , gave a very good result.

However, there is a disadvantage in working with such low frequencies namely, along with the fact of encountering some drifts in the electronic components of the analog computer, the long time necessary to conduct the measurements. Thus it takes, for example, about twelve hours to obtain one complete resonance curve for the forced vibrations.

Finally, the magnitude- and time-scaled equation reads

$$\left[ \frac{\ddot{x}(\tau)}{\Omega_n^2 x_{IC}} \right] = -2\zeta \left[ \frac{\dot{x}(\tau)}{\Omega_n x_{IC}} \right] - \left[ \frac{x(\tau)}{x_{IC}} \right] - \alpha(\tau) \left[ \frac{\ddot{x}(\tau)}{\Omega_n^2 x_{IC}} \right] + \begin{cases} 0 \\ F^0 \sin \Omega_f \tau \end{cases}, \quad (5-7)$$

in which it is remembered that

$$\tau = 10t; \quad \Omega_n = \frac{\omega_n}{10} \quad \text{and} \quad \Omega_f = \frac{\omega_f}{10}.$$

The circuit diagram finally adopted may be found in Fig. 42.

## 5.2 Free Vibration Results.

In this case, we examine the response frequency as a function of the magnitude of  $\alpha_{rms}$ . The study is conducted for different values of  $x_{IC}$ , namely  $x_{IC} = 0.8, 0.7, 0.6, 0.5, 0.4$  and  $0.3$  (in machine-units, which means that actual voltages are obtained by multiplying these figures by 5).

For each value of  $x_{IC}$ , different values of  $\alpha(\tau)$  are applied and the response frequency is measured. For each such point, a set of 10 or more measurements is conducted over different lengths of time ( $\#A=1$  and  $\#A=250$  or  $300$ ) in order to take the randomness of  $\alpha(\tau)$  into account. The system is "restarted" every time it damps out (or, quite seldom, when it overflows too much), then averages of  $\alpha_{rms}$  and  $f_{response}$  are calculated,

and in the case of  $\alpha_{rms}$ , they are transformed into "a equivalents", which means that the given  $\alpha(\tau)$  has the same r.m.s. value as a deterministic  $\alpha(\tau)$ , typically  $\alpha(\tau) = a \sin \Omega \tau$ . In fact,

$$\text{"a equiv."} = \alpha_{rms} \times \sqrt{2} \times \text{scale factor depending on } x_{IC}.$$

The results are then given in the form of rectangles of uncertainty, in terms of "a equiv." and  $f_{resp}$ . The average value is roughly in the center of the rectangle, the bounds of which are obtained from the maximum and minimum values measured. These results are plotted in Fig. 43. It is quite interesting to notice that a general trend appears from data which primarily seem to be rather unexploitable.

The shift which is observed between the curves corresponding to different values of  $x_{IC}$  is thought to be due to a lower accuracy of the analog computer when operating within smaller voltage ranges\*, which actually occurs when  $x_{IC}$  is decreased.

It could be that our method of calculation of "a equiv.", which seems quite logical (by imposing equality of pseudo-random and deterministic r.m.s. values), is not valid, in which case  $\alpha_{rms}$  should be calculated as it is done for the forced cases (see Section 5.3 below).

The preceding remarks deal with the relative position of the curves corresponding to different values of  $x_{IC}$ . Nevertheless, the general effect is clear and consists of an increase of the oscillation frequency, corresponding to an increase in  $\alpha_{rms}$ . This effect, which is evident and is in agreement with our previous results, remains however low:

---

\*The best results are obtained indeed when the analog computer is used in its full range, i.e. between -5V and +5V.

$(1.402 - 1.4)/1.4 = 0.15\%$  for  $\alpha_{\text{rms}} = 0.1$ , and

$0.5\%$  for  $\alpha_{\text{rms}} = 0.2$ .

For the higher "unrealistic" values of  $\alpha_{\text{rms}}$ , one finds about 1.5% for  $\alpha_{\text{rms}} = 0.5$  and about 3.5% for  $\alpha_{\text{rms}} = 0.8$  (or more than 3.5%, since the curves are interrupted due to overflow).

This is the same behaviour pattern that we observed previously with the digital computer approaches of Chapters III and IV.

Let us finally mention that all free vibration experiments have been conducted with the usual small value of  $\zeta$ , i.e.  $\zeta = 0.005$ .

### 5.3 Forced Vibration Results

These runs are some of the most interesting in this thesis, since the forced vibration response curve gives direct access to the resonance frequency, as well as to the response damping which can be measured at the half-power points. On the whole, ten response curves  $x/F_0 = f(\Omega/\Omega_n)$  have been plotted and one of them may be found in Fig. 44. Each such plot consists of about fifteen measurement points, calculated for a number of averages #A equal to 300, in order to take the random fluctuations of the response into account. Working on the frequency range (0 - 4 Hz) and with this value of #A, it takes more than ten minutes to obtain one response measurement. In fact, the whole procedure to obtain one point includes (a) a measurement of the forcing function (with #A = 1), (b) for the sake of comparison, a measurement of the deterministic response with  $\alpha(\tau) = 0$  (also with #A = 1), (c) the measurement of the pseudo-random response (with #A = 300), (d) again a deterministic measurement (#A = 1) in order to check eventual drifts in the analog computer, and finally (e) a measurement of

the forcing function ( $\#A=1$ ) in order to check eventual drifts in the function generator. The whole procedure, including handling and reading the resonance frequency and r.m.s. value (POWER key), takes about forty minutes to obtain one measurement point.

The results obtained are shown below; before discussing them, let us give just a few words on how the value of  $\alpha_{rms}$  is determined. Since we take here  $x_{IC} = 0$ , we can no longer proceed as for free vibration, and now we have to measure both  $\alpha(\tau)[\ddot{x}/\Omega_n^2 x_{IC}]$  depicted on Fig. 45(a) and  $[\ddot{x}/\Omega_n^2 x_{IC}]$  shown on Fig. 45(b). The ratio of their r.m.s. values gives us the value of  $\alpha_{rms}$ . Unfortunately  $\alpha(\tau)[\ddot{x}/\Omega_n^2 x_{IC}]$  has some power above 4 Hz, as may clearly be seen on Fig. 45(a). The value of 4 Hz being our upper analysis limit, the values of  $\alpha_{rms}$  indicated here are therefore minimum values.

The results below have been obtained by using equation (5-7) — which is equivalent to the circuit diagram given in Fig. 42 — of course including the forcing function. It should also be mentioned that, in order to have a broader peak and not too high a resonance peak, the value of  $\zeta$  has been increased to 0.02 and also 0.05.

$\zeta$	$\alpha_{rms}$ (minimum value)	$\zeta$ measured <sup>§</sup> at half-power point	$(\frac{\Omega}{\Omega_n})$ resonance
0.02	0	0.0205	1.0005
"	0.10	0.022	1.002
0.05	0	0.05	0.998
"	0.10	0.0515	0.998
"	0.32	0.059	1.032

<sup>§</sup>Here " $\zeta$  measured" is calculated as  $\zeta = \Delta\Omega/2$ , where  $\Delta\Omega$  is the frequency interval between the two points located at  $x_{max}/\sqrt{2}$ .

Again, we obtain results which are coincident with those already found in the free vibration cases. As a matter of fact, the shift towards higher frequencies is very weak, only of 0.2% for  $\alpha_{\text{rms}} = 0.10$  (when  $\zeta = 0.02$ ; even less when  $\zeta = 0.05$ ), and of 3.2% for  $\alpha_{\text{rms}} = 0.32$ . It is simply recalled that the effect sought is of the order of 6%, and should occur below the upper "realistic" bound of  $\alpha_{\text{rms}} = 0.20$ . Nevertheless, the effect sought appears and, moreover, occurs in the desired direction and this, by itself, can be considered as a positive result.

Fortunately, this also occurs for damping, and it may be worth mentioning that it is the first time that this effect appears so significantly (in the previous free vibration studies it was never very evident). However, we remain far from the desired effect of 100%, since for  $\alpha_{\text{rms}} = 0.10$  the effect is of 10% (when  $\zeta = 0.02$ ) or only 3% (when  $\zeta = 0.05$ ), and only 18% (when  $\zeta = 0.05$ ) for  $\alpha_{\text{rms}} = 0.32$ .

Another finding can be presented here: mostly when  $(\Omega/\Omega_n) > 1.3$ , and even below when  $\alpha_{\text{rms}} = 0.32$ , the power spectral density of the response exhibits not only the sharp peak at  $f = f_f$  (forcing frequency), but also a broader peak about the natural frequency  $f_n = 1.4$  Hz [see Figs. 46(a) and (b), and equally Fig. 44 on which it clearly appears that the pseudo-random response is above the deterministic response — i.e., when  $\alpha(\tau) = 0$ ]. This, of course, does not occur for a classical oscillator. For  $\alpha_{\text{rms}} = 0.32$ , this broad peak contains much more power than the sharp peak at the forcing frequency. But nevertheless this unexpected effect is not important as far as the determination of the damping is concerned, since it becomes significant far enough from the resonance region, even though it already appears with a very small peak when  $f_f$  is below  $f_n$ .

Finally, in the hope of discovering a more important effect, an attempt is made to apply pseudo-random perturbations, not only on the mass coefficient, but also on the damping coefficient. Equation (5-7) is thus modified, for the forced case of course, into equation (5-8):

$$\begin{aligned} \left[ \frac{\ddot{x}(\tau)}{\Omega_n^2 x_{IC}} \right] = & -2\zeta \left[ \frac{\dot{x}(\tau)}{\Omega_n x_{IC}} \right] - \left[ \frac{x(\tau)}{x_{IC}} \right] - \alpha_1(\tau) \left[ \frac{\ddot{x}(\tau)}{\Omega_n^2 x_{IC}} \right] \\ & - 2\zeta \delta \alpha_2(\tau) \left[ \frac{\dot{x}(\tau)}{\Omega_n x_{IC}} \right] + F^o \sin \Omega_f \tau. \end{aligned} \quad (5-8)$$

Two cases are distinguished:

$$\delta = 1 \quad \text{Equation (5-8,a)}$$

$$\delta = -1 \quad \text{Equation (5-8,b).}$$

The procedure is exactly similar to the one used previously (for  $\delta=0$ ).

The results obtained are shown in the table below.

$\delta$	$\zeta$	$\alpha_{1rms}$ (minimum value)	$\alpha_{2rms}$ (minimum value)	$\zeta$ measured at half- power point	$\left(\frac{\Omega}{\Omega_n}\right)$ resonance
+1	0.05	0.32	0.032	0.058	1.024
"	"	0.32	0.32	0.047	1.029
"	"	0.032	0.32	0.049	0.997
-1	0.05	0.32	0.032	0.0565	1.03
"	"	0.32	0.32	0.059	1.03

The effect of applying such random perturbations on the damping coefficient  $\zeta$  is not very evident and, anyway, generates no important new kind of behaviour of the system. Adding the perturbations  $\alpha_2(\tau)$ , however,

seems to lower the effective damping, whereas subtracting it increases the response damping.

We could also consider applying such pseudo-random perturbations on the last coefficient of the second-order differential equation envisaged, namely the stiffness coefficient, but no interesting effect is suspected, at least from the hydrodynamic mass point of view.

Therefore, the first results obtained in this Section 5.3 with  $\alpha_2(\tau) = 0$  are the most significant found with the one-degree-of-freedom model and agree, at least qualitatively, with Carlucci's experimental discoveries.

## CHAPTER VI

### CONCLUSION

The behaviour of the hydrodynamic mass and damping of a flexible cylinder immersed in two-phase axial flow was investigated in this research. It was in fact attempted to explain the two effects observed by Carlucci in simulated two-phase flow, namely a significant increase of damping, depending on the flow regime, and a decrease of the hydrodynamic mass occurring at a higher rate than that of the mixture density. The basic hypothesis made is that these two effects arise from random perturbations affecting the hydrodynamic mass. In fact this question brings us to the very nature of the fluid-structure coupling, this interaction being essentially probabilistic due to the presence of two-phase flow.

After a too involved theoretical attempt, aiming at obtaining a general model of the fluid-structure interaction by starting from a molecular level, it was decided to dwell on a numerical simulation of a one-degree-of-freedom system. The purpose was then to verify whether the fact of applying pseudo-random perturbations (pseudo-random because they are generated artificially) can account for the two effects described by Carlucci. With this model, three studies have been conducted in which both the response frequency and damping were the parameters of interest. The two first studies were digital, whereas the last was analog (the first was conducted in the time domain, and the two others in the frequency domain).

The results of these three approaches are consistent, the last, however, being the most explicit. Agreement is best, as far as the response

frequency is concerned. As a matter of fact, a shift towards higher frequencies is exhibited in all three studies, and this is in agreement with a decrease of the hydrodynamic mass. The magnitude of this effect is, however, found to remain weak, namely less than 1% for "realistic" values of perturbation amplitudes. This is low, when compared to the 6% effect found by Carlucci. (On the other hand, for highly "unrealistic" values of the perturbation amplitudes, this value of 6% can be reached, but has not much physical meaning and, moreover, already occurs in the region of perturbation amplitudes which could give rise to instabilities.)

The damping effect does not appear significantly in the two digital approaches, but in the last analog simulation (forced case) a higher damping is exhibited, however, not exceeding 15% (for "realistic" values of the perturbation amplitudes). This is still small when compared to the 100% expected, which corresponds to Carlucci's observations.

It is true that the model investigated is not very sophisticated, especially for such a complex system. This could explain why the expected magnitude for the effects involved was not obtained. Nevertheless, the fact of having obtained similar results by the three approaches implemented can by itself be considered as a partial success.

It could also simply be that the two effects sought are not, or are not mainly, the consequence of random fluctuations of the added mass, but are due to another, still unknown, cause.

We do not think that one should expect much more from such a type of numerical simulation, for example by increasing the number of degrees-of-freedom. The only remaining aspect which could have been interesting to investigate would have been the introduction of a time

delay between two pseudo-random added mass perturbations  $\alpha(\tau)$  applied to the two mass coefficients of a two-degree-of-freedom system. This would have modelled the propagation of the flow disturbances on the surface of the cylinder, along the axis of the cylinder.

However, it will be very interesting to develop fundamental research on the fluid-solid interaction, in the future, by starting at the molecular level and implementing the transition to the macroscopic level by use of the theory of stochastic processes. Proper modelling of two-phase flow is in itself still a challenge for science. A good understanding of the fluid-structure interaction would finally provide a continuous passage between solid and fluid mechanics and a general theory of flow-induced vibrations.

## REFERENCES

1. Blevins, R.D., "Flow-Induced Vibration", Van Nostrand Reinhold Co., New York, 1977.
2. Bisplinghoff, R.L., Ashley, H., & Halfman, R.L., "Aeroelasticity", Addison-Wesley Publishing Company, Reading, Mass., 1955.
3. Dowell, E.H., "Panel Flutter: A Review of the Aeroelastic Stability of Plates and Shells", AIAA Journal, Vol.8, 1970, pp.385-399.
4. Dowell, E.H., "Aeroelasticity of Plates and Shells", Noordhoff International Publishing, Leyden, 1975.
5. Hawthorne, W.R., "The Early Development of the Dracone Flexible Barge", Proceedings of the Institution of Mechanical Engineers, Vol.175, 1961, pp.52-83.
6. Paidoussis, M.P., "Stability of Towed, Totally Submerged Flexible Cylinders", Journal of Fluid Mechanics, Vol.34, 1968, pp.273-297.
7. Burgreen, D., Byrnes, J.J., & Benforado, D.M., "Vibration of Rods Induced by Water in Parallel Flow", Transactions of the ASME, Vol. 80, 1958, pp.991-1003.
8. Paidoussis, M.P., "Dynamics of Flexible Slender Cylinders in Axial Flow. Part 1: Theory; Part 2: Experiments", Journal of Fluid Mechanics, Vol.26, 1966, pp.717-736 and 737-751.
9. Chen, S.-S., & Wambsganss, M.W., "Parallel-Flow-Induced Vibration of Fuel Rods", Nuclear Engineering & Design, Vol.18, 1972, pp.253-278.
10. Paidoussis, M.P., "Dynamics of Cylindrical Structures Subjected to Axial Flow", Journal of Sound & Vibration, Vol.29, 1973, pp.365-385.
11. Chen, S.-S., "Vibration of Nuclear Fuel Bundles", Nuclear Engineering & Design, Vol.35, 1975, pp.399-422.
12. Paidoussis, M.P., "The Dynamics of Clusters of Flexible Cylinders in Axial Flow: Theory and Experiments", Journal of Sound & Vibration, Vol.65, 1979, pp.391-417.

13. Paidoussis, M.P., "Vibration of Cylindrical Structures Induced by Axial Flow", Transactions of the ASME, Journal of Engineering for Industry, Vol.96, 1974, pp.547-552.
14. Paidoussis, M.P., "The Dynamical Behaviour of Cylindrical Structures in Axial Flow", Annals of Nuclear Science & Engineering (Annals of Nuclear Energy), Vol.1, 1974, pp.83-106.
15. Chen, S.-S., "Parallel Flow-Induced Vibrations and Instabilities of Cylindrical Structures", Shock & Vibration Digest, Vol.6, 1974, pp.2-12.
16. Shin, Y.S., & Wambsganss, M.W., "Flow-Induced Vibration in LMFBR Steam Generators: A State-of-the-Art Review", Nuclear Engineering & Design, Vol.40, 1977, pp.235-284.
17. Lane, A.D., et al., "The Measurement and Prediction of Vibration in CANDU-PHW Fuel and Channel Assemblies", Paper 1.1, Proc. Int'l Conf. on Vibration in Nuclear Plant (ViNP), Keswick, May 1978.
18. Pettigrew, M.J., Sylvestre, Y., & Campagna, A.O., "Vibration Analysis of Heat Exchanger and Steam Generator Designs", Nuclear Engineering Design, Vol.48, 1978, pp.97-115.
19. Paidoussis, M.P., "Flow-Induced Vibrations in Nuclear Reactors and Heat Exchangers: Practical Experiences and State of Knowledge", in [20], pp.1-81.
20. "Practical Experiences with Flow-Induced Vibrations", Proceedings of IAHR/IUTAM Symposium, Karlsruhe, Sept. 1979, ed. E. Naudascher and D. Rockwell; Springer-Verlag, Berlin, 1980.
21. Paidoussis, M.P., "Fluidelastic Vibration of Cylinder Arrays in Axial and Cross Flow: State of the Art", Journal of Sound & Vibration, Vol.76, 1981, pp.329-360.
22. Shin, Y.W., "Two-Phase Flow-Induced Vibrations of Rods In Parallel Flow: A State-of-the-Art Review", General Electric Report GEAP-24148, Oct. 1978.

23. Belytschko, T., & Schumann, U., "Fluid-Structure Interactions in Light Water Reactor Systems", Nuclear Engineering & Design, Vol.60, 1980, pp.173-195.
24. Hara, F., "A Theory on the Vibrations of a Fuel Pin Model in Parallel Two-Phase Flow", Paper D2/4, Trans. 3rd Int'l Conf. on Structural Mechanics in Reactor Technology (SMiRT), London, Sept. 1975.
25. Hara, F., "Experimental Study of the Vibrations of a Fuel Pin Model in Parallel Two-Phase Flow", Paper D2/3, 3rd SMiRT, London, Sept. 1975.
26. Hara, F., & Yamashita, T., "Parallel Two-Phase-Flow-Induced Vibrations in Fuel Pin Model", Journal of Nuclear Science and Technology, Vol.15, 1978, pp.346-354.
27. Pettigrew, M.J., & Gorman, D.J., "Experimental Studies on Flow Induced Vibration to Support Steam Generator Design, Part I: Vibration of a Heated Cylinder in Two-Phase Axial Flow", Paper 424, Proc. Int'l Symp. on Vibration Problems in Industry (VPII), Keswick, April 1973.
28. Gorman, D.J., "An Analytical and Experimental Investigation of the Vibration of Cylindrical Reactor Fuel Elements in Two-Phase Parallel Flow", Nuclear Science & Engineering, Vol.44, 1971, pp.277-290.
29. Cedolin, L., Hassid, A., Rossini, T., & Solieri, R., "Vibrations Induced by the Two-Phase (Gas and Liquid) Coolant Flow in the Power Channels of a Pressure Tube Type Nuclear Reactor", Paper E4/5, 1st SMiRT, Berlin, Sept. 1971.
30. Pettigrew, M.J., & Paidoussis, M.P., "Dynamics and Stability of Flexible Cylinders Subjected to Liquid and Two-Phase Axial Flow in Confined Annuli", Paper D2/6, 3rd SMiRT, London, Sept. 1975.
31. Paidoussis, M.P., & Pettigrew, M.J., "Dynamics of Flexible Cylinders in Axisymmetrically Confined Flow", Journal of Applied Mechanics, Vol.46, 1979, pp.37-44.
32. Carlucci, L.N., "Hydrodynamic Mass and Fluid Damping of Rod Bundles Vibrating in Confined Water and Air-Water Mixtures", Paper D3/11, 4th SMiRT, San Francisco, August 1977.

33. Carlucci, L.N., "Damping and Hydrodynamic Mass of a Cylinder in Simulated Two-Phase Flow", Transactions of the ASME, Journal of Mechanical Design, Vol.102, 1980, pp.597-602.
34. Ostoja-Starzewski, M., "Dynamics of a Single Flexible Cylinder in External Axial Compressible Fluid Flow", M.Eng. Thesis, Dept. Mech. Eng., McGill University, May 1980.
35. Paidoussis, M.P., & Ostoja-Starzewski, M., "Dynamics of a Flexible Cylinder in Subsonic Axial Flow", Paper 81-0605-CP, AIAA/ASME/ASCE/AHS 22nd Structures, Structural Dynamics & Materials Conference, Atlanta, April 1981, published as AIAA Publication CP812, AIAA Journal, Vol.19, 1981, pp.1467-1475.
36. Schumann, U., "Virtual Density and Speed of Sound in Fluid-Solid Mixture with Periodic Structure", to be published in the Int. Journal of Multiphase Flow.
37. Collier, J.G., "Convective Boiling and Condensation", McGraw-Hill, London, 1972.
38. Hewitt, G.F., & Roberts, D.N., "Studies of Two-Phase Flow Patterns by Simultaneous X-Ray and Flash Photography", AERE-M2159, H.M.S.O., 1969.
39. Baker, O., "Design of Pipe Lines for Simultaneous Flow of Oil and Gas", Oil and Gas Journal, 26 July, 1954.
40. Milne-Thomson, L.M., "Theoretical Hydrodynamics", Chapter IX, The MacMillan Company, London, 1968 (5th edition).
41. Morton, J.B., & Corrsin, S., "Experimental Confirmation of the Applicability of the Fokker-Planck Equation to a Nonlinear Oscillator", Journal of Mathematical Physics, Vol.10, 1969, pp.361-368.
42. Einstein, A., Annalen der Physik, Vol.17, 1905, p.549, translated in: Einstein, A., "Investigations on the Theory of Brownian Motion", edited with notes by Fürth, R., Dover Publications, Inc., New York, 1956 (unabridged and unaltered republication of the translation originally published in 1926).

43. Uhlenbeck, G.E., & Ornstein, L.S., "On the Theory of Brownian Motion", Physical Review, Vol.36, 1930, pp.823-841; reprinted in [46].
44. Chandrasekhar, S., "Stochastic Problems in Physics and Astronomy", Chapter II, Reviews of Modern Physics, Vol.15, 1943, pp.20-44; reprinted in [46].
45. Wang, M.C., & Uhlenbeck, G.E., "On the Theory of Brownian Motion II", Reviews of Modern Physics, Vol.17, 1945, pp.323-342; reprinted in [46].
46. Wax, N., "Selected Papers on Noise and Stochastic Processes", Dover Publications, Inc., New York, 1954.
47. Nelson, E., "Dynamical Theories of Brownian Motion", Princeton University Press, Princeton, New Jersey, 1967.
48. Doob, J.L., "Stochastic Processes", John Wiley & Sons, Inc., New York, 1953.
49. Feller, W., "An Introduction to Probability Theory and Its Applications", Vol.I, John Wiley & Sons, Inc., New York, 1950 (3rd edition: 1968).
50. Papoulis, A., "Probability, Random Variables, and Stochastic Processes", McGraw-Hill Book Company, New York, 1965.
51. Stern, J., de Barbeyrac, J., & Poggi, R., "Méthodes Pratiques d'Etudes des Fonctions Aléatoires", Dunod, Paris, 1967.
52. Yaglom, A.M., "An Introduction to the Theory of Stationary Random Functions", Prentice-Hall, Inc., Englewood Cliffs, New Jersey, 1962.
53. Beran, M.J., "Statistical Continuum Theories", John Wiley & Sons, Inc., New York, 1968.
54. Samuels, J.C., "Elements of Stochastic Processes", Part VI in: Eringen, A.C., "Continuum Physics", Vol.1, Academic Press, Inc., New York, 1971, pp.605-663.
55. Bharucha-Reid, A.T., "Elements of the Theory of Markov Processes and Their Applications", McGraw-Hill Book Company, New York, 1960.
56. Montroll, E.W., & Lebowitz, J.L., "Fluctuation Phenomena", North-Holland Publishing Company, Amsterdam, 1979.

57. Axelrad, D.R., "Micromechanics of Solids", PWN-Polish Scientific Publishers, Warsaw, and Elsevier Scientific Publishing Company, Amsterdam, 1978.
58. Hansen, J.P., & McDonald, I.R., "Theory of Simple Liquids", Academic Press, Inc. (London) Ltd., London, 1976.
59. Boon, J.P., & Yip, S., "Molecular Hydrodynamics", McGraw-Hill Advanced Series, New York, 1980.
60. Meirovitch, L., "Analytical Methods in Vibrations", The MacMillan Company, New York, 1967.
61. Thomson, W.T., "Theory of Vibration with Applications", Prentice-Hall, Inc., Englewood Cliffs, New Jersey, 1972.
62. "IMSL Library Reference Manual", 8th edition, IMSL, Inc., Houston, Texas, June 1980.
63. "Calcomp Digital Plotter — User's Manual", 6th edition, McGill University Computing Centre, Montreal, Quebec, May 1978.
64. Paidoussis, M.P., Issid, N.T., & Tsui, M., "Parametric Resonance Oscillations of Flexible Slender Cylinders in Harmonically Perturbed Axial Flow. Part 1: Theory", Journal of Applied Mechanics, Vol.47, 1980, pp.709-714.
65. Bolotin, V.V., "The Dynamic Stability of Elastic Systems", Holden-Day, Inc., San Francisco, 1964.
66. Bracewell, R.N., "The Fourier Transform and Its Applications", McGraw-Hill, Inc., New York, 1965.
67. Cooley, J.W., & Tukey, J.W., "An Algorithm for the Machine Calculation of Complex Fourier Series", Journal of Mathematical Computation, Vol.19, 1965, pp.297-301.
68. Brigham, E.O., "The Fast Fourier Transform", Prentice Hall, Inc., New York, 1974.
69. Bergland, G.D., "A Guided Tour of the Fast Fourier Transform", IEEE Spectrum, July 1969, pp.41-52.

70. Collacott, R.A., "Vibration Monitoring and Diagnosis", George Godwin Limited, London, 1979.
71. "Digital Signal Analyzer HP 5420A: User's Guide", Hewlett-Packard, Palo Alto, California, 1978.
72. "EAI 1000: Reference and Maintenance Manual", EAI-Electronic Associates Pty. Ltd., Sydney, Australia, 1978.
73. Korn, G.A., & Korn, T.M., "Electronic Analog Computers", McGraw-Hill, New York, 1956.
74. Bennett, A.W., "Introduction to Computer Simulation", West Publishing Company, St. Paul, 1974.
75. Pettigrew, M.J., "Flow Induced Vibration of Nuclear Power Station Components", Atomic Energy of Canada Limited Report AECL - 5852, Sept. 1977.
76. Proceedings, Symposium on Two-Phase Flow Dynamics, Session V - Propagation Phenomena, B., Eindhoven, Sept. 1967.
77. Yih, T.S., & Griffith, P., "Unsteady Momentum Fluxes in Two-Phase Flow and the Vibration of Nuclear System Components", ANL - 7685, Proc. Conf. on Flow-Induced Vibrations in Reactor System Components, Argonne National Laboratories, Argonne, Illinois, May 1970, pp.91-111.
78. Wallis, G.B., "One Dimensional Two-Phase Flow", McGraw-Hill Book Co., 1969.
79. Parthasarathy, A., "Deterministic and Stochastic Stability of a Nonautonomous Circulatory System", Ph.D. Thesis, Syracuse University, Syracuse, N.Y., 1972.

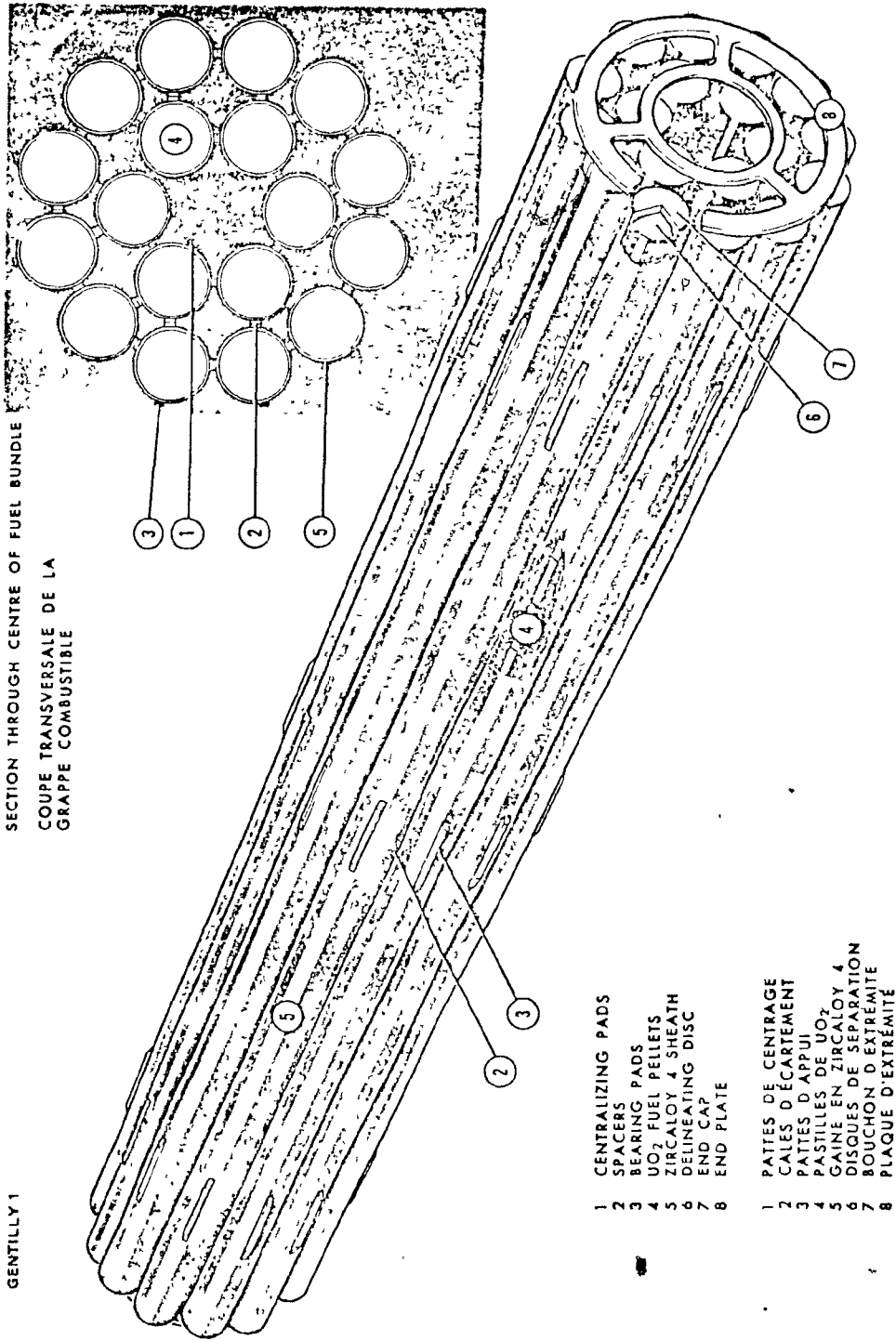


Fig.1. Bundle of nuclear - reactor fuel elements as reproduced in Ref.[75].

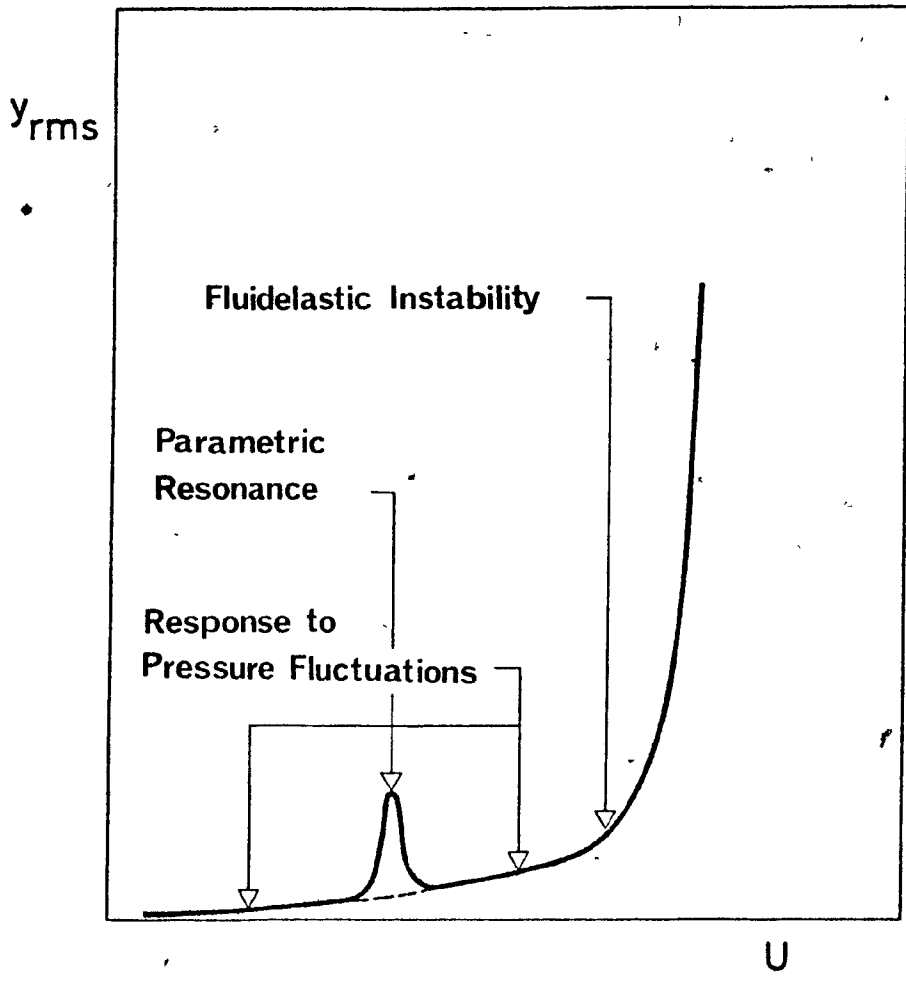


Fig.2. Idealized response of a cylinder, in an array of cylinders subjected to axial flow. (From Ref.[21]).

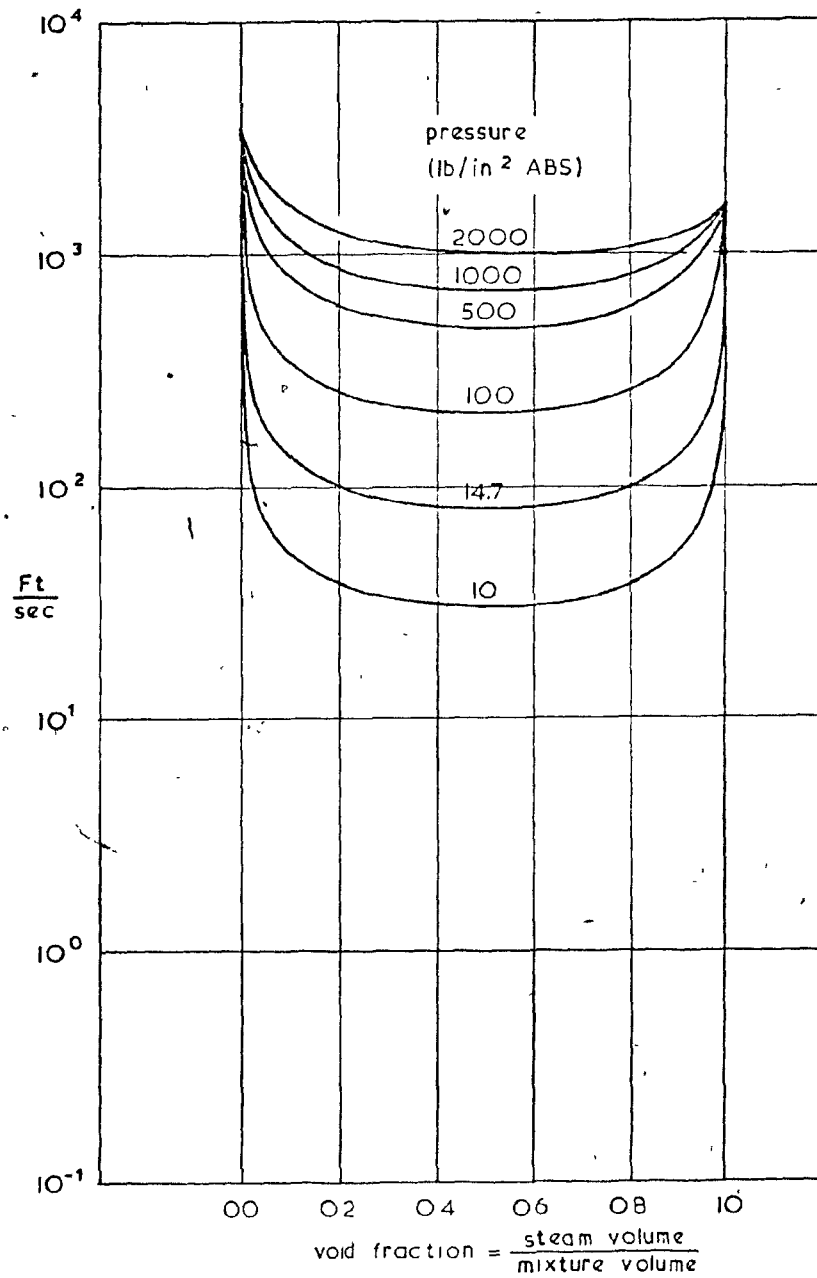


Fig.3. Sonic speed variation with void fraction and according to pressure in a mixture of steam and water. No mass transfer assumed. (From Ref.[76], as reproduced in [34]).

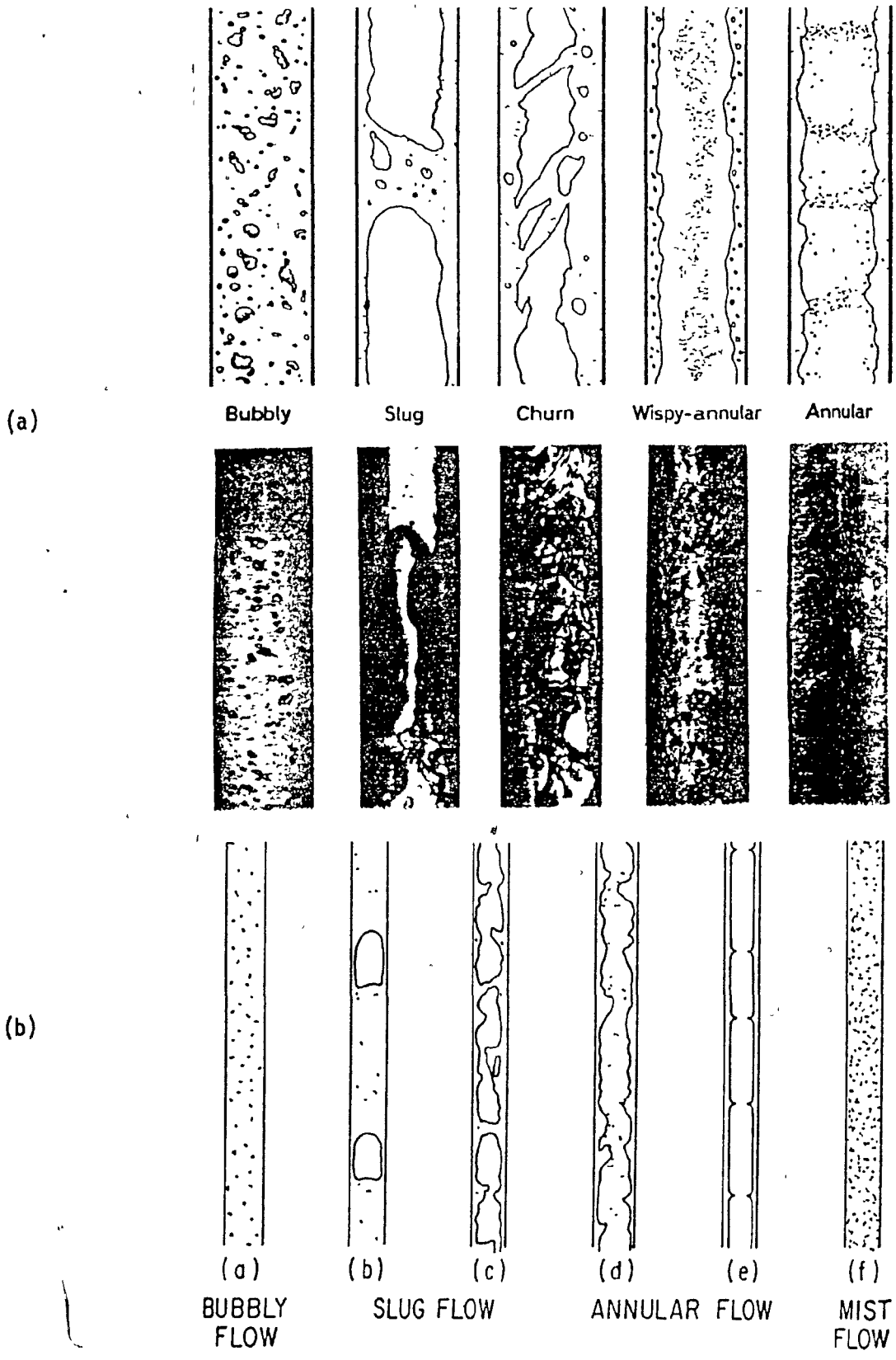


Fig.4. Sketches of flow regime geometries in two-phase vertical upflow.  
 {(a) from Ref.[37]; (b) from Ref.[77] as reproduced in Ref.[22]}.

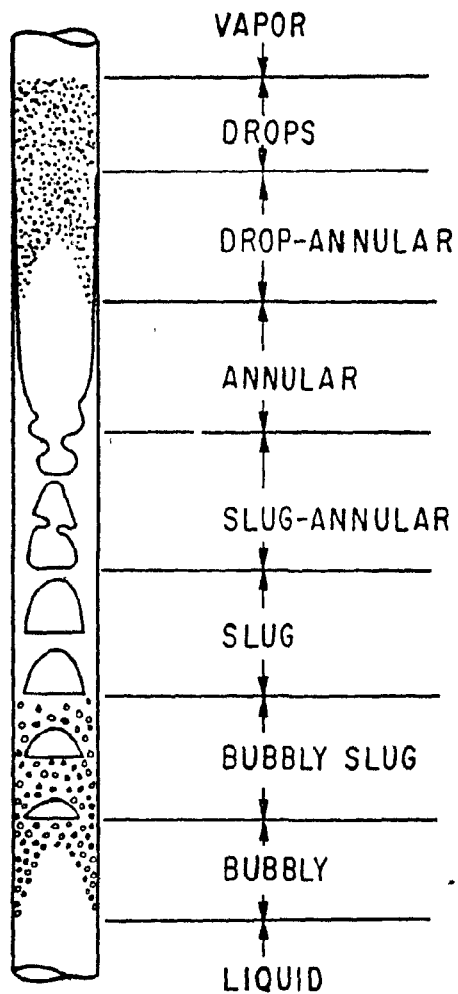


Fig.5. Approximate sequence of flow patterns in a vertical tube evaporator.  
 (From Ref:[78], as reproduced in [22]).

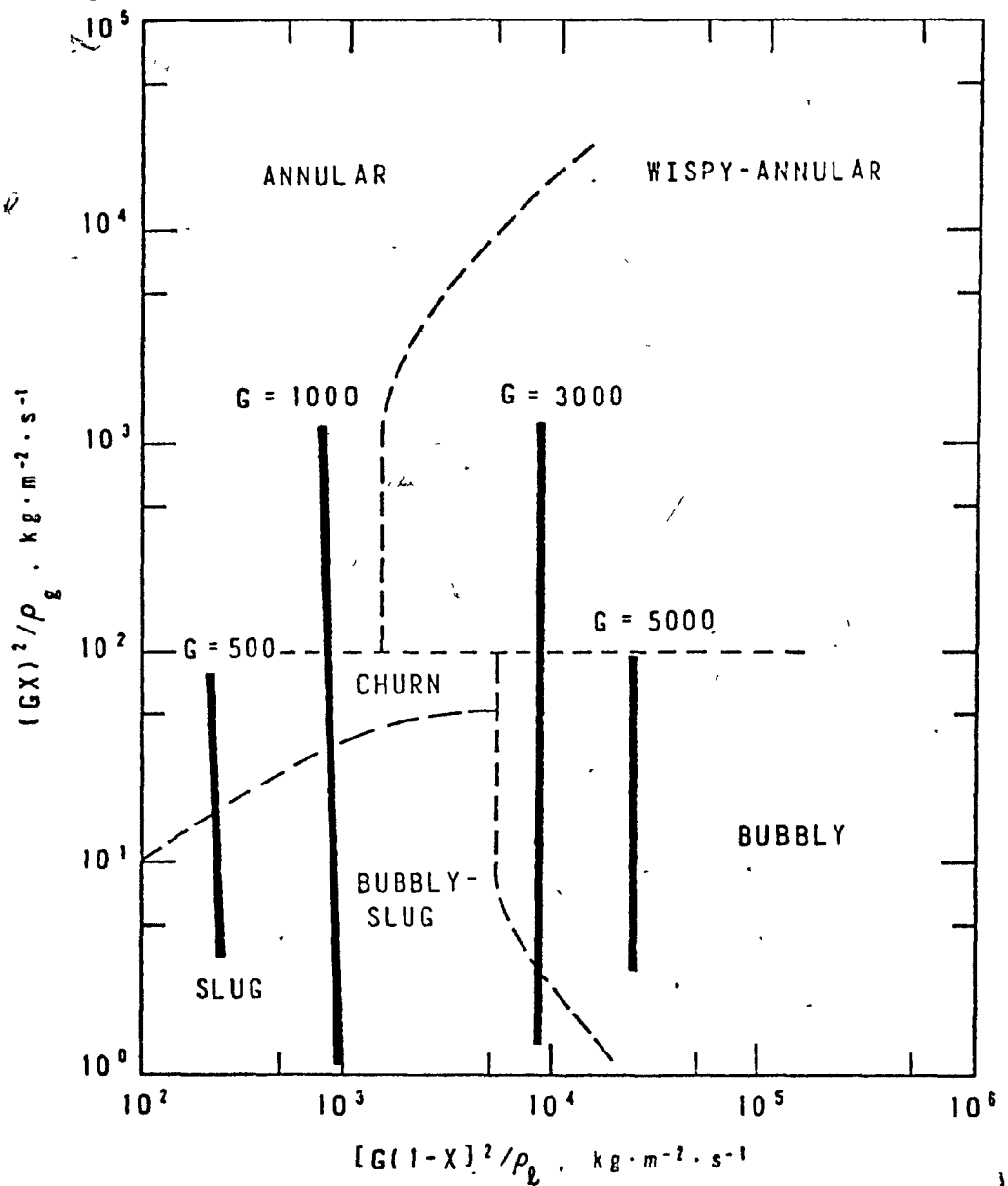


Fig.6. Flow pattern map for vertical upflow [38] as reproduced in [37], on which test conditions covered in [33] are shown as vertical bars.

Mass flux,  $G$ , is in  $\text{kg} \cdot \text{m}^{-2} \cdot \text{s}^{-1}$ ;  $\chi$  is the void fraction,  $\rho_g$  is the density of the gaseous phase and  $\rho_l$  that of the liquid phase.

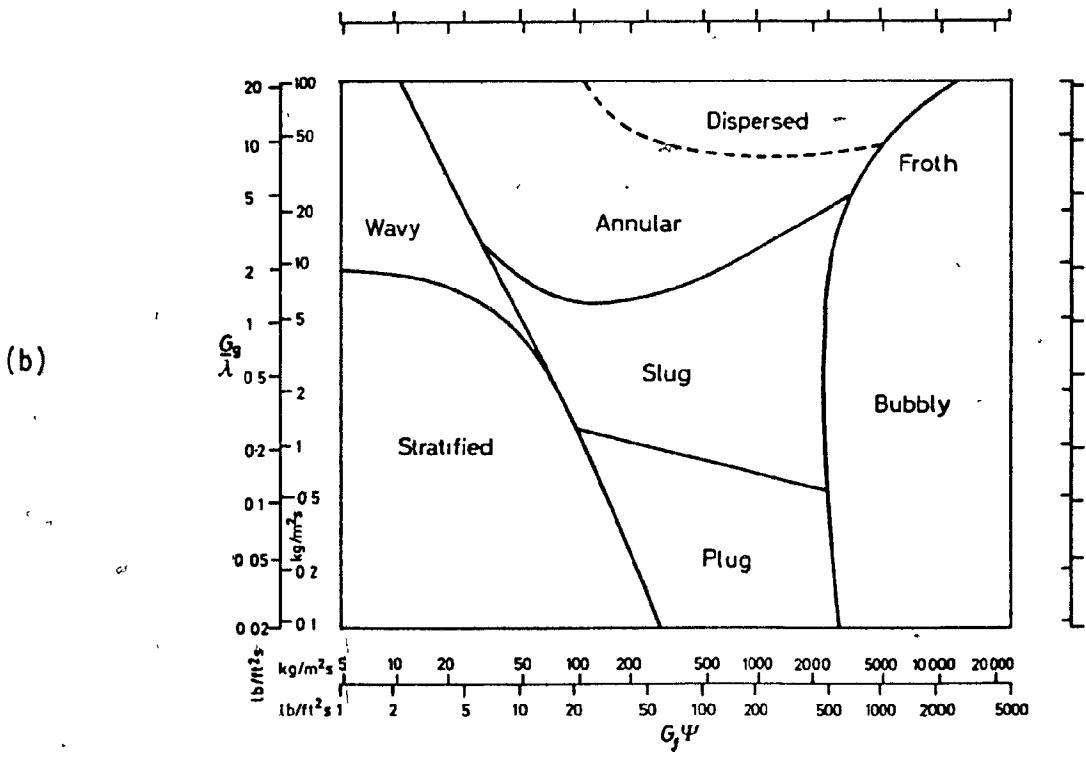
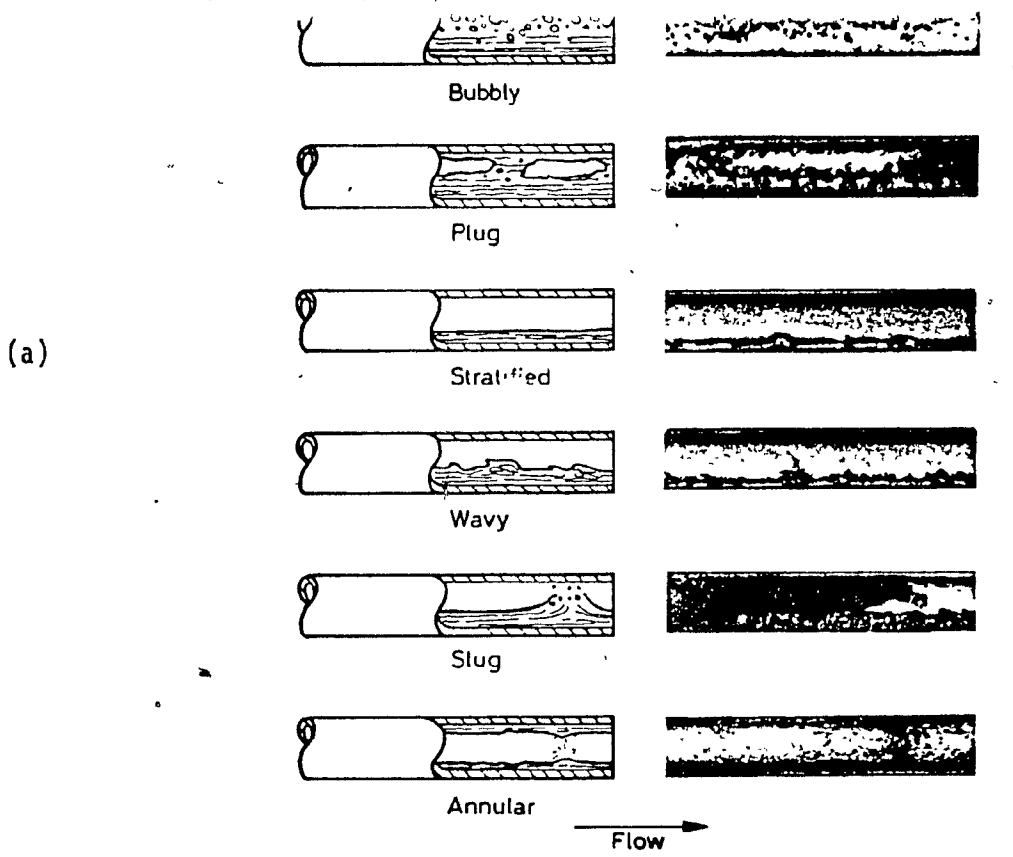


Fig.7. Horizontal flow: (a) Flow regime geometries, and (b) Flow pattern map [39] as reproduced in Ref.[37].

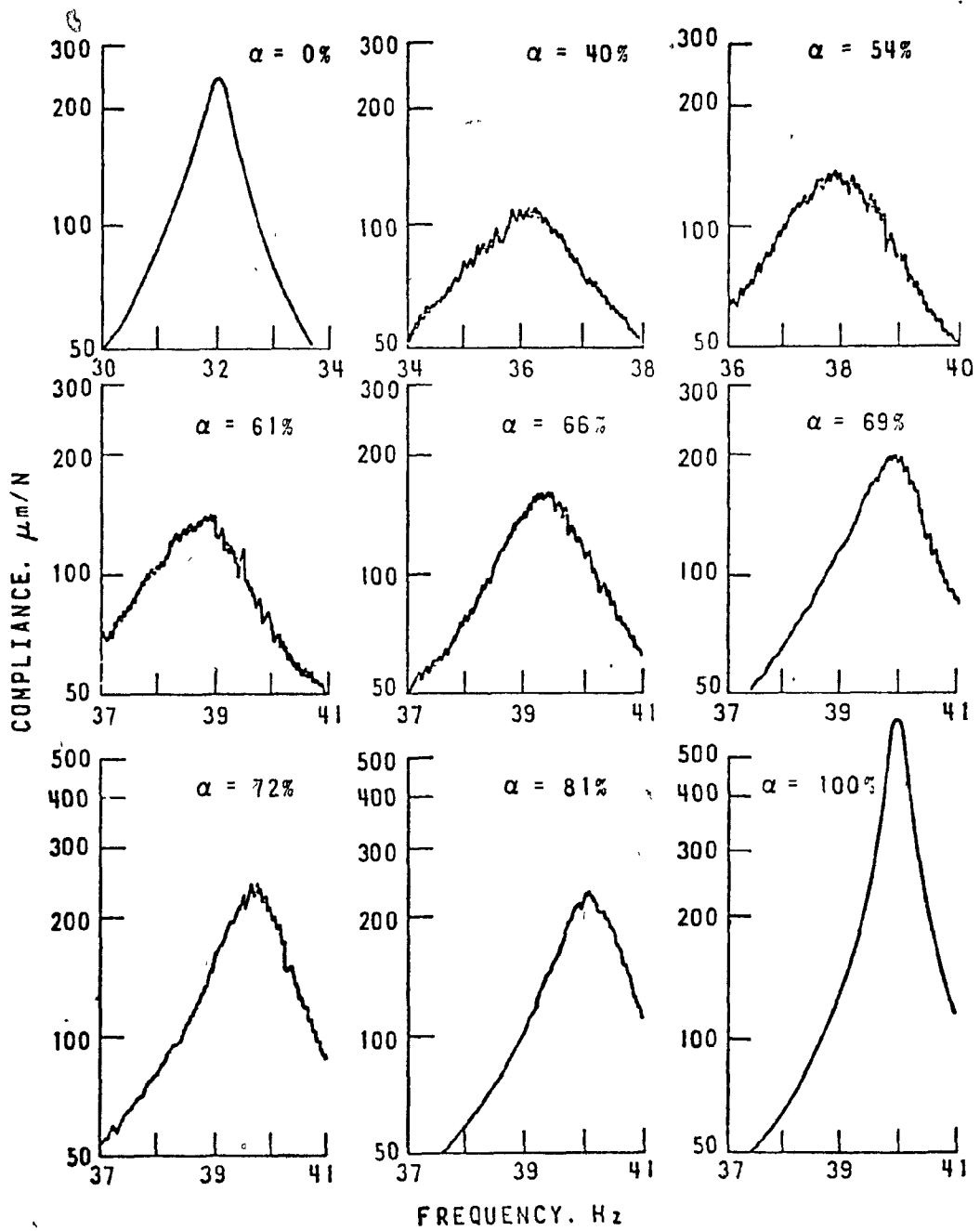


Fig.8. Typical response curves; mass flux =  $1000 \text{ Kg. m}^{-2} \cdot \text{s}^{-1}$ , and flow tube inside diameter =  $31.5 \text{ mm}$ . (From Ref. [33]).

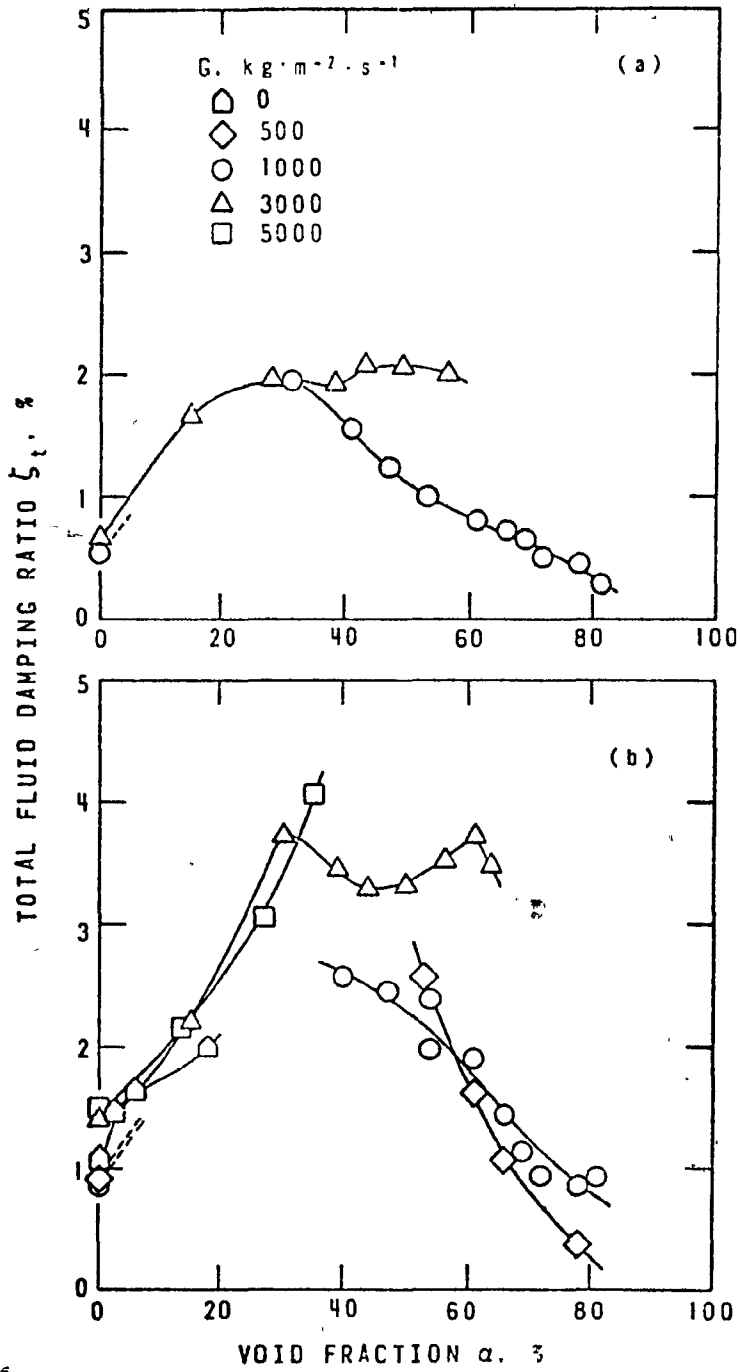


Fig.9. Variation of the total fluid damping ratio with void fraction in flow tubes of inside diameter (a) 40.0 mm and (b) 31.5 mm.

(From Ref.[33]).

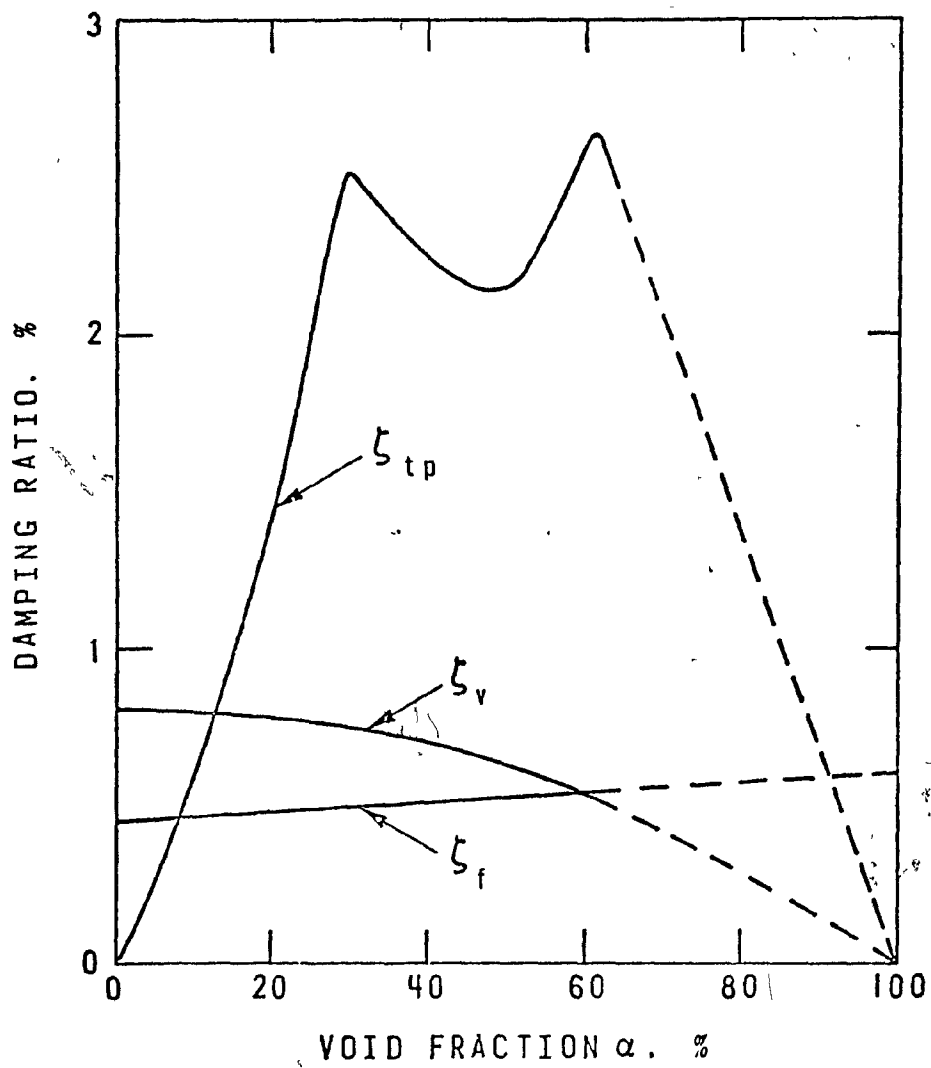


Fig.10. Variation of the components of the total fluid damping ratio with void fraction; mass flux =  $3000 \text{ kg. m}^{-2} \cdot \text{s}^{-1}$ , flow tube inside diameter = 31.5 mm. (From Ref.[33]).

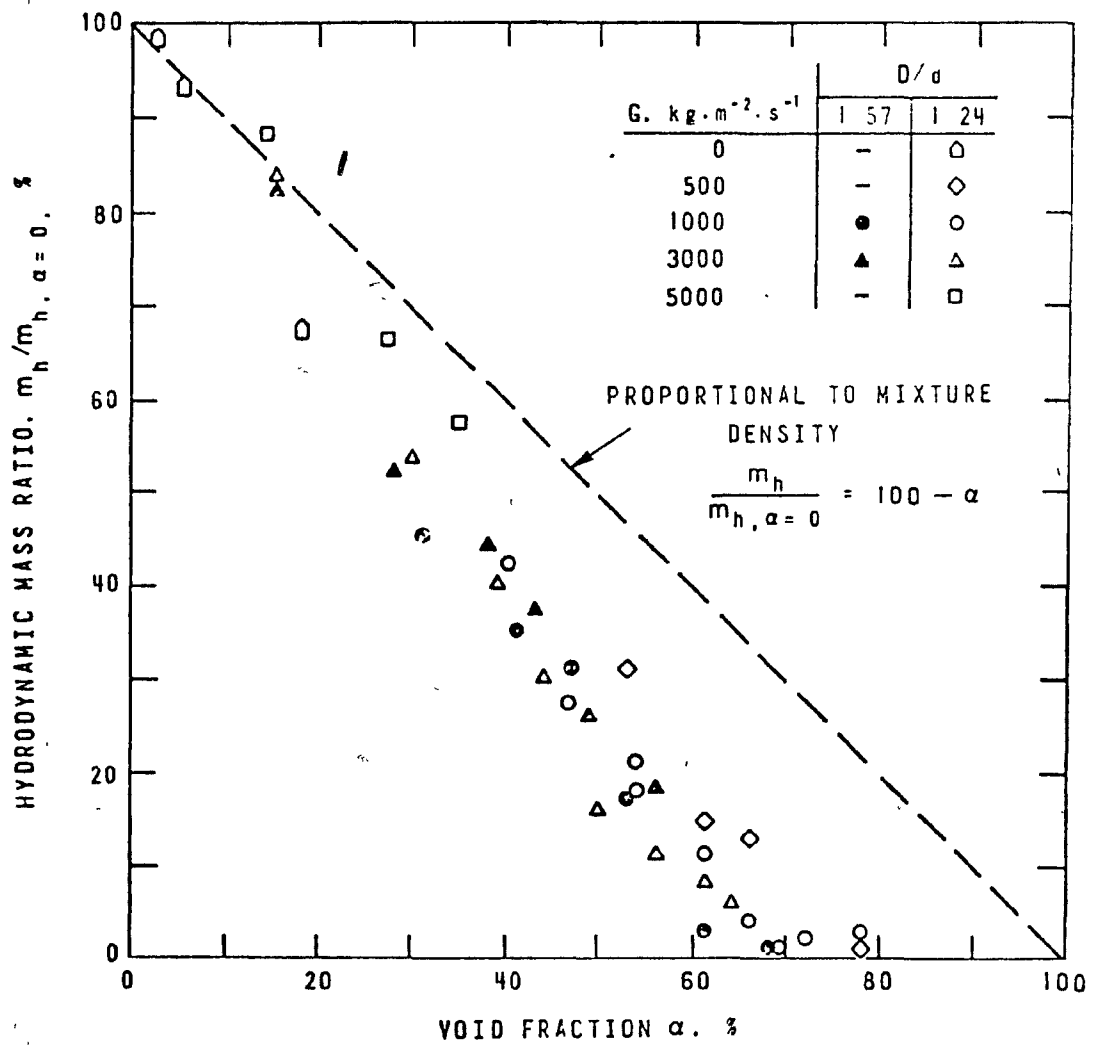


Fig.11. Variation of hydrodynamic mass with void fraction.  
(from Ref.[33]).

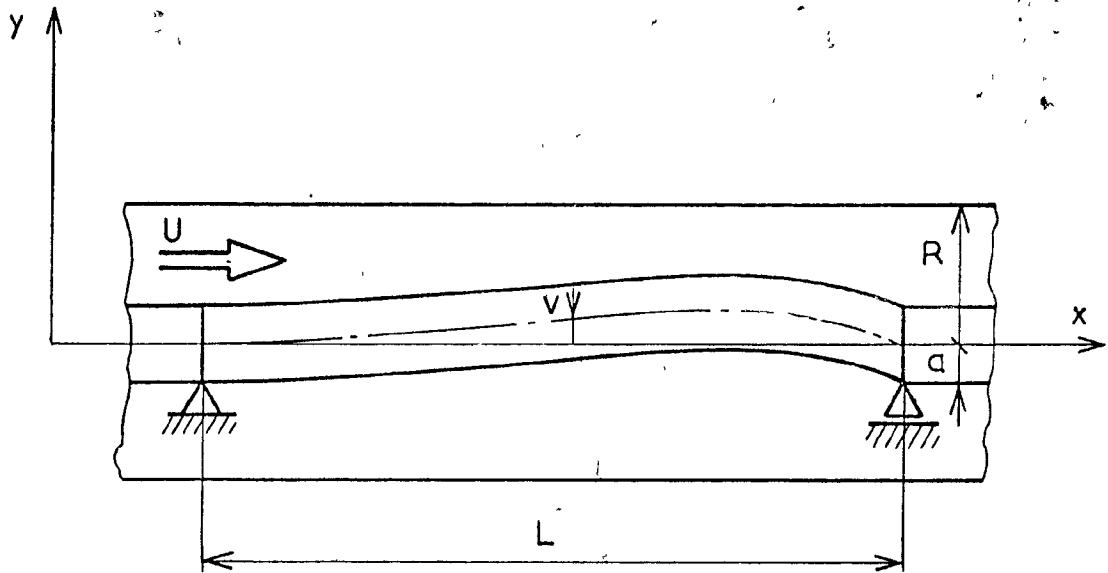


Fig.12. A flexible slender cylinder subjected to bounded axial flow.

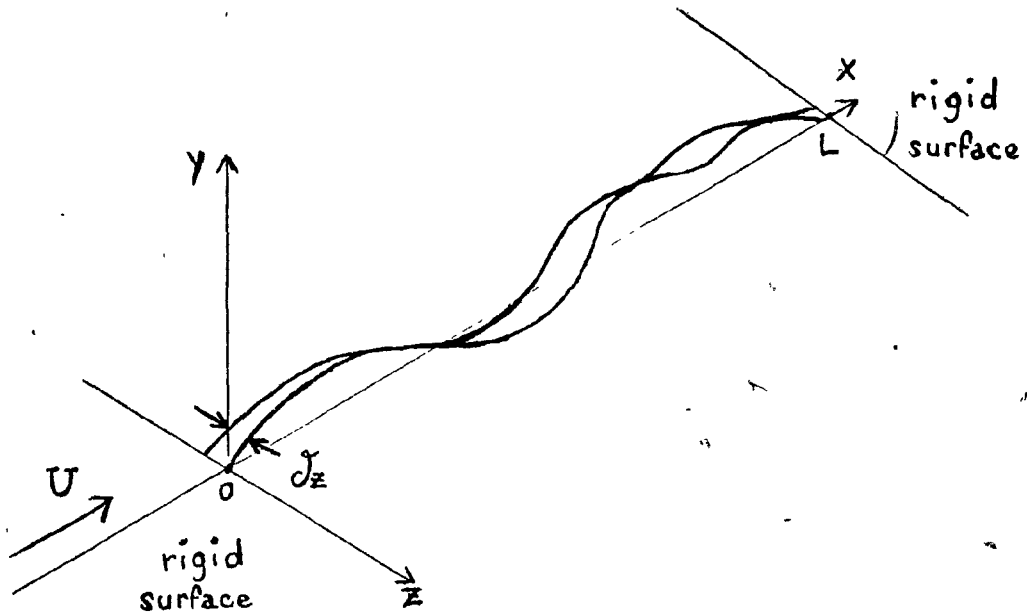


Fig.13(a). Strip of membrane adopted as model of the structure for the probabilistic approach.

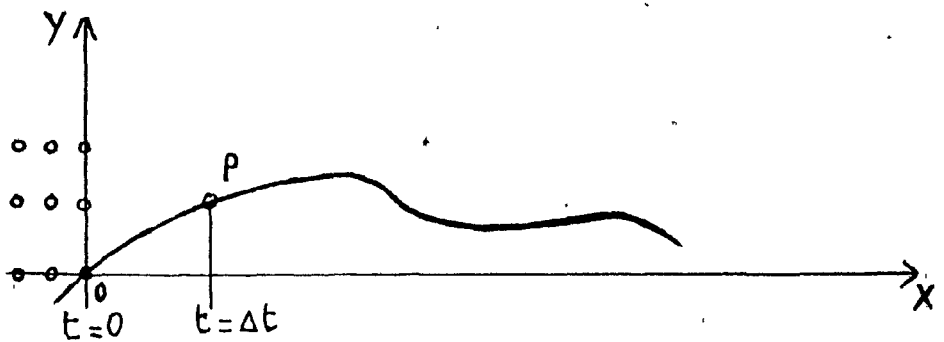


Fig.13(b). Lattice model adopted for the fluid flowing over the membrane (or string) in the probabilistic approach.



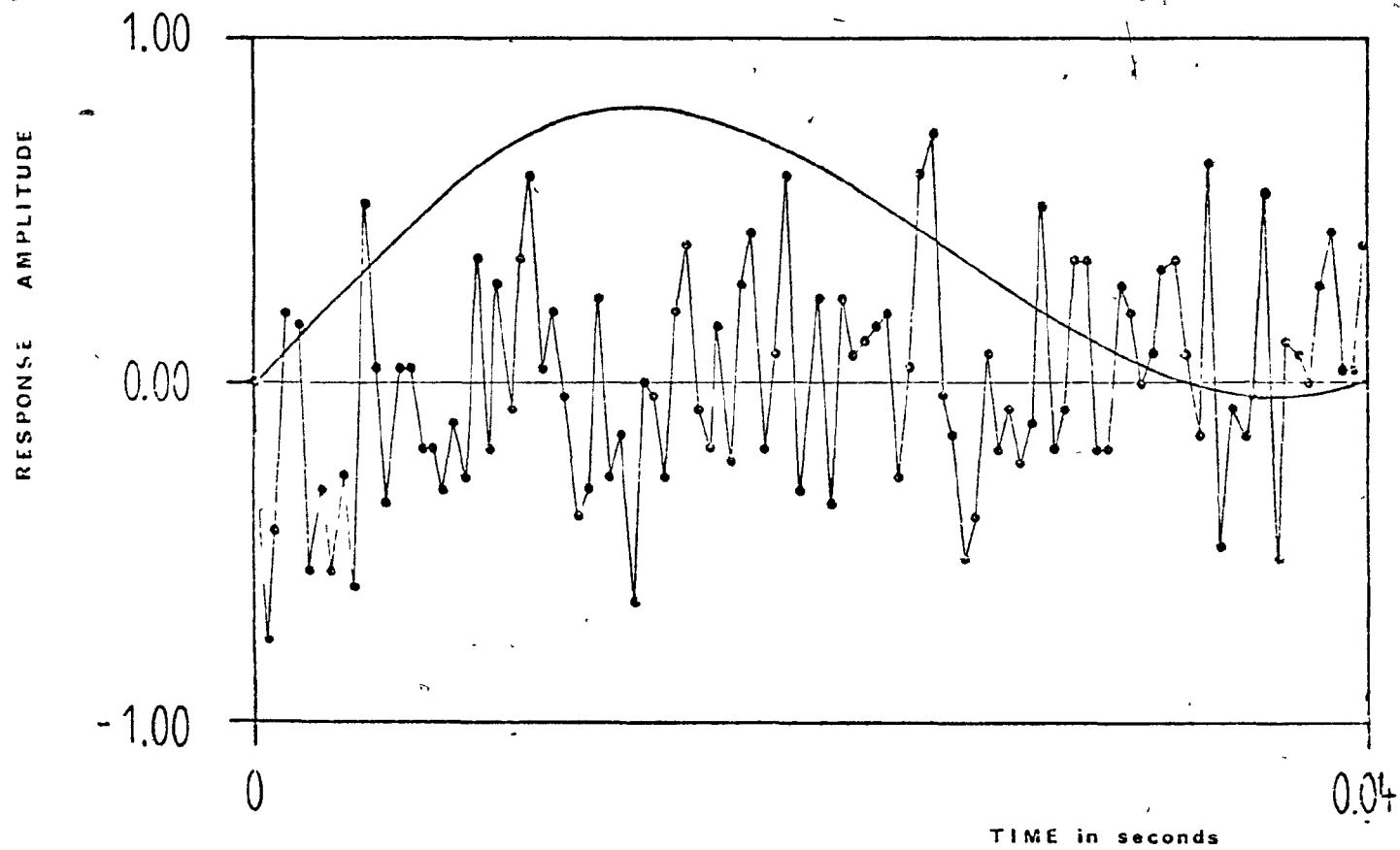


Fig.15(a). Time record of the pseudo-random Gaussian variates generated by the Monte-Carlo method (Appendix C.2), stretching between -1 and +1. These variates are compared to the deterministic  $\alpha(t) = \sum_{i=1}^5 \sin(2\pi f_i t)$ , in which  $f_i = 5, 10, 15, 20, 25$  Hz.

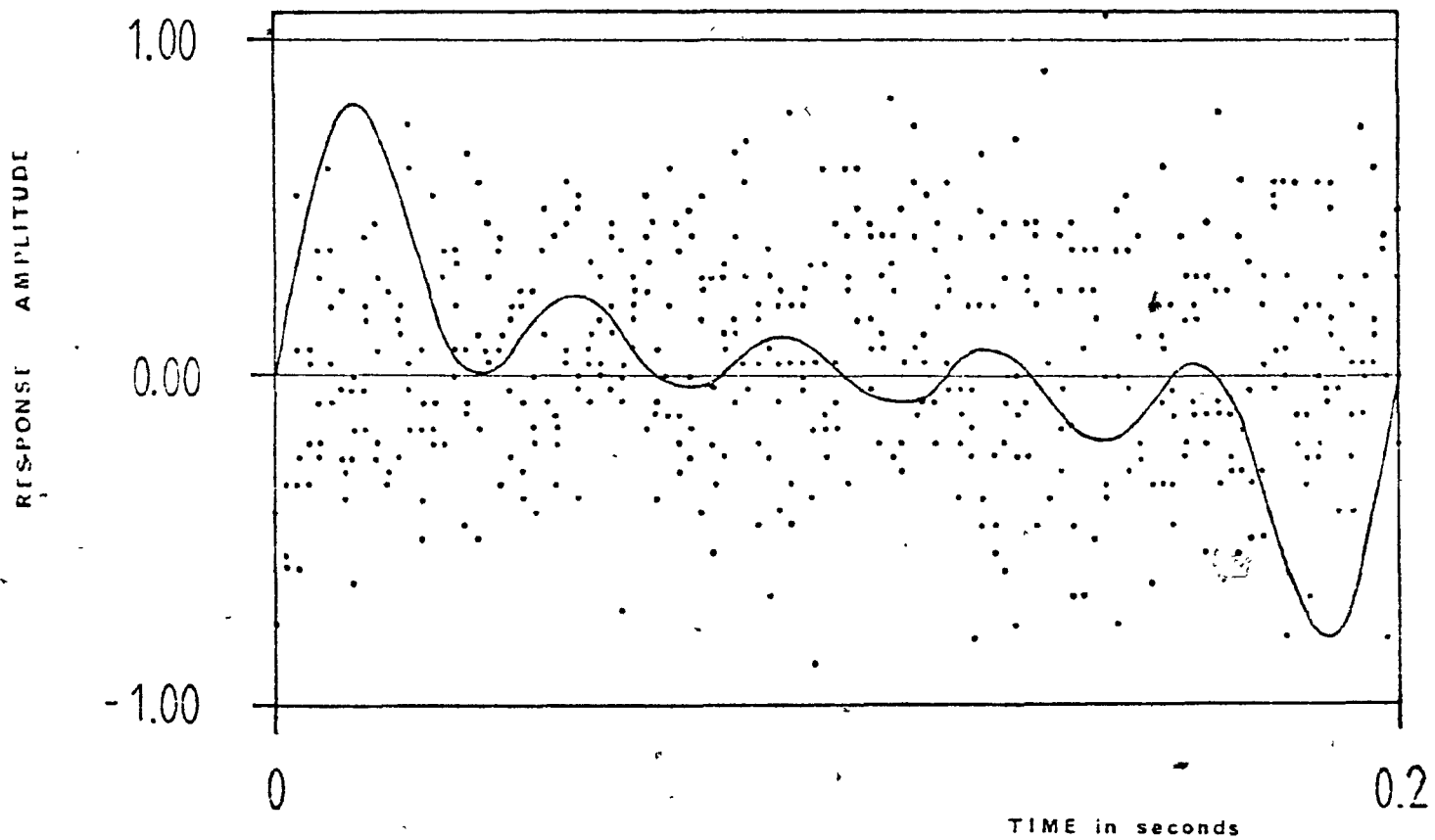


Fig.15(b). Same comparison as in Fig.15(a) between the time records of the pseudo-random and deterministic added mass perturbations, but measured over a longer interval of time (0.2s instead of 0.04s).

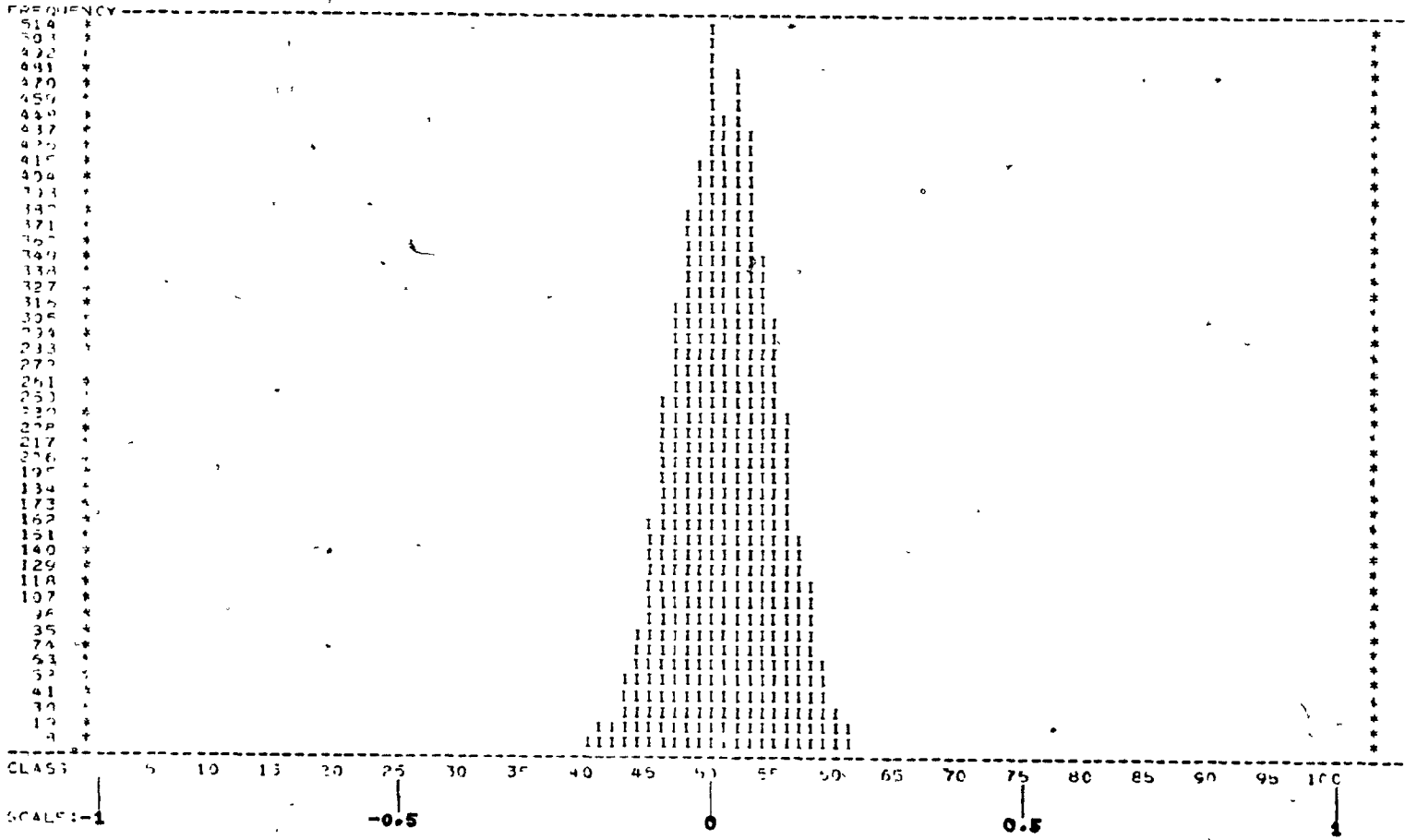


Fig.16(a). Histogram of the pseudo-random Gaussian number generated by the Monte-Carlo algorithm (given in Appendix C.2 and called scheme [c] of  $\alpha(t)$  in Appendix D.2). For  $\bar{\alpha} = 0.25$ .



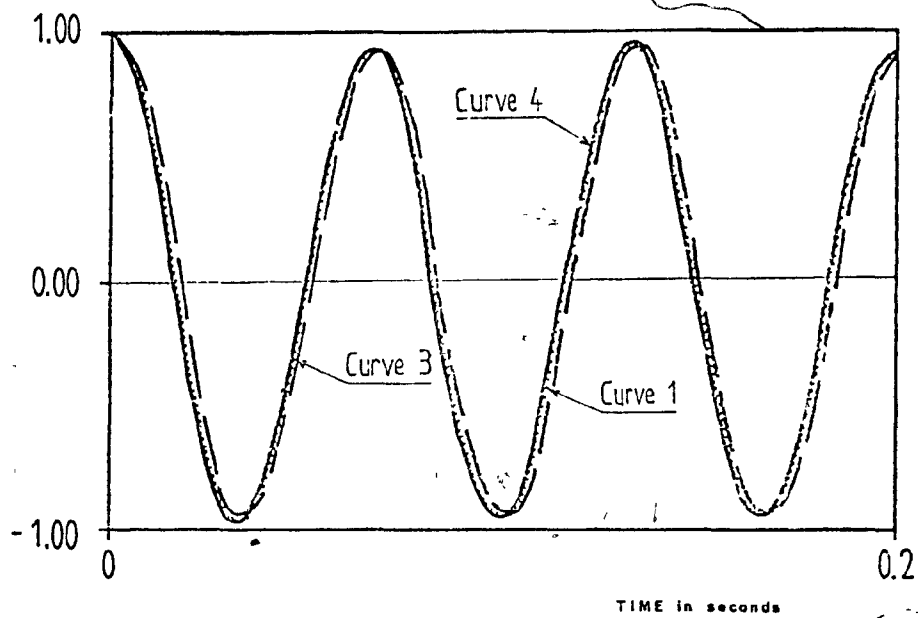


Fig.17(a). Time record of system response, for Run C1 with  $\bar{\alpha} = 0.25$  (see Appendix C.6). Considered for cycles #1,2,3 of Curve 1.

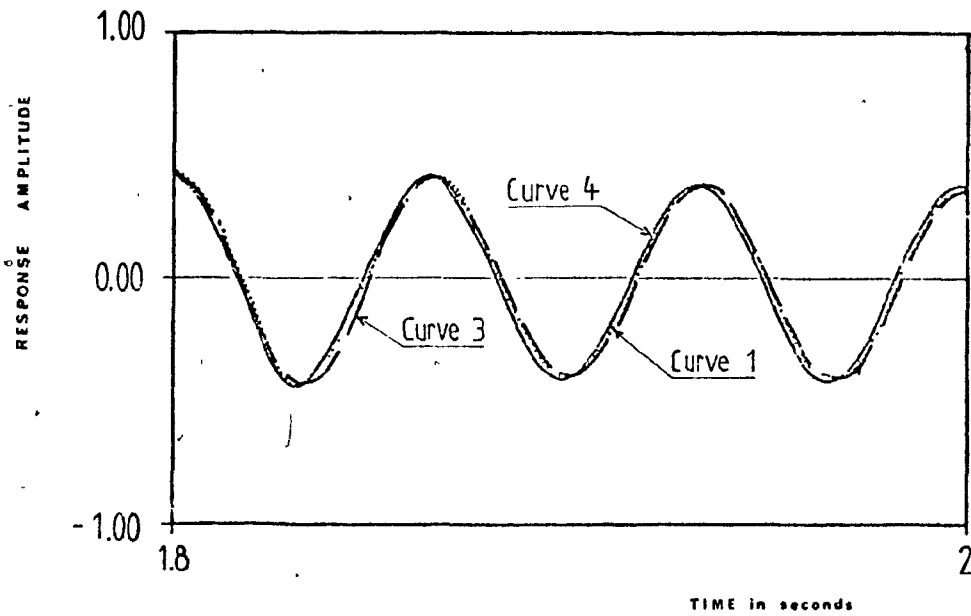


Fig.17(b). Run C1, considered for cycles #28,29,30 of Curve 1.

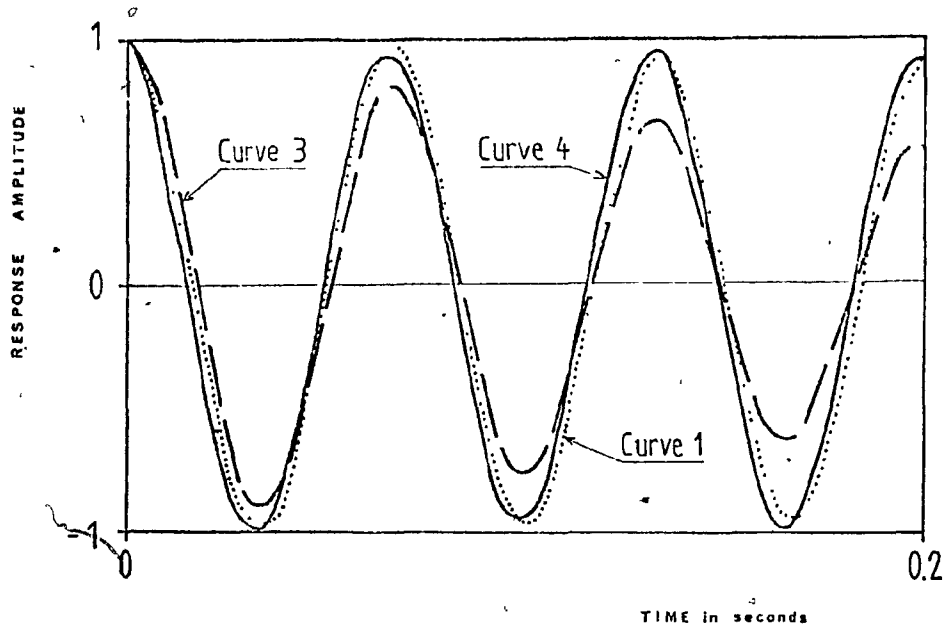


Fig.18(a). Time record of system response, for Run G2 with  $\bar{\alpha} = 0.50$  (see Appendix C.6). Considered for cycles #1,2,3 of Curve 1.

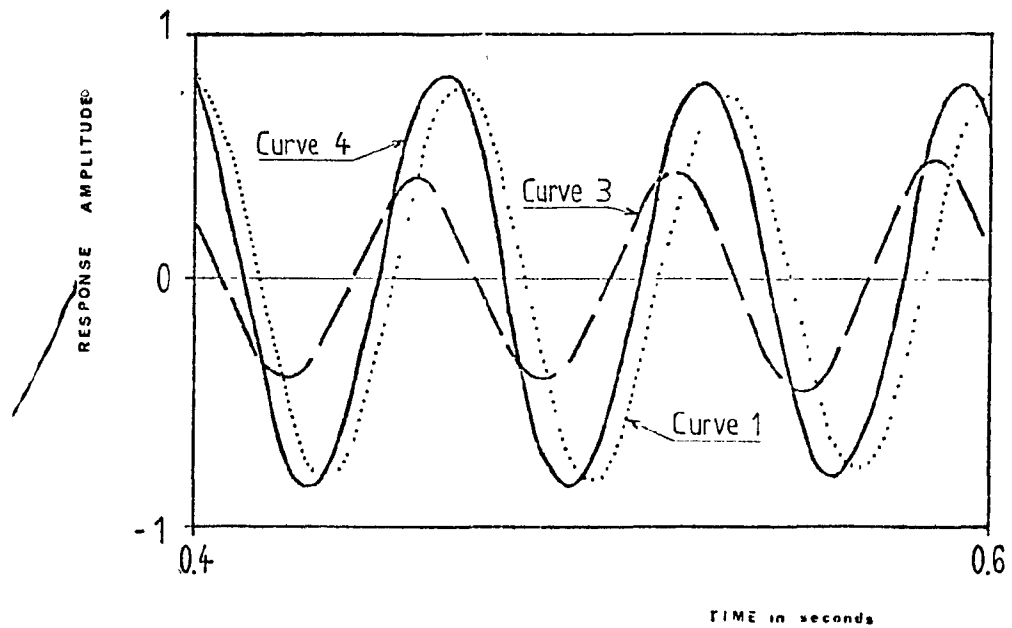


Fig.18(b). Run G2, considered for cycles #7,8,9 of Curve 1.

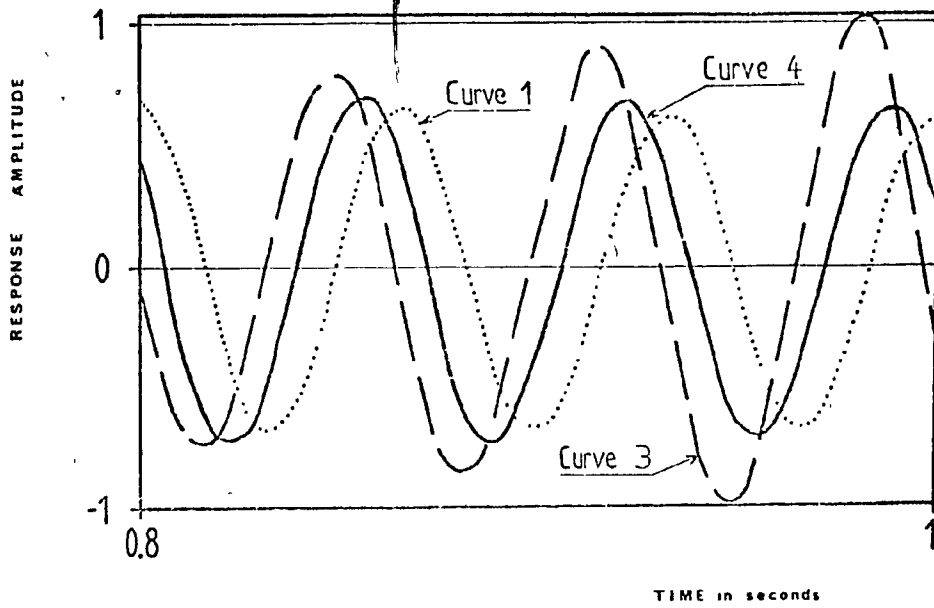


Fig.18(c). Run G2, considered for cycles #13,14,15 of Curve 1.

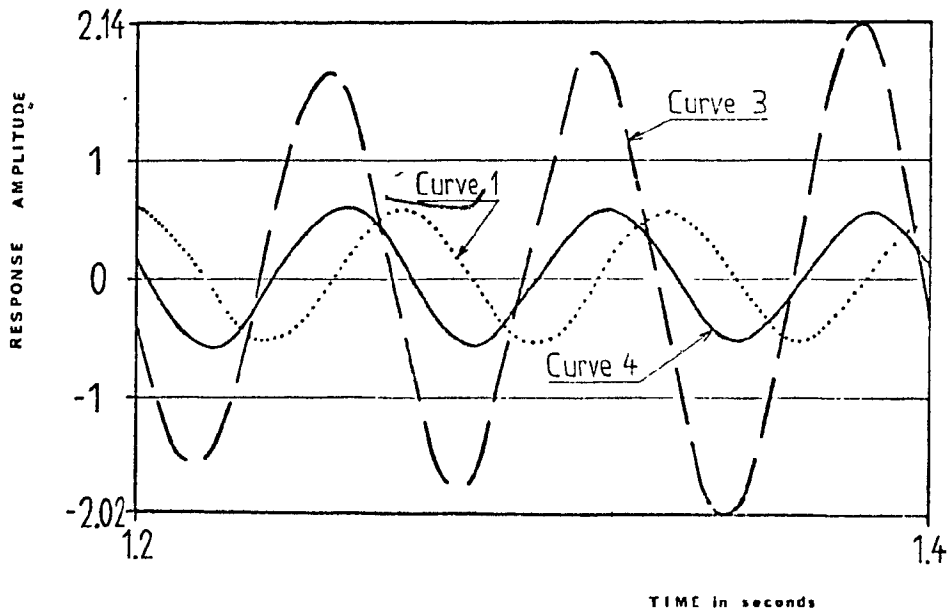


Fig.18(d). Run G2, considered for cycles #19,20,21 of Curve 1.

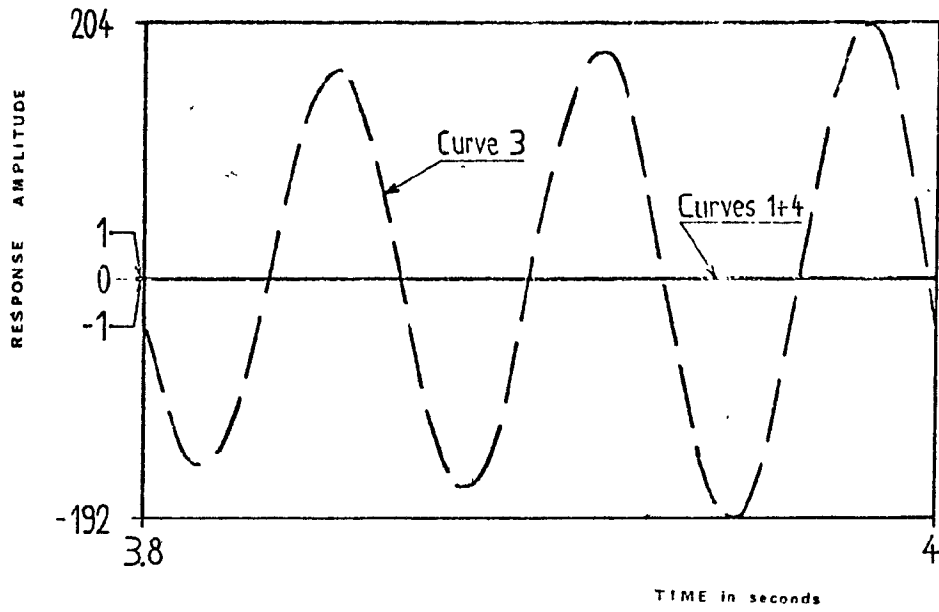


Fig.18(e). Run G2, considered for cycles #58,59,60 of Curve 1.

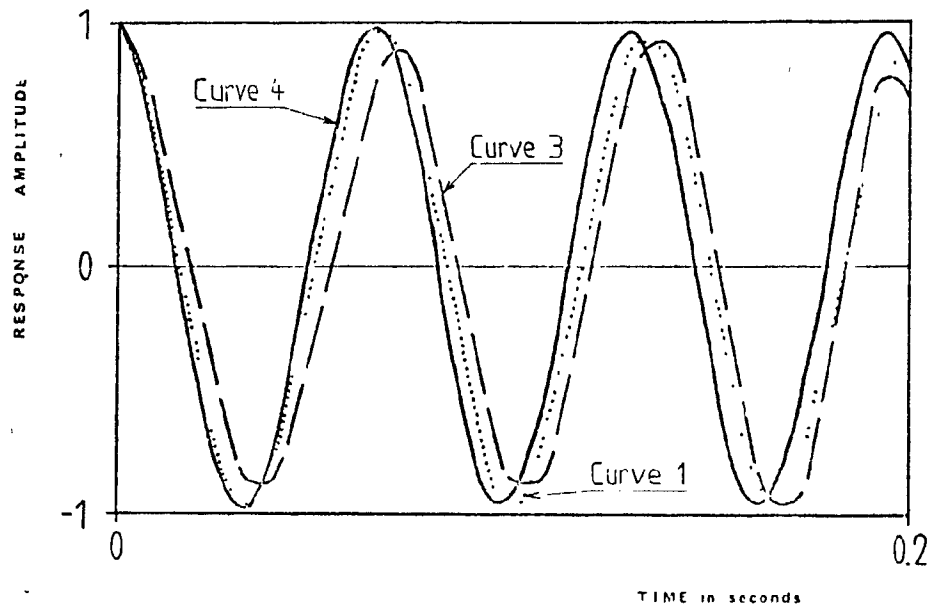


Fig.19(a). Time record of system response, for Run C3 with  $\bar{\alpha} = 0.75$  (see Appendix C.6). Considered for cycles #1,2,3 of Curve 1.

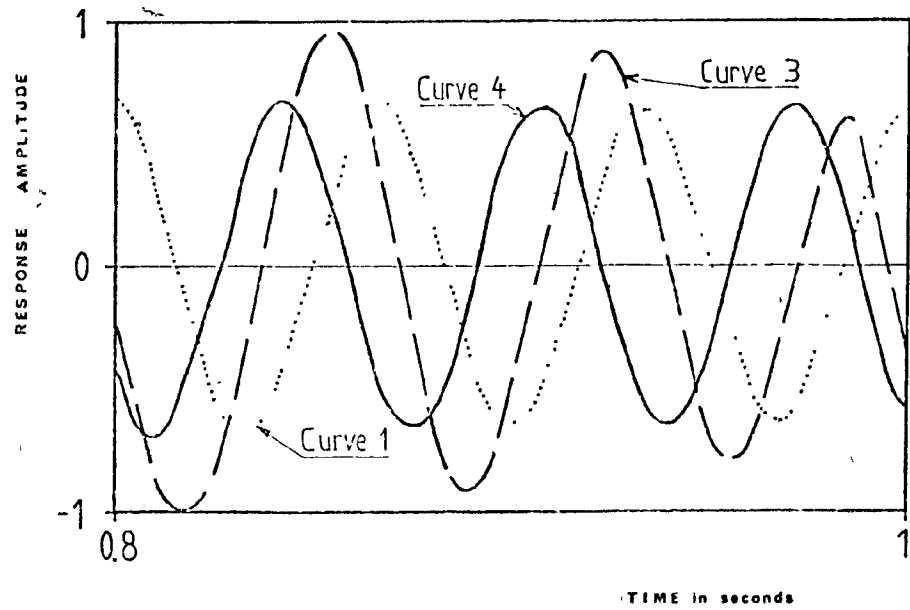


Fig.19(b). Run C3, considered for cycles #13,14,15 of Curve 1.

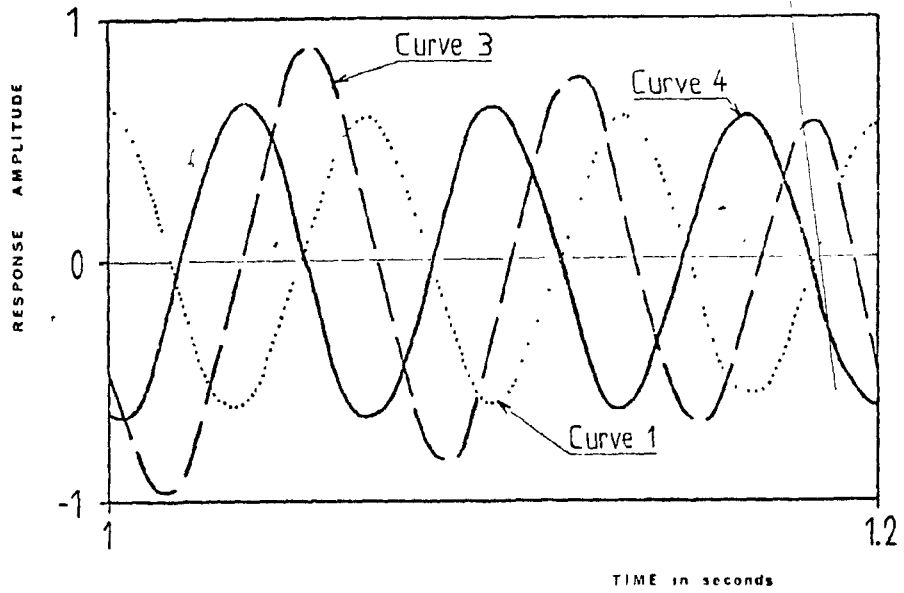


Fig.19(c). Run C3, considered for cycles #16,17,18, of Curve 1.

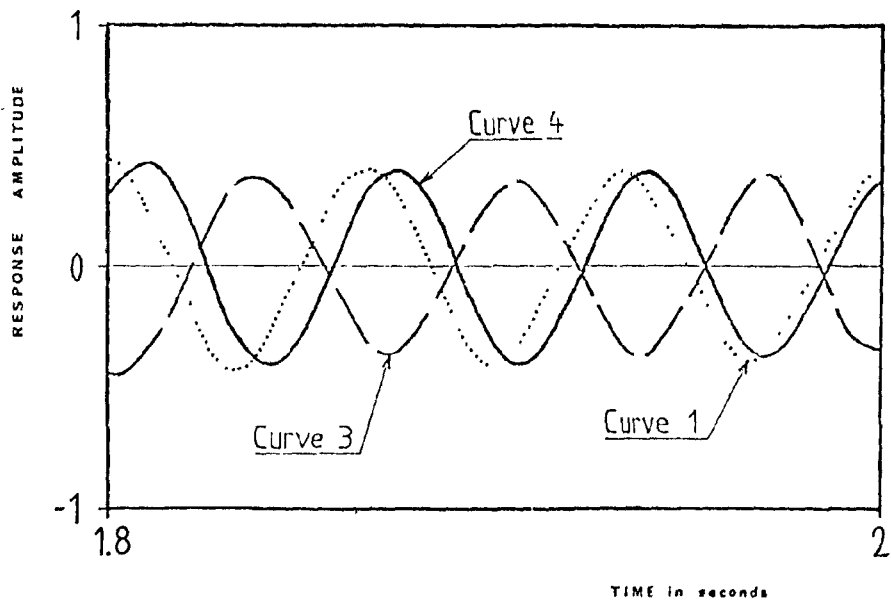


Fig.19(d). Run C3, considered for cycles #28,29,30 of Curve 1.

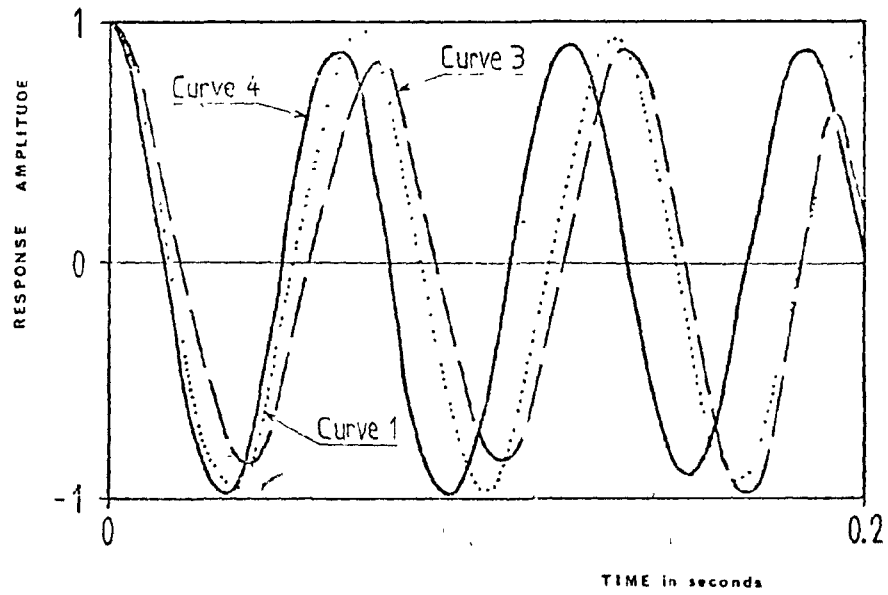


Fig.20(a). Time record of system response, for Run C4 with  $\bar{\alpha}=1$  (see Appendix C.6). Considered for cycles #1,2,3 of Curve 1.

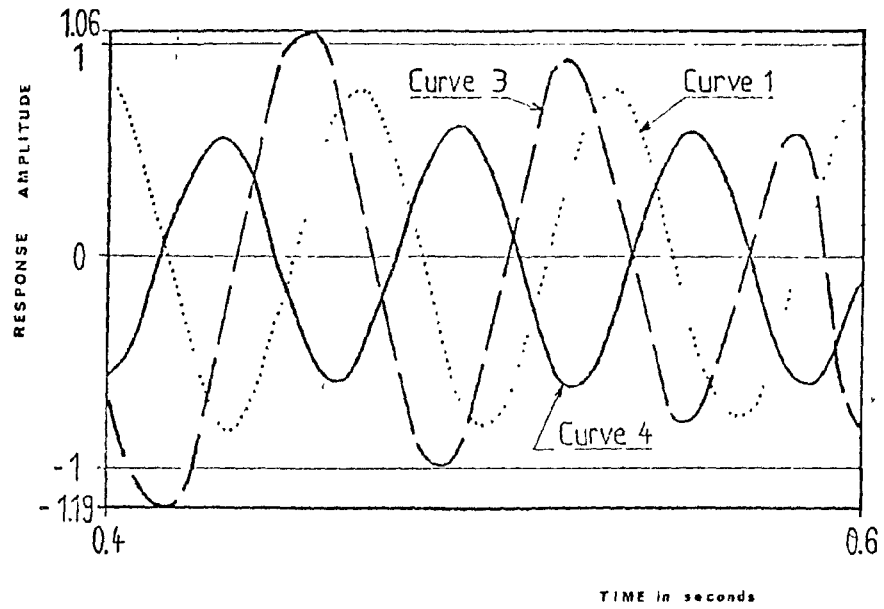


Fig.20(b). Run C4, considered for cycles #7,8,9 of Curve 1.

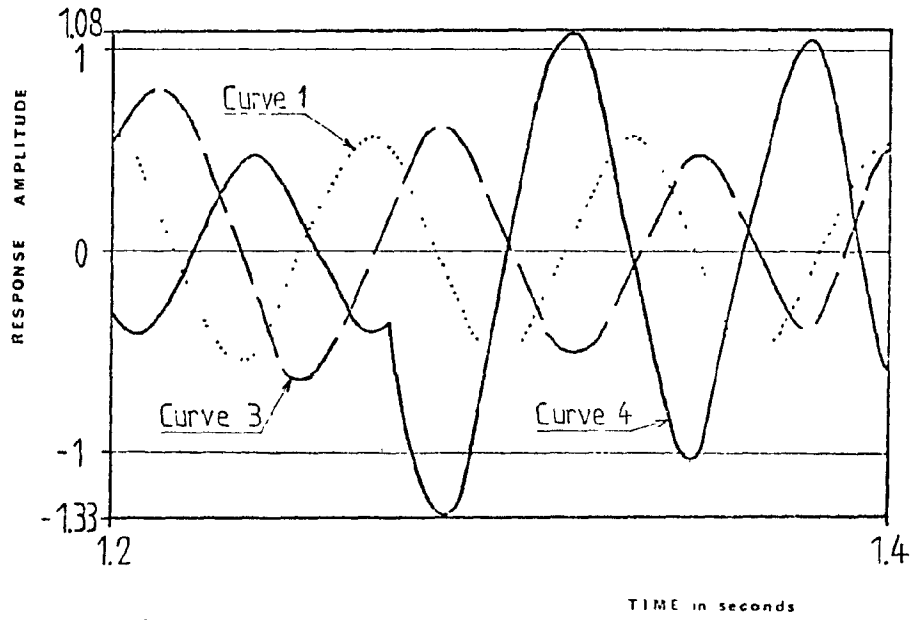


Fig.20(c). Run C4, considered for cycles #19,20,21 of Curve 1.

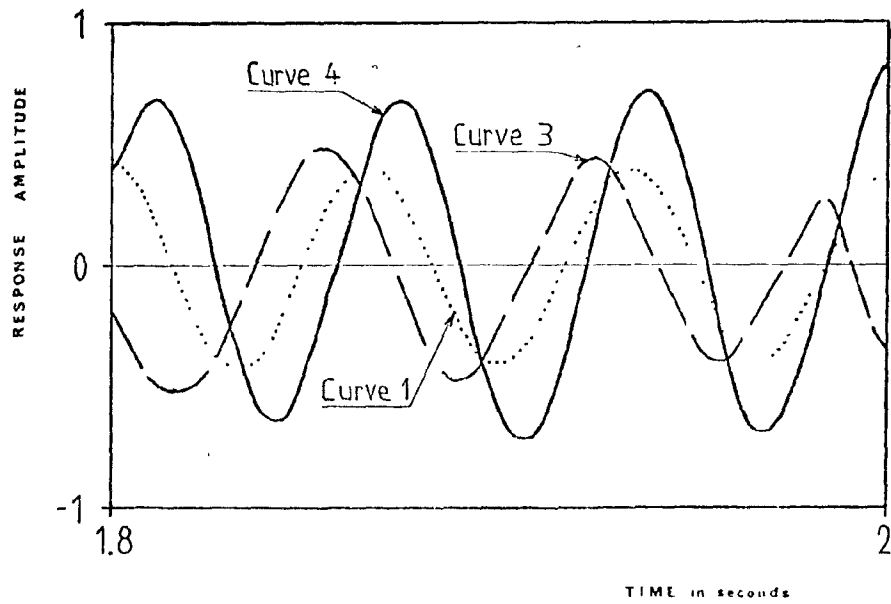


Fig.20(d). Run C4, considered for cycles #28,29,30 of Curve 1.

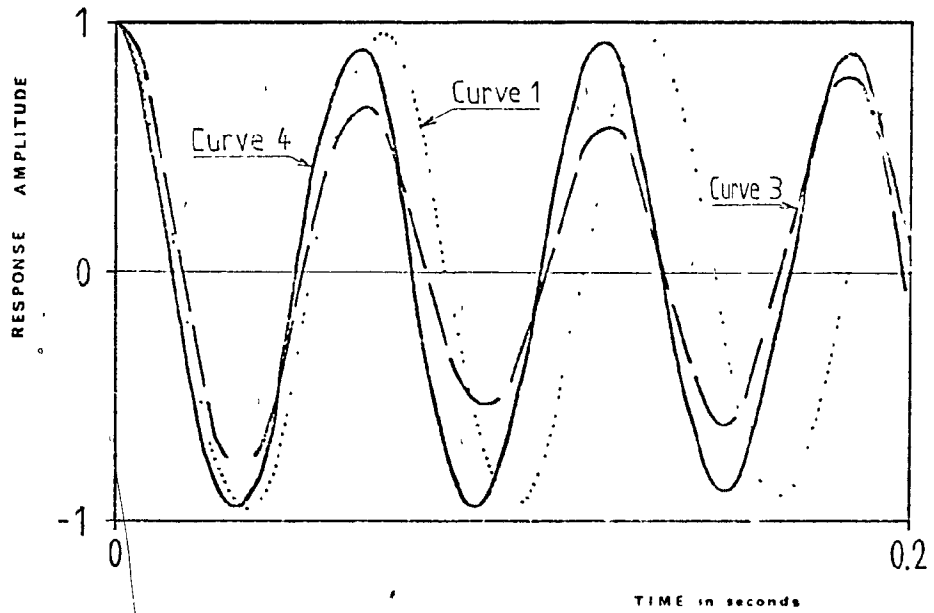


Fig.21(a). Time record of system response, for Run G4 with  $\bar{\alpha} = 1$  (see Appendix C.6). Considered for cycles #1,2,3 of Curve 1.

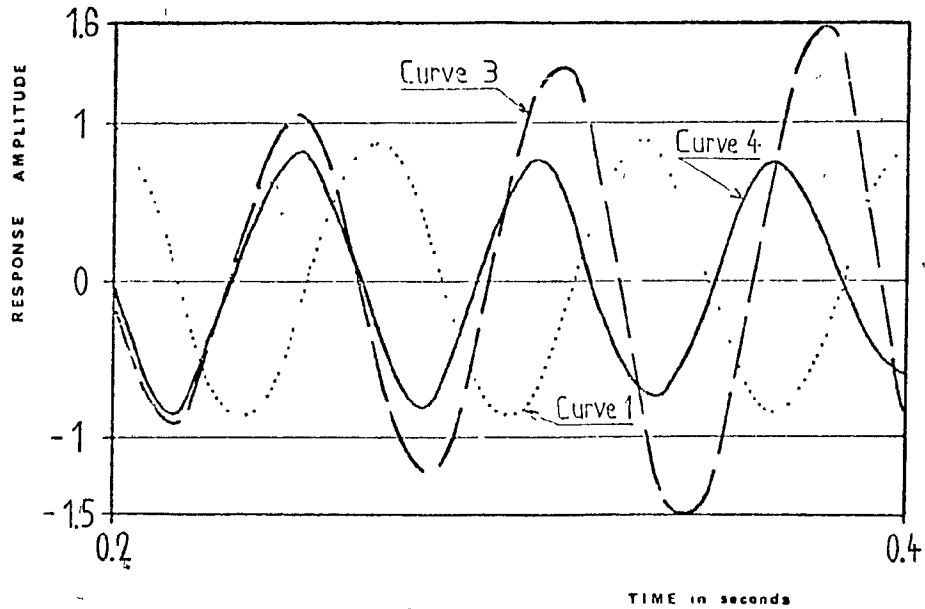


Fig. 21(b). Run G4, considered for cycles #4,5,6 of Curve 1.

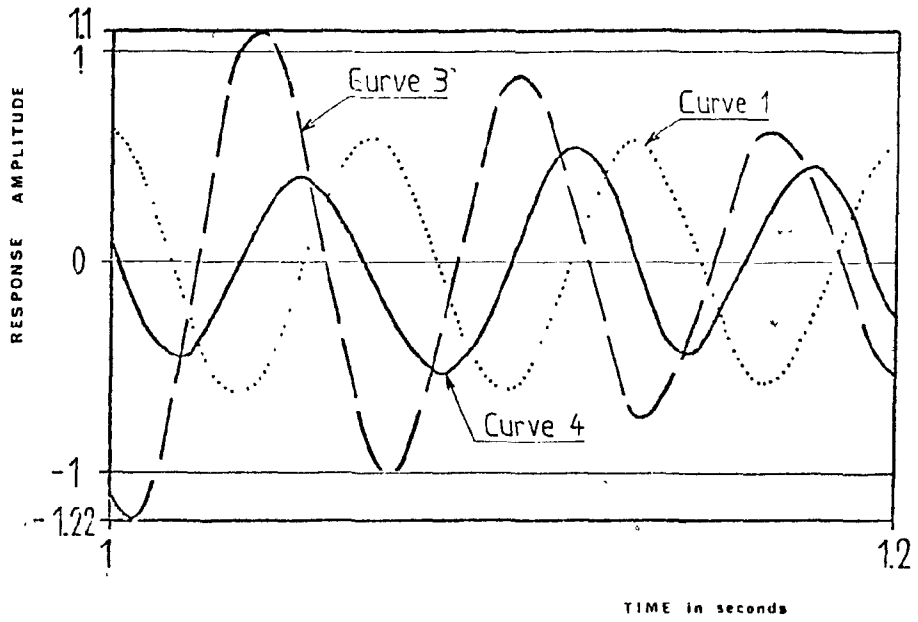


Fig.21(c). Run G4, considered for cycles #16,17,18 of Curve 1.

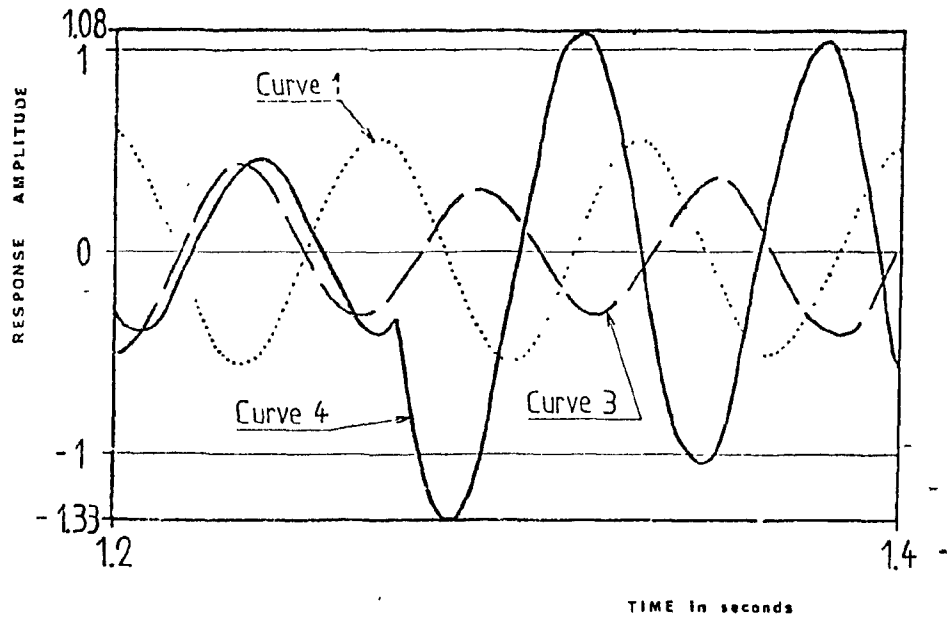


Fig.21(d). Run G4, considered for cycles #19,20,21 of Curve 1.

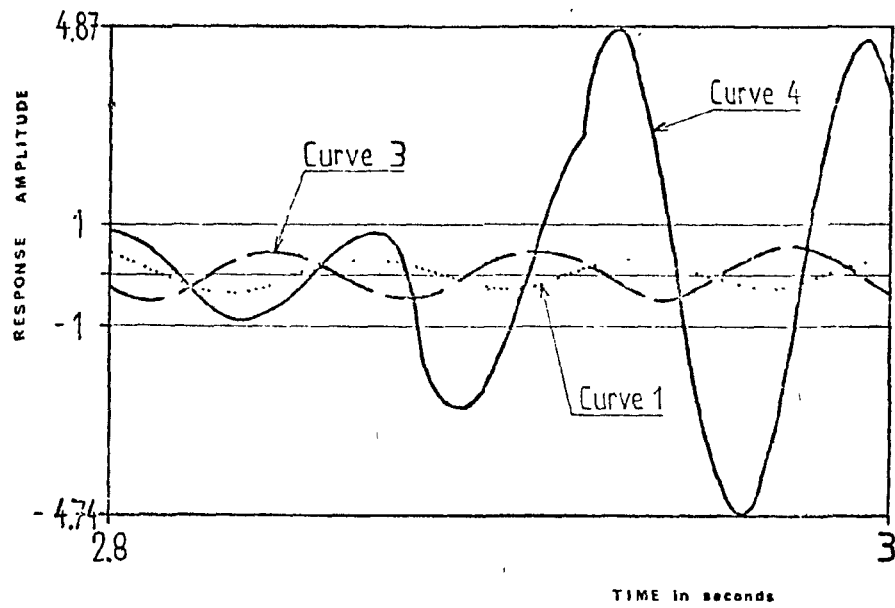


Fig.21(e). Run G4, considered for cycles #43,44,45 of Curve 1.

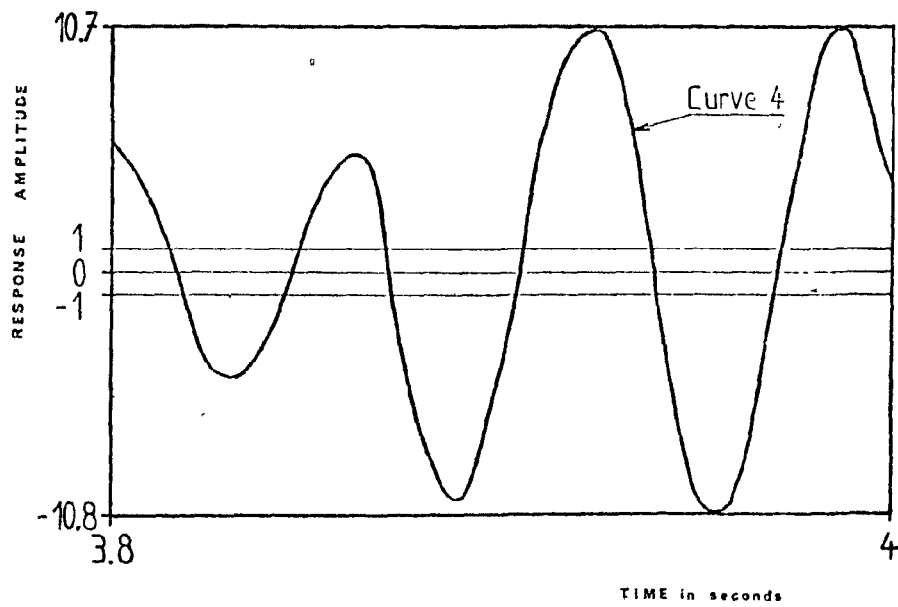


Fig.21(f). Run G4, considered for cycles #58,59,60 of Curve 1.

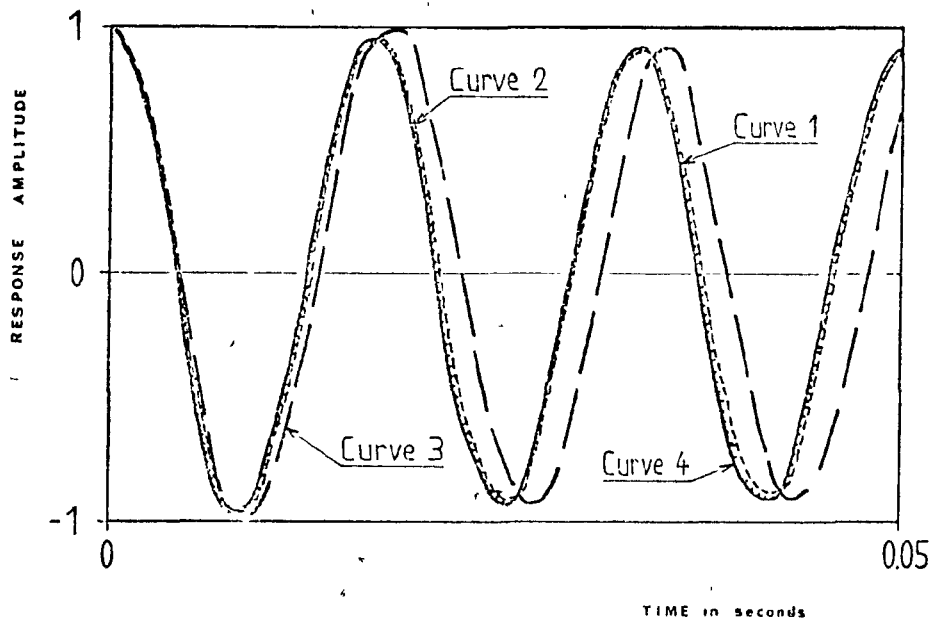


Fig.22(a). Time record of system response, for Run B3 with  $\bar{\alpha} = 0.25$  and  $f_n = 60$  Hz (see Appendix C.6). Considered for cycles #1,2,3 of Curve 1.

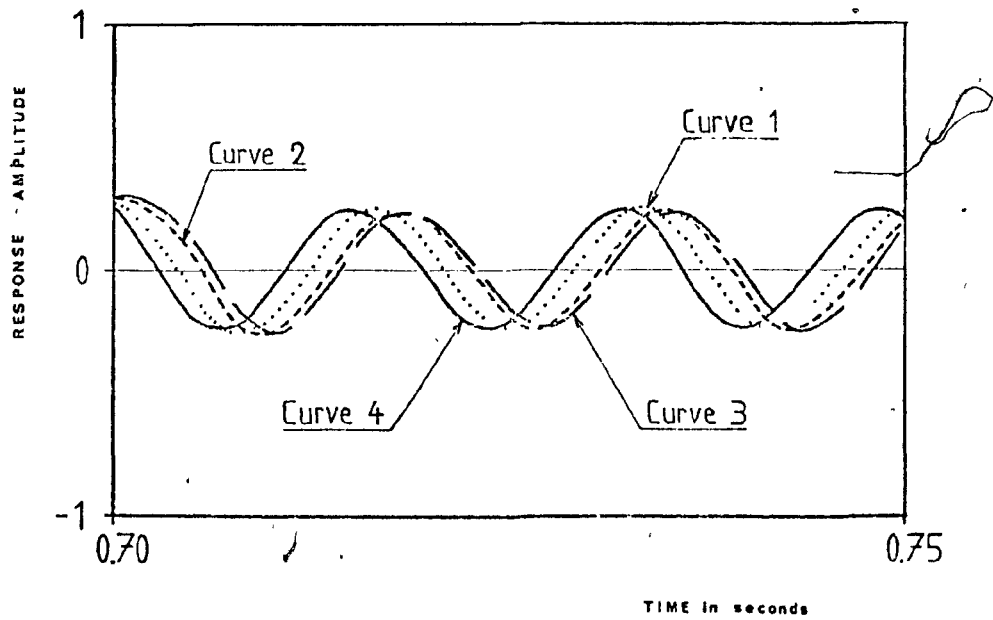


Fig.22(b). Run B3, considered for cycles #43,44,45 of Curve 1.

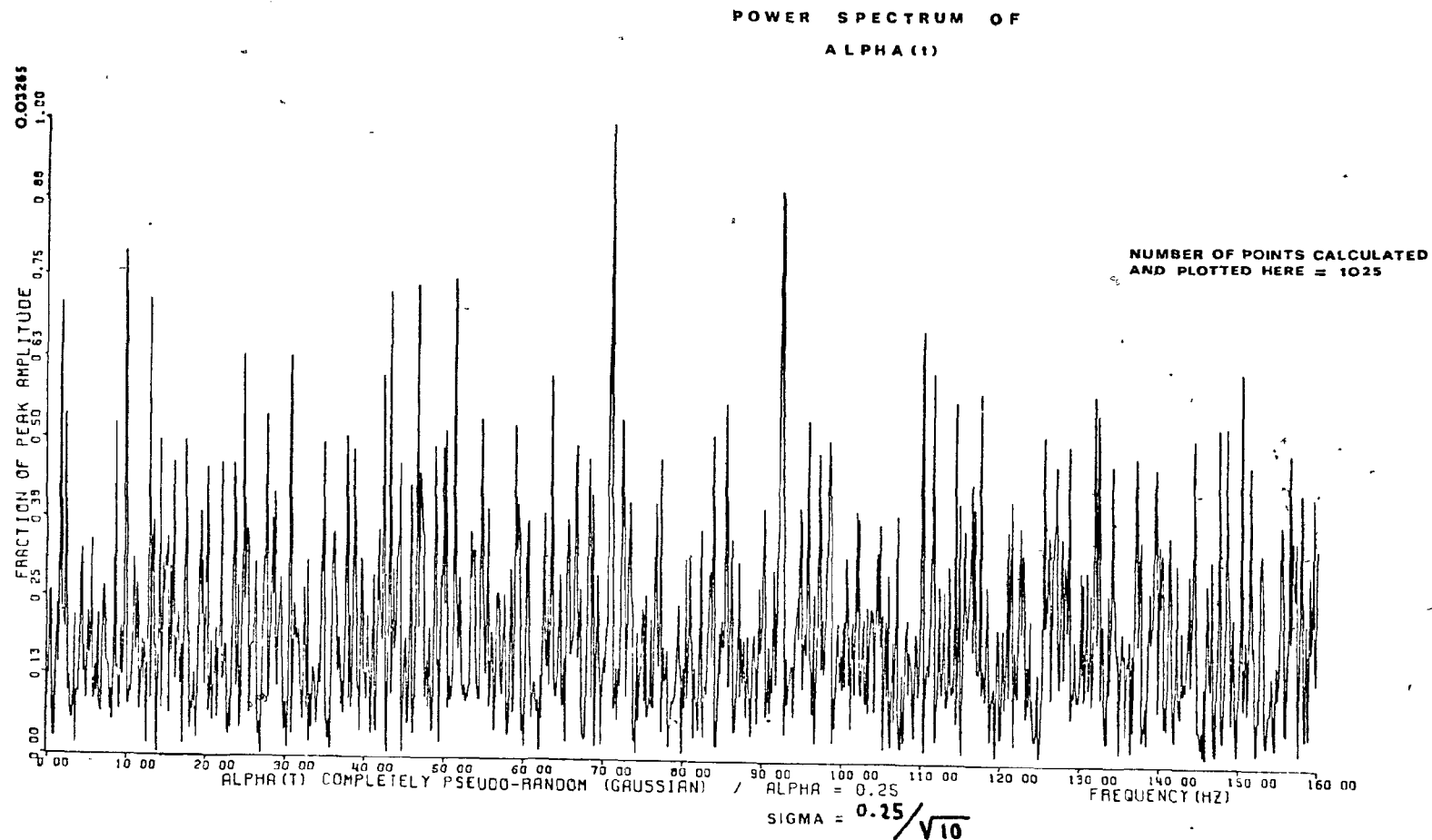


Fig.23. Power spectrum of the completely pseudo-random  $\alpha(t)$  of scheme  $[c]^\dagger$ , i.e., generated by the Monte-Carlo algorithm.

For  $\bar{\alpha} = 0.25$ . {Case A[c]}.

$^\dagger$ cf. Appendix D.2.

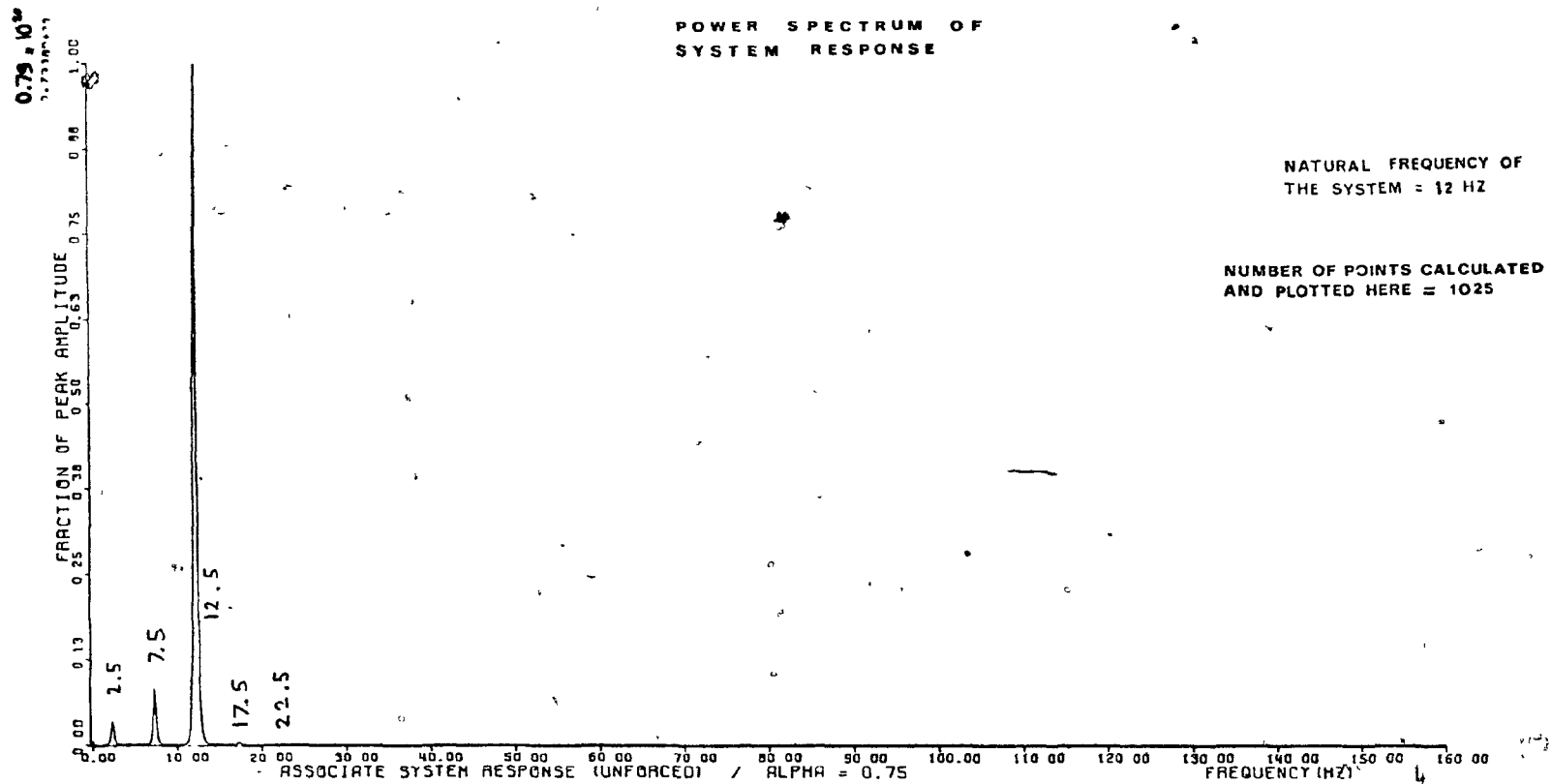


Fig.24. Power spectrum of the response to the deterministic  $\alpha(t)$  of scheme [b] with  $N=5$  and  $\bar{\alpha} = 0.75$ .

-Occurrence of parametric resonance. {Case A[b]}.

POWER SPECTRUM OF  
ALPHA (t)

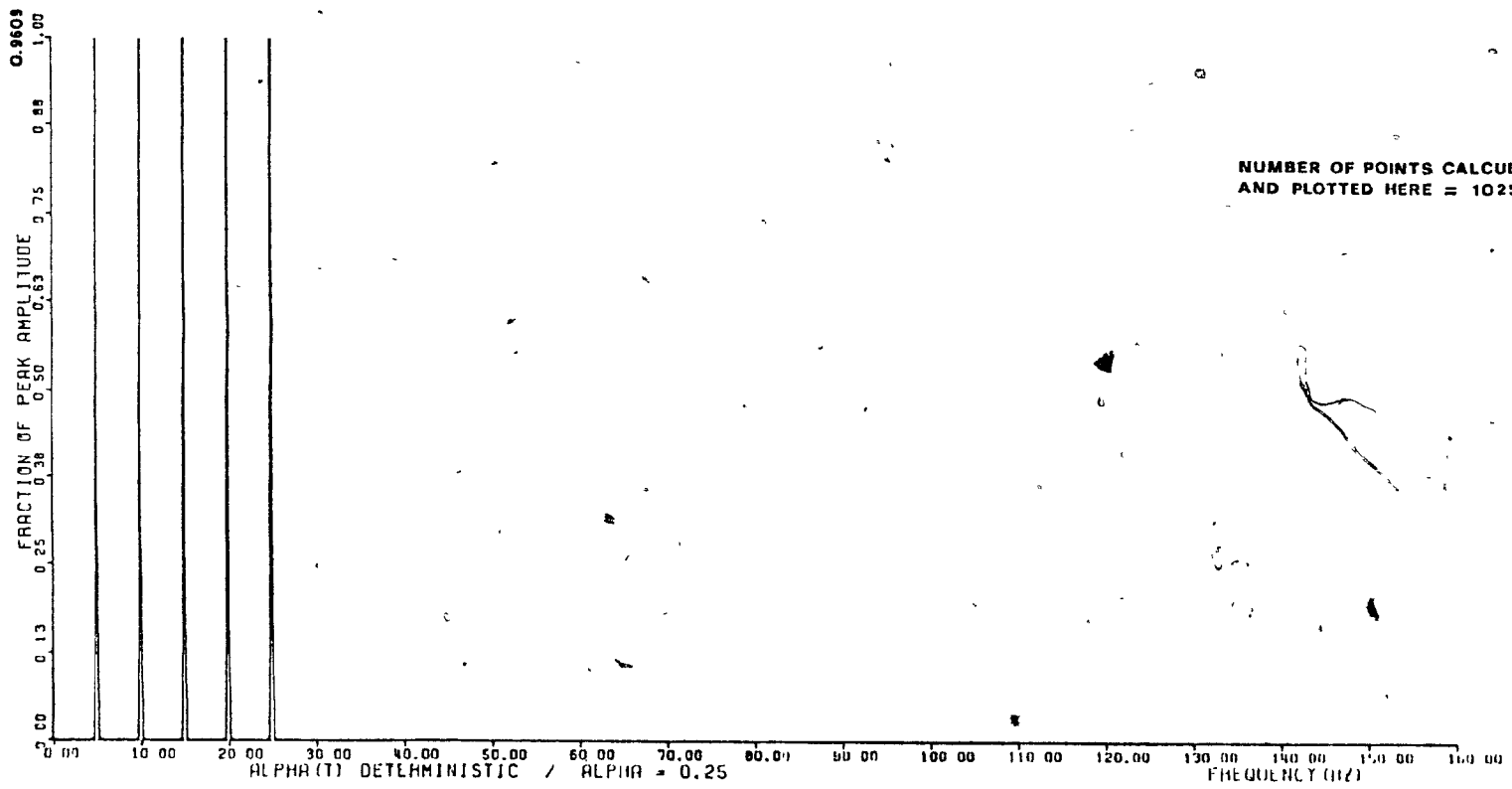


Fig.25(a). Power spectrum of the deterministic  $\alpha(t)$  of scheme [b] for  $N=5$  and  $\alpha = 0.25$ . {Case A[b]}.

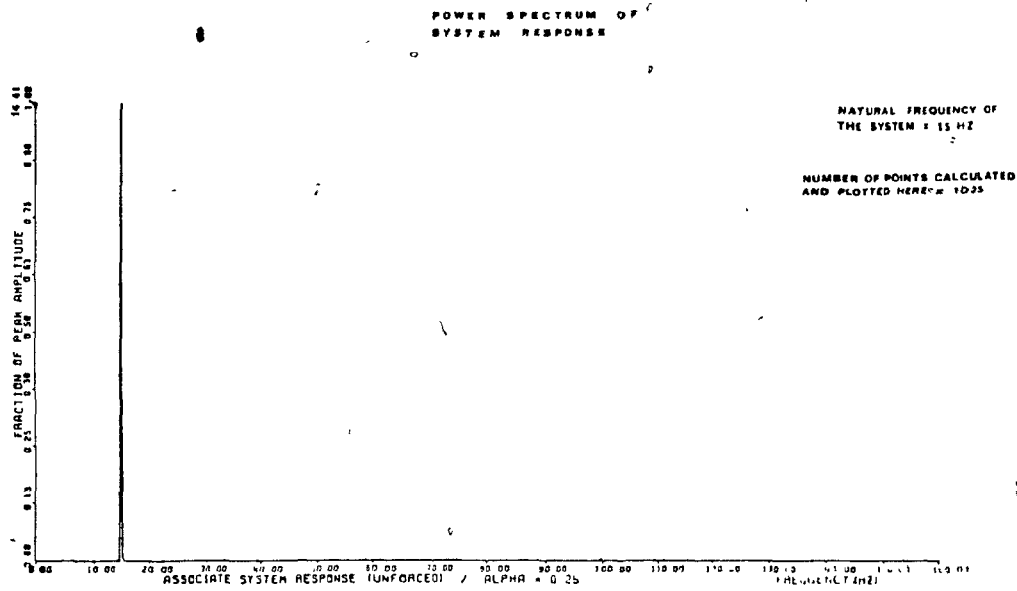


Fig.25(b). Power spectrum of the response to the deterministic  $\alpha(t)$  of scheme [b] with  $N=5$  and  $\bar{\alpha} = 0.25$ ; for  $f_n = 15$  Hz. {Case A[b]}..

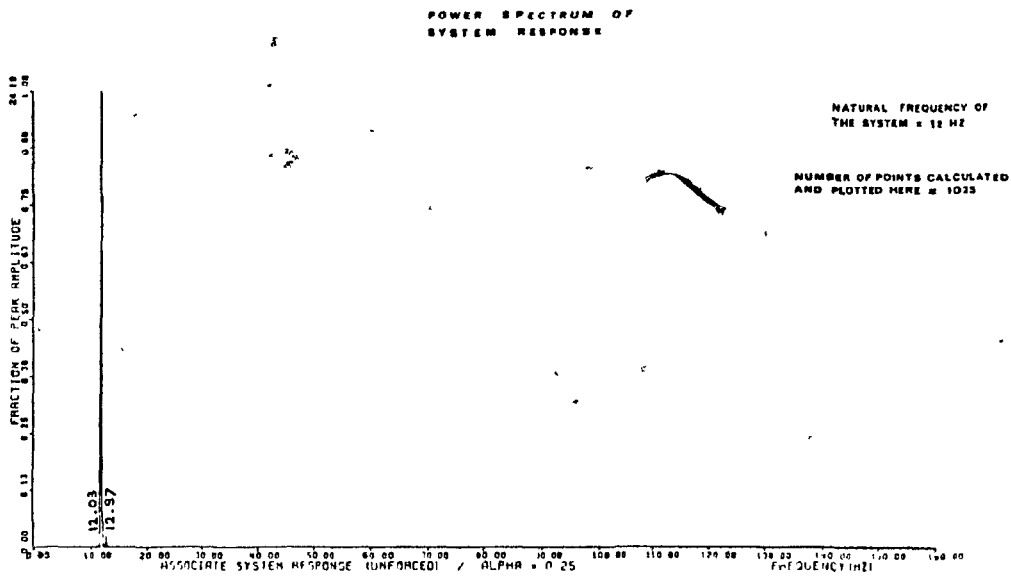


Fig.25(c): Power spectrum of the response to the deterministic  $\alpha(t)$  of scheme [b] with  $N=5$  and  $\bar{\alpha} = 0.25$ ; for  $f_n = 12$  Hz. {Case A[b]}.

POWER SPECTRUM OF  
ALPHA (t)

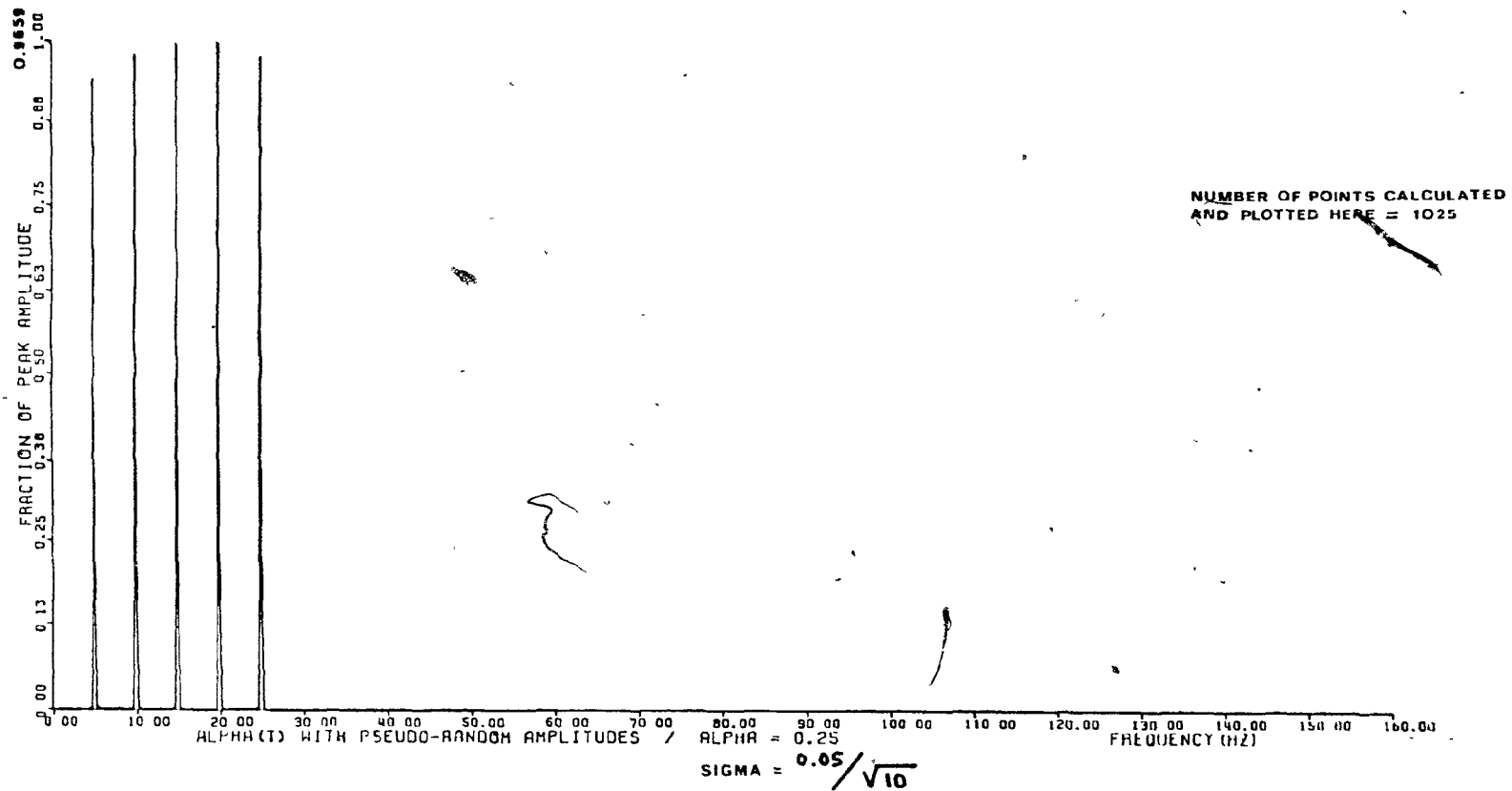


Fig.26. Power spectrum of pseudo-random  $\alpha(t)$  of scheme [d], with pseudo-random amplitudes. For  $N=5$  and  $\bar{\alpha} = 0.25$ . {Case A[d]}.

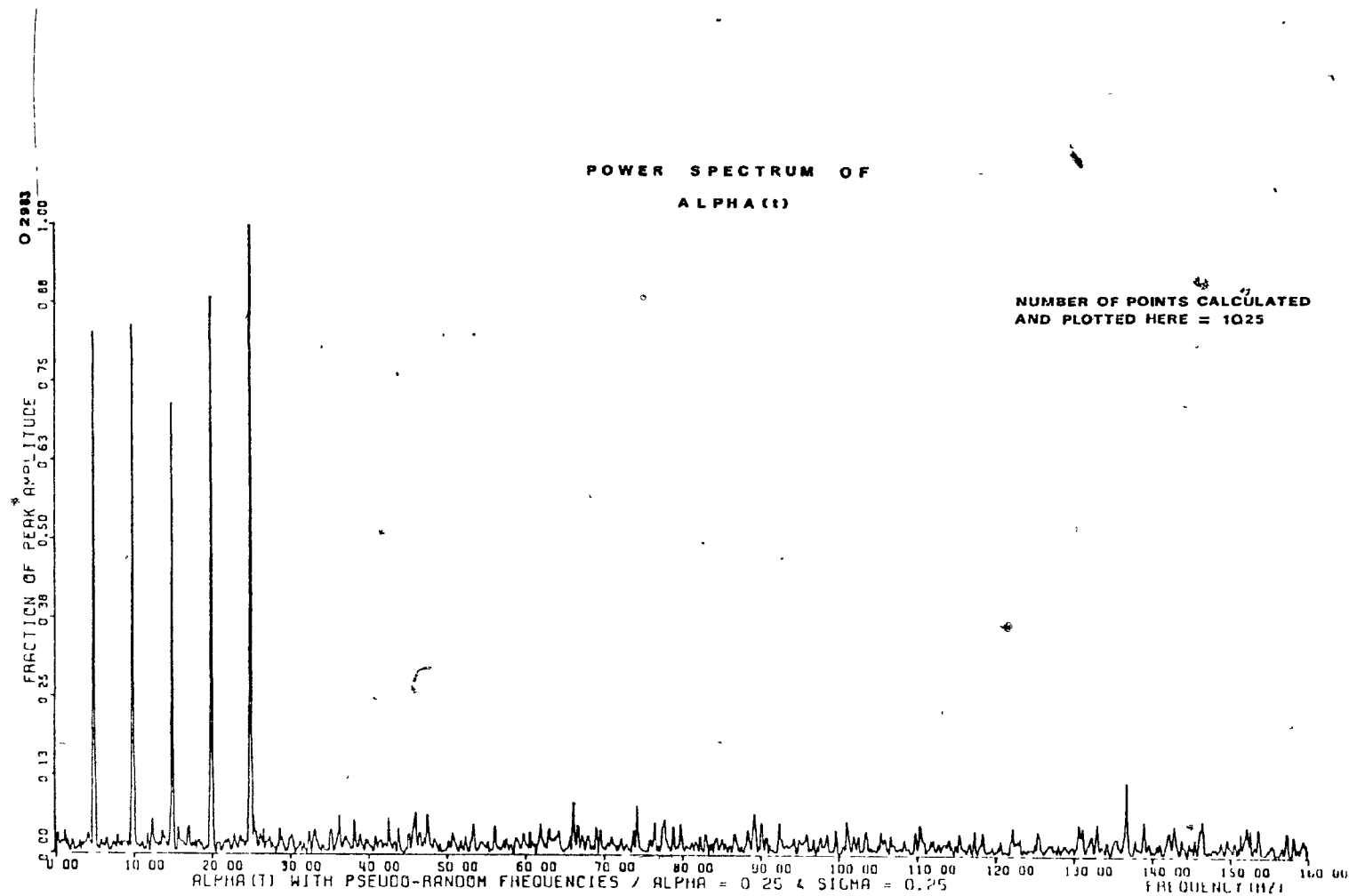


Fig.27(a). Power spectrum of pseudo-random  $\alpha(t)$  of scheme [e], with pseudo-random frequencies. For  $N=5$ ,  $\bar{\alpha} = 0.25$  and  $\sigma = 0.25$ . {Case A[e]}.

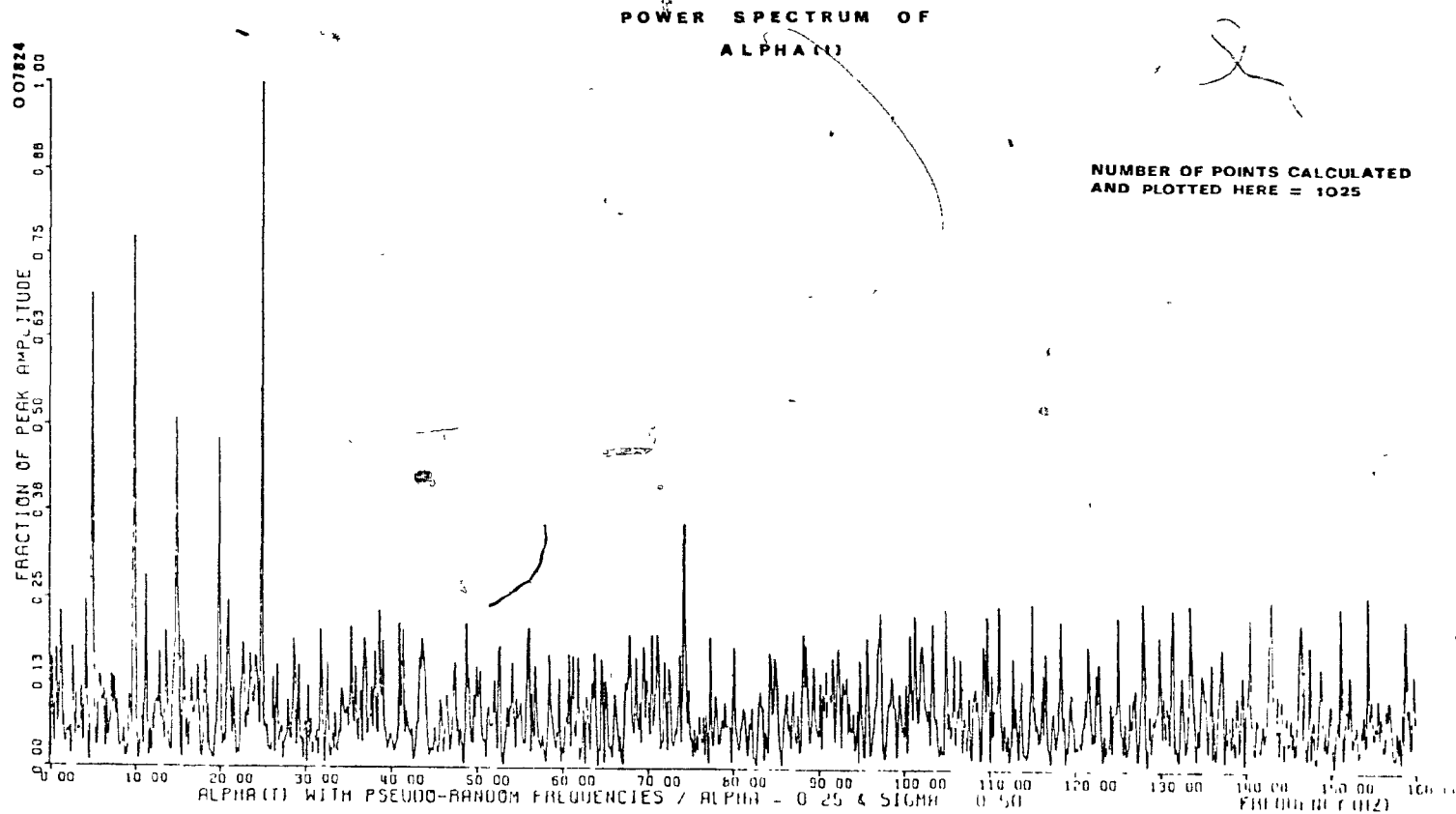


Fig.27(b). Power spectrum of pseudo-random  $\alpha(t)$  of scheme [e]. For  $N=5$ ,  $\bar{\alpha} = 0.25$  and  $\sigma = 0.50$ . {Case A[e]}.

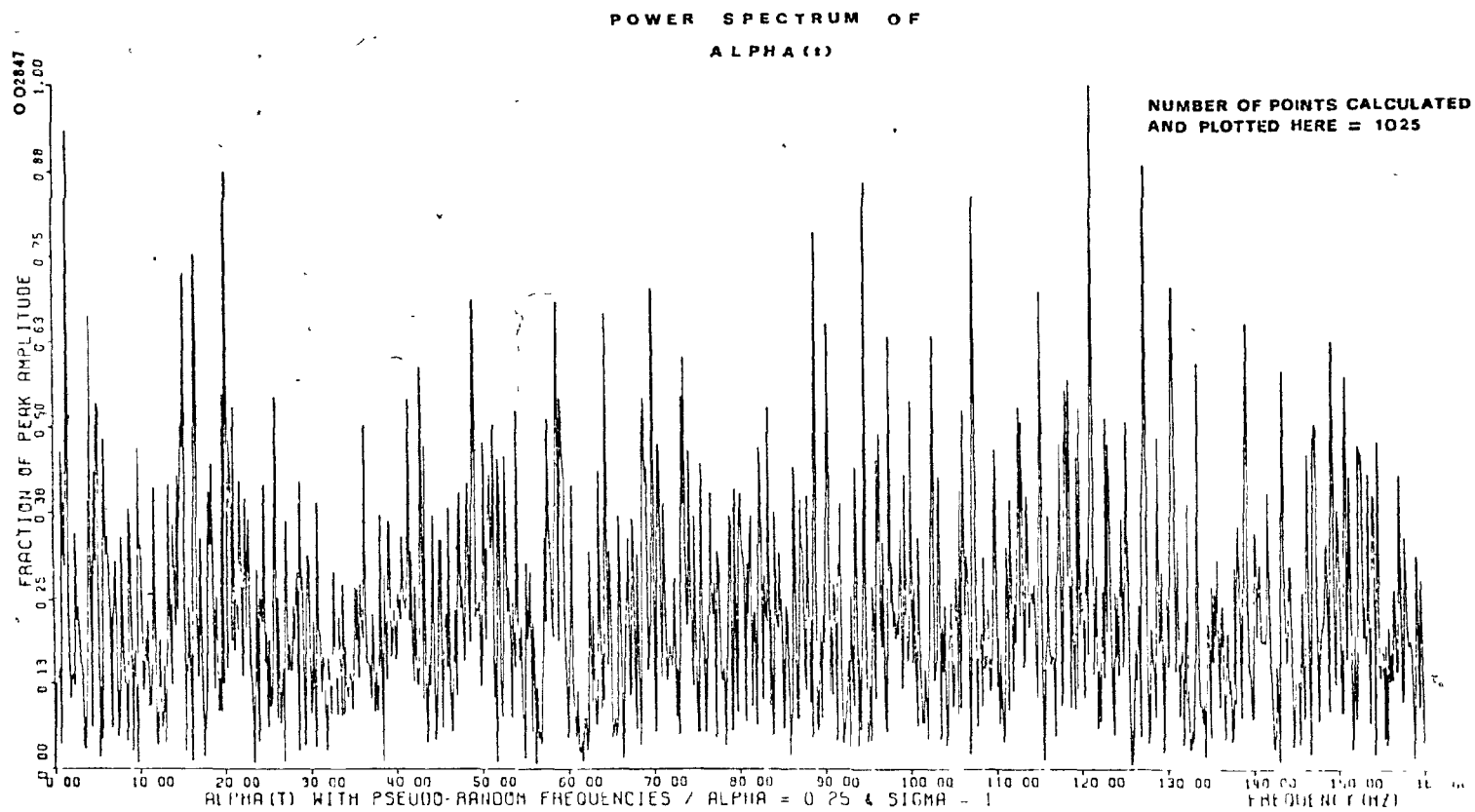


Fig.27(c). Power spectrum of pseudo-random  $\alpha(t)$  of scheme [e]. For  $N=5$ ,  $\bar{\alpha} = 0.25$  and  $\sigma = 1$ . {Case A[e]}.

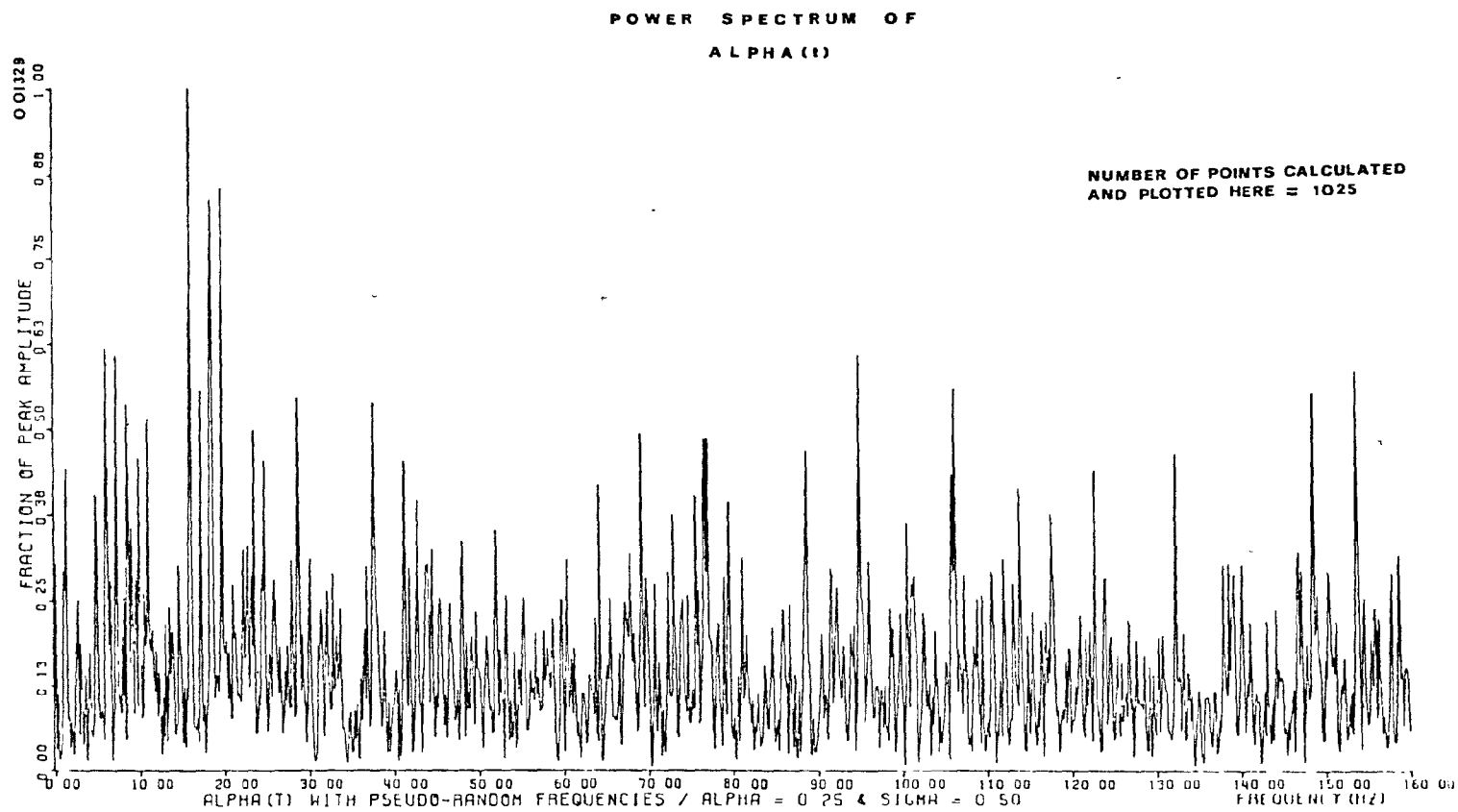


Fig.28. Power spectrum of pseudo-random  $\alpha(t)$  of scheme [e]. For  $N=17$ ,  $\bar{\alpha} = 0.25$  and  $\sigma = 0.50$ . {Case A[e]}.

POWER SPECTRUM OF  
ALPHA (t)

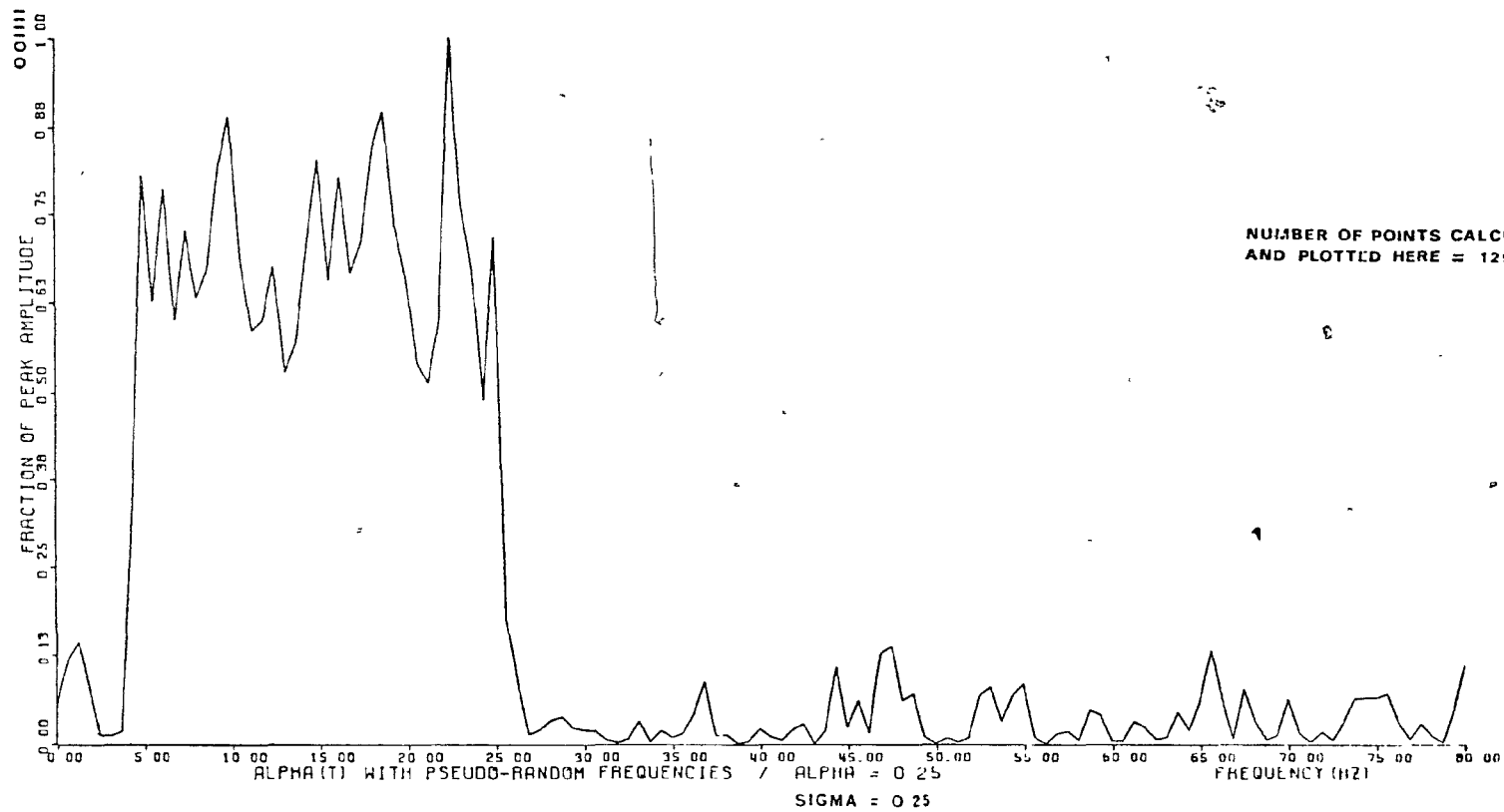


Fig.29(a). Power spectrum of pseudo-random  $\alpha(t)$  of scheme [e], obtained by decreasing the discrimination of the calculation. For  $N=17$ ,  $\bar{\alpha} = 0.25$  and  $\sigma = 0.25$ .

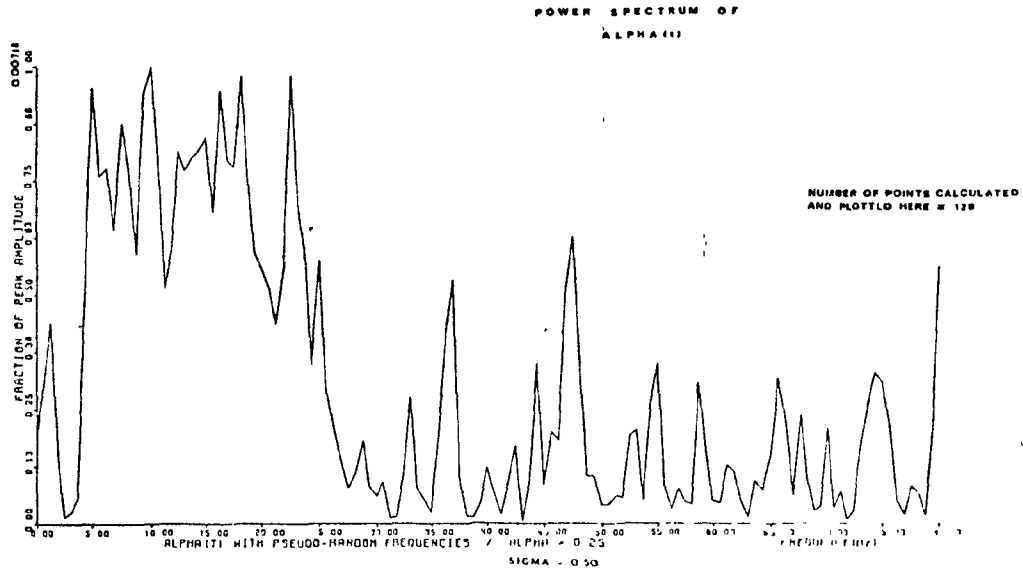


Fig.29(b). Same case as on Fig.29(a), but with  $\sigma = 0.50$  instead of 0.25.

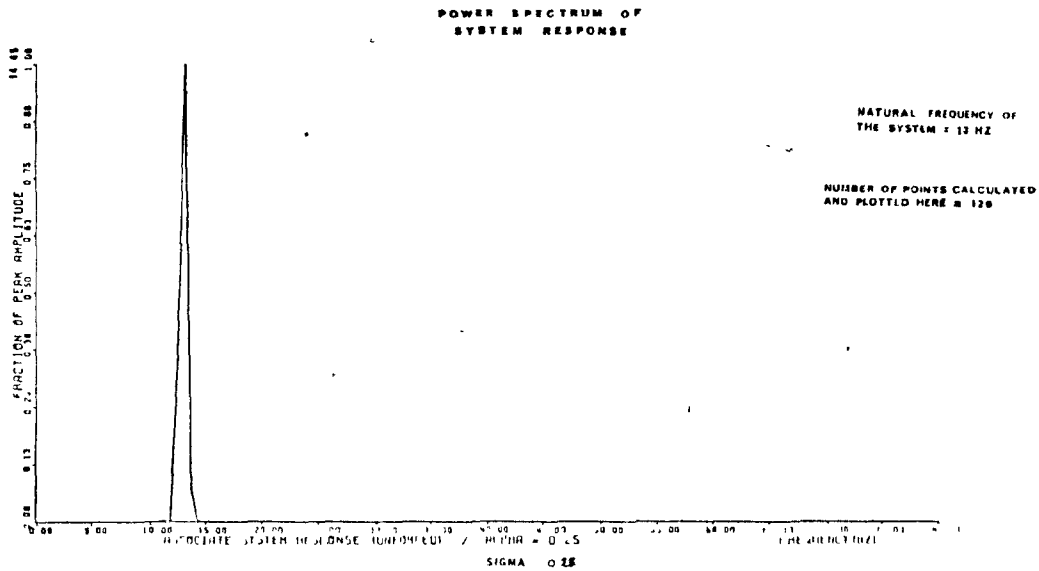
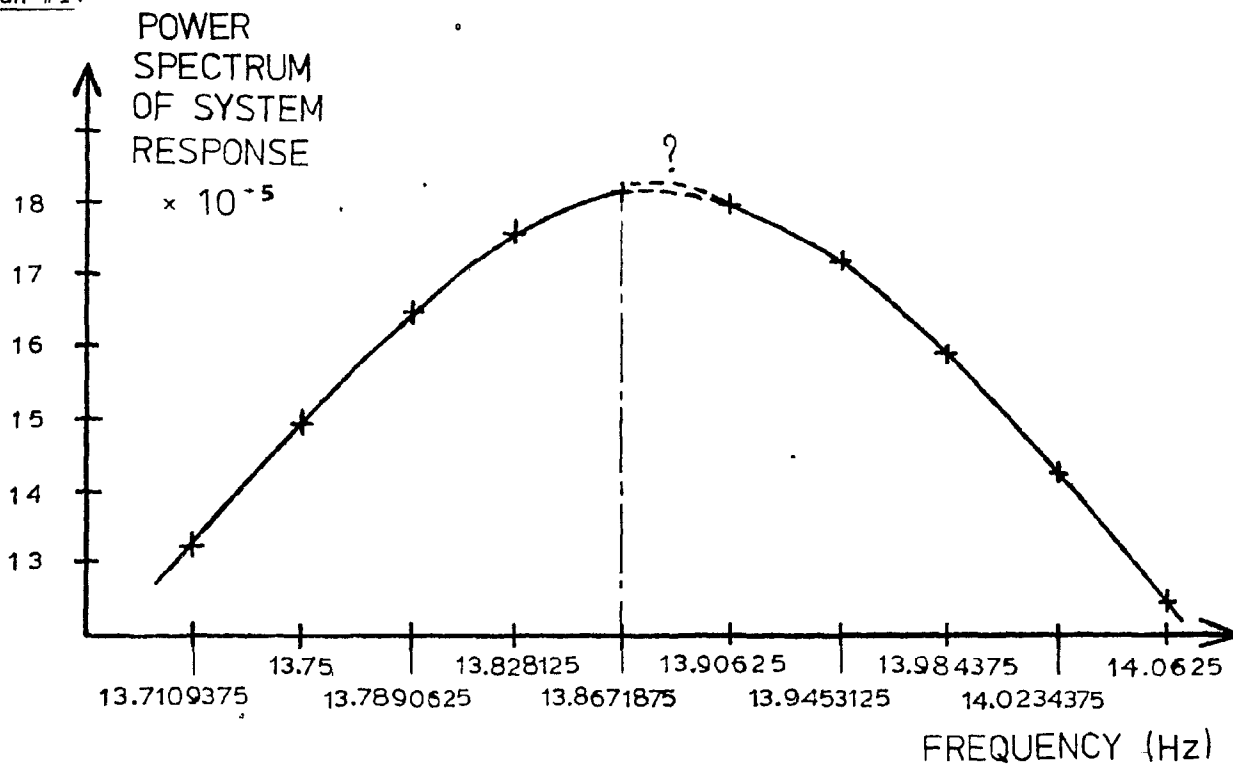


Fig.29(c). Power spectrum of the response associated to the  $\alpha(t)$  considered in Fig.29(a).

run #1:



run #2:

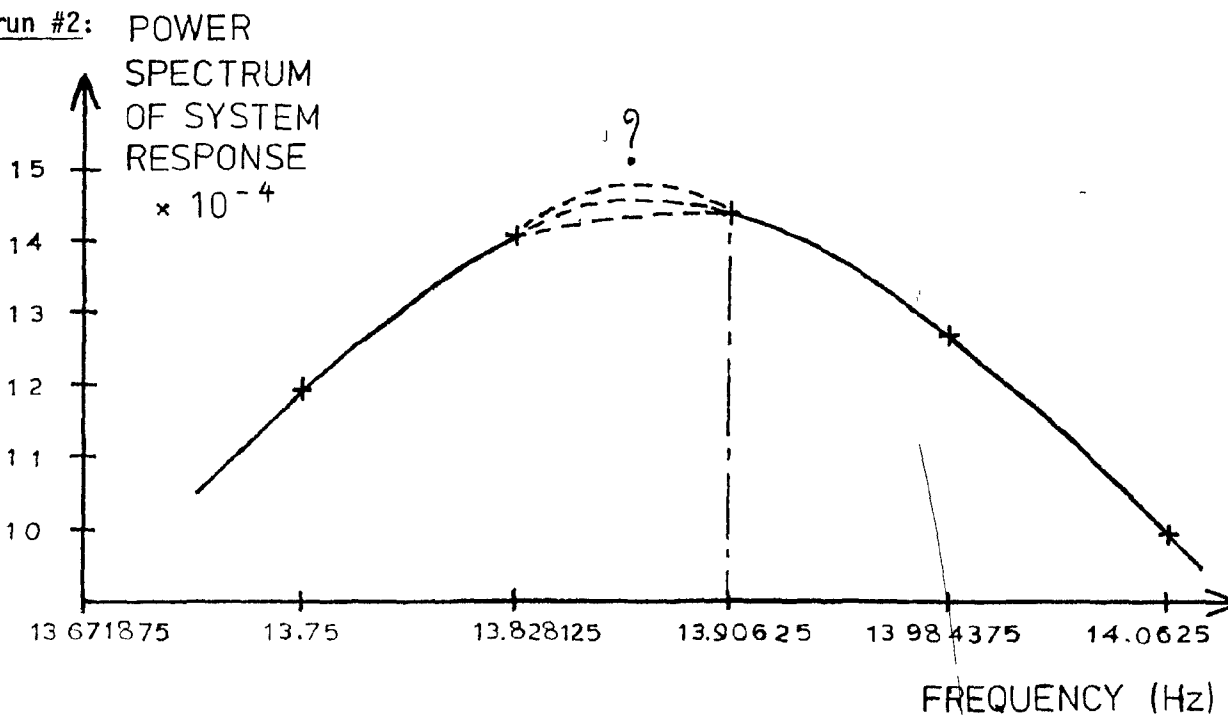


Fig.30. Local comparison of the two peaks obtained for Case B[a], using two different values of  $N_{ps}$ : 1025 (run #1) and 513 (run #2).

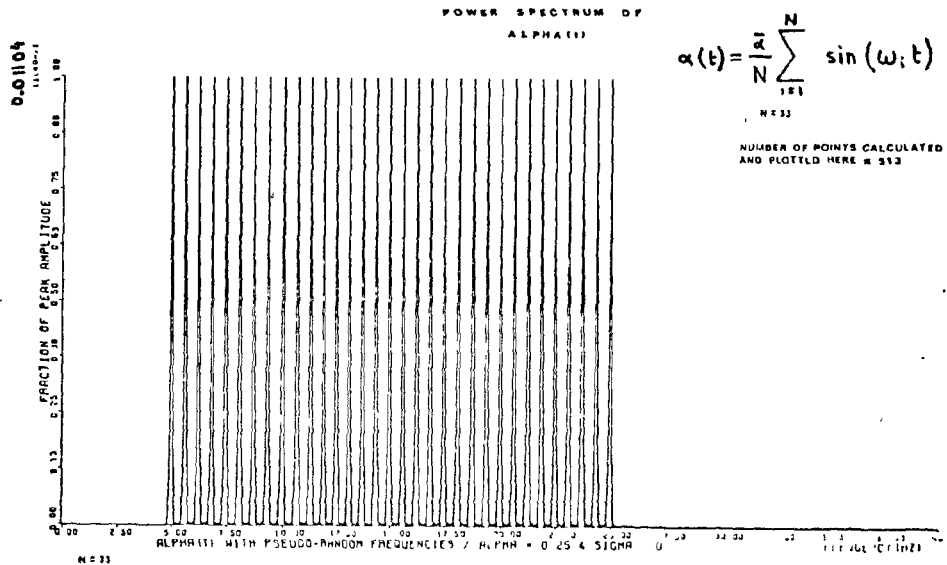


Fig.31(a). Power spectrum of the deterministic  $\alpha(t)$  of scheme [b] for  $N=33$  and  $\bar{\alpha} = 0.25$ . {Case B[b]}.

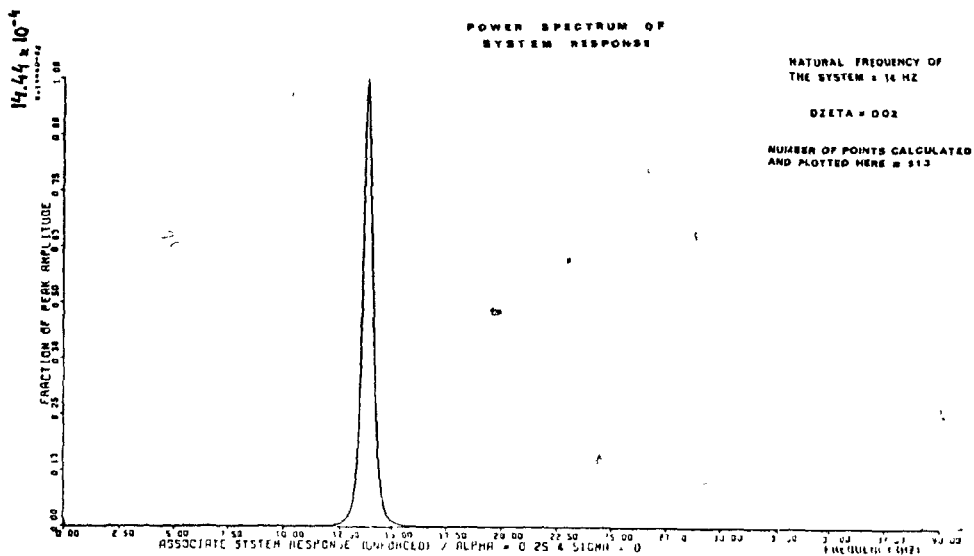


Fig.31(b). Power spectrum of the response associated to the  $\alpha(t)$  of Fig.31(a).

$38.62 \times 10^{-4}$

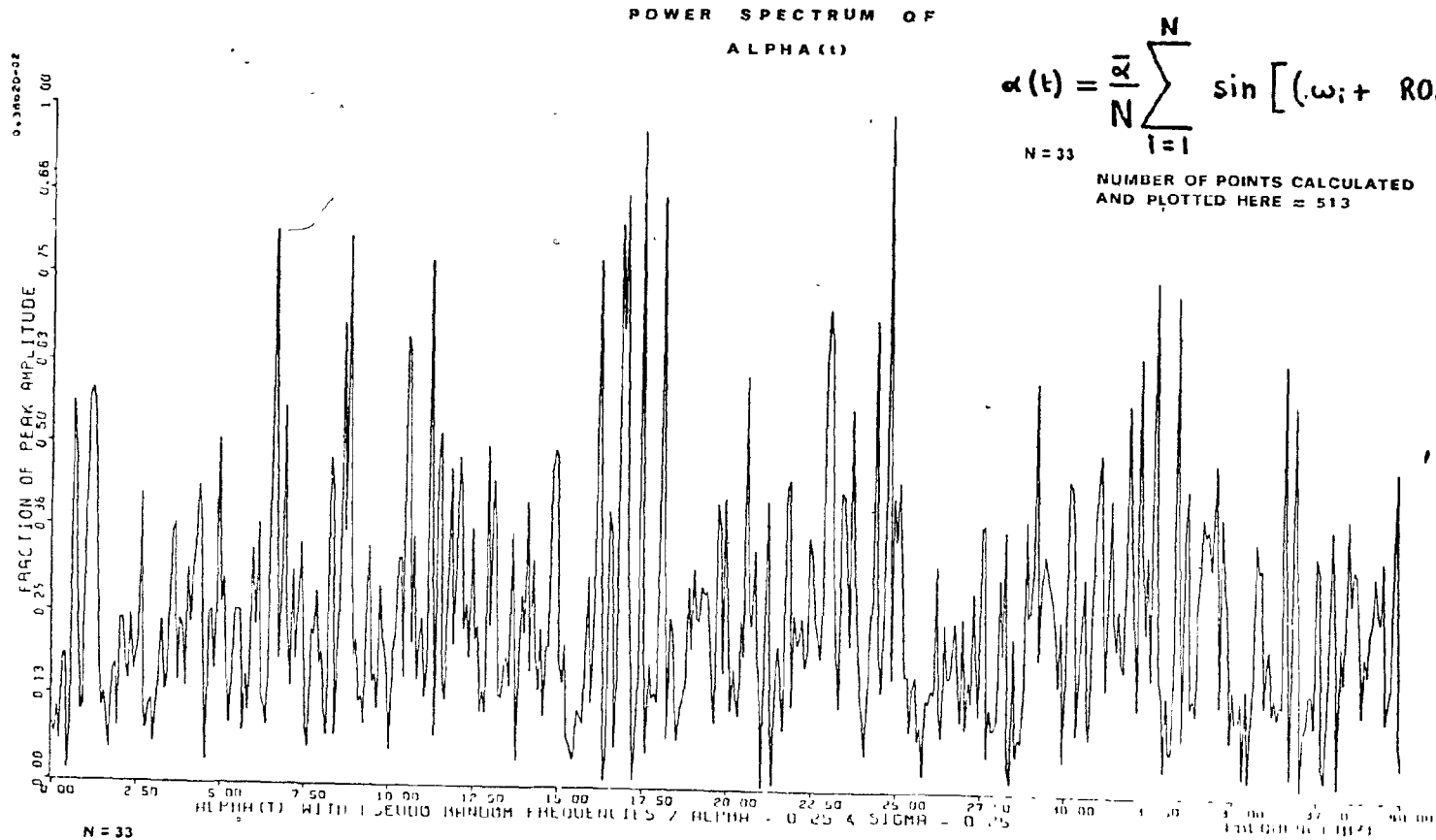


Fig.32. Power spectrum of the pseudo-random  $\alpha(t)$  of scheme [e] for  $N=33$ ,  $\bar{\alpha} = 0.25$  and  $\sigma = 0.25$ . {Case B[e]}.

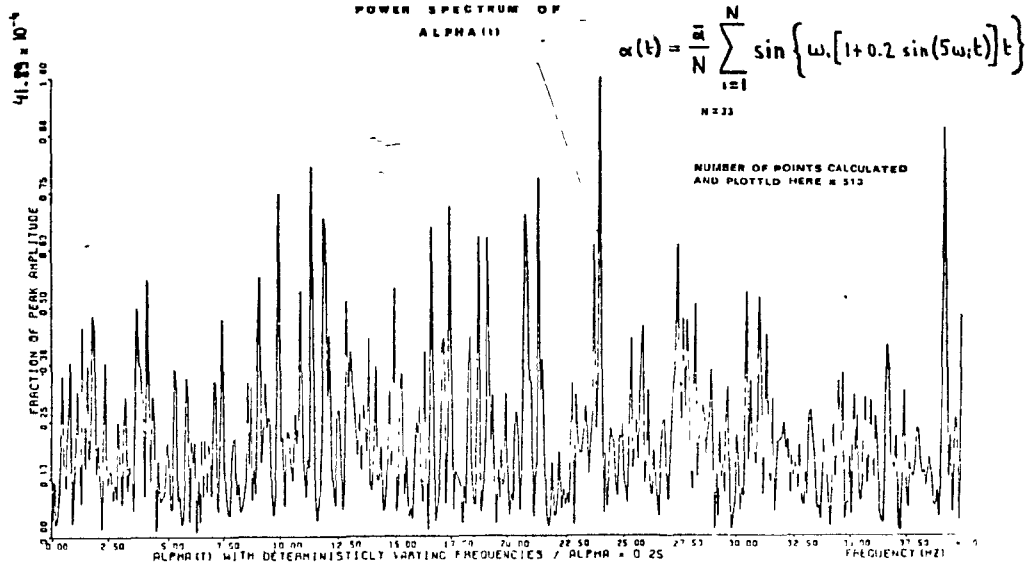


Fig.33. Power spectrum of  $\alpha(t)$  of scheme [g] with  $N=33$ ,  $\bar{\alpha} = 0.25$ ,  $\mu_i = 0.2$  and  $\lambda = 5$ . {Case B[g]}.

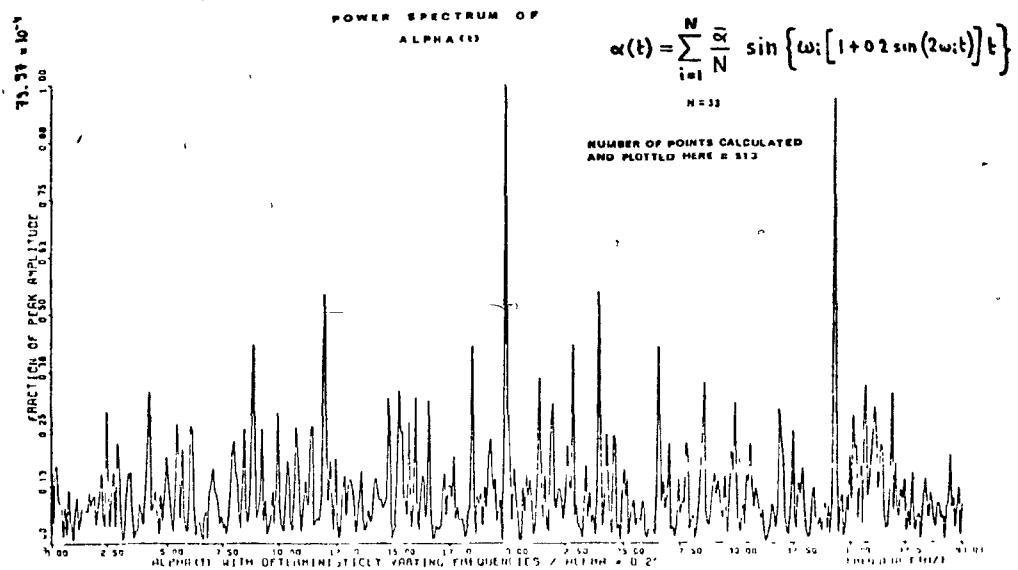


Fig.34. Power spectrum of  $\alpha(t)$  of scheme [g] with  $N=33$ ,  $\bar{\alpha} = 0.25$ ,  $\mu_i = 0.2$  and  $\lambda = 2$ . {Case B[g]}.

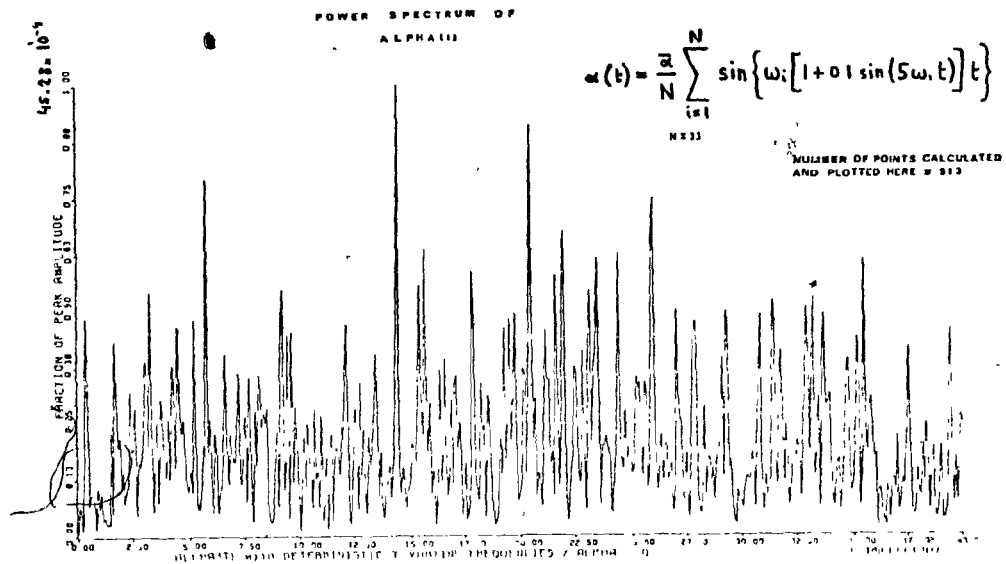


Fig. 35. Power spectrum of  $\alpha(t)$  of scheme [g] with  $N=33$ ,  $\bar{\alpha} = 0.25$ ,  $\mu_i = 0.1$  and  $\lambda = 5$ . {Case B[g]}.

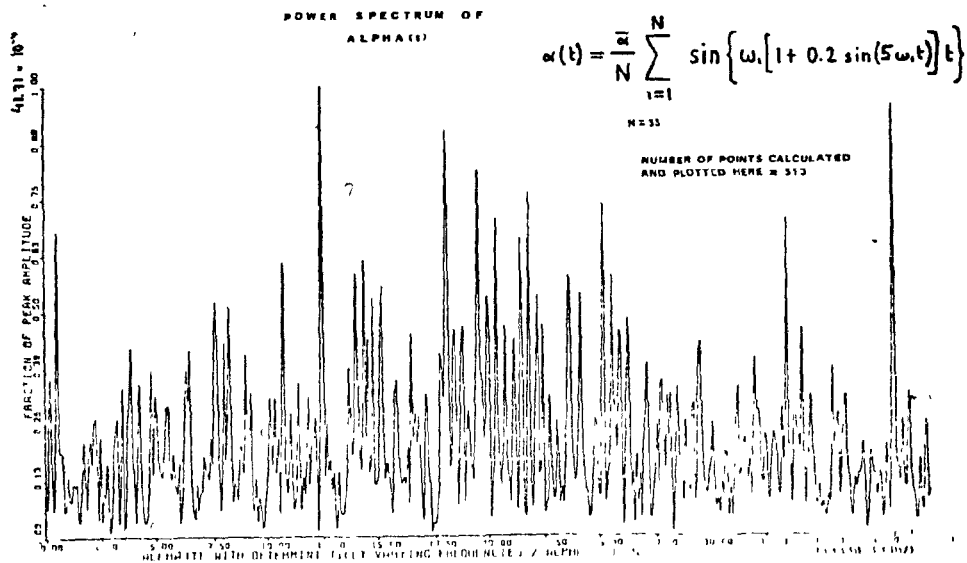


Fig. 36. Power spectrum of  $\alpha(t)$  of scheme [h] with  $N=33$ ,  $\bar{\alpha} = 0.25$ ,  $\mu_i = 0.2$  and  $\lambda = 5$ . {Case B[h]}.

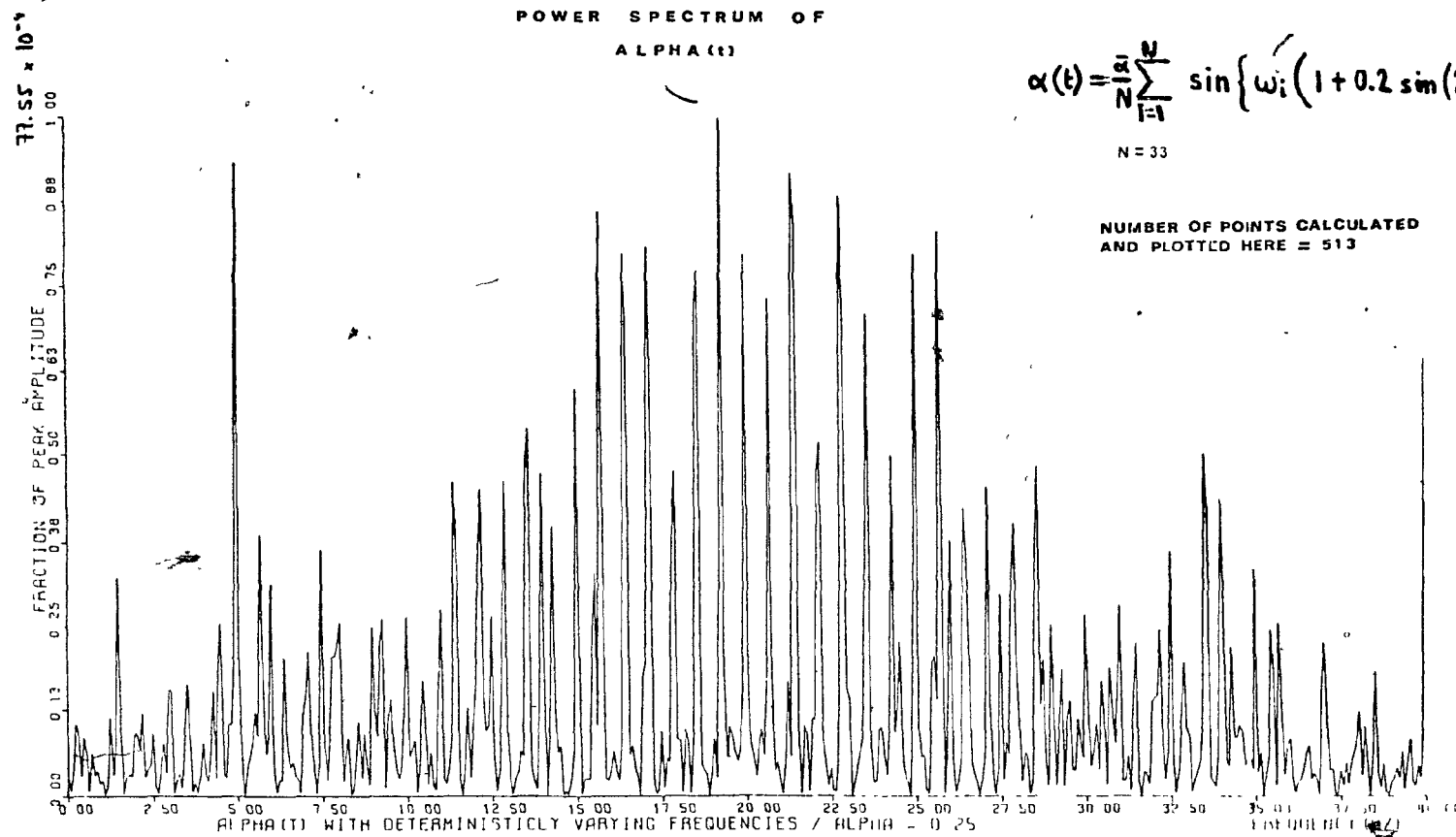


Fig.37. Power spectrum of  $\alpha(t)$  of scheme [h] with  $N=33$ ,  $\bar{\alpha} = 0.25$ ,  $\mu_i = 0.2$  and  $\lambda = 2$ .

{Case B[h]}.

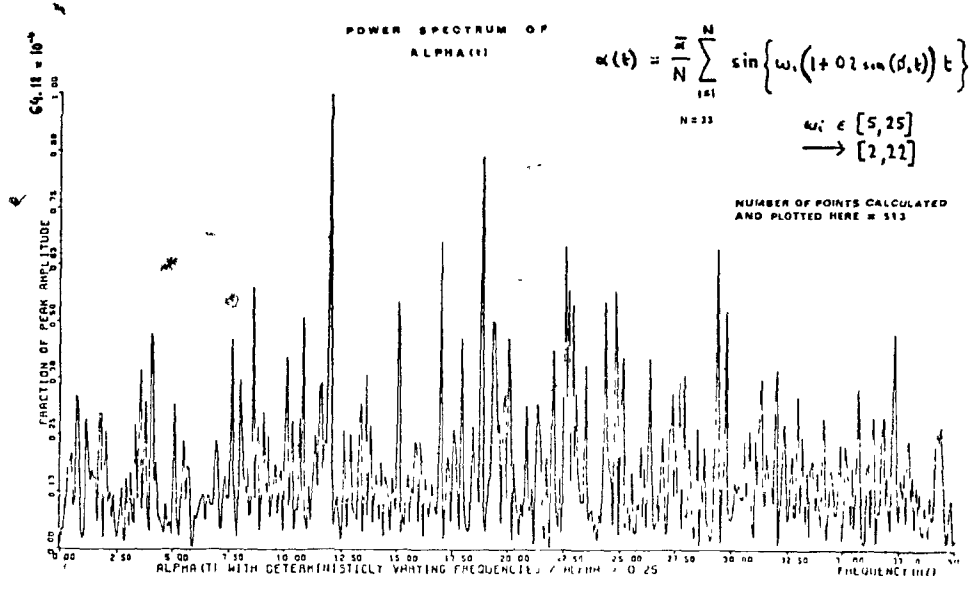


Fig.38. Power spectrum of  $\alpha(t)$  of scheme [j] with  $N=33$ ,  $\bar{\alpha} = 0.25$ ,  $\mu_j = 0.2$  and  $\lambda = 1$ . {Case B[j]}.

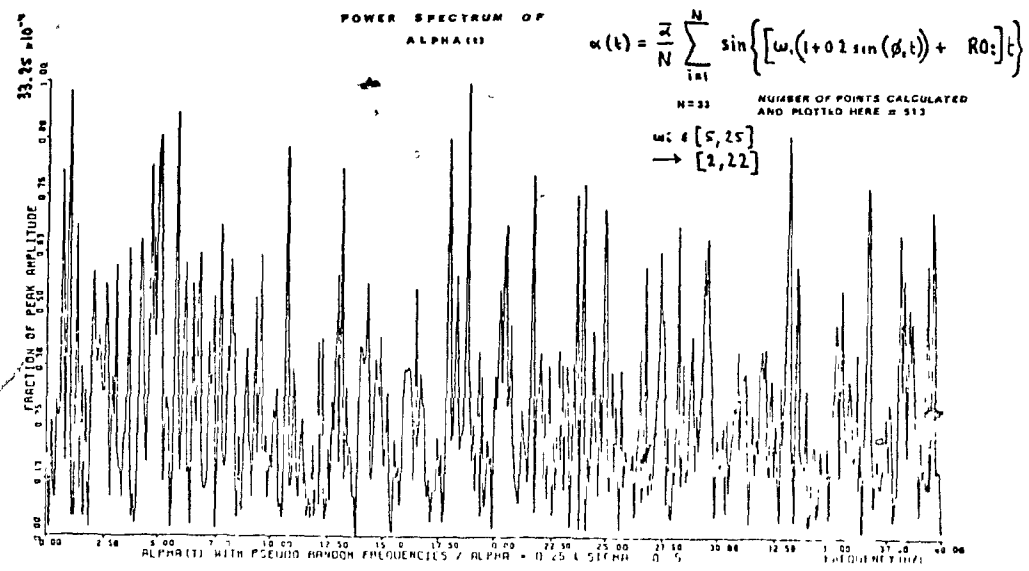


Fig.39. Power spectrum of  $\alpha(t)$  of scheme [k] with  $N=33$ ,  $\bar{\alpha} = 0.25$ ,  $\mu_j = 0.2$ ,  $\lambda = 1$  and  $\sigma = 0.25$  (pseudo-random case). {Case B[k]}.

X: 500.00 Hz  
A SPEC 1

$\Delta X: 2.0000$

#A: 1

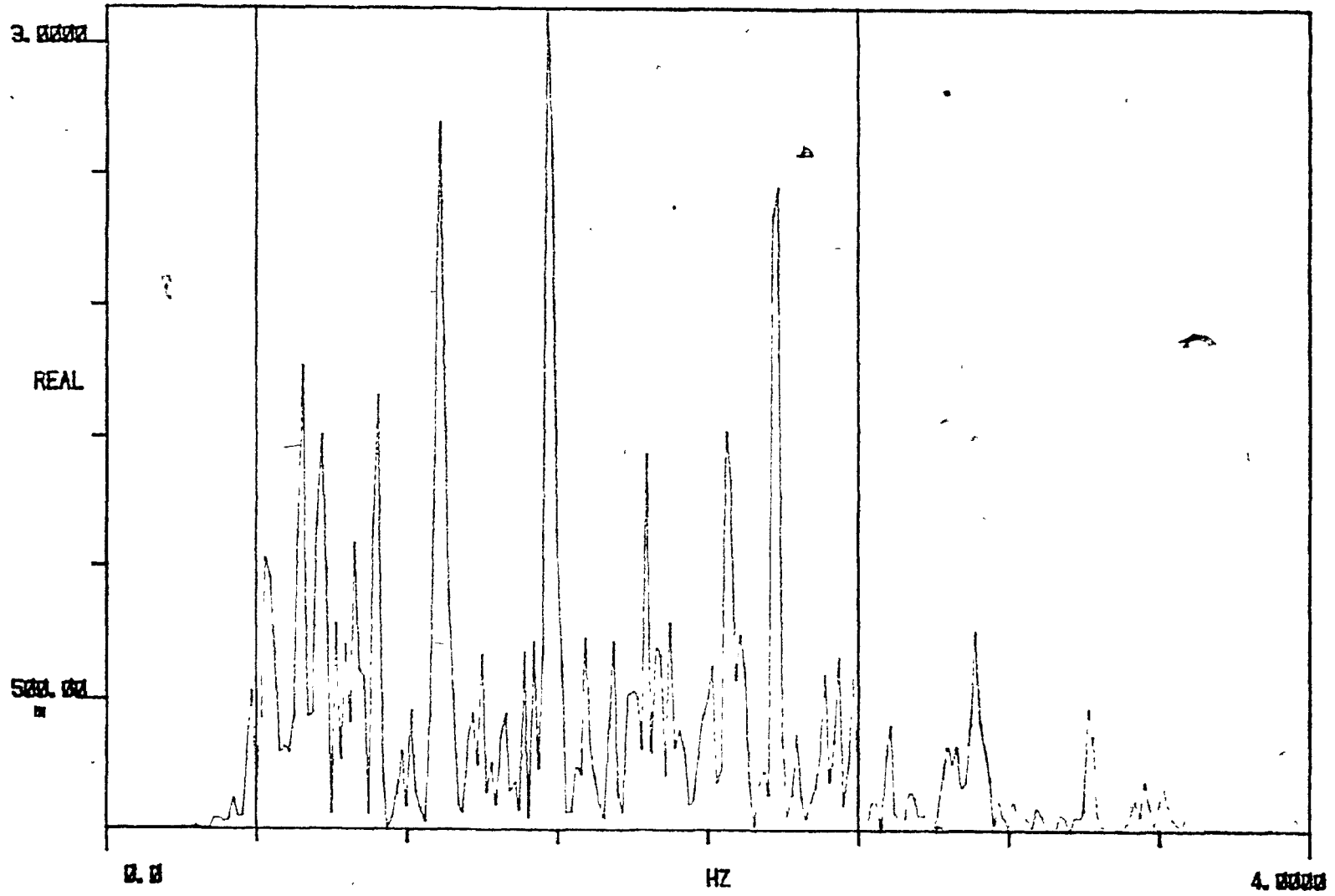


Fig.40(a). Power spectral density of the pseudo-random added mass perturbations generated for Chapter V, measured over one averaging step (256 samples during 64 seconds).

X: 500.00 m  
A SPEC 1

$\Delta X: 2.0000$

#A: 100

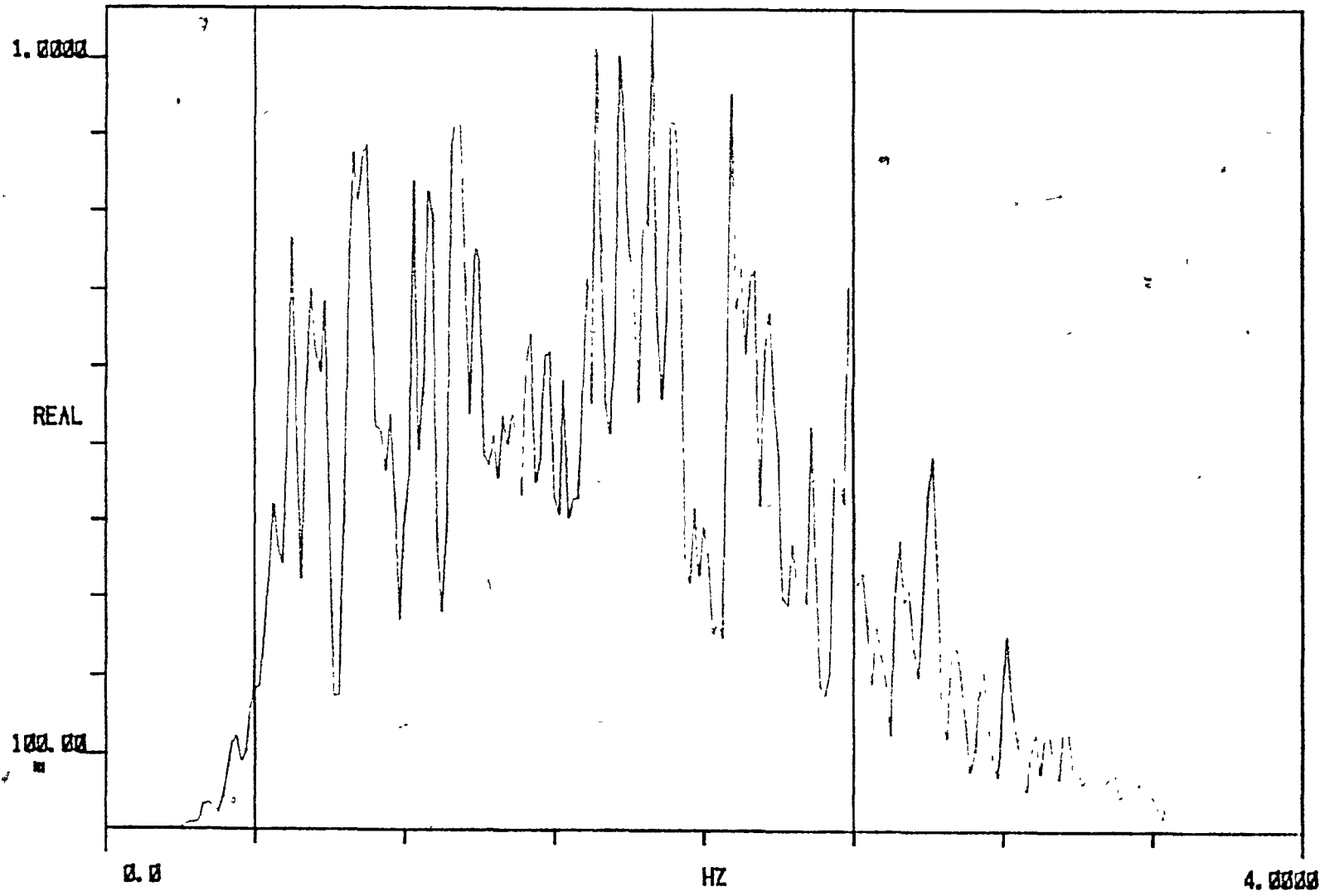


Fig.40(b). Power spectral density of the pseudo-random added mass perturbations generated for Chapter V, measured over 100 averaging steps.

X: 500.00 m  
A SPEC 1

$\Delta X: 2.0000$

#A: 1000

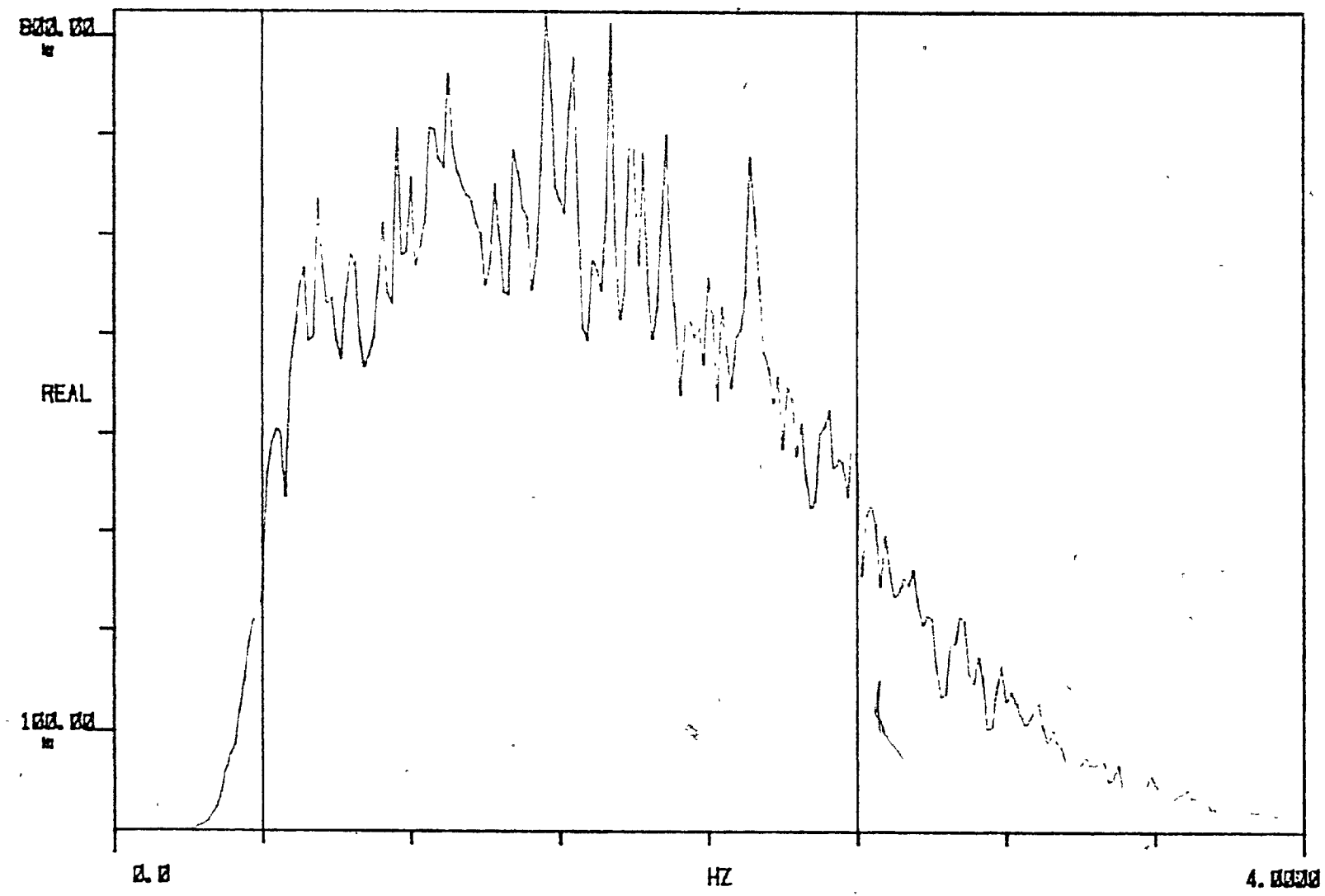


Fig.40(c). Power spectral density of the pseudo-random added mass perturbations generated for Chapter V, measured over 1000 averaging steps.

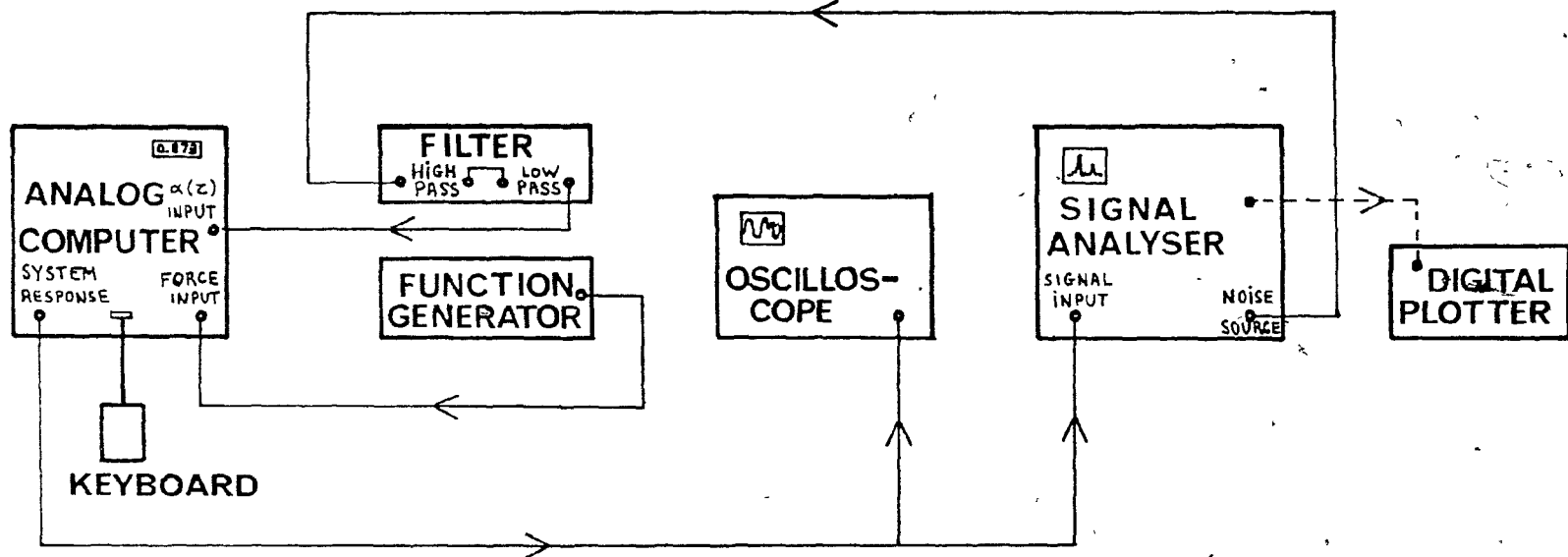


Fig.41. Schematic description of the analog experiment of Chapter V.

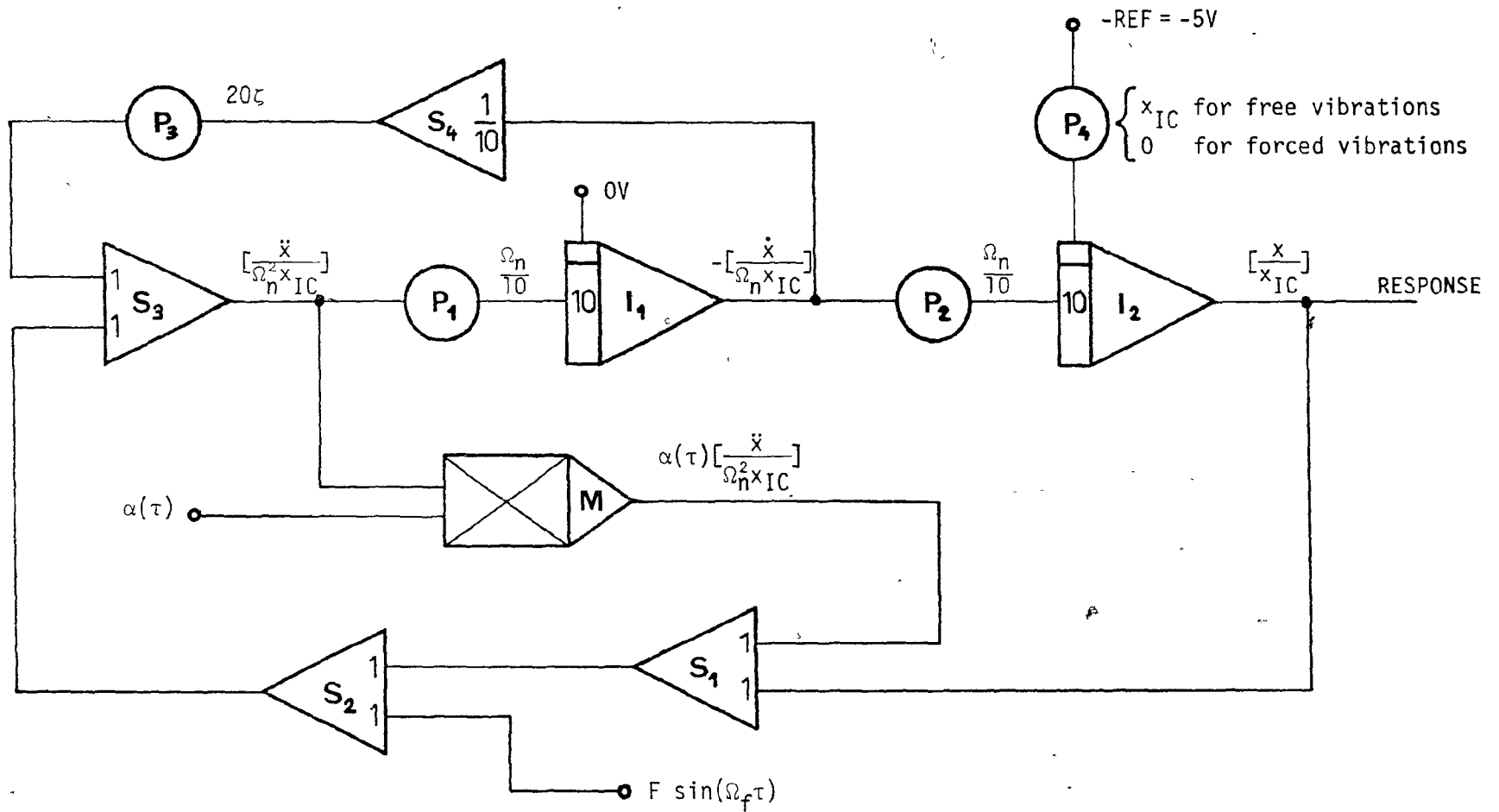


Fig.42. Circuit diagram used to solve equation (5-7) on the analog computer.

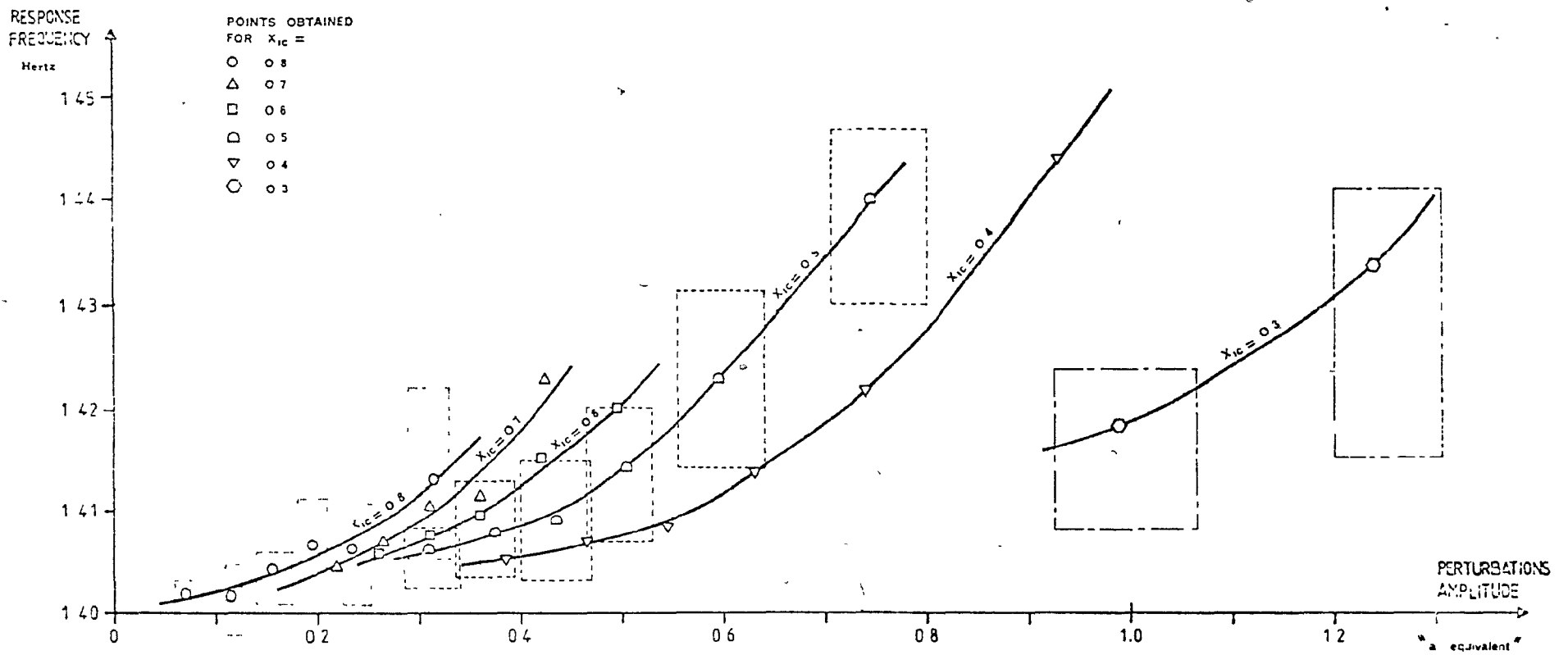


Fig.43. Free vibrations results obtained for six values of  $x_{IC}$ . For reasons of clarity, the rectangles of uncertainty are only given for  $x_{IC} = 0.8, 0.5$  and  $0.3$ .

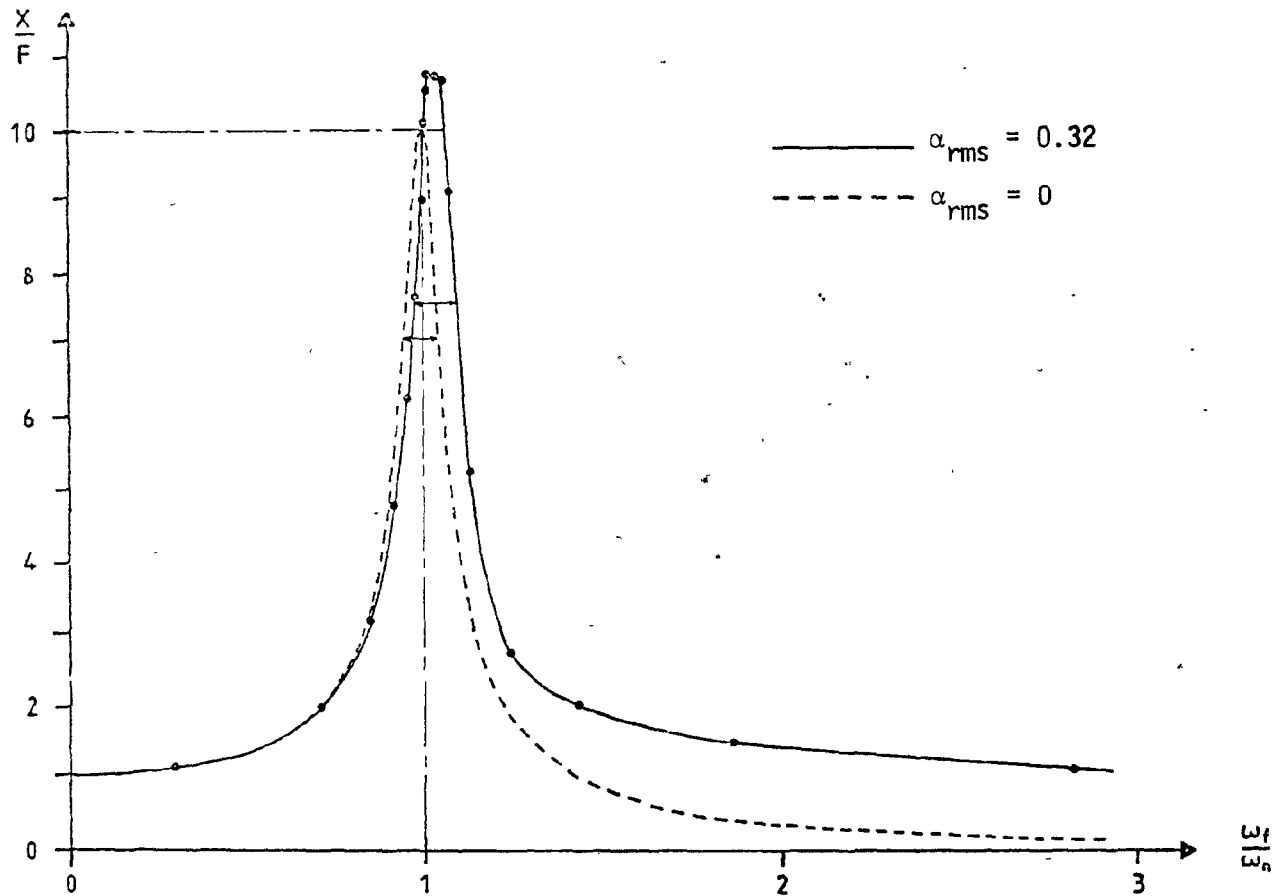


Fig.44. Forced vibrations results. The response curve  $X/F = f(\Omega_f/\Omega_n)$  corresponding to equation (5-7) with  $\alpha_{rms} = 0.32$  is compared to the reference case with  $\alpha_{rms} = 0$ .

X: 0.0  
A SPEC 1

$\Delta X: 3.9844$

#A: 300

POWER: 215.21  $\mu$

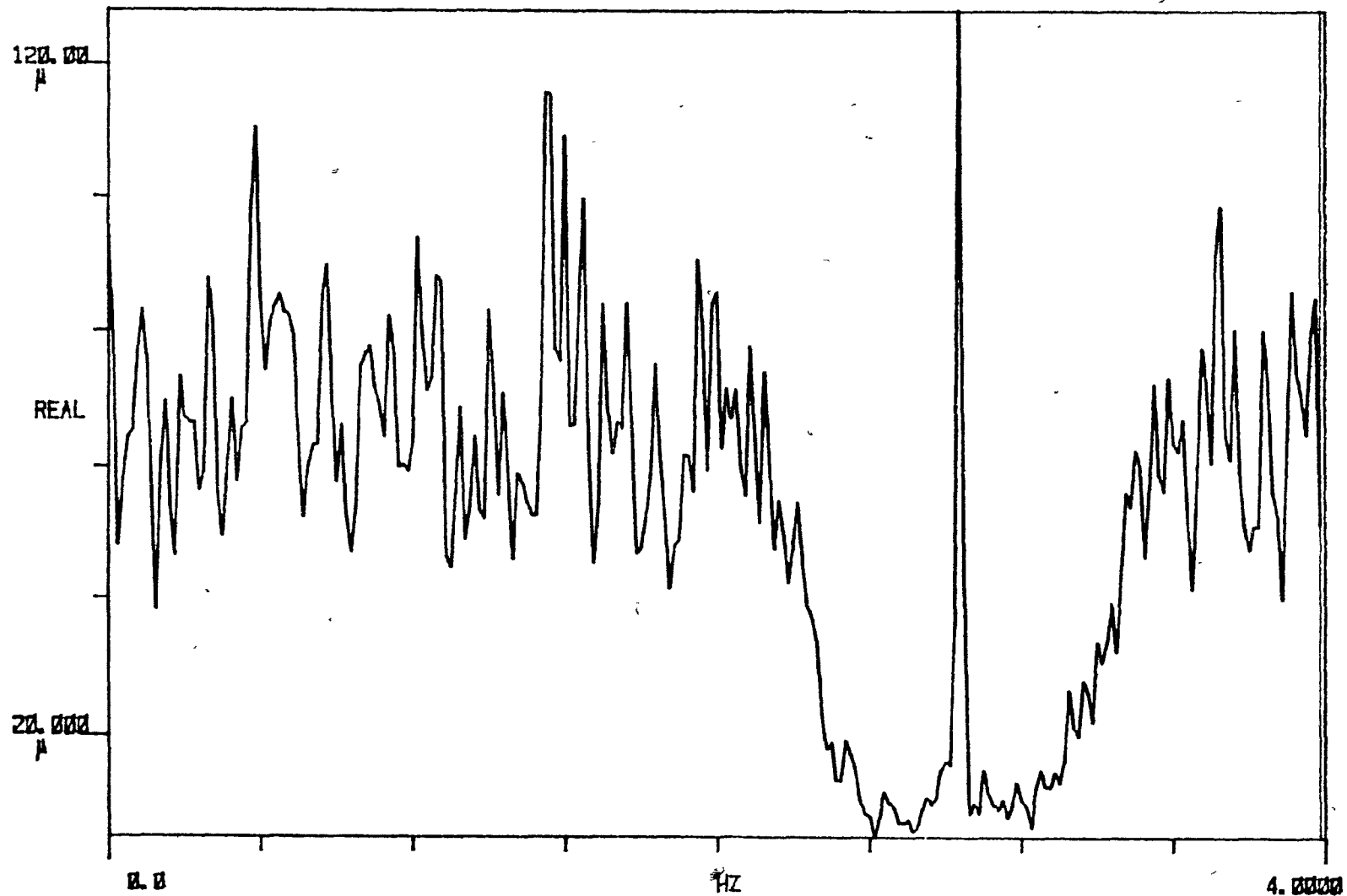


Fig.45(a). Power spectral density of  $\alpha(\tau)[\ddot{x}/\Omega_n^2 \times I_C]$ , obtained during the forced vibrations measurements. We have  $\zeta = 0.02$ ,  $\alpha_{rms} = 0.10$ , and the forcing frequency is 2.8 Hz.

X: 0.0  
A SPEC 1

$\Delta X: 3.9844$

#A: 300

POWER: 26.042 W

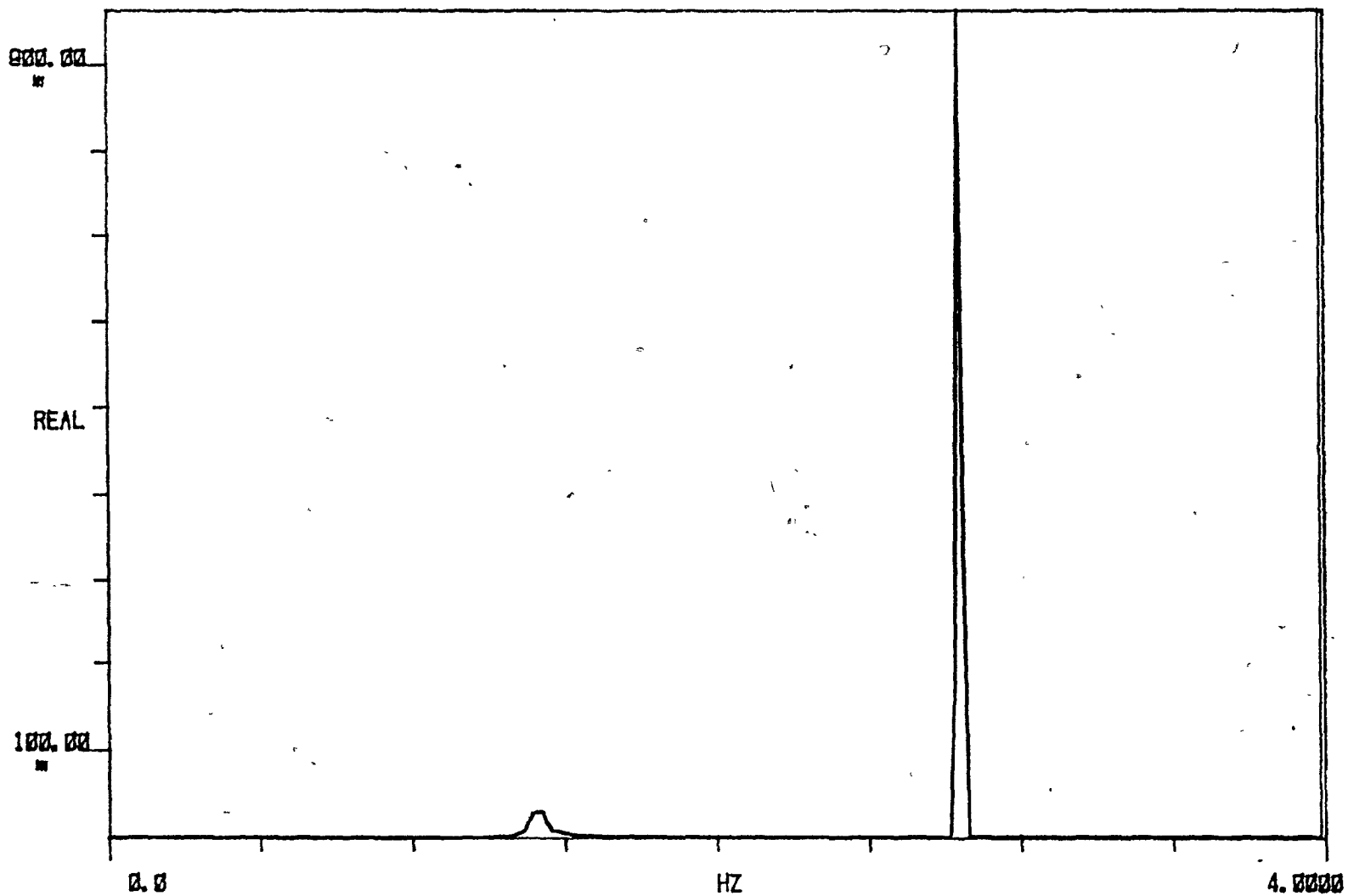


Fig. 45(b). Power spectral density of  $[\dot{x}/\omega_n^2 x_{IC}]$ , obtained during the forced vibrations measurements. We have  $\zeta = 0.02$ ,  $\alpha_{rms} = 0.10$ , and the forcing frequency is 2.8 Hz (whereas  $f_n = 1.4$  Hz).

X: 2.5783  
A SPEC 1

$\Delta X: 77.958$  m

#A: 300

POWER: 2.4580 m

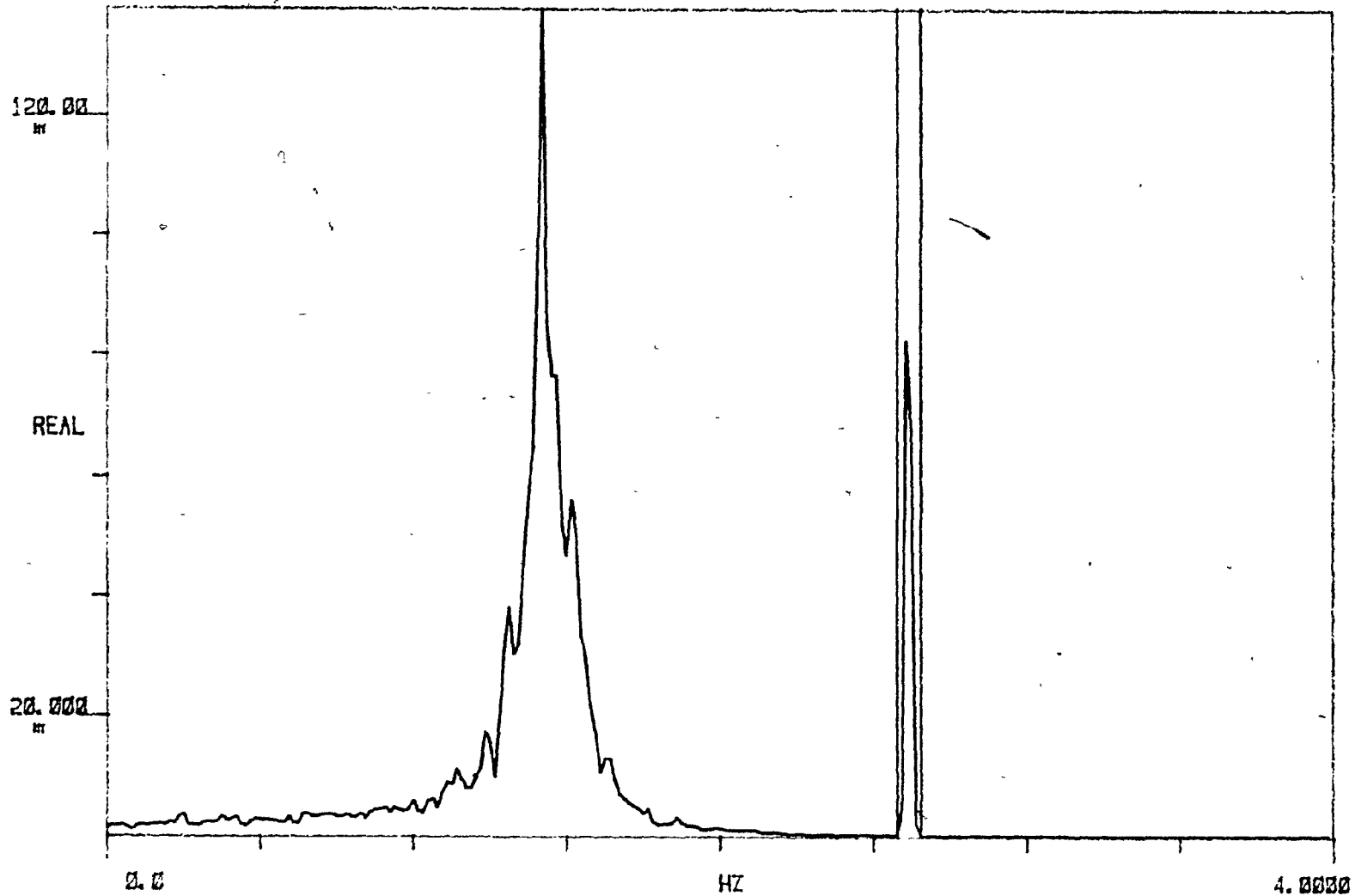


Fig.46(a). Power spectral density of the system response (forced vibrations). We have  $\zeta = 0.05$ ,  $\alpha_{rms} = 0.32$ , and the forcing frequency is 2.62 Hz ( $f_0 = 1.4$  Hz). Here the power  $(V_{rms})^2$  is measured about the forcing frequency peak.

X: 0.0  
A SPEC 1

ΔX: 3.9844

#A: 300

POWER: 26.721

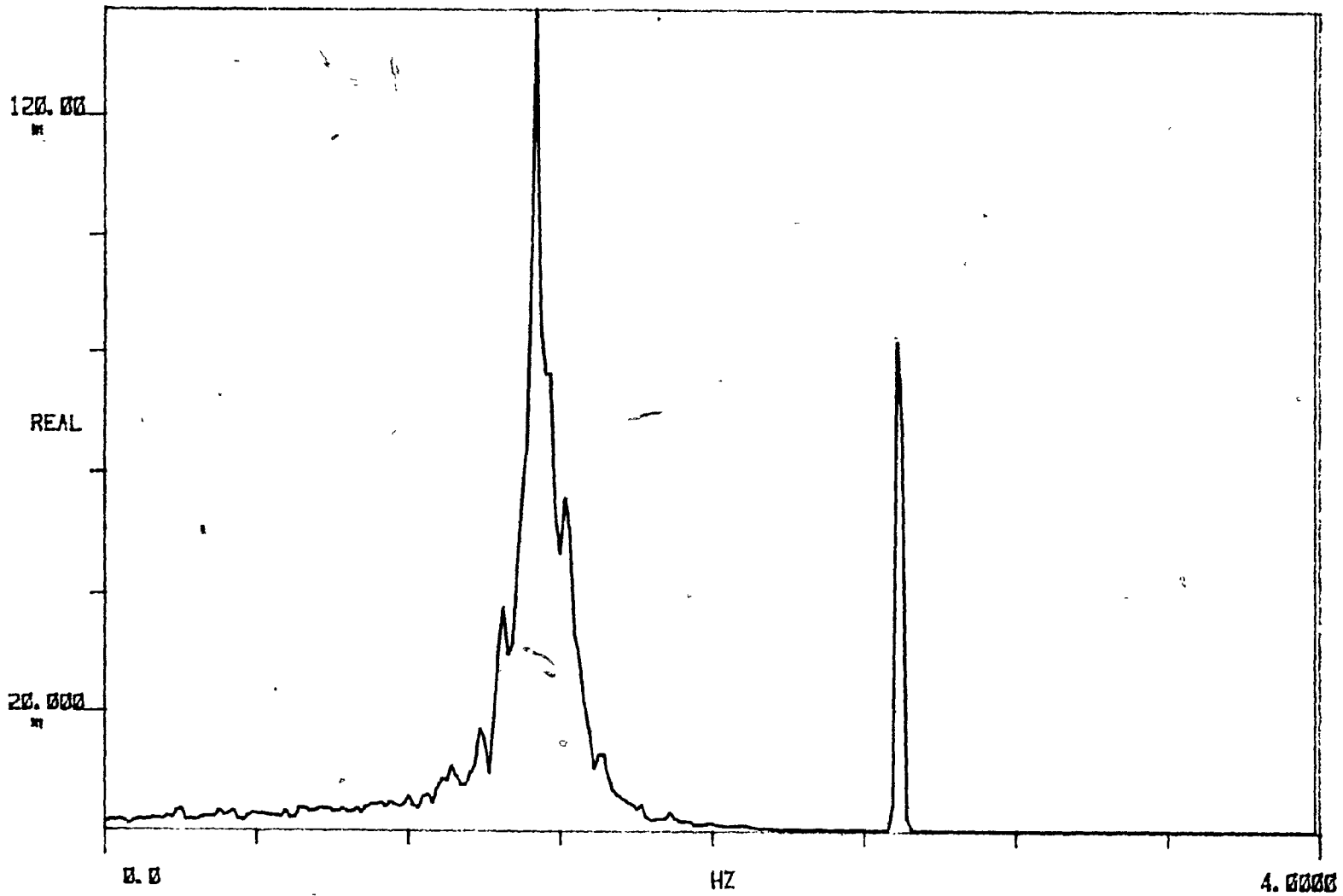


Fig.46(b). Same power spectral density of the system response as in Fig.46(a), but here the power  $(V_{rms})^2$  is measured over the whole frequency range (0 - 4 Hz).

## APPENDIX A

Discretization of the Equation of Small  
Lateral Motions in an Attempt to Obtain  
a Fokker-Planck Equation

Let us first give the values of the coefficients  $A_1$  to  $A_{10}$  of equation (2-9):

$$A_1 = \alpha_0$$

$$A_2 = 1$$

$$A_3 = u^2 [\chi - \frac{1}{2} \epsilon c_f (1 - \xi)(1 + h_0) - \frac{1}{2} c_b]$$

$$A_4 = 2\chi\beta_0^{\frac{1}{2}}u$$

$$A_5 = \chi\beta_0^{\frac{1}{2}}u = A_4/2$$

$$A_6 = \frac{1}{2}u^2\epsilon c_f(1 + h_0)$$

$$A_7 = \chi\beta_0$$

$$A_8 = \frac{1}{2}u\beta_0^{\frac{1}{2}}\epsilon c_f$$

$$A_9 = 1 - \beta_0$$

$$A_{10} = \chi\beta_0 = A_7$$

(A-1)

The first question arising now is to decide which stochastically varying quantity —  $U$ ,  $\rho$ , or even the momentum  $\rho U$  — is to be chosen as the principal random variable. We finally choose the density  $\rho$  (or  $s_1$ ) as the main random input and express all the other random variables in terms of  $s_1$ . To do so, we assume that:  $\overline{\rho U} = \bar{\rho}\bar{U}$  and  $\overline{\rho U^2} = \bar{\rho}\bar{U}^2$  so that

$$s_3 = s_1 s_2 \quad \text{and} \quad s_4 = s_1 s_2^2$$

(A-2)

We also assume that continuity is preserved at every cross-section at all times, i.e.

$$\rho UA = \text{constant.} \quad (\text{A-3})$$

Since  $A$  is constant, this yields:  $\rho U = \text{constant}$ , hence  $\rho U = \bar{\rho} \bar{U}$  and  $s_2 = s_1^{-1}$ . Finally we have

$$\begin{aligned} s_2 &= s_4 = s_1^{-1} \\ s_3 &= 1; \end{aligned} \quad (\text{A-4})$$

$s_3 = 1$  implies that  $\partial s_3 / \partial \tau = 0$ . If we furthermore assume that incompressibility is also preserved at every cross-section at all times (a strong assumption), we also have  $\partial s_1 / \partial \tau = 0$ .

The cylinder in axial flow may be subjected to an arbitrary force field  $f(\xi, \tau)$ ; hence, the dimensionless equation of small lateral motions reads

$$\begin{aligned} A_1 \frac{\partial^5 \eta}{\partial \xi^4 \partial \tau} + \frac{\partial^4 \eta}{\partial \xi^4} + \frac{A_3}{s_1} \frac{\partial^2 \eta}{\partial \xi^2} + A_4 \frac{\partial^2 \eta}{\partial \xi \partial \tau} + \frac{A_6}{s_1} \frac{\partial \eta}{\partial \xi} + A_8 \frac{\partial \eta}{\partial \tau} \\ + [A_9 + A_7 s_1] \frac{\partial^2 \eta}{\partial \tau^2} = f(\xi, \tau). \end{aligned} \quad (\text{A-5})$$

Our goal now is to transform equation (A-5) into an equation of the type of (2-11) in order to apply to it a procedure similar to that of Morton and Corrsin [41].

This transformation is done by the Galerkin approximation technique, which means that our continuous system is approximated by a  $n$ -degree-of-freedom discrete system, the accuracy of the method increasing with  $n$ .

To do this, we apply solutions of the type

$$\eta(\xi, \tau) = \sum_{i=1}^n \phi_i(\xi) q_i(\tau), \quad (\text{A-6})$$

where  $q_i(\tau)$  are the generalized coordinates and  $\phi_i(\xi)$  are eigenfunctions (at zero-flow velocity) of a beam with the same boundary conditions as the cylinder.

Due to the boundary conditions, the eigenfunctions  $\phi_i(\xi)$  are orthonormal, i.e.

$$\int_0^1 \phi_i(\xi) \phi_j(\xi) d\xi = \delta_{ij}, \quad (\text{A-7})$$

where  $\delta_{ij}$  is the Kronecker symbol.

Substituting (A-6) into (A-5), multiplying by  $\phi_r(\xi)$ ,  $r=1,2,\dots,n$ , and integrating over the domain (0,1) yields an equation of the type

$$[M]\{\ddot{q}\} + [C]\{\dot{q}\} + [K]\{q\} = \{Q\}, \quad (\text{A-8})$$

in which dots denote differentiation with respect to  $\tau$ .

Here  $\{q\}$  stands for the vector of the generalized coordinates:

$$\{q\} = \{q_1, q_2, \dots, q_n\}^T, \quad T \text{ denoting the transpose.}$$

$[Q]$  is also a column-matrix:  $[Q] = [Q_i]$ , whereas  $[M]$ ,  $[C]$  and  $[K]$  are  $n \times n$  square matrices:  $[M] = [m_{ij}]$

$$[C] = [c_{ij}]$$

$$[K] = [k_{ij}].$$

We have

$$m_{ij}(\xi, \tau) = A_9 \delta_{ij} + A_7 \int_0^1 s_1(\xi, \tau) \phi_i(\xi) \phi_j(\xi) d\xi,$$

$$c_{ij}(\xi, \tau) = [A_1 \lambda_i^4 + A_0] \delta_{ij} + A_4 \int_0^1 \phi_j'(\xi) \phi_i(\xi) d\xi,$$

$$k_{ij}(\xi, \tau) = \lambda_i^4 \delta_{ij} + A_3 \int_0^1 \frac{\phi_j''(\xi) \phi_i(\xi)}{s_1(\xi, \tau)} d\xi \\ + A_6 \int_0^1 \frac{\phi_j'(\xi) \phi_i(\xi)}{s_1(\xi, \tau)} d\xi,$$

$$Q_i(\xi, \tau) = \int_0^1 f(\xi, \tau) \phi_i(\xi) d\xi. \quad (\text{A-9})$$

$\lambda_i$  are the beam eigenvalues corresponding to the eigenfunctions  $\phi_i$ , and primes denote differentiation with respect to  $\xi$ .

Unfortunately we are still far from being able to follow a procedure similar to that of Morton and Corrsin [41], even in the first-mode approximation. The same holds for the procedure followed by Parthasarathy [79].

## APPENDIX B

Some Elements on the Probabilistic  
Formulation of the Fluid-Structure Interaction

B.1 Membrane in planar turbulent flow

We could undertake this study by considering the structural member to be a flexible cylinder, part of an infinitely long rigid beam, as described in Section 2.2 of Chapter II and as shown in Fig. 12. The cylinder would then undergo lateral motions in the (x,y)-plane, as assumed in Section 2.2, the equation of which would be

$$M \frac{\partial^2 y}{\partial t^2} + EI \frac{\partial^4 y}{\partial x^4} = F(x,t),$$

in which  $y(x,t)$  is the cylinder deformation and  $M$ ,  $EI$  and  $F(x,t)$  are, respectively, the mass of the cylinder, its flexural rigidity, and the hydrodynamic force in the (x,y)-plane, per unit length.

But, for simplicity, let us assume that the member consists of a membrane, or rather a strip of membrane, of width  $\delta z$  and extending from  $x=0$  to  $x=L$  [see Fig. 13(a)]. The membrane undergoes motion in the vertical plane (x,y), and the fluid-solid interaction is assumed to be exactly the same at each instant in each plane parallel to the (x,y)-plane. This means that we deal with a purely two-dimensional phenomenon. Moreover, the whole system is assumed to extend laterally to infinity ( $-\infty < z < +\infty$ ) and the fluid flow is unbounded. Actually, due to this configuration, we choose to work only on a strip of membrane, or even a string, by letting  $\delta z \rightarrow 0$ .

As far as the fluid flow is concerned, we consider the flow above this string, in the particular  $(x,y)$ -plane chosen as reference. We regard the fluid as a discrete medium made up of particles of same size, mass and all other physical characteristics. Thus, we still deal with a homogeneous model of the fluid. The fluid flow is supposed to enter the string region and pass over it in the form of a lattice-like structure, with the velocity  $U$  parallel to  $x$  [see Fig. 13(b)].

We focus our attention on a single fluid particle  $P$ , which enters the string region sliding on the string, at the instant  $t=0$ . Its initial position  $(x_0, y_0)$  is thence the origin  $(0,0)$  of the  $(x,y)$  reference plane, whilst its initial velocity is  $(v_{x_0}, v_{y_0}) = (U, 0)$ . It is then assumed that this particle will continue to slide on the surface of the string during its entire passage over the string, and will not "take off" from it. Our approach to the problem is inspired by the studies conducted on the Brownian motion, a good selection of which may be found in Ref. [46]. The dynamics of this fluid particle is described by a "generalized Langevin equation", expressed by equation (2-12). This two-dimensional Langevin equation can also be written in matricial form, as

$$\frac{d^2}{dt^2} \begin{bmatrix} x \\ y \end{bmatrix} + \begin{bmatrix} \beta & 0 \\ 0 & 0 \end{bmatrix} \frac{d}{dt} \begin{bmatrix} x \\ y \end{bmatrix} + \begin{bmatrix} \omega_0^2 & 0 \\ 0 & \omega_0^2 \end{bmatrix} \begin{bmatrix} x \\ y \end{bmatrix} = \begin{bmatrix} A_x(t) \\ A_y(t) \end{bmatrix}, \quad (\text{B-1})$$

or explicitly,

$$\text{in the } x\text{-direction: } \frac{d^2x}{dt^2} + \beta \frac{dx}{dt} + \omega_0^2 x = A_x(t), \quad (\text{B-2,a})$$

$$\text{in the } y\text{-direction: } \frac{d^2y}{dt^2} + \omega_0^2 y = A_y(t) . \quad (\text{B-2,b})$$

In the above,  $x$  and  $y$  are the co-ordinates of the fluid particle  $P$  considered, whereas  $\beta$  is the Stokes' drag denoting the interaction between the particle  $P$  and the string (membrane) surface. Usually  $\beta$  is taken to be equal to  $f/m$  where  $f$  is the friction coefficient and  $m$  is the mass of  $P$  (another expression of  $\beta$  has been adopted by Chandrasekhar and may be found as equation (133) of Ref. [44]). This friction exists here in the  $x$ -direction only, i.e. along the string surface.  $K(x) = -\omega_0^2 x$  and  $K(y) = -\omega_0^2 y$  are the two components of a harmonic-type force denoting the attraction of the particle  $P$  to its neighbours. Finally,  $A_x(t)$  and  $A_y(t)$  are the components of a randomly fluctuating loading force representing the hydrodynamic disturbing force due to the surrounding particles.

The motion of this particle  $P$  is coupled with the motion of the string by the following two relations:

(i) the equation of lateral motions of the string

$$M \frac{\partial^2 f(x,t)}{\partial t^2} - T \frac{\partial^2 f(x,t)}{\partial x^2} = -A_y(t) , \quad (\text{B-3})$$

in which  $f(x,t)$  is the string deformation,  $T$  is the constant tension in the string, whereas  $M$  and  $-A_y(t)$  are respectively the mass of the string and the vertical hydrodynamic force per particle length  $dx$ ; this last term is identical with the loading in equation (B-2).

(ii) the kinematic boundary condition

$$v_y = v_x \frac{\partial f(x,t)}{\partial x} + \frac{\partial f(x,t)}{\partial t} , \quad (\text{B-4})$$

which arises from the assumption that the particle of co-ordinates  $(x,y)$  slides continuously on the string.  $(v_x, v_y)$  are the components of the particle velocity and are equal to  $(\frac{dx}{dt}, \frac{dy}{dt})$ .

## B.2 Investigation of the random loading force $\vec{A}(t)$

$\vec{A}(t)$ , and in particular its component  $A_y(t)$ , is the looked-for solution to the problem. We cannot assume white noise for  $\vec{A}(t)$ , not even for  $A_x(t)$ , because we know from theoretical continuum studies, as well as from experiments, that the system (beam + fluid) vibrates at certain discrete frequencies. These are macroscopic waves in the fluid, propagating radially as well as axially. It is therefore proposed to regard  $\vec{A}(t)$  as a superposition of two kinds of perturbation:

- (a)  $\vec{A}^m(t)$  stemming from molecular hydrodynamics. This part is white noise since a Brownian particle under normal conditions in liquid will suffer about  $10^{21}$  collisions per second and its motion can be assumed to be purely random on the macroscopic scale.
- (b)  $\vec{A}^c(t)$  stemming from flow-elastic coupled motions, where  $c$  stands for coupling. This term is the unknown.

We hence have

$$\vec{A}(t) = \vec{A}^m(t) + \vec{A}^c(t), \quad (\text{B-5})$$

which can be written down more precisely by rendering explicit its components,

$$\text{in the } x\text{-direction: } A_x(t) = A_x^m(t) + A_x^c(t) \quad (\text{B-5', a})$$

$$\text{in the } y\text{-direction: } A_y(t) = A_y^m(t) + A_y^c(t). \quad (\text{B-5',b})$$

We now make some assumptions on the microscopic randomly fluctuating components  $A_x^m(t)$  and  $A_y^m(t)$ , in a procedure similar to the one followed by Wang and Uhlenbeck (equations (41a) and (41b) of Ref. [45]).

In the x-direction, we assume that

$$\langle A_x^m(t) \rangle = 0, \quad (\text{B-6,a})$$

$$\langle A_x^m(t_1) A_x^m(t_2) \rangle = 2D\delta(t_1 - t_2), \quad (\text{B-6,b})$$

where  $\langle \rangle$  represents the average value and is defined as

$$\langle u(t) \rangle = \lim_{T \rightarrow \infty} \frac{1}{2T} \int_{-T}^T u(t) dt,$$

$$\text{and } \langle u(t) u(t+\tau) \rangle = \lim_{T \rightarrow \infty} \frac{1}{2T} \int_{-T}^T u(t) u(t+\tau) dt$$

(thus  $\langle \rangle$  denotes a long time-average).  $\delta$  is the Dirac delta function, and we also have

$$D = \frac{\beta k T}{m},$$

in which  $k$  is the Boltzmann constant and  $T$  is the absolute temperature.

In the y-direction, we assume that

$$\langle A_y^m(t) \rangle = 0, \quad (\text{B-7,a})$$

$$\langle A_y^m(t_1) A_y^m(t_2) \rangle = 0, \quad (\text{B-7,b})$$

since we have assumed there is no friction in the y-direction.

### B.3 Integration of the generalized Langevin equation over a specific time interval $\Delta T$

Having given these details on  $\vec{A}(t)$ , we are now able to integrate the generalized Langevin equation over a specific time interval  $\Delta t$  which first needs to be rendered more precise. It is the essence of Brownian motion that there exist time intervals  $\Delta T$  during which the physical parameters (such as position or velocity of the particle) change only by "infinitesimal" amounts, i.e. they remain nearly constant, whilst there occur a very large number of fluctuations of the two microscopic fluctuators  $A_x^m(t)$  and  $A_y^m(t)$ . We can say furthermore that the variations of  $A_x^C(t)$  and  $A_y^C(t)$ , which would be in synchronism with the vibrating string, will be slower than the variations of the position or velocity of P.

Three time scales of vibration have thus been identified, and we choose  $\Delta T$  such that it be still very long compared to the longest characteristic times in  $A_x^m(t)$  and  $A_y^m(t)$ , but very short compared with the shortest characteristic times in  $x$ ,  $y$ ,  $v_x$ ,  $v_y$ ,  $A_x^C(t)$  and  $A_y^C(t)$ , which can thus be considered as essentially constant. The existence of such a doubly asymptotic time interval is crucial to the standard Fokker-Planck formulation.

Let us now start the integration. In the x-direction, we obtain from (B-2,a) and (B-5',a):

$$\frac{d^2x}{dt^2} + \beta \frac{dx}{dt} + \omega_0^2 x = A_x^C(t) + A_x^m(t),$$

which can be written as

$$\frac{dx}{dt} = v_x$$

$$\frac{dv_x}{dt} = -\beta v_x - \omega_0^2 x + A_x^C(t) + A_x^m(t).$$

Integrating over the afore-defined time interval  $\Delta T$ , we get

$$\Delta x = v_x \Delta t \quad (\text{B-8,a})$$

$$\Delta v_x = (-Bv_x - \omega_0^2 x + A_x^c) \Delta t + \int_t^{t+\Delta t} A_x^m(\xi) d\xi, \quad (\text{B-8,b})$$

in which  $\Delta x = x(t+\Delta t) - x(t)$ , and  $\xi$  is a dummy variable.

Having done this, it is easy to obtain the coefficients of the two-dimensional Fokker-Planck equation, following a procedure similar to those of Wang and Uhlenbeck (page 334 of Ref.[45]), or Morton and Corrsin [41].

This equation, in the x-direction, reads

$$\begin{aligned} \frac{\partial P_x}{\partial t} = & -\left(\frac{\partial}{\partial x} [A_1^x P_x] + \frac{\partial}{\partial v_x} [A_2^x P_x]\right) \\ & + \frac{1}{2} \left(\frac{\partial^2}{\partial x^2} [B_{11}^x P_x] + \frac{\partial^2}{\partial x \partial v_x} [B_{12}^x P_x] + \frac{\partial^2}{\partial v_x^2} [B_{22}^x P_x]\right). \end{aligned} \quad (\text{B-9})$$

To obtain the Fokker-Planck equation in the y-direction, one has to replace  $x$  by  $y$ ,  $v_x$  by  $v_y$ , the  $A_i^x$  and  $B_{ij}^x$  coefficients by  $A_i^y$  and  $B_{ij}^y$ , respectively, and  $P_x$  by  $P_y$  are conditional probabilities which will be specified later on.

We have

$$A_1^x = \lim_{\Delta t \rightarrow 0} \frac{\langle \Delta x \rangle}{\Delta t} \quad (\text{B-10,a})$$

$$A_2^x = \lim_{\Delta t \rightarrow 0} \frac{\langle \Delta v_x \rangle}{\Delta t} \quad (\text{B-10,b})$$

$$B_{11}^x = \lim_{\Delta t \rightarrow 0} \frac{\langle (\Delta x)^2 \rangle}{\Delta t} \quad (\text{B-10,c})$$

$$B_{12}^x = \lim_{\Delta t \rightarrow 0} \frac{\langle \Delta x \Delta v_x \rangle}{\Delta t} \quad (\text{B-10,d})$$

$$B_{22}^x = \lim_{\Delta t \rightarrow 0} \frac{\langle (\Delta v_x)^2 \rangle}{\Delta t} \quad (\text{B-10,e})$$

The relations for obtaining the  $A_i^y$  and  $B_{ij}^y$  are quite similar, and one merely needs to replace the letter x by the letter y, as appropriate.

Let us now calculate these coefficients.

- From (B-8,a):

$$\Delta x = v_x \Delta t,$$

and

$$\langle \Delta x \rangle = \langle v_x \Delta t \rangle = v_x \langle \Delta t \rangle = v_x \Delta t;$$

hence,

$$A_1^x = \lim_{\Delta t \rightarrow 0} \frac{\langle \Delta x \rangle}{\Delta t} = v_x. \quad (\text{B-11,a})$$

- From (B-8,b):

$$\Delta v_x = (-\beta v_x - \omega_0^2 x + A_x^c) \Delta t + \int_t^{t+\Delta t} A_x^m(\xi) d\xi$$

Averaging and taking (B-6,a) into account,

$$\langle \Delta v_x \rangle = (-\beta v_x - \omega_0^2 x + A_x^c) \Delta t;$$

hence,

$$A_2^x = \lim_{\Delta t \rightarrow 0} \frac{\langle \Delta v_x \rangle}{\Delta t} = -\beta v_x - \omega_0^2 x + A_x^c. \quad (\text{B-11,b})$$

$$\langle (\Delta x)^2 \rangle = \langle v_x^2 (\Delta t)^2 \rangle = v_x^2 (\Delta t)^2;$$

hence,

$$B_{11}^x = \lim_{\Delta t \rightarrow 0} \frac{\langle (\Delta x)^2 \rangle}{\Delta t} = \lim_{\Delta t \rightarrow 0} v_x^2 \Delta t = 0 \quad (\text{B-11,c})$$

$$\begin{aligned} \langle \Delta x \Delta v_x \rangle &= v_x (-\beta v_x - \omega_0^2 x + A_x^C) (\Delta t)^2 + v_x \Delta t \cdot \int_t^{t+\Delta t} \langle A_x^m(\xi) \rangle d\xi \\ &= v_x (-\beta v_x - \omega_0^2 x + A_x^C) (\Delta t)^2, \end{aligned}$$

because of (B-6,a); hence,

$$B_{12}^x = \lim_{\Delta t \rightarrow 0} \frac{\langle \Delta x \Delta v_x \rangle}{\Delta t} = \lim_{\Delta t \rightarrow 0} v_x (-\beta v_x - \omega_0^2 x + A_x^C) \Delta t = 0 \quad (\text{B-11,d})$$

$$\begin{aligned} \langle (\Delta v_x)^2 \rangle &= (-\beta v_x - \omega_0^2 x + A_x^C)^2 (\Delta t)^2 \\ &\quad + 2(-\beta v_x - \omega_0^2 x + A_x^C) \Delta t \cdot \int_t^{t+\Delta t} \langle A_x^m(\xi) \rangle d\xi \\ &\quad + \int_t^{t+\Delta t} \int_t^{t+\Delta t} \langle A_x^m(t_1) A_x^m(t_2) \rangle dt_1 dt_2, \end{aligned}$$

where  $t_1$  and  $t_2$  are dummy variables. The limit of the first term is zero because of the factor  $(\Delta t)^2$ ; the limit of the second term is also zero, because of (B-6,a); hence, we are left with the third term which, due to (B-6,b), becomes

$$\langle (\Delta v_x)^2 \rangle = 2D \int_t^{t+\Delta t} \int_t^{t+\Delta t} \delta(t_1 - t_2) dt_1 dt_2,$$

and finally

$$B_{22}^x = \lim_{\Delta t \rightarrow 0} \frac{\langle (\Delta v_x)^2 \rangle}{\Delta t} = 2D. \quad (\text{B-11,e})$$

The same type of procedure can be pursued on the Langevin equation in the  $y$ -direction (equation B-2,b), and we finally end up with a set of two coupled Fokker-Planck (or Kramers) equations

$$\frac{\partial P_x}{\partial t} = -v_x \frac{\partial P_x}{\partial x} + \frac{\partial}{\partial v_x} [(\beta v_x + \omega_0^2 x - A_x^C) P_x] + D \frac{\partial^2 P_x}{\partial v_x^2}, \quad (\text{B-12,a})$$

$$\frac{\partial P_y}{\partial t} = -v_y \frac{\partial P_y}{\partial y} + \frac{\partial}{\partial v_y} [(\omega_0^2 y - A_y^C) P_y], \quad (\text{B-12,b})$$

where

$$P_x = P(x, v_x, t | x_0, v_{x0})$$

and

$$P_y = P(y, v_y, t | y_0, v_{y0})$$

are conditional probability density functions, defined by the statement that if the system is at  $x_0$  and  $v_{x0}$  at time zero, then  $P(x, v_x, t | x_0, v_{x0}) \times dx dv_x$  is the probability that it will be between  $x$  and  $x + dx$  and have a velocity between  $v_x$  and  $v_x + dv_x$  at time  $t$ . The definition of  $P_y$  is quite similar.

## APPENDIX C

Complements to the Digital  
Time Domain Analysis of Chapter III

C.1 Runge-Kutta method

The Runge-Kutta (4-point) scheme is used here to solve the differential equation (2-16) representing the system finally adopted. Actually, we use form (2-14) of this equation, but this does not matter at all since the two forms are equivalent. We also take equation (2-15) into account and introduce CM which stands for the constant (time-invariant) mass and is equal to

$$CM = M + \overline{m}_h. \quad (C-1)$$

By introducing the time derivative of  $x$  with respect to time,

$$y = \dot{x} = \frac{dx}{dt},$$

equation (2-14), which is a second-order differential equation, can be written as a set of two first-order differential equation as follows;

$$\frac{dx}{dt} = f(t, x, y) = y \quad (C-2, a)$$

$$\frac{dy}{dt} = g(t, x, y) = -\frac{K}{CM + \mu(t)} x - \frac{C}{CM + \mu(t)} y + \frac{f_0(t)}{CM + \mu(t)}. \quad (C-2, b)$$

To solve this, we then apply the Runge-Kutta iteration formulae,

namely

$$x_1 = x_0 + \frac{1}{6}(k_1 + 2k_2 + 2k_3 + k_4) \quad (C-3, a)$$

$$y_1 = y_0 + \frac{1}{6}(l_1 + 2l_2 + 2l_3 + l_4), \quad (C-3,b)$$

in which

$$k_1 = h f(t_0, x_0, y_0)$$

$$l_1 = h g(t_0, x_0, y_0)$$

$$k_2 = h f(t_0 + \frac{h}{2}, x_0 + \frac{k_1}{2}, y_0 + \frac{l_1}{2})$$

$$l_2 = h g(t_0 + \frac{h}{2}, x_0 + \frac{k_1}{2}, y_0 + \frac{l_1}{2})$$

$$k_3 = h f(t_0 + \frac{h}{2}, x_0 + \frac{k_2}{2}, y_0 + \frac{l_2}{2})$$

$$l_3 = h g(t_0 + \frac{h}{2}, x_0 + \frac{k_2}{2}, y_0 + \frac{l_2}{2})$$

$$k_4 = h f(t_0 + h, x_0 + k_3, y_0 + l_3)$$

$$l_4 = h g(t_0 + h, x_0 + k_3, y_0 + l_3),$$

f and g being respectively the functions defined in (C-2,a) and (C-2,b), whereas h is the step-size chosen.

The very first pair  $(x_0, y_0)$  is obtained from the initial conditions applied to the system.

## C.2 Generation of pseudo-random Gaussian perturbations

The perturbations  $\alpha(t)$  of the hydrodynamic mass are obtained in two steps.

First pseudo-random numbers are generated according to the uniform probability distribution

$$p_u(x) = 1; \quad 0 \leq x \leq 1. \quad (C-4)$$

This is classically achieved by the following sub-program (given in Fortran):

Initial values (in main program):

$$IR = 1$$

$$J = 5 * 13$$

Iteration scheme (in sub-program):

```

D01  I = 1,N
      IR = IR*J
      IF (IR.LT.0)  IR = IR+2*(2**30-1)+2
      R = DFLOAT (IR)/2.DO**31
1    RU(I) = R

```

RU(I) denotes the ith uniform random variate.

The next step is now to transform these numbers into another set of random numbers according to another probability distribution  $p(x)$ . It may be mentioned here that, according to exact terminology, we should call  $p(x)$  a probability density rather than a probability distribution since the latter is defined as  $F(x) = \int_{-\infty}^{+\infty} p(x) dx$ , but such a distinction is not fundamental at this stage and the vocabulary confusion may be considered permissible.

If we call  $r_i$  the ith random variate according to the uniform distribution (C-4) generated by the subroutine above, then  $x_i$ , the ith variate according to the new distribution  $p(x)$ , is obtained as solution to the equation

$$\int_a^{x_i} p(x) dx = r_i. \quad (C-5)$$

In our case we consider the Gaussian distribution, i.e. we have

$$p(x) = \frac{1}{\sqrt{2\pi} \sigma} e^{-\frac{(x-\mu)^2}{2\sigma^2}}, \quad (C-6)$$

in which  $\mu$  and  $\sigma^2$  are respectively the mean and variance of the Gaussian distribution (the square root  $\sigma$  of the variance is called the standard deviation).

Hence, the pseudo-random number  $x_i$  is obtained by solving

$$\int_a^{x_i} e^{-\frac{(x-\mu)^2}{2\sigma^2}} dx = \sqrt{2\pi} \sigma r_i. \quad (C-5')$$

Before solving this equation, the constants  $a$ ,  $\mu$  and  $\sigma$  have to be known;  $a$  can be chosen to be equal to  $\mu - 3\sigma$ , and a few words on the determination of  $\mu$  and  $\sigma$  will be given in Appendix C.3. Having specified that, we can now indicate the numerical method used to solve equation (C-5'). The secant method is chosen to solve it, whereas Simpson's method is adopted to evaluate the numerous integrals required by the use of the secant method. But such a procedure is obviously very long, requiring a great number of calculations (and, hence computer time) to obtain merely one random number  $x_i$ . Moreover, when considering that only for one oscillation cycle, we need 300 or 500 (cf. Appendix C.3) such random variates, it becomes clear enough that a simpler procedure has to be found to generate the normal (Gaussian) variates. Anyway, an approximately Gaussian  $\alpha(t)$  is sufficient for our purpose.

The new procedure which was actually adopted is a consequence of the Central Limit Theorem [50], which states that

"if  $y_1, y_2, \dots, y_n$  are independent random samples of a stochastic event following a certain distribution characterized by its mean  $\mu^*$  and variance  $\sigma^{*2}$ , and if we consider the change of variable

$$z = \left[ \frac{1}{n} \sum_{i=1}^n y_i - \mu^* \right] \frac{\sqrt{n}}{\sigma^*}, \quad (C-7)$$

then  $z$  follows a standard normal distribution as  $n \rightarrow \infty$ ."

In our case, we start from the uniform distribution defined by relation (C-4) and intend to calculate its mean  $\mu_u$  and variance  $\sigma_u^2$ . But before doing this, let us shortly remind the definition of the moment of a function  $H(x)$ , in case of a continuous probability density  $f(x)$ . This moment is given by

$$\langle H(x) \rangle = \int_a^b H(x) f(x) dx, \quad (\text{C-8})$$

where  $a$  and  $b$  are the limits of the domain of validity of  $H(x)$  and  $f(x)$ .

We now apply this to the calculation of  $\mu_u$  and  $\sigma_u^2$ , associated to the uniform probability density (C-4). Here we have  $(a,b) = (0,1)$ .

Hence,

$$\bullet \mu_u = \langle x \rangle \quad (\text{C-9,a})$$

$$\mu_u = \int_0^1 x p_u(x) dx = \int_0^1 x dx = \frac{1}{2}$$

$$\bullet \sigma_u^2 = \langle (x - \langle x \rangle)^2 \rangle. \quad (\text{C-9,b})$$

By using the definition (C-8) and carrying out the calculation, we obtain

$$\sigma_u^2 = \langle x^2 \rangle - \langle x \rangle^2 \quad (\text{C-9,b'})$$

$$= \int_0^1 x^2 dx - \frac{1}{4}$$

$$= \left[ \frac{x^3}{3} \right]_0^1 - \frac{1}{4} = \frac{1}{3} - \frac{1}{4} = \frac{1}{12}.$$

Summing up, we have found that

$$\mu_u = \frac{1}{2} \quad \text{and} \quad \sigma_u = \frac{1}{2\sqrt{3}} = \frac{1}{\sqrt{12}} \quad (\text{C-10})$$

All the details of the demonstration leading to the fast technique of generation of a normal distribution will not be given here. Suffice it to say that by introducing the change of variables

$$y = Ax + B \quad (C-11)$$

and

$$z = \sum_{i=1}^n y_i \quad (C-12)$$

and using relations (C-10) and some consequences of the Central Limit Theorem, we obtain

$$\mu_z = n\mu_y = n\left(\frac{A}{2} + B\right) \quad (C-13,a)$$

$$\sigma_z = \sqrt{n} \sigma_y = A \sqrt{\frac{n}{12}}, \quad (C-13,b)$$

in which  $(\mu_y, \sigma_y)$  and  $(\mu_z, \sigma_z)$  respectively denote the mean and standard deviation associated to the distributions applied to  $y$  and  $z$ , the latter being a normal (Gaussian) distribution. The greater  $n$  is taken, the better the approximation of a normal distribution will be. For reasons of simplicity in equation (C-13,b) and since such an approximation is sufficient [see the histograms in Figs. 16(a) and (b)], the truncation to  $n=12$  is chosen. Equations (C-13,a) and (C-13,b) then become

$$\mu_z = 6A + 12B$$

$$\sigma_z = A.$$

Hence we can solve for  $A$  and  $B$  in terms of  $\mu_z$  and  $\sigma_z$ , which gives

$$A = \sigma_z, \quad (\text{C-14,a})$$

$$B = \frac{\mu_z}{12} - \frac{\sigma_z}{6}. \quad (\text{C-14,b})$$

These results allow us now to indicate the various steps of the fast technique used in Chapters III and IV to generate pseudo-random numbers from a Gaussian distribution of mean  $\mu$  and variance  $\sigma^2$ .

- (i) We first have to obtain  $\mu$  and  $\sigma$  — or  $\mu_z$  and  $\sigma_z$  in equations (C-14,a) and (C-14,b) — which stem from the deterministic  $\alpha(t)$  given in equation (3-1) adopted for Curve 3 (see Appendix C.3).
- (ii) We then select a random number  $r_i$  from the uniform distribution (C-4).
- (iii) This  $r_i$  is then multiplied by  $\sigma$ .
- (iv) To this product is then added the expression  $\frac{\mu}{12} - \frac{\sigma}{6}$  (or B, according to equation (C-14,b)). This means that we have now obtained a variate of the variable  $y$ , following equation (C-11).
- (v) We finally add up twelve of these variates  $y_i$ , and obtain one variate of the variable  $z$  which follows a normal distribution (equation (C-12) in which  $n=12$ ).

This procedure may still seem rather long, but it is nevertheless much more efficient than solving equation (C-5'). The output may be observed in Figs. 15 and 16, the latter being a histogram obtained by means of the IMSL subroutine USHIST.

### C.3 Determination of the mean $\mu$ and variance $\sigma^2$ of the random fluctuator $\alpha(t)$

According to the definition of the moment of a function  $H(x)$ , given by equation (C-8), and to equations (C-9,a) and (C-9,b'), we have

$$\mu = \langle \alpha \rangle = \int_{-\infty}^{+\infty} \alpha p(\alpha) d\alpha$$

and

$$\begin{aligned}\sigma^2 &= \langle \alpha^2 \rangle - \langle \alpha \rangle^2 \\ &= \int_{-\infty}^{+\infty} \alpha^2 p(\alpha) d\alpha - \mu^2,\end{aligned}$$

in which  $\alpha = \alpha(t)$  and  $p(\alpha)$  is the normal probability density given by equation (C-6). Making the hypothesis of ergodicity, we can identify ensemble and time averages. Hence, we also have

$$\mu = \lim_{T \rightarrow \infty} \frac{1}{2T} \int_{-T}^T \alpha(t) dt \quad (\text{C-15,a})$$

and

$$\sigma^2 = \lim_{T \rightarrow \infty} \frac{1}{2T} \int_{-T}^T \alpha^2(t) dt - \mu^2 \quad (\text{C-15,b})$$

It is now desired that the pseudo-random  $\alpha(t)$  of Curve 4 and the deterministic  $\alpha(t)$  of Curve 3 have the same mean and variance, in order to allow comparison between the two responses. The deterministic  $\alpha(t)$  of Curve 3 is given by equation (3-1) and since in all cases  $\phi_i = 0$ , it can be written, taking also (3-2) and (3-3) into account,

$$\alpha(t) = \sum_{i=1}^5 a_i \sin(\omega_i t) = \frac{\bar{\alpha}}{5} \sum_{i=1}^5 \sin(\omega_i t). \quad (\text{C-16})$$

- From (C-15,a) and (C-16), we have

$$\mu = \frac{\bar{\alpha}}{10} \lim_{T \rightarrow \infty} \frac{1}{T} \int_{-T}^T \sum_{i=1}^5 \sin(\omega_i t) dt.$$

Due to periodicity of the five sine functions, this can be written as

$$\mu = \frac{\bar{\alpha}}{10} \sum_{i=1}^5 \frac{1}{T_i} \int_{-T_i}^{T_i} \sin(\omega_i t) dt,$$

in which  $T_i$  is the period of the oscillation of circular frequency  $\omega_i$ , i.e.

$$T_i = \frac{2\pi}{\omega_i}. \quad (C-17)$$

For a given  $i$ , we have

$$\int_{-T_i}^{T_i} \sin(\omega_i t) dt = \left[ -\frac{\cos(\omega_i t)}{\omega_i} \right]_{-T_i}^{T_i} = 0,$$

hence

$$\mu = 0. \quad (3-7,a)$$

● Let us now calculate the variance. From (C-15,b), (C-16) and (3-7,a), we have

$$\sigma^2 = \frac{\bar{\alpha}^2}{50} \lim_{T \rightarrow \infty} \frac{1}{T} \int_{-T}^T \left[ \sum_{i=1}^5 \sin(\omega_i t) \right]^2 dt.$$

Due to the periodicity of the sine function, this can also be written

$$\sigma^2 = \frac{\bar{\alpha}^2}{50} \frac{1}{T_m} \int_{-T_m}^{T_m} \left[ \sum_{i=1}^5 \sin(\omega_i t) \right]^2 dt,$$

in which  $T_m$  is a time duration defined as the least common multiple of all the periods  $T_i$ ,  $T_{(i+j)}$  and  $T_{(i-j)}$ , associated respectively to the oscillations of circular frequencies  $\omega_i$ ,  $\omega_i + \omega_j$  and  $\omega_i - \omega_j$ . The need to integrate over such a period  $T_m$  will become evident very soon. By conducting the calculation, the variance becomes

$$\sigma^2 = \frac{\bar{\alpha}^2}{50T_m} \left[ \sum_{i=1}^5 \int_{-T_m}^{T_m} \sin^2 \omega_i t \, dt + 2 \sum_{i=1}^5 \sum_{\substack{j=1 \\ j \neq i}}^5 \int_{-T_m}^{T_m} \sin \omega_i t \sin \omega_j t \, dt \right] \quad (C-18)$$

Let us analyse separately the two kinds of integrals appearing here.

$$\begin{aligned} * \int_{-T_m}^{T_m} \sin^2 \omega_i t \, dt &= \frac{1}{2} \int_{-T_m}^{T_m} (1 - \cos 2\omega_i t) \, dt \\ &= \frac{1}{2} \left[ t - \frac{\sin 2\omega_i t}{2\omega_i} \right]_{-T_m}^{T_m} = T_m \end{aligned} \quad (C-19, a)$$

$$* \int_{-T_m}^{T_m} \sin \omega_i t \sin \omega_j t \, dt = \frac{1}{2} \int_{-T_m}^{T_m} [\cos(\omega_i - \omega_j)t - \cos(\omega_i + \omega_j)t] \, dt.$$

Due to the choice of  $T_m$ , it follows that

$$\int_{-T_m}^{T_m} \sin \omega_i t \sin \omega_j t dt = 0. \quad (C-19,b)$$

Plugging (C-19,a) and (C-19,b) into (C-18), we finally obtain

$$\sigma^2 = \frac{\bar{\alpha}^2}{50T_m} \sum_{i=1}^5 T_m = \bar{\alpha}^2 \frac{5T_m}{50T_m} = \frac{\bar{\alpha}^2}{10};$$

hence,

$$\sigma = \frac{\bar{\alpha}}{\sqrt{10}}, \quad (3-7,b)$$

which can also be written as

$$\sigma = a_i \sqrt{\frac{5}{2}},$$

because of equation (3-2).

#### C.4 Study of convergence of the Runge-Kutta solutions

This short study is mainly concerned with the comparison between the two reference cases in which  $\alpha(t) = 0$ , i.e. Curves 1 and 2 of Chapter III. Nevertheless, Curves 3 and 4 are also considered. The parameter of interest here is  $n$ , the number of discretization points used to conduct the Runge-Kutta iteration scheme, or, what is equivalent, the size of the constant step-size  $h$ . The number  $n$  envisaged is considered over one page of USPLTD plot, which was chosen to be 3 cycles of the reference curve, i.e. Curve 1. If  $T_n$  is the natural period of equation (2-16) with  $\alpha(t) = 0$  and without forcing function, the step-size  $h$  is therefore equal to

$$h = \frac{3T_n}{n-1}.$$

The study was conducted for the following values of  $n$ : 100, 200, 300, 400, 500, 600. The values of the responses were taken at the following instants of time:  $t = 3T_n, 6T_n, 9T_n$ , i.e. after 3, 6 and 9 cycles.

The case envisaged here is for parameters

$$f_n = \frac{1}{T_n} = 15 \text{ Hz,}$$

$$f_1 = \frac{\omega_1}{2\pi} = 30 \text{ Hz, } f_2 = 150 \text{ Hz, } f_3 = 240 \text{ Hz, } f_4 = 300 \text{ Hz, } f_5 = 450 \text{ Hz,}$$

$$\zeta = 0.01, \quad \bar{\alpha} = 1.$$

The results of the comparison between responses of Curves 1 and 2 are given in the table below.

$n$	$[x(\text{Curve 2}) - x(\text{Curve 1})]/[x(\text{Curve 1})]$		
	at $t = 3T_n$	at $t = 6T_n$	at $t = 9T_n$
100	$-3.42 \times 10^{-5}$	$-1.86 \times 10^{-2}$	$-7.32 \times 10^{-2}$
200	$-1.00 \times 10^{-5}$	$-4.69 \times 10^{-3}$	$-1.85 \times 10^{-2}$
300	$-9.54 \times 10^{-6}$	$-2.13 \times 10^{-3}$	$-8.33 \times 10^{-3}$
400	$-9.42 \times 10^{-6}$	$-1.22 \times 10^{-3}$	$-4.76 \times 10^{-3}$
500	$-9.42 \times 10^{-6}$	$-8.04 \times 10^{-4}$	$-3.10 \times 10^{-3}$
600	$-9.42 \times 10^{-6}$	$-5.73 \times 10^{-4}$	$-2.19 \times 10^{-3}$

It may be noticed here that a systematical error is introduced by the use of the Runge-Kutta method, which is  $9.42 \times 10^{-6}$  after 3 cycles (after 6 and 9 cycles, the limit is not yet reached for  $n = 600$ ). Fortunately this error remains small, at least as long as the number of cycles considered does not

become too large. The first runs were conducted with  $n = 300$ ; after this study of convergence,  $n = 500$  was preferred (an even higher value of  $n$  was not envisaged because of increasing computer costs).

As far as the frequency is concerned, there seems to occur a very slight systematic shift towards lower frequencies, of the order of 0.2%. In fact, for  $f_n = 15$  Hz, the frequency of Curve 1 is effectively 15 Hz (which is expected from the analytical solution), whereas the frequency of Curve 2, measured over 15, 30 or 45 cycles, is found to be only 14.97 Hz. If this effect is supposed to occur for Curves 3 and 4 within the same order of magnitude, then the frequencies measured from these curves (if they are about 15 Hz) should all be increased by 0.03 Hz.

The results for Curves 3 and 4 were also obtained during this study, but need not be given here. The response for  $n = 600$  was compared to the response obtained for the other values of  $n$ . At least when starting from  $n = 300$ , convergence was observed for Curve 3. To give an idea, at  $t = 9T_n$ , the ratio  $[x(\text{Curve 3})_{n=300} - x(\text{Curve 3})_{n=600}] / [x(\text{Curve 3})_{n=600}]$  is equal to  $1.03 \times 10^{-1}$ , whereas the ratio  $[x(\text{Curve 3})_{n=500} - x(\text{Curve 3})_{n=600}] / [x(\text{Curve 3})_{n=600}]$  is equal to  $1.60 \times 10^{-2}$ . For Curve 4, no such convergence is observed, which is expected, since using a different value of  $n$  actually means that a different number of random numbers (which is precisely  $n$ , since each integration point requires the generation of one pseudo-random number) is used in the scheme.

### C.5 Listing of the program

A typical listing of the program is given in the five following pages. The case considered is Run 2 of Series E (see Appendix C.6).

```

1  $WATFIV ,TIME=99,PAGES=40,NOEXT
   IMPLICIT REAL*8(A-H,K-L,O-Z)
2  C***** PART ONE OF PLOTTING PROGRAM :
   INTEGER IY,N,M,INC,ICPT,IMAG4(5151),IER,ITITLE(144),ICHR(10)
3  REAL RANGE(4)
4  DOUBLE PRECISION X(300),Y(300,4)
5  DATA ICHR(1)/1H /,RANGE/4*0.0/
6  CALL UGETIO(1,NIN,NOUT)
7  READ(NIN,5) (ITITLE(I), I = 1,144 )
8  5 FORMAT(72A1)
9  PI = 3.1415926536D0
C***** PARAMETERS TO BE CHANGED IN STUDY :
10  FN = 15.DC
11  DZETA = 0.01D0
12  F1 = 30.D0
13  F2 = 150.D0
14  F3 = 240.D0
15  F4 = 300.D0
16  F5 = 450.D0
17  O1 = 2.D0*PI*F1
18  O2 = 2.DC*PI*F2
19  O3 = 2.D0*PI*F3
20  O4 = 2.D0*PI*F4
21  O5 = 2.DC*PI*F5
22  A1 = 0.15D0
23  A2 = A1
24  A3 = A1
25  A4 = A1
26  A5 = A1
27  PHI1 = 0.D0
28  PHI2 = PHI1
29  PHI3 = PHI1
30  PHI4 = PHI1
31  PHI5 = PHI1
C***** FROM THESE PARAMETERS , WE NOW DEFINE :
32  TN = 1.D0/FN
33  T1 = 1.D0/F1
34  H = TN/299.D0*3.D0
35  CN = 2.D0*PI*FN
36  ALPHA = A1 + A2 + A3 + A4 + A5
C***** EXACT SOLUTION IN CASE M(T) = 0 :
C -----> COURBE NO 1 ( 2 CARTES )
37  UD = ON*DSQRT( 1.D0 - DZETA*DZETA )
38  PHI = 0.D0
C*****
39  CMASS = 1.D0
40  KA = CMASS*ON*ON
41  C = 2.D0*DZETA*ON*CMASS

```

```

42 C*****
43 T = 0.D0
44 X0= 1.D0
45 Y0= 0.D0
46 X1= 1.D0
47 Y1= 0.D0
48 X2= 1.D0
49 Y2= 0.D0
50 X(1) = T
51 Y(1,1) = X0
52 Y(1,2) = X0
53 Y(1,3) = X0
53 Y(1,4) = X0
C*****
C
C
C
54 A = 0.D0
55 TMIU = 0.D0
56 SIGMA = ALPHA / DSQRT(10.D0)
57 IR = 1
58 JJ= 5**13
C*****
59 J = 1
60 4 I = 2
C*****
61 1 CONTINUE
C*****
62 CALL F(H, Y1 , P )
63 CALL GZERO(H,KA,C,CMASS , X1 , Y1 , Q )
64 CALL F(H, Y1+ Q /2.D0 , PP )
65 CALL GZERO(H,KA,C,CMASS , X1+ P /2.D0 , Y1+ Q /2.D0 , QQ )
66 CALL F(H, Y1+ QQ/2.D0 , PPP )
67 CALL GZERO(H,KA,C,CMASS , X1+ PP/2.D0 , Y1+ QQ/2.D0 , QQQ )
68 CALL F(H, Y1+ QQQ , PPPP )
69 CALL GZERO(H,KA,C,CMASS , X1+ PPP , Y1+ QQQ , QQQQ )
70 XXX= X1+ (P + 2.D0*PP + 2.D0*PPF + PPPP)/6.D0
71 YYY= Y1+ (Q + 2.D0*QQ + 2.D0*QQQ + QQQQ)/6.D0
C*****
C
72 CALL F(H, Y0 , K )
73 CALL G(H,KA,C,T , X0 , Y0 , L )
* ,PI ,F1 ,A1 ,PHI1 ,CMASS ,
* O1 ,O2 ,O3 ,O4 ,O5 ,A2 ,A3 ,A4 ,A5 ,PHI2 ,PHI3 ,PHI4 ,PHI5 )
74 CALL F(H, Y0+ L /2.D0 , KK )
75 CALL G(H,KA,C,T+ H/2.D0 , X0+ K /2.D0 , Y0+ L /2.D0 , LL )
* ,PI ,F1 ,A1 ,PHI1 ,CMASS ,
* O1 ,O2 ,O3 ,O4 ,O5 ,A2 ,A3 ,A4 ,A5 ,PHI2 ,PHI3 ,PHI4 ,PHI5 )
76 CALL F(H, Y0+ LL/2.D0 , KKK )
77 CALL G(H,KA,C,T+ H/2.D0 , X0+ KK/2.D0 , Y0+ LL/2.D0 , LLL )
* ,PI ,F1 ,A1 ,PHI1 ,CMASS ,
* O1 ,O2 ,O3 ,O4 ,O5 ,A2 ,A3 ,A4 ,A5 ,PHI2 ,PHI3 ,PHI4 ,PHI5 )

```

INITIALIZATION :

ELEMENTS FOR THE GAUSSIAN DISTRIBUTION AND MONTE-CARLO :

-----> CCURBE NO 4

KEEP THIS :

RUNGE-KUTTA METHOD :

CASE 1 : WITH M(T) = 0<sup>-</sup>  
-----> CCURBE NO 2

CASE 2 : FOR M(T) = SUM OF AI\*SIN(OI\*T + PHI)  
-----> COURBE NO 3

```

78      CALL F(H, Y0+ LLL      , KKKK )
79      CALL G(H, KA, C, T+ H      , X0+ KKK      , Y0+ LLL      , LLLL
* , PI, F1, A1, PHI1, CMASS,
* 01, 02, 03, 04, 05, A2, A3, A4, A5, PHI2, PHI3, PHI4, PHI5)
80      XX = X0+ (K + 2.00*KK + 2.00*KKK + KKKK)/6.00
81      YY = Y0+ (L + 2.00*LL + 2.00*LLL + LLLL)/6.00
C*****
C----->          CJURBE NO 4
82      CALL F(H, Y2      , U
83      CALL CARLO(H, KA, C, CMASS , X2      , Y2      , V
* , TMIU, SIGMA, JJ, IR)
84      CALL F(H, Y2+ V /2.00 , UU )
85      CALL CARLO(H, KA, C, CMASS , X2+ U /2.00 , Y2+ V /2.00 , VV
* , TMIU, SIGMA, JJ, IR)
86      CALL F(H, Y2+ VV/2.00 , UUU )
87      CALL CARLO(H, KA, C, CMASS , X2+ UU/2.00 , Y2+ VV/2.00 , VVV
* , TMIU, SIGMA, JJ, IR)
88      CALL F(H, Y2+ VVV      , UUUU )
89      CALL CARLO(H, KA, C, CMASS , X2+ UUU      , Y2+ VVV      , VVVV
* , TMIU, SIGMA, JJ, IR)
90      XXXX=X2+ (U + 2.00*UU + 2.00*UUU + UUUU)/6.00
91      YYY=Y2+ (V + 2.00*VV + 2.00*VVV + VVVV)/6.00
C*****          SUITE :
92      T = T + H
93      X(I) = T
94      Y(I,1) = DEXP( -DZETA*ON*T ) * DCOS( DD*T + PHI )
95      Y(I,2) = XXX
96      Y(I,3) = XX
97      Y(I,4) = XXXX
98      IF(I.GE.300) GO TO 2
99      X0= XX
100     Y0= YY
101     X1= XXX
102     Y1= YYY
103     X2= XXXX
104     Y2= YYY
105     I = I + 1
106     GO TO 1
C*****          END OF RUNGE-KUTTA USES :
107     2 CONTINUE
108     Y(75,1) = 1.00
109     Y(76,1) = -1.00
C*****          PART TWO OF PLOTTING PROGRAM :
110     INC = 1
111     N = 300
112     M = 4
113     IOPT = 1
114     IY = 300
115     CALL USPLTD(X, Y, IY, N, M, INC, I, TITLE, RANGE, ICHAR, IOPT, IMAG, IER)
C*****          TRACER D'AUTRES TABLEAUX :
116     IF ( J.GE.12 ) GO TO 3
117     WRITE(6, 77) J
118     77 FORMAT('0', 5X, 'TABLEAU NO ', 11)

```

```

119      J = J + 1
120      X(I) = X(300)
121      Y(1,1) = Y(300,1)
122      Y(1,2) = Y(300,2)
123      Y(1,3) = Y(300,3)
124      Y(1,4) = Y(300,4)
125      GO TO 4
126      3 WRITE(6,78) J
127      78 FORMAT(' ',5X,'TABLEAU NO ',I1)
128      WRITE(6,88)      TMIU,SIGMA,ALPHA
129      88 FORMAT(' ',2X,'GAUSSIAN DISTRIBUTION :  MIU = ',D20.13,'  &  SI
      *GMA = ',D20.13,'      ;  *** -ALPHA = ',D12.5)
130      WRITE(6,333)
131      333 FORMAT(1H1)
132      STOP
133      END

```

```

134      SUBROUTINE F(H,Y,K)
135      IMPLICIT REAL*8(A-Z)
136      K = H*Y
137      RETURN
138      END

```

```

139      SUBROUTINE GZERO(H,KA,C,CMASS,X,Y,Q)
140      IMPLICIT REAL*8(A-Z)
141      Q = H*( - KA/CMASS *X - C/CMASS *Y )
142      RETURN
143      END

```

```

144 SUBROUTINE G(H,K,A,C,T,X,Y,L,PI,F1,A1,PHI1,CMASS,
* O1,O2,O3,O4,O5,A2,A3,A4,A5,PHI2,PHI3,PHI4,PHI5)
145 IMPLICIT REAL*8(A-Z)
146 CALL MOFT(PI,F1,A1,PHI1,T,MM,
* O1,O2,O3,O4,O5,A2,A3,A4,A5,PHI2,PHI3,PHI4,PHI5)
147 L = H*( -KA/( CMASS + MM ) *X - C/( CMASS + MM ) *Y )
148 RETURN
149 END

```

```

150 SUBROUTINE CARLO(H,K,A,C,CMASS,X,Y,CARL,TMIU,SIGMA,J,IR)
C***** MONTE CARLO :
151 IMPLICIT REAL*8(A-H,K-L,O-Z)
152 RRR = 0.D0
153 DO 7 III = 1,12
154 IR = IR*J
155 IF(IR.LT.0) IR = IR + 2*(2**30 - 1) + 2
156 R = DFLOAT(IR)/2.D0**31
157 RR = R*SIGMA + TMIU/12.D0 - SIGMA/2.D0
158 RRR = RRR + RR
159 7 CONTINUE
160 RN = RRR
161 CARL = H*( -KA/( CMASS + RN ) *X - C/( CMASS + RN ) *Y )
162 RETURN
163 END

```

```

164 SUBROUTINE MOFT(PI,F1,A1,PHI1,T,MM,O1,O2,O3,O4,O5,A2,A3,A4,A5,
*PHI2,PHI3,PHI4,PHI5)
165 IMPLICIT REAL*8(A-Z)
166 MM = A1*DSIN(O1*T + PHI1 ) + A2*DSIN( O2*T +PHI2 ) + A3*DSIN( O3*T
* + PHI3 ) + A4*DSIN( O4*T + PHI4 ) + A5*DSIN( O5*T + PHI5 )
167 RETURN
168 END

```

\$DATA

### C.6 Various series of computer runs investigated

#### Series A,B,C

Curve 3 of these series is discussed in Section 3.2.3 (and Curve 4 in Section 3.2.2).

These three series consist of ten computer runs which have in common the perturbation frequencies

$$f_i = \omega_i/2\pi = 5, 10, 15, 20, 25 \text{ Hz.}$$

The other parameters of each run are detailed in the table below (when no value is given for a parameter for a second, third or fourth run, it means that the parameter in question has the same value as for the first run of the series considered).

Series & Run	$f_n$ (Hz)	$\zeta$	$\bar{\alpha}$	$n$	$N_c$	Remarks
A	1	0.01	0.50	300	15	Large amplitudes
	2		0.75			
	3		1			
B	1	0.005	0.25	500	45	Small amplitudes and $\zeta$ - test on $f_n$
	2	30				
	3	60				
C	1	0.005	0.25	500	30	Basically the same as Series A, but $\zeta = 0.005$ instead of 0.01
	2		0.50			
	3		0.75			
	4		1			

In all series:  $f_i = 5, 10, 15, 20, 25 \text{ Hz.}$

$f_n$  is the natural frequency of the system and is equal to  $\omega_n/2\pi$ , in which  $\omega_n$  is defined by equation (2-16', a).  $\zeta$  and  $\bar{\alpha}$  are respectively defined by

equations (2-16',b) and (3-3).  $n$  is the number of calculation points used over three cycles (cf. Appendix C.4), whereas  $N_c$  is the number of cycles computed.

#### Series D to H

Curve 3 of these series is discussed in Section 3.2.4 (and Curve 4 in Section 3.2.2).

These five series consist of seventeen computer runs which have in common the natural frequency  $f_n = 15$  Hz. The other parameters are given below.

Series & Run	$\zeta$	$f_i$ (in Hz) $i = 1$ to 5	$\bar{\alpha}_i$	$n$	$N_c$	Remarks
D	1	30,123,263,333,543 ( $f_n = 15$ Hz)	0.50	300	15	Large amplitudes — to test for parametric resonance; $f_1 =$ $2f_n$
	2		0.75			
	3		1			
E	1	30,150,240,300,450 ( $f_n = 15$ Hz)	0.50	300	15	Large amplitudes — to test for parametric resonance; $f_1 = 2f_n$
	2		0.75			
	3		1			
F	1	15,150,240,300,450 ( $f_n = 15$ Hz)	0.50	300	15	Large amplitudes — to test for parametric resonance; $f_1 = f_n$
	2		0.75			
	3		1			
G	1	30,150,240,300,450 (same as in Series E)	0.25	500	60	Same as Series E, but $\zeta = 0.005$ in- stead of 0.01
	2		0.50			
	3		0.75			
	4		1			
H	1	30,150,240,300,450 (same as in Series E)	0.25	500	30	To measure $x_{rms}$ when $\zeta = 0$
	2		0.50			
	3		0.75			
	4		1			

## APPENDIX D

Complements to the Digital  
Frequency Domain Analysis of Chapter IV

D.1 Fast Fourier transform

The fast Fourier transform can reduce the time involved in finding a discrete Fourier transform from several minutes to less than a second and, consequently, lower the computer cost. The Fourier transform, of course, is used to identify the frequency components making up a continuous waveform. For sampled data, as is the case in this digital analysis, the discrete Fourier transform (DFT) is used and the fast Fourier transform (FFT) is precisely an efficient algorithm to determine the DFT.

The Fourier transform for continuous signals and its inverse transform can be written in the form

$$X(f) = \int_{-\infty}^{+\infty} x(t) e^{-i2\pi ft} dt \quad (D-1,a)$$

$$x(t) = \int_{-\infty}^{+\infty} X(f) e^{i2\pi ft} df \quad (D-1,b)$$

for  $-\infty < f < \infty$  and  $-\infty < t < \infty$ .

In these equations  $x(t)$  represents the function considered in the time domain while  $X(f)$  is its representation in the frequency domain (also called its linear spectrum).

The analogous discrete Fourier transform pair that applies to sampled versions of these functions can be written in the form

$$X(j) = \frac{1}{N} \sum_{k=0}^{N-1} x(k) e^{-i2\pi jk/N} \quad (D-2,a)$$

$$x(k) = \sum_{j=0}^{N-1} X(j) e^{i2\pi jk/N} \quad (D-2,b)$$

for  $j = 0, 1, \dots, N-1$ ;  $k = 0, 1, \dots, N-1$ ; and  $N$  is the number of real sampled points used for the DFT (we called it  $N_{\text{DFT}}$  in Section 4.1). Both  $X(j)$  and  $x(k)$  are, in general, complex series.

If we replace  $e^{2\pi i/N}$  by the term  $W_n$ , the DFT becomes

$$X(j) = \frac{1}{N} \sum_{k=0}^{N-1} x(k) W_n^{-jk}$$

$$x(k) = \sum_{j=0}^{N-1} X(j) W_n^{+jk}$$

Each  $j$  is a harmonic number; that is, the true frequency is the product  $jf_0$  where  $f_0$  is the fundamental frequency and the true time is the product  $k\Delta t$  where  $\Delta t$  is the sample period. The real part of  $X(j)$  is an even function and the imaginary part of  $X(j)$  is an odd function which implies that the Fourier coefficients  $N/2$  and  $N-1$  can be viewed as "negative frequency" harmonics between  $-N/2$  and  $-1$ . Furthermore, the last half of the time series can be interpreted as negative time (that is, as occurring before  $t=0$ ).

The Cooley-Tukey FFT algorithm was developed in 1965 [67] and led to all the numerous subsequent publications on this topic. Using the notation of Cooley, the FFT algorithm involves evaluating the expression

$$\hat{X}(j) = \sum_{k=0}^{N-1} A(k) W^{jk} \quad (D-3)$$

for  $j = 0, 1, \dots, N-1$ ;  $k = 0, 1, \dots, N-1$ ; and  $W = e^{2\pi i/N}$ .

We will take the case for  $N=8$ , and then it is convenient to represent  $j$  and  $k$  as binary numbers. This is to say that for

$$j = 0, 1, \dots, 7 \quad \text{and} \quad k = 0, 1, \dots, 7$$

we can write

$$j = 4j_2 + 2j_1 + j_0 \quad \text{and} \quad k = 4k_2 + 2k_1 + k_0.$$

In these expressions,  $j_0, j_1, j_2, k_0, k_1$  and  $k_2$  can take on a value of either 0 or 1.

Therefore, equation (D-3) becomes

$$\hat{X}(j_2, j_1, j_0) = \sum_{k_0=0}^1 \sum_{k_1=0}^1 \sum_{k_2=0}^1 A(k_2, k_1, k_0) W^{(4j_2+2j_1+j_0)(4k_2+2k_1+k_0)} \quad (D-4)$$

Since  $W^{m+n} = W^m \cdot W^n$ , we have

$$W^{(4j_2+2j_1+j_0)(4k_2+2k_1+k_0)} = W^{(4j_2+2j_1+j_0)4k_2} \\ \times W^{(4j_2+2j_1+j_0)2k_1} W^{(4j_2+2j_1+j_0)k_0}.$$

The two first factors can be written in the form

$$W^{(4j_2+2j_1+j_0)4k_2} = [W^{8(2j_2+j_1)k_2}] W^{4j_0k_2}$$

$$W^{(4j_2+2j_1+j_0)2k_1} = [W^{8j_2k_1}] W^{2(2j_1+j_0)k_1}.$$

However,

$$W^8 = (e^{2\pi i/8})^8 = e^{2\pi i} = 1.$$

Hence the terms in brackets above equal 1 and equation (D-4) becomes

$$\hat{X}(j_2, j_1, j_0) = \sum_{k_0=0}^1 \sum_{k_1=0}^1 \sum_{k_2=0}^1 A(k_2, k_1, k_0) W^{4j_0 k_2} \\ \times W^{2(2j_1+j_0)k_1} W^{(4j_2+2j_1+j_0)k_0} \quad (D-5)$$

It is most convenient to perform the summations separately and label the intermediate results where only the latest set needs to be saved (each set contains only eight terms). Thus the equations can be rewritten in the form

$$A_1(j_0, k_1, k_0) = \sum_{k_2=0}^1 A(k_2, k_1, k_0) W^{4j_0 k_2} \\ A_2(j_0, j_1, k_0) = \sum_{k_1=0}^1 A_1(j_0, k_1, k_0) W^{2(2j_1+j_0)k_1} \\ A_3(j_0, j_1, j_2) = \sum_{k_0=0}^1 A_2(j_0, j_1, k_0) W^{(4j_2+2j_1+j_0)k_0}$$

and finally

$$\hat{X}(j_2, j_1, j_0) = A_3(j_0, j_1, j_2). \quad (D-6)$$

In this case ( $N=8$ ) a direct evaluation requires 64 complex multiply-and-add operations. Using the FFT equation and noting that the bracketed terms in the previous equations equal 1 and that  $W^0 = -W^4$ ,  $W^1 = -W^5$ , etc., only 12 operations are needed. More generally, for  $N=2^n$ , the reduction is from  $N^2$  to  $\frac{1}{2} N \log_2 N$  complex multiplications, as many complex additions and also as many subtractions. For  $N=1024$  for example, this represents a computational reduction of more than 200 to 1.

The three most often encountered problems (or pitfalls) in using the discrete Fourier transform appear to be aliasing, leakage, and the picket-fence effect.

The term "aliasing" refers to the fact that high-frequency components of a time function can impersonate low frequencies if the sampling rate is too low. This problem can be removed by making certain that the sampling rate is at least twice as high as the highest frequency in the signal (this minimum sample rate is known as the Nyquist Criterion). If there is a large amount of high frequency noise present, it is best to pass the signal through a low pass filter and to sample at a rate twice the frequency at which the signal is being filtered.

"Leakage" is an effect which is inherent in the DFT because of the required time domain truncation. The time domain truncation may be thought of as multiplying the signal by a unit-amplitude data window,  $w(t)$ , which has a Fourier transform  $\sin(f)/f$ , where  $f$  is the value of the frequency in the frequency domain. Therefore, the truncation of a sampled wave form results in a frequency domain convolution of the signal with the  $\sin(f)/f$  function. This convolution introduces additional components in the frequency domain, because of the side-lobe characteristic of the  $\sin(f)/f$  function, unless the truncation interval is chosen to be equal to a multiple of the period. To reduce leakage, it is necessary to employ a time domain truncation function, which has side-lobe characteristics which are smaller in magnitude than that of  $\sin(f)/f$ . A good truncation function is the Hamming window,

$$w(t) = \begin{cases} (1-b) + b \cos\left(\pi \frac{\tau}{m}\right) & \text{for } -m+1 < \tau < m-1 \\ 0 & m \leq |\tau| \end{cases} \quad (D-7)$$

where  $T_t$  is the length of the time record in seconds. If we let  $b=0.46$ , then this is the Hamming window. If we let  $b=0.5$ , then this is the Hanning window of the Hamming window class. Actually, we chose the FTFPS routine (from the IMSL Library) to obtain the power spectrum of a time function. This routine uses the symmetric window

$$w(j) = 1 - \left| \frac{j - \frac{L-1}{2}}{\frac{L+1}{2}} \right|, \quad \text{for } j=0,1,\dots,L-1 \quad (D-8)$$

which is approximately the Parzen window. ( $L$  is an input parameter to the FTFPS routine used to segment the time series, and must be a power of two.)

In order to understand the "picket-fence effect", it is necessary to understand the nature of the results of the FFT. The FFT produces a spectrum of  $N_f$  frequency components spaced at intervals of  $\Delta f = 1/T_t$ . If a unit frequency component occurs at  $f_c$ , such that  $f_c$  is an integer multiple of  $\Delta f$ , then its magnitude will be expressed as unity. If, however,  $f_c$  does not occur with such an integral relationship, then it will appear in the surrounding frequency components  $n \cdot \Delta f$  and  $(n+1) \cdot \Delta f$ . Its amplitude in this case will be  $\sin(f)/f$ , where  $f = f_c - f_n$  and  $f = f_{n+1} - f_c$ . In the worst case when  $f_c$  is located half-way between  $n \cdot \Delta f$  and  $(n+1) \cdot \Delta f$ , it will be seen as 0.637 of the amplitude at both of these frequencies. Therefore, the FFT could result in an error of 27.3% in the value of the amplitude. This effect is referred to as the picket-fence effect. A possible cure to this problem is to double the record length with a set of samples which are all zero. This would cause the FFT to calculate a redundant set of terms which would be between the original terms. Now, the maximum error

would occur when  $f_c$  is  $1/4$  of the way between successive frequency components, and would then reach 10%. However, in practice the picket-fence problem is not as great as this discussion implies.

## D.2 Various schemes of $\alpha(t)$ generated in the digital study

The following schemes of  $\alpha(t)$  have been generated in Chapters III and IV. They are presented in a discretized form, their general variate being given at a specific instant of time  $t_k$ . Each model of  $\alpha(t)$  thus characterized is denoted by a small bracketed letter, i.e., [a], [b], ..., [k]. Besides the schemes of  $\alpha(t)$  are indicated the names of the cases under which the scheme in question has been considered in the various chapters or sections. Not all schemes have been used in Chapter III or in one of the two sections of Chapter IV considered, as can be seen below. In Chapter III, the cases envisaged have previously been called Curve 1, ..., up to Curve 4. For Chapter IV, they are called A[v] or B[w] where the capital letters A and B show that the cases considered belong, respectively, to Section 4.2 or Section 4.3, whereas the small letters inside brackets (hypothetic [v] and [w] used here) indicate which model of  $\alpha(t)$  is taken. The various schemes of  $\alpha(t)$  are presented in the table on the next page.

Scheme considered		Cases examined		
Name	$\alpha(t_k) =$	Chapter III	Section 4.2	Section 4.3
[a]	0	Curve 2 (Curve 1)	A[a]	B[a]
[b]	$\frac{1}{N} \sum_{i=1}^{N_0} \sin(\omega_i t_k)$	Curve 3	A[b]	B[b]
[c]	$RO_k$	Curve 4	A[c]	
[d]	$\sum_{i=1}^N RA_{ik} \sin(\omega_i t_k)$		A[d]	
[e]	$\frac{1}{N} \sum_{i=1}^N \sin[(\omega_i + RO_{ik}) t_k]$		A[e]	B[e]
[f]	$\frac{1}{N} \sum_{i=1}^N \sin[\omega_i t_k + RO_{ik}]$		A[f]	
[g]	$\frac{1}{N} \sum_{i=1}^N \sin[\omega_i (1 + \mu_i \sin(\lambda \omega_i t_k)) t_k]$			B[g]
[h]	$\frac{1}{N} \sum_{i=1}^N \sin[\omega_i (1 + \mu_i \sin(10\lambda \pi t_k)) t_k]$			B[h]
[i]	$\frac{1}{N} \sum_{i=1}^N \sin[\omega_i (1 + \mu_i \sin(\lambda \omega_i t_k)) + RO_{ik} t_k]$			B[i]
[j]	$\frac{1}{N} \sum_{i=1}^N \sin[\omega_{i_{new}} (1 + \mu_i \sin(10\lambda \pi t_k)) t_k]$			B[j]
[k]	$\frac{1}{N} \sum_{i=1}^N \sin[\omega_{i_{new}} (1 + \mu_i \sin(10\lambda \pi t_k)) + RO_{ik} t_k]$			B[k]

For the values of  $f_i$  and the methods of generation of  $RO_i$  for each scheme, see Remark 3 below.

Remarks

1. As a first remark, let us notice that not all these schemes are random; in fact we have:

pseudo-random schemes: [c],[d],[e],[f],[i],[k]

deterministic schemes: [a],[b],[g],[h],[j]

2. It may also be noticed that, similarly to equation (3-2), all amplitudes  $a_i$  of the individual sine functions are being taken to be equal, hence  $\bar{\alpha}$  is again defined, similarly to equation (3-3), as

$$\bar{\alpha} = \sum_{i=1}^N a_i = Na_i, \quad (4-4) \text{ or } (D-9)$$

hence the amplitude of one sine function is equal to

$$a_i = \frac{\bar{\alpha}}{N} \quad (D-9')$$

and appears under the latter form as a common factor in most schemes of  $\alpha(t)$ . The only difference between equations (3-2) and (3-3), and (D-9) and (D-9') is that the latter ones are generalized for any N.

3. After these two global remarks, we still have to examine the schemes one by one in order to specify some characteristics, especially the different methods used to generate the random variates  $RO_{ik}$  which have all been noted in the same way for simplicity.

Scheme [a]: This the fundamental reference case since it represents the homogeneous model of two-phase flow for which  $m_h(t) = \bar{m}_h$  (it is recalled that in Chapter III, Curves 1 and 2 denote, respectively, the analytical and numerical solution).

Scheme [b]: This is the deterministic reference case and consists of the sum of N sine functions in the time domain, or a juxtaposition of

$N$  identical peaks in the frequency domain [see Fig. 25(a)]. To make these peaks equidistant, we choose equidistant frequencies, according to  $N$ , as follows:

$N =$  Values of  $f_i = \omega_i/2\pi$

5	$\begin{array}{c} \text{5 Hz} \\ \underbrace{\hspace{2cm}} \\ 5, 10, 15, 20, 25 \end{array}$
9	$\begin{array}{c} \text{2.5 Hz} \\ \underbrace{\hspace{2cm}} \\ 5, 7.5, 10, 12.5, 15, 17.5, 20, 22.5, 25 \end{array}$
17	$\begin{array}{c} \text{1.25 Hz} \\ \underbrace{\hspace{2cm}} \\ 5, 6.25, 7.5, 8.75, 10, 11.25, 12.5, 13.75, 15, \\ 16.25, 17.5, 18.75, 20, 21.25, 22.5, 23.75, 25 \end{array}$
33	$\begin{array}{c} \text{0.625 Hz} \\ \underbrace{\hspace{2cm}} \\ 5, 5.625, 6.25, 6.875, 7.5, 8.125, 8.75, 9.375, 10, 10.625, \\ 11.25, 11.875, 12.5, 13.125, 13.75, 14.375, 15, 15.625, 16.25, \\ 16.875, 17.5, 18.125, 18.75, 19.375, 20, 20.625, 21.25, 21.875, \\ 22.5, 23.125, 23.75, 24.375, 25 \end{array}$

Let us specify that these values of the perturbation frequencies,  $f_i$ , are also those for schemes [d] to [i], in case the corresponding value of  $N$  is used.

Scheme [c]: This is the random reference case (completely pseudo-random without favouring any specific frequency). Its generation by a normal Monte-Carlo technique is given in Appendix C.2. As far as its mean  $\mu$  and standard deviation  $\sigma$  are concerned, it was found in Appendix C.3 that for  $N = 5$  we have  $\mu = 0$  and  $\sigma = \bar{\alpha}/\sqrt{10}$ . By a similar demonstration, it is established that for any  $N$ , we have

$$\mu = 0 \quad (4-8,a)$$

and

$$\sigma = \bar{\alpha}/\sqrt{2N} . \quad (4-8,b)$$

Scheme [d]: In this case, the amplitudes of scheme [b] are made random.

To see this better, scheme [b] has to be written again in its initial form using (D-9'),

$$\alpha(t_k) = \frac{\bar{\alpha}}{N} \sum_{i=1}^N \sin(\omega_i t_k) = \sum_{i=1}^N a_i \sin(\omega_i t_k).$$

By replacing  $a_i$  by the pseudo-random sequences  $RA_{ik}$  (RA standing for "Random Amplitude"), we obtain scheme [d]. The new subscript  $k$  stems from the fact that the random variates are different for each instant of time  $t_k$ . Defining  $a_i = \tilde{a} (= \frac{\bar{\alpha}}{N})$  — the common value of all the amplitudes  $a_i$  of scheme [b] — the  $N$  sequences  $RA_{ik}$  at a given instant  $t_k$  are all chosen to have the same mean  $\mu_i = \tilde{a}$ , and also standard deviation  $\sigma_i = \tilde{a}/\sqrt{2N}$  which distributes their deviates from 0 to  $2\tilde{a}$  about the mean  $\tilde{a}$ . To obtain given deviates of the random sequences  $RA_{ik}$ , the  $N$  associate deviates of the pseudo-random Monte-Carlo sequence (as for scheme [c]) are generated by assigning the first one to  $RA_{1k}$ , the second to  $RA_{2k}$ , and so forth to  $RA_{Nk}$ . It was verified for  $N=5$  that, by doing so, one still obtains normal (Gaussian) sequences for each  $RA_{ik}$  — provided, of course, that a sufficient number of deviates has been generated.

Scheme [e]: Here the amplitudes  $a_i$  remain constant as in scheme [b] (hence the common amplitude  $\frac{\bar{\alpha}}{N}$  can again be written outside the summing operator  $\Sigma$ ), but the frequencies are randomly perturbed. In this case  $RO_{ik}$  are random sequences of mean  $\mu_i = 0$  and of variable standard deviation  $\sigma$  (now being,

used as a parameter independent of  $\bar{\alpha}$ ). The  $\omega_i$  are constants as in scheme [b] — so that  $RO_{ik}$  acts as a fluctuator to  $\omega_i$ . As already mentioned, the values of  $f_i$  are the same as for scheme [b].

Scheme [f]: In this case it is attempted to achieve the same goal as above (scheme [e]) by randomly perturbing the phase between the frequency components of  $\alpha(t)$ , rather than the "predominant" frequencies themselves.

$RO_{ik}$  are pseudo-random numbers defined as for scheme [e], hence  $\sigma$  can again be chosen independently of  $\bar{\alpha}$ .

Scheme [g]: This is a new deterministic case in which the circular frequencies  $\omega_i$  are deterministically perturbed by the factor  $1 + \mu_i \sin(\lambda \omega_i t_k)$ .

Scheme [h]: This is the same deterministic case as scheme [g], but in the aforementioned factor, all the frequencies  $\omega_i$  of the term  $\sin(\lambda \omega_i t_k)$  are replaced by the lowest of them,  $\omega_1 = 2\pi f_1 = 10\pi$  (since  $f_1 = 5$  Hz).

Scheme [i]: This is again a pseudo-random scheme. In fact, the deterministically varying frequencies of scheme [g] are further disturbed randomly by pseudo-random deviates  $RO_{ik}$  defined as for scheme [e].

Scheme [j]: This case is the same as the deterministic scheme [h] with, in addition, a systematic frequency shift of -3 Hz, translating thus all the frequencies  $f_i$  from the range (5 - 25 Hz) down to the new range (2 - 22 Hz).

Scheme [k]: This is a pseudo-random scheme with the new range of frequencies (2 - 22 Hz) obtained by randomly perturbing the already deterministically varying frequencies of scheme [j]. As a matter of fact, going from scheme [j] to scheme [k] is exactly similar to going from scheme [g] to scheme [i].

### D.3 Listing of the program

The listing given below corresponds to run A[e], for which the deterministic frequencies  $f_i$  are perturbed by a pseudo-random fluctuator. The parameters considered here are  $N = 5$ ,  $f_n = 14$  Hz,  $\bar{\alpha} = 0.25$  and  $\sigma = 0.50$ . The listing may be found in the following pages, as well as the 161 first digital output data, i.e. up to the frequency of 25 Hz. Both power spectra of the fluctuator  $\alpha(t)$  and of the response  $x(t)$  are given.

```

0001      ***      RUN A[C]
0002      IMPLICIT REAL*8(A-H,K-L,O-R,T-Z)
0003      INTEGER IY,N,M,INC,ICPT,IMAG4(5151),IER,ITITLE(144),ICHAR(10)
0004      INTEGER NN ,L,IND,IWK(11)
0005      REAL RANGE(4)
0006      REAL FX , FXINC , PS(1025) , PBIG , DDD , FLOAT
0007      DOUBLE PRECISION X(1025),Y(1025,1) , SIGMA , SIGMA2
0008      DOUBLE PRECISION XX(4096),PSX(1025),WK(1024)
0009      DOUBLE PRECISION YY(4096),PSY(1025),XPS(2050)
0010      COMPLEX*16 CWK(2050)
0011      DATA ICHAR(1)/1H /,RANGE/4*0.0/
0012      CALL UGETIC(1,NIN,NOUT)
0013      SEAS(NIN,5) (ITITLE(1), I = 1,144 )
0014      5 FORMAT(72A1)
0015      L = 2048
0016      NN = 4096
0017      IND = 1
0018      PI = 3.1415926536DC
0019      F1 = 5.00
0020      FN = F1
0021      TN = 1.00/FN
0022      T1 = 1.00 / F1
0023      H = TN/64.00
0024      C1 = 2.00*PI*F1
0025      C2 = C1*2.00
0026      C3 = C1*3.00
0027      C4 = C1*4.00
0028      C5 = C1*5.00
0029      ALPHA = 0.2500
0030      A1 = ALPHA / 5.00
0031      A2 = A1
0032      A3 = A1
0033      A4 = A1
0034      A5 = A1
0035      PHI1 = 0.00
0036      PHI2 = PHI1
0037      PHI3 = PHI1
0038      PHI4 = PHI1
0039      PHI5 = PHI1
0040      ***** ELEMENTS FOR THE GAUSSIAN DISTRIBUTION
0041      SIGMA = 0.5000
0042      TMIU = 0.00
0043      WRITE(6,88) TMIU,SIGMA,ALPHA
0044      88 FORMAT('1',2X,'GAUSSIAN DISTRIBUTION : MIU = ',D20.13,' 3 SI
0045      *GMA = ',D20.13,' ; *** ALPHA = ',D12.5)
0046      IR = 1
0047      IR1 = 1
0048      J = 5**13
0049      ***** INITIALIZATION :
0050      FNN = 14.00
0051      CN = 2.00*PI*FNN
0052      ZETA = 0.00500
0053      CMASS = 1.00
0054      KA = CMASS*ON*ON

```

```

0051      C = 2.00*OZETA*DN*CMASS
0052      RF = 0.00
0053      OMEGA = 0.00
0054      T = 0.00
0055      X0 = 1.00
0056      Y0 = 0.00
0057      X1 = 1.00
0058      Y1 = 0.00
0059      X2 = 1.00
0060      Y2 = 0.00
0061      XX(1) = 0.00
0062      YY(1) = 1.00
0063      XXSUM = 0.00
0064      YYSUM = 0.00
0065      XX2SUM = 0.00
0066      YY2SUM = 0.00
0067      DO1 I = 2, NN
0068      CALL ALEPH(IR1, TMIU, SIGMA, T, O1, O2, O3, O4, O5, PHI1, PHI2, PHI3, PHI4, PHI5
          $S, ALPH, J, A1, A2, A3, A4, A5)
0069      CALL FF(H, Y2, U)
0070      CALL PERTU(H, KA, C, CMASS, X2, Y2, V)
          $, TMIU, SIGMA, J, IR, RF, OMEGA, T,
          $O1, O2, O3, O4, O5, PHI1, PHI2, PHI3, PHI4, PHI5, A1, A2, A3, A4, A5)
0071      CALL FF(H, Y2+ V /2.00, UU)
0072      CALL PERTU(H, KA, C, CMASS, X2+ U /2.00, Y2+ V /2.00, VV)
          $, TMIU, SIGMA, J, IR, RF, OMEGA, T + H/2.00,
          $O1, O2, O3, O4, O5, PHI1, PHI2, PHI3, PHI4, PHI5, A1, A2, A3, A4, A5)
0073      CALL FF(H, Y2+ VV/2.00, UUU)
0074      CALL PERTU(H, KA, C, CMASS, X2+ UU/2.00, Y2+ VV/2.00, VVV)
          $, TMIU, SIGMA, J, IR, RF, OMEGA, T + H/2.00,
          $O1, O2, O3, O4, O5, PHI1, PHI2, PHI3, PHI4, PHI5, A1, A2, A3, A4, A5)
0075      CALL FF(H, Y2+ VVV, UUUU)
0076      CALL PERTU(H, KA, C, CMASS, X2+ UUU, Y2+ VVV, VVVV)
          $, TMIU, SIGMA, J, IR, RF, OMEGA, T + H,
          $O1, O2, O3, O4, O5, PHI1, PHI2, PHI3, PHI4, PHI5, A1, A2, A3, A4, A5)
0077      XXXX=X2+ (U + 2.00*UU + 2.00*UUU + UUUU)/6.00
0078      YYYY=Y2+ (V + 2.00*VV + 2.00*VVV + VVVV)/6.00
0079      T = T + H
0080      XX(I) = ALPH
0081      YY(I) = XXXX
0082      X2= XXXX
0083      Y2= YYYY
0084      XXSUM = XXSUM + XX(I)
0085      YYSUM = YYSUM + YY(I)
0086      XX2SUM = XX2SUM + XX(I)*XX(I)
0087      YY2SUM = YY2SUM + YY(I)*YY(I)
0088      1 CONTINUE
0089      XXSUM = XXSUM / NN
0090      YYSUM = YYSUM / NN
0091      XXRMS = DSQRT( XX2SUM / NN )
0092      YYRMS = DSQRT( YY2SUM / NN )
0093      WRITE(6,7) XXSUM, XXRMS
0094      WRITE(6,8) YYSUM, YYRMS
0095      7 FORMAT(////////'0', 8X, 'XXSUM = ', D20.13, 6X, 'XXRMS = ', D20.13)

```

```

0096      8 FORMAT('0',          6X,'YYSUM = ',F20.13,6X,'YYRMS = ',D20.13)
0097      DO6   I = 1,NN
0098      XX(I) = XX(I) -XXSUM
0099      YY(I) = YY(I) -YYSUM
0100      6 CONTINUE
0101      CALL FTFFS (XX,YY,NN,L,IND,PSX,PSY,XPS,IWK,WK,CWK,IER)
0102      WRITE(6,66)      IER
0103      66 FORMAT(////////'0',6X,'IER = ',I4,' '////////)
0104      DENOM = L#H
0105      WRITE(6,333)
0106      333 FORMAT(////////'0',10X,'          FREQUENCY          ',3X,
*          'POWER SPECTRUM OF X ',3X,
*          'POWER SPECTRUM OF Y ',3X,
*          'MAGN. OF X-SPECTRUM ',3X,
*          'PHASE OF X-SPECTRUM '////////)
0107      IL = L/2 + 1
0108      DO2   I = 1,IL
0109      X(I) = DFLOAT(I - 1) / DENOM
0110      2 WRITE(6,3) I,X(I)      , PSX(I) , PSY(I) , XPS(I) , XPS(I + IL)
0111      3 FORMAT(' ',2X,I4,5(3X,D20.13))
0112      INC = 1
0113      N = IL
0114      M = 1
0115      IOPT = 1
0116      IY = IL
0117      X(1) = 0.D0
0118      ITEST = 1
0119      CALL PLOT0N
0120      GO TO 11
0121      22 DO55 I = 1,IL
0122      55 PSX(I) = PSY(I)
0123      11 DO4 I = 1,IL
0124      4 Y(I,1) = PSX(I)
0125      CALL USPLTD(X,Y,IY,N,M,INC,ITITLE,RANGE,ICHAR,IOPT,IMAG4,IER)
0126      CALL LARGE(PSX,IL,BIG)
0127      RBIG = SNGL(BIG)
0128      IF(RBIG.EQ.0.0) GO TO 72
0129      DO42 I = 1,IL
0130      42 PS(I) = SNGL( PSX(I) ) * 8.0 / RBIG
0131      FX = 0.0
0132      DDD = FLOAT( L/2 )
0133      FXINC = 16.0/DDD
0134      CALL PLOT(4.0,1.5,-3)
0135      CALL AXIS(C.0,0.0,'FRACTION OF PEAK AMPLITUDE',26,8.0,90.0,0.0,0.0,125
*25)
0136      IF(ITEST.NE.1) GO TO 90
0137      CALL AXIS(0.0,0.0,
*4-1 : ALPHA(T) WITH PSEUDO-RANDOM FREQUENCIES / ALPHA = 0.25 & SIGMA = .1
$MA = 0.50      FREQUENCY(HZ)',-111,16.0,0.0,0.0,10.0)
0138      GO TO 91
0139      90 CALL AXIS(0.0,0.0,
*4-1 : ASSOCIATE SYSTEM RESPONSE (UNFORCED) / ALPHA = 0.25 & SIGMA
$= 0.50      FREQUENCY(HZ)',-111,16.0,0.0,0.0,10.0)
0140      91 CALL PLOT(FX,PS(1),3)

```

```

0141          D041      I = 1, IL
0142          CALL PLOT(FX,PS(I),2)
0143          41      FX = FX + FXINC
0144          CALL PLOT(FX,-1.5,-3)
0145          IF(ITEST.NE.1)      GO TO 24
0146          ITEST = 2
0147          GO TO 22
0148          72      WRITE(6,20)
0149          20      FORMAT('0',8X,'RBIG IS EQUAL TO ZERO')
0150          24      CONTINUE
0151          CALL ENDPLT
0152          STOP
0153          END

```

```

*OPTIONS IN EFFECT*  NOTERM, ID, EBCDIC, SOURCE, NOLIST, NODECK, LOAD, NOMAP, NOTE ST
*OPTIONS IN EFFECT*  NAME = MAIN      , LINECNT =      56
*STATISTICS*        SOURCE STATEMENTS =      153, PROGRAM SIZE =      186328
*STATISTICS*        NO DIAGNOSTICS GENERATED

```

FORTRAN IV G1 RELEASE 2.0

LARGE

```

0001          SUBROUTINE LARGE(E,N,BIG)
0002          IMPLICIT REAL*8(A-H,K-L,O-Z)
0003          EQUABLE PRECISION E(N)
0004          BIG=0.00
0005          DO 40 I=1,N
0006          IF(BIG.GE.CABS(E(I))) GOTO 40
0007          BIG=CABS(E(I))
0008          40      CONTINUE
0009          RETURN
0010          END

```

```

*OPTIONS IN EFFECT*  NOTERM, ID, EBCDIC, SOURCE, NOLIST, NODECK, LOAD, NOMAP, NOTE ST
*OPTIONS IN EFFECT*  NAME = LARGE     , LINECNT =      56
*STATISTICS*        SOURCE STATEMENTS =      10, PROGRAM SIZE =      448
*STATISTICS*        NO DIAGNOSTICS GENERATED

```

FORTRAN IV G1 RELEASE 2.0

FF

```
0001      SUBROUTINE FF(H,Y,K)
0002      IMPLICIT REAL*8(A-Z)
0003      K = H*Y
0004      RETURN
0005      END
```

```
*OPTIONS IN EFFECT*  NOTERM, ID, EBCDIC, SOURCE, NOLIST, NODECK, LOAD, NOMAP, NOTEST
*OPTIONS IN EFFECT*  NAME = FF      , LINECNT =      56
*STATISTICS*        SOURCE STATEMENTS =      5, PROGRAM SIZE =      344
*STATISTICS*        NO DIAGNOSTICS GENERATED
```

FORTRAN IV G1 RELEASE 2.0

PERTU

```
0001      SUBROUTINE PERTU(H,KA,C,CMASS,X,Y,CARL,TMIU,SIGMA,J,IR,F,OMEGA,T,
0002      *O1,O2,O3,O4,O5,PHI1,PHI2,PHI3,PHI4,PHI5,A1,A2,A3,A4,A5)
0003      IMPLICIT REAL*8(A-H,K-L,O-Z)
0003      CALL ALEPH(IR,TMIU,SIGMA,T,O1,O2,O3,O4,O5,PHI1,PHI2,PHI3,PHI4,PHI5,
0004      $,ALPH,J,A1,A2,A3,A4,A5)
0004      CARL = H*( -KA*X - C*Y + F*DSIN(OMEGA*T) ) / ( CMASS + ALPH )
0005      RETURN
0006      END
```

```
*OPTIONS IN EFFECT*  NOTERM, ID, EBCDIC, SOURCE, NOLIST, NODECK, LOAD, NOMAP, NOTEST
*OPTIONS IN EFFECT*  NAME = PERTU   , LINECNT =      56
*STATISTICS*        SOURCE STATEMENTS =      6, PROGRAM SIZE =      1260
*STATISTICS*        NO DIAGNOSTICS GENERATED
*STATISTICS*        NO DIAGNOSTICS THIS STEP
```

FORTRAN IV G1 RELEASE 2.0

ALEPH

```
0001      SUBRCUTINE ALEPH(IR,TMIU,SIGMA,T,01,02,03,04,05,PHI1,PHI2,PHI3,PHI4,PHI5
          *4,PHI5,ALPH,J,A1,A2,A3,A4,A5)
          C VARIANTE 1
0002      IMPLICIT REAL*8(A-H,K-L,O-Z)
0003      DOUBLE PRECISION RO(5) , RRO(5)
0004      RO(1) = 01
0005      DO351 I = 2,5
0006      351 RO(I) = RO(I-1) + RO(1)
0007      DO 44 I = 1,5
0008      RRR = 0.00
0009      DO 7 III = 1,12
0010      IP = IR*J
0011      IF(IP.LT.0) IR = IR + 2*(2**30 - 1) + 2
0012      R = DFLOAT(IR)/2.D0**31
0013      RR = R*SIGMA + TMIU/12.D0 - SIGMA/2.D0
0014      RRR = RRR + RR
0015      7 CONTINUE
0016      44 RRO(I) = RRR
0017      ALPH = 0.00
0018      DO45 I = 1,5
0019      45 ALPH = ALPH + A1*DSIN((RO(I) + RRO(I)) * T )
0020      RETURN
0021      END
```

```
*OPTIONS IN EFFECT* NOTERM, ID, EBCDIC, SOURCE, NOLIST, NODECK, LOAD, NOMAP, NCTEST
*OPTIONS IN EFFECT* NAME = ALEPH , LINECNT = 56
*STATISTICS* SOURCE STATEMENTS = 21, PROGRAM SIZE = 1434
*STATISTICS* NO DIAGNOSTICS GENERATED
```

XXSUM = 0.1080448528083D-02

XXRMS = 0.8180185779995D-01

YYSUM = 0.3254633933068D-03

YYRMS = 0.2045174642750D+00

IER = 0

	FREQUENCY	POWER SPECTRUM OF X	POWER SPECTRUM OF Y
1	0.0	0.1153654668890D-02	0.1089817177585D-03
2	0.1562500000000D+00	0.1269820182186D-01	0.2245525513456D-04
3	0.3125000000000D+00	0.5649646766322D-02	0.1773976578099D-05
4	0.4687500000000D+00	0.2619439283272D-02	0.4683531113154D-04
5	0.6250000000000D+00	0.1036025464383D-01	0.4946708245725D-04
6	0.7812500000000D+00	0.1366929024661D-01	0.9082362463446D-03
7	0.9375000000000D+00	0.4971783548602D-02	0.2435100243476D-02
8	0.1093750000000D+01	0.7253630196079D-02	0.1010712565139D-02
9	0.1250000000000D+01	0.1803081068235D-01	0.2179581533239D-03
10	0.1406250000000D+01	0.1204143689600D-01	0.7146601697157D-04
11	0.1562500000000D+01	0.4856117023344D-02	0.4877622031194D-05
12	0.1718750000000D+01	0.2688561309063D-02	0.3384158038688D-04
13	0.1875000000000D+01	0.2676563711132D-02	0.2259069168967D-04
14	0.2031250000000D+01	0.4192573047166D-02	0.5698789456491D-04
15	0.2187500000000D+01	0.3632139114023D-02	0.3895253261019D-04
16	0.2343750000000D+01	0.4564171774483D-02	0.3086222957834D-04
17	0.2500000000000D+01	0.1311262861889D-02	0.1429615458502D-05
18	0.2656250000000D+01	0.1373645955792D-01	0.2707600632907D-04
19	0.2812500000000D+01	0.6605431475156D-02	0.2595098016090D-04
20	0.2968750000000D+01	0.3340321027528D-02	0.7204004912666D-05

21	0.31250000000000+01	0.86771557627220-02	0.25947504125940-04
22	0.32812500000000+01	0.37865902992450-02	0.72283016088220-04
23	0.34375000000000+01	0.40511005985870-02	0.62702635899380-04
24	0.35937500000000+01	0.52959544180460-02	0.71098519551400-04
25	0.37500000000000+01	0.93871405634320-02	0.43013857207560-03
26	0.39062500000000+01	0.27270787677590-02	0.13439972131390-02
27	0.40625000000000+01	0.73020096388130-02	0.23469272758270-02
28	0.42187500000000+01	0.19305206492830-01	0.80917308628990-03
29	0.43750000000000+01	0.49813010358590-02	0.30191037710480-04
30	0.45312500000000+01	0.24653805700680-02	0.20842147130520-04
31	0.46875000000000+01	0.48300245292340-03	0.22497186543930-04
32	0.48437500000000+01	0.27753837623920-01	0.58724872490320-05
33	0.50000000000000+01	0.53549599874010-01	0.26996512006080-04
34	0.51562500000000+01	0.14448121864530-01	0.30111208346530-04
35	0.53125000000000+01	0.48630939561420-02	0.47228431031180-04
36	0.54687500000000+01	0.21215941103210-02	0.13893160132330-04
37	0.56250000000000+01	0.42852396757600-02	0.37725566038970-04
38	0.57812500000000+01	0.10661636367140-01	0.12775135428050-02
39	0.59375000000000+01	0.10330539243990-01	0.33545687943850-02
40	0.60937500000000+01	0.73578418449860-02	0.18476112690860-02
41	0.62500000000000+01	0.79646791136840-02	0.26493507661970-03
42	0.64062500000000+01	0.90907889169510-02	0.11887614969680-03
43	0.65625000000000+01	0.20849667155530-02	0.31480340567220-04
44	0.67187500000000+01	0.85464528687720-02	0.59603995210580-04
45	0.68750000000000+01	0.33407239245970-02	0.51236864642020-04
46	0.70312500000000+01	0.46698354320890-02	0.13948511562540-03
47	0.71875000000000+01	0.53237550817610-02	0.45996921555190-04
48	0.73437500000000+01	0.10746428907430-01	0.90836302863850-04
49	0.75000000000000+01	0.69676034228130-02	0.59520961330950-04
50	0.76562500000000+01	0.10361339454090-01	0.37552169897560-04
51	0.78125000000000+01	0.58110022541520-02	0.10891141609670-04
52	0.79687500000000+01	0.77864633059980-02	0.39476957557230-04
53	0.81250000000000+01	0.24907121067460-02	0.76761231395460-04
54	0.82812500000000+01	0.21151885160850-02	0.56384800210270-04
55	0.84375000000000+01	0.24670099464640-02	0.19008551097350-04
56	0.85937500000000+01	0.27891708951970-02	0.18413489610620-03
57	0.87500000000000+01	0.43567440374840-02	0.65345974862550-03
58	0.89062500000000+01	0.10239904160200-02	0.35038492589290-02
59	0.90625000000000+01	0.13350310058960-02	0.55114884390870-02
60	0.92187500000000+01	0.22760718186680-02	0.25728802767390-02
61	0.93750000000000+01	0.84183845080900-02	0.11617772388140-03
62	0.95312500000000+01	0.63534514777410-02	0.10473237469260-03
63	0.96875000000000+01	0.46927178495860-02	0.69943709790940-04
64	0.98437500000000+01	0.24552340235740-01	0.99457115823640-04
65	0.10000000000000+02	0.60563683682760-01	0.22254430006140-03
66	0.10156250000000+02	0.21039161165180-01	0.31040057034420-03
67	0.10312500000000+02	0.40526048531330-02	0.33181521531930-03
68	0.10468750000000+02	0.76745359367490-03	0.23075957917540-03
69	0.10625000000000+02	0.25672610193110-02	0.21006660779820-03
70	0.10781250000000+02	0.55118029981990-02	0.42522079832720-02

71	0.10937500000000+02	0.5734770068291D-02	0.1721081546667D-01
72	0.11093750000000+02	0.2235463578493D-02	0.1031966470233D-01
73	0.11250000000000+02	0.9462304995018D-02	0.1636217051289D-02
74	0.11400250000000+02	0.2230000362696D-01	0.4577612012949D-03
75	0.11562500000000+02	0.5999933374036D-02	0.1899067430725D-04
76	0.11718750000000+02	0.10970241500004D-02	0.4542500098476D-03
77	0.11875000000000+02	0.4638603484695D-02	0.5815524098536D-03
78	0.12031250000000+02	0.1685273833383D-02	0.9854356203265D-04
79	0.12187500000000+02	0.5989083872975D-02	0.3432348873741D-03
80	0.12343750000000+02	0.3955814265246D-02	0.1762876400618D-03
81	0.12500000000000+02	0.7329923197110D-02	0.2680387886640D-03
82	0.12656250000000+02	0.7824017034056D-02	0.4351469390850D-03
83	0.12812500000000+02	0.7195014995302D-02	0.1001987588993D-02
84	0.12968750000000+02	0.1320552126506D-01	0.1393086228825D-02
85	0.13125000000000+02	0.5495806811567D-02	0.3376274621097D-02
86	0.13281250000000+02	0.5449294810821D-02	0.1149883501750D-01
87	0.13437500000000+02	0.4260354687627D-02	0.1158809337515D-02
88	0.13593750000000+02	0.2963553196593D-02	0.6355210941927D-01
89	0.13750000000000+02	0.1561430234707D-01	0.1485926521152D+00
90	0.13906250000000+02	0.5407847280259D-02	0.4767373668144D+01
91	0.14062500000000+02	0.2527334611764D-02	0.1342849086294D+02
92	0.14218750000000+02	0.1926184069326D-02	0.1948009036776D+01
93	0.14375000000000+02	0.1628001498310D-02	0.1421383876999D-02
94	0.14531250000000+02	0.9958424086619D-02	0.5378710617470D-01
95	0.14687500000000+02	0.1314915125928D-01	0.4691433946692D-03
96	0.14843750000000+02	0.1446309406090D-01	0.1184279073447D-01
97	0.15000000000000+02	0.3987088995489D-01	0.1636069735093D-03
98	0.15156250000000+02	0.2106304005228D-01	0.1596637733004D-02
99	0.15312500000000+02	0.1405080516111D-01	0.1053366978949D-02
100	0.15468750000000+02	0.2136720440694D-02	0.1185585468058D-02
101	0.15625000000000+02	0.9049416400197D-03	0.5231350733003D-04
102	0.15781250000000+02	0.1465655903299D-01	0.4221644298249D-03
103	0.15937500000000+02	0.7522786069046D-02	0.8630590332323D-03
104	0.16093750000000+02	0.3047306266267D-02	0.1731487195497D-02
105	0.16250000000000+02	0.6291864695659D-02	0.6713558477247D-03
106	0.16406250000000+02	0.2155692770161D-02	0.1138840334576D-02
107	0.16562500000000+02	0.5361164314883D-02	0.1208830394641D-03
108	0.16718750000000+02	0.1046926904283D-01	0.7734411912787D-04
109	0.16875000000000+02	0.7039222050789D-02	0.6564059908719D-04
110	0.17031250000000+02	0.5953675969060D-02	0.9635667916361D-04
111	0.17187500000000+02	0.7333483330622D-02	0.6256892424323D-05
112	0.17343750000000+02	0.7696940244094D-02	0.3652597149421D-04
113	0.17500000000000+02	0.1180707074049D-01	0.2144445586627D-04
114	0.17656250000000+02	0.6523820606960D-02	0.3204239651491D-03
115	0.17812500000000+02	0.1884245356787D-02	0.1295340077813D-03
116	0.17968750000000+02	0.1040845448587D-02	0.8553547141136D-04
117	0.18125000000000+02	0.3329765276506D-02	0.2085772537895D-03
118	0.18281250000000+02	0.1017058957473D-01	0.9440908944759D-04
119	0.18437500000000+02	0.1283146788528D-01	0.2185907157340D-03
120	0.18593750000000+02	0.2239643090917D-02	0.3901203414342D-04

121	0.1875000000000000+02	0.74385912848840-02	0.44753107559340-03
122	0.1890625000000000+02	0.16849931287510-02	0.18726022504430-02
123	0.1906250000000000+02	0.15203623052710-02	0.23730910236250-02
124	0.1921375000000000+02	0.10380206182940-02	0.91437518725750-03
125	0.1937500000000000+02	0.11541215330670-02	0.61199678749830-04
126	0.1953125000000000+02	0.39116301620030-02	0.30633513432260-04
127	0.1968750000000000+02	0.53484414264480-02	0.46213302411970-04
128	0.1984375000000000+02	0.13788394908930-01	0.19390590626720-04
129	0.2000000000000000+02	0.37698583561300-01	0.17495287428550-04
130	0.2015625000000000+02	0.17075633332930-01	0.40023406658770-04
131	0.2031250000000000+02	0.23570173259560-02	0.14730065194160-04
132	0.2046875000000000+02	0.35566624984450-02	0.33107817495340-05
133	0.2062500000000000+02	0.28223507179290-02	0.40430694668680-04
134	0.2078125000000000+02	0.69115118734900-02	0.15554534254060-04
135	0.2093750000000000+02	0.15597517907490-01	0.54702902199300-04
136	0.2109375000000000+02	0.19271624010260-01	0.37284178333650-04
137	0.2125000000000000+02	0.10294621641440-01	0.72626057864880-05
138	0.2140625000000000+02	0.62876006287750-02	0.74968356174040-05
139	0.2156250000000000+02	0.36698520381220-02	0.92882999710050-05
140	0.2171875000000000+02	0.93075529765020-02	0.16755729610400-05
141	0.2187500000000000+02	0.53735702435710-02	0.64880055075650-05
142	0.2203125000000000+02	0.13624018988750-02	0.13497088443280-04
143	0.2218750000000000+02	0.19553371646930-02	0.30187173738620-06
144	0.2234375000000000+02	0.15043567185200-02	0.17946331147170-06
145	0.2250000000000000+02	0.45031379423670-02	0.11938049022220-05
146	0.2265625000000000+02	0.99193694674410-02	0.52091237446660-06
147	0.2281250000000000+02	0.14321872530120-01	0.41043581295750-05
148	0.2296875000000000+02	0.94955127946600-02	0.16745875199530-05
149	0.2312500000000000+02	0.42103637123720-02	0.59326764185820-07
150	0.2328125000000000+02	0.64755571383770-02	0.34477352671530-05
151	0.2343750000000000+02	0.57705006491900-02	0.10505373293120-04
152	0.2359375000000000+02	0.13012630255830-01	0.14915401869310-04
153	0.2375000000000000+02	0.10997022526210-01	0.29299325487130-04
154	0.2390625000000000+02	0.76806075631820-02	0.36332203365640-03
155	0.2406250000000000+02	0.73597663398130-02	0.58341068692520-03
156	0.2421875000000000+02	0.12819219167670-01	0.12523229121290-03
157	0.2437500000000000+02	0.12463798658280-01	0.10806286453640-04
158	0.2453125000000000+02	0.89190928144490-02	0.12890031278010-04
159	0.2468750000000000+02	0.48727962726050-02	0.13197406194730-05
160	0.2484375000000000+02	0.18663817867720-01	0.22533058752260-05
161	0.2500000000000000+02	0.78244759800560-01	0.37555466814550-05

## APPENDIX E

Complements to the Analog  
Frequency Domain Analysis of Chapter VE.1 Measurement characteristics of the HP 5420A Digital Signal Analyser

The HP 5420A Digital Signal Analyser performs a variety of time domain and frequency domain measurements. The input signal is a continuous waveform which is filtered, sampled (or discretized) and analysed using digital signal processing techniques. The process of the analysis involves the following steps:

- analog low-pass filter,
- analog-to-digital converter,
- digital filter,
- digital processor, and finally
- display of the result.

The analog low-pass filter is used to prevent aliasing. In fact, according to the Nyquist criterion given in Appendix D.1, when a signal is sampled, frequencies above one half of the sampling frequency will fold back into the analysis range, causing aliasing errors. The use of the anti-aliasing filters in the analyser allows alias-free measurements at frequencies below one fourth of the sampling frequency.

The analog-to-digital converter (ADC) converts voltages into numbers, namely the input waveform into the discrete input samples required by the analyser. The converter used is the HP 54410A ADC converter. The sampling is conducted at given intervals of time  $t_n = n\Delta t$ , in which  $\Delta t$  is the constant sample period. Its inverse  $1/\Delta t$  is the sample rate FS (or frequency of sampling).

The digital filter produces bandwidths that are powers of two sub-multiples of one quarter of the sample rate, e.g.,  $f_s/2$ ,  $f_s/4$ ,  $f_s/8$ ,... in which  $f_s = FS/4$ . This is so because the analyser uses only two sample rates, requiring two anti-aliasing filter cutoffs per input channel (there are two input channels available). Hence, all other bandwidths are produced by digitally filtering the ADC output with the hardware digital filter. Usually Fourier analysis produces a baseband (dc to BW) spectrum; here BW stands for bandwidth. In our study, a baseband spectrum is effectively considered. However, the digital filter makes it possible to implement a band selectable analysis (BSA), allowing the full resolution of the analyser to be focused in a narrow band, by specifying a non-zero center frequency as well as the desired bandwidth.

As far as the digital processor — in fact the analyser itself — is concerned, it manipulates the discrete data obtained through the three previous devices presented above. The continuous stream of samples are grouped into ensembles, or arrays, of  $N_t$  samples each. These ensembles may or may not overlap but, of course, overlapped processing is preferable since in this case, more data are processed, thus enhancing statistical confidence.

The relations between the time domain and frequency domain parameters are related (for baseband) by the following expressions:

$$T_t = N_t \Delta t$$

$$\Delta f = 1/T_t$$

$$BW = (N/4) \Delta f,$$

in which  $T_t$  is the length of one time ensemble,  $N_t$  is the number of samples

in the input ensemble, BW is the frequency bandwidth of the measurement,  $\Delta t$  and  $\Delta f$  are the time and frequency sample spacings. It may be noticed that the result of the Fourier transform is one ensemble of uniformly spaced frequency domain samples, whereas the time domain data are in the form of several ensembles of uniformly spaced time samples.

The process used to take into account the individual results obtained for each ensemble in order to obtain a single ensemble of results in the frequency domain is a process of averaging. Signal averaging also reduces variance when analysing random data and recovers coherent signals buried in noise.

The simplest form of averaging is the summation averaging. The summation average of N ensembles,  $A_N$ , is given by

$$A_N = \frac{1}{N} \sum_{i=1}^N Z_i,$$

where the  $i$ th ensemble is  $Z_i$ . But summation averaging does not produce a calibrated result until all N ensembles are averaged, and this is why it is not used in the analyser.

Two main types of averaging are used in the HP 5420A analyser, namely stable averaging and exponential decay averaging. Stable averaging gives an equal weight to all data, being thus most useful when the characteristics of the signal to be measured are not changing — except for noise — during the averaging process. On the contrary, exponential averaging discounts old data more and more as the averaging process continues, giving added weight to new data as it comes in; it is thus most useful when the characteristics of the signal being measured change significantly during

the averaging process (e.g. changes in the frequency of vibration components of a rotating machine as a function of machine speed, or optimization of the transfer function of control systems).

In our study, stable averaging is adopted, for obvious reasons. It produces the same result as summation averaging; however, the stable average is always calibrated properly. The equation for stable averaging is

$$A_N = A_{N-1} + \frac{Z_N - A_{N-1}}{N} ,$$

where  $A_N$  is the average after  $N$  ensembles. Stable averaging terminates after the specified "number of averages" (noted #A on the plots, as may be seen in Figs.40) has been performed. With the analyser in the stable averaging mode, any number of averages up to 32,767 may be specified. The measurement can be stopped before this specified number has been taken and the result will still be calibrated.

The analyser has two methods of initiating a measurement once the START button has been pushed. One method uses the internal clock and is referred to as "free run" mode; the other method uses a trigger condition, either internal or external. We chose to use the free run mode, for which the ADC never waits for a trigger of any kind to start sampling. The samples are stored in a buffer and the instrument controller is free to ask for a new record whenever it has finished processing the previous one. If the processing time is lower than the time record length, as it occurs in our case, the controller comes back for another record before the ADC has all new samples. Then the latter of the former samples are processed again. This is referred to as overlap processing, and has already been

mentioned above. The amount of overlap will depend on the bandwidth selected, whether the display is active or not, and on what coordinates have been selected if the display is active. Overlap processing has the benefit of greater variance reduction per unit time, i.e., as already mentioned, better statistical confidence can be achieved in any given analysis time.

On the analyser, there also exists the possibility of specifying the type of signal being processed in terms of three different signal types: sinusoidal, random or transient (or impact). It may be made clear that signal type has meaning only for frequency domain measurements, where it affects data processing and specifies the calibration applied to auto- and cross-spectrum measurements. Since we consider auto spectra, we effectively have to choose the signal type. Selecting sinusoidal signal type allows the analyser to make the most accurate amplitude measurements on signals that contain spectral components that are separated by at least  $5\Delta f$ . Transient signal type is used when an integer number of periods of the time waveform are included in the analyser time record or when the time waveform is short-lived and decays to zero before the end of the time record; it has the best frequency resolution characteristics (it allows signals as close as  $1\Delta f$  to be resolved) but also the poorest accuracy ( $-4\text{dB}$  for the worst case).

But in our case, the random signal type is adopted, because of the pseudo-random nature of the added mass perturbations  $\alpha(t)$ . This signal type allows the analyser to resolve frequencies more closely spaced ( $2\Delta f$ ) than for the sinusoidal signal type; however, absolute amplitude accuracy with this type is less than with sinusoidal (in the worst case, signal amplitude can be off by as much as  $-3\text{dB}$ ). The result obtained is in fact

a spectral density and is expressed in  $(\text{volts})^2/\text{Hz}$ . The dimension associated with the random signal type and the auto spectrum measurement is  $(K \cdot V_{\text{rms}})^2/\text{Hz}$ , where K represents a calibration factor in terms of engineering units/volt.

The type of window used for random signal is the Hanning window, given in Appendix D.1 (it is a variant of the Hamming window). This is one of the differences between the two frequency analysis methods of Chapters IV and V.

To read the value of the response amplitude, there is the POWER key which, among others in the case of auto spectrum measured with the random signal type, gives the r.m.s. power ( $V_{\text{rms}}^2$ ). The range on which this power is measured may include the entire data block (no cursors), the portion of the data between the two cursors when used, or a single cursor location.

Another difference between the two frequency analysis methods lies in the numbers  $N_t$  and  $N_{ps}$  of time domain and frequency domain samples. In the FTFPS sub-program (Chapter IV), these parameters could be chosen as powers of two (at least for  $N_t$ ) and different values were adopted during the study: mainly  $N_t = 4096$  and  $N_{ps} = 1025$  in Section 4.2 (at the end of that section, the values  $N_t = 512$  and  $N_{ps} = 129$  were also taken), and  $N_t = 2048$  and  $N_{ps} = 513$  in Section 4.3. On the contrary, in the program used by the HP 5420A analyser, the values of  $N_t$  and  $N_{ps}$  are fixed and are respectively equal to 512 and 256. These values are lower than the ones used in Chapter IV, but, due to the possibility of using ensemble averaging with overlapped processing, the capacity of the analyser is much greater.

## E.2 The EAI 1000 Analog Computer

The EAI 1000 Analog Computer is microprocessor controlled and is composed of solid-state computing elements. It allows the rapid solution of scientific and engineering problems. It is basically a set of mathematical building blocks, or computing components, each able to perform specific mathematical operations on direct voltages (between -5 and +5 volts). The input and output terminations of the computing components are brought out to a patch panel, and can be easily interconnected with wires called patch cords. By appropriately interconnecting these building blocks, an electrical model is produced in which the voltages at the outputs of the blocks obey the relations given in the mathematical description of a physical problem. This is done on a removable patch panel which is then fitted to the computer and the initial problem parameters are set by adjusting the coefficient potentiometers to their appropriate values. The EAI 1000 is constructed with a modular housing system. These modules are fitted together, and interconnections between trays made with standard flat strip cables. The modules included in a basic system are

(i) Analog module – Containing analog and digital computer elements.

Amongst the analog elements are four integrators, six summers, two multipliers, ten grounded and two ungrounded potentiometers. (Up to three analog modules may be accommodated in any one system).

(ii) Display module – Containing all necessary displays for value readout, function addressing and overload.

(iii) Control module – Containing power supplies, microprocessor control system multiplexor, mode control and keyboard. The control module can support up to three analog modules.

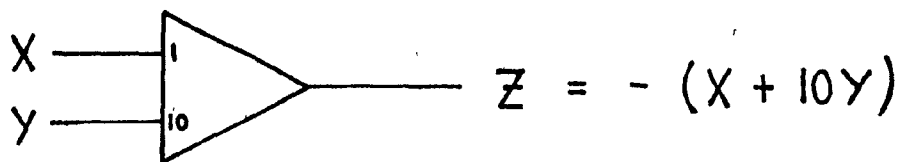
Expansion modules are

- (i') Analog modules – As previously described. Two expansion trays can be added to a basic system.
- (iv) Digital module – Containing additional digital computing elements plus facilities for hybridisation. One digital tray can be fitted to a basic system.

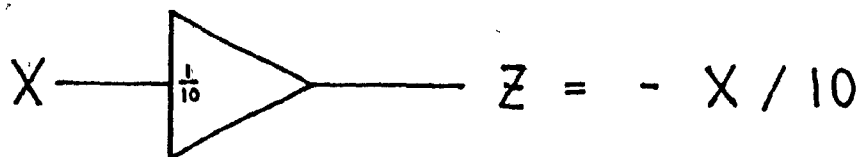
The fundamental components of the analog computer is the operational amplifier. It is an inverting amplifier of very high gain (typically  $-10^7$ , where the negative sign indicates inversion), high input impedance (several megohms), low output impedance (less than 100 ohms), and it is direct-coupled. It is the operational amplifier which, when connected to different types of its input and feedback impedances, enables the computer to sum, differentiate, integrate, invert and multiply by a constant.

We now indicate the various symbols used in Chapter V for a summer, an integrator, a multiplier and a potentiometer.

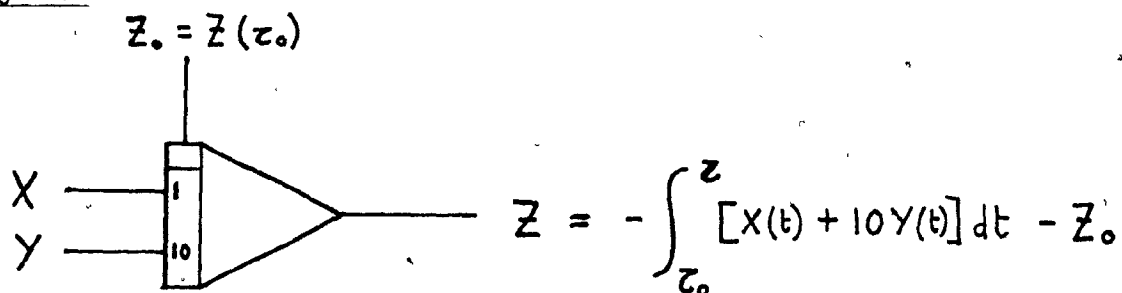
Summer:



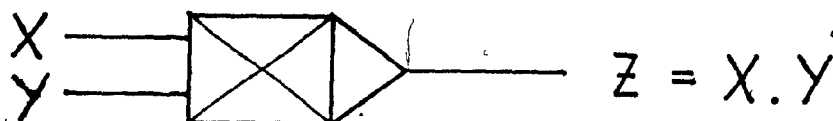
This is obtained when an output point is connected with an input point of gain 1, by means of a patch cord. However, when an output point is connected to an input point of gain 10, then the gain 1/10 is obtained for the summer:



Integrator:



Multiplier:



Potentiometer:



These analog computing elements are used to solve equation (5-7) and the circuit diagram may be found in Fig. 42.